X-713-67-73

NASA TM X-55735

RADIOMETRY RESEARCH

MARCH 1967

GODDARD SPACE FLIGHT CENTER

GREENBELT, MARYLAND

3 RADIOMETRY RESEARCH 9

Radiometry Section
Thermophysics Branch
Spacecraft Technology Division

9 February 1967 10 CV

GODDARD SPACE FLIGHT CENTER
Greenbelt, Maryland 3

FOREWORD

This report is a summary of some of the activities of the Radiometry Section for the latter part of 1966. It is divided into three parts: part I covers the progress accomplished by personnel of the section; part II covers progress accomplished by on-site contractor personnel under Task Assignment 713-2132; and, part III covers progress accomplished by off-site contractor personnel under Task Assignment 713-2149. Electro-Mechanical Research performed this work under Contract NAS-5-9244.

CONTENTS

PART I

RADIOMETRY RESEARCH

Charles Duncan
Alfred Hobbs
Carmen Nicoletta
James Webb
John Flemming
Stanley Neuder
Benjamin Seidenberg

ILLUSTRATIONS

TABLES

41. SUMMARY 8

3 SOLAR SIMULATION STUDIES 4 (713-124-09-05-06)

A-1200 Solar Simulator

N 67-[illegible]42

The RAE-TTU-(R82) satellite was scheduled to be tested for the greater part of this quarter. This test did not require any solar simulation. No work was planned on improving the uniformity, spectrum, or other characteristics of the simulator which would involve use of the lamps. Work planned for this quarter included: movement of control console into solar simulator room; design of modifications to power supplies to allow 150 amp operation; design of mechanical and electronic modifications which would result in more economical and reliable operation of the simulator; and, cleaning and re-aluminizing of the optical components of the system.

A paint sample test was performed in the early part of the quarter. Requirements for the test were: 1) solar spectral correspondence as good as possible; 2) uniformity as good as possible; and, 3) 140 mw/cm^2 irradiation. This required the use of seven spectral and seven uniformity filters which reduced the efficiency of the system to approximately 3.5%.

The uniformity filters which had been designed to improve the uniformity of irradiance in the test volume were not available until the test was scheduled to begin. No delay could be granted to start the test to allow the proper alignment of the lamps, collectors, and new uniformity filters in the system. These factors resulted in a situation where 140 mw cm^{-2} could be obtained only if the lamps were operated at 110-115 amps. Spectrolab had recommended that current not exceed 105 amps for long periods; but, that 110 amp operation should not damage the electronic components of the system. The test was performed with the lamps operating at 110-115 amps. After 48 hours, electronic problems developed which resulted in several lamp failures and power supply component failures. The uniformity before the test was ±5.5% and after the test ±6%.

The experience of the paint sample test demonstrated that the system could not be expected to perform with good uniformity and spectrum at 140 mw cm^{-2} unless major modifications were made to the system.

At the conclusion of the test, emphasis was placed on the design of modifications to the power supplies which would allow operation up to 150 amps. These modifications have been designed and orders have been placed for the new components needed.

A circuit has also been designed which allows the solar cell intensity sensor to be placed in one position for any position of the lamp and to still maintain proper control of the power supply when in the "light" mode. This has resulted in the elimination of two operators when the power supplies are aligned electronically in the current and light modes. Another monitor circuit has been designed which will display continuously the condition of the power supply characteristics. This will indicate to the operator on duty immediately which power supply is malfunctioning and permit corrective measures to be applied before a lamp fails. In the past, lamp failure or fluctuation of temperatures of samples was the first indication of malfunction of electronic components. The control console has been moved into the simulator area and rewired. Calculations made in the current capacity of the wires furnished by spectrolab showed that 10% of the power from the supplies was being lost in the cables. New cables have been ordered which will reduce this loss to less than 1%.

The optics have been cleaned and collectors are in the process of being re-aluminized.

The next quarter plans include: 1) completion of all electronic modifications to system; 2) modifications to collectors to allow 5kw lamp use; 3) uniformity and spectral work using new uniformity filters; and 4) installation of krypton lamps, if received in time.

Long range planning includes: 1) redesign of lenticular system to increase efficiency and uniformity; 2) development of spectral filters for krypton-xenon combinations of lamps; 3) installation of in-vacuum uniformity and spectral measuring equipment; 4) design and installation of data acquisition system to handle all data related to solar simulator; and 5) installation of 5kw lamps in system.

Convair 990 Flight Experiment

Uncertainties exist in the published values of the solar spectral irradiance. New data should be obtained under conditions more favorable than ground measurements to eliminate these uncertainties. An experiment has been proposed which would allow measurements to be made at 40,000 feet aboard a Convair 990 aircraft. Ames Research Center owns this plane and it has been modified for scientific experiments. A proposal has been submitted to HQ NASA requesting use of this aircraft. This proposal has been approved by Dr. J. Clark.

Design of modifications to the Leiss which will be needed to qualify it for flight have been conceived. The details have not been worked out completely yet.

Fixtures to hold the Leiss and the electronic scanning spectrometer are also being designed. Calculations have been made on sources of possible error in the experiment, flight paths which could be used, and other aspects of the experiment.

Plans for the next quarter are: 1) submit work order to EMR to finalize design modifications to Leiss and fixtures to hold instrumentation and to fabricate same; 2) complete error analysis of experiment; and 3) assemble equipment together in Building 7 for final checkout and calibration. The flight will probably be the two weeks from 7 August to 21 August 1967 which leaves very little time to accomplish everything. It is critical that work begin on final design and fabrication of fixtures and modifications to the Leiss.

Arc Research

The existing sources available for solar simulation are inadequate for efficient simulation of the solar spectral irradiance, total solar irradiance, and collimation of the solar irradiation. Sources more suitable for ultra-violet degradation experiments are also needed. The sources most generally in use, high to medium pressure mercury lamps, consist totally of line emissions in the ultra-violet region. A lamp with continuous radiation in the v.v. region and good spectral correspondence with the solar irradiation would be of great value. Work is being conducted with a pressure arc system and a vortex stabilized radiation system (VSRS) to improve spectrum, brightness and mechanical size of fireball. Measurements have been made with argon, krypton, neon, and helium at various pressure, power, and gas flow levels.

Fifteen sets of measurements have been made with the VSRS this quarter. The results of the neon-argon measurements indicate that a significant improvement can be made in spectral match to solar irradiance with the proper ratio of these two gases in a system of this type. Argon is very rich in μ.v. emission which may make it useful for degradation studies. Other results have indicated that krypton, xenon combinations of compact arc lamps would improve the spectral characteristics of the A-1200 simulator.

Plans for the next quarter include: 1) completion of the neon-argon series of measurements; 2) measurements with varying flow rates; and 3) xenon measurements.

COATINGS QUALIFICATION

Flight data from several satellites have demonstrated the need for thorough testing of thermal control coatings as to: 1) ultra-violet stability; 2) charged

particle stability; and 3) adhesion characteristics. In addition, the reproducibility of paint mixtures and paint films needs to be established. Measurements of the optical properties of thermal control coatings in air after u.v. or particle irradiation have proven to be useless. No definite standards have been established by NASA or GSFC to ensure that paint mixtures and paint films are of uniform quality or can be accurately reproduced. The effects of the substrate surface or contour of the object to which the coating is applied have not been determined in any scientific manner. These facts indicate that immediate measures should be employed, to qualify certain types of coatings for space applications and to establish definitely the optical, mechanical, and chemical properties of these coatings. This would ensure the thermal design engineer that the coatings used would not change optical or mechanical properties during the life of the spacecraft or inform him very specifically what changes would occur and at what time.

Work has been in progress this quarter to obtain data in support of the above areas. Thermal shock tests have been performed on several thermal coatings. This effort has been delayed due to a lack of facilities within this group and to a lack of a priority at T&E Division. The results of the RAE-TTU unit test in the A-1200 indicate that more emphasis should be placed in this area.

Work also has been in progress to establish the validity of accelerated solar ultra-violet irradiation of samples and the effects of spectrum upon the thermal coatings optical properties. Preliminary results have been obtained which are detailed in the EMR monthly reports. Several more tests are needed to complete this work which are not possible to be performed at present due to the elimination of overtime usage. The change in optical properties is measured "in situ" for these tests.

Electron irradiation at 400 kev to a total accumulated flux of 10^{15} e cm^{-2} in air has been accomplished for several coatings. The results indicated no change. One of the coatings (Alkali silicate - TiO_2) was subsequently irradiated in vacuum to 10^{15} e cm^{-2} and measured in air within 15 minutes after exposure and showed approximately 25% change in absorptance. The sample was allowed to remain in air for 10 days, was remeasured and showed essentially no change from the original characteristics.

Plans for the next quarter include: 1) electron irradiation at 400 kev, 700 kev, and 1 Mev to a flux accumulation of 10^{15} e cm^{-2} for 10 thermal control coatings; 2) proton irradiation at 400 kev for 10 coatings; 3) completion of tests to establish reciprocity relationships for silicone, silicate, and epoxy paints; 4) completion of tests to establish effect of spectrum on paints mentioned in 3; and 5) thermal shock, adhesion, and chemical tests on several coatings now used on satellites.

All measurements of changes will be made "in situ" for the ultra-violet irradiation and within 15 minutes upon removal to air for the particle irradiation.

SOLAR CELL CALIBRATIONS (713-120-33-01-01)

Work has been in progress developing reliable and accurate techniques and instrumentation for determination of solar cell characteristics.

This quarter's work was concerned with the evaluation of 1Ω-cm and 10Ω-cm cells of 8 mil and 16 mil thickness. 1 Mev electron radiation experiments were conducted to define energy conversion characteristics of these cells. Other work was performed on Li doped solar cells and the angular dependence of incident radiation on cells. This is detailed in Part III.

23 VORTEX ARC STUDIES 6

6 Stanley Neuder 7

ABSTRACT

Measurements of the spectral distribution of vortex stabilized, inert gas plasmas and mixed inert gas plasmas, continues to be made with the vortex stabilized arc (VSA) in order to attain an improved externally-unmodified, single source of solar simulation.

INTRODUCTION

During this quarter, the following spectral measurements were made on the vortex arc.

I.	a) Neon		4kw—8 atm
	b) Neon		16kw—8 atm
II.	a) Argon (75%)—Neon (25%)		8kw—10 atm
	b) Argon (75%)—Neon (25%)		13kw—10 atm
III.	a) Argon (50%)—Neon (50%)		4kw—4 atm
	b) Argon (20%)—Neon (80%)		4kw—4 atm
	c) Argon (10%)—Neon (90%)		4kw—10 atm
IV.	a) Argon	1600 cc/min	4kw—5 atm
	b) Argon	1200 cc/min	4kw—5 atm
	c) Argon	1200 cc/min	3kw—5 atm
	d) Argon	360 cc/min	2kw—5 atm
	e) Argon	maximum flow rate	3.5kw—5 atm
V.	a) Helium	open loop	4kw
	b) Helium	open loop	13kw incomplete
VI.	a) Xenon		incomplete

The results of these measurements will be discussed subsequently.

Much of this material has been presented at the NASA conference on coatings and solar simulation, Oct. 1966 at JPL in Pasadena.

Progress is being made towards completion of contract No. NAS 5-12450 by spectrolab. Delivery is anticipated in the near future.

Maximum permitted plasma current levels have been found to differ for the various inert gases.

DISCUSSION

Series I.

Neon emission has been measured and plotted as % energy per bandwidth at two power levels, 4kw and 16kw, at constant pressure. The UV energy content

has increased by approximately 40% in the wavelength range .25 to .55μ with the 4-fold power increase. An accompanying reduction in energy content beyond .8μ was also noted. The neon plasma at 4kw is relatively poor in UV content.

Series II, III.

Comparison of neon and argon spectra shows that argon is rich in the .25 to .5μ wavelength range and deficient in the .5μ to .8μ region. Neon is quite the reverse. Various % mixtures were spectrally measured. The 75 argon—25 neon mixture was measured at 8kw and 13kw. Both exhibited the pure argon characteristic spectral variations with power. Argon 50—neon 50 at 4kw was still primarily an argon distribution. Equal spectral excitation was achieved with 20 argon—80 neon at 4kw and 4 atm, while predominant neon excitation was exhibited by the 10 argon—90 neon mixture. These results indicate that a significant improvement in spectral matching is attainable. Further developmental steps will be taken along several lines in order to achieve the desired spectral distribution.

Series IV.

Different vortex flow rates have been tried from a low rate of 360 cc/min argon to well over 2500 cc/min, all at relatively low power. This data has been reduced but not plotted. Preliminary results indicate no major changes in the energy distribution. This remains to be verified. (The plasma goes from a short arc configuration to sharp cylindrical symmetry, with increased flow rate.)

Series V.

The helium spectrum was obtained by starting in argon, then transferring to helium, (blue-white to red-orange color). The run was "open-loop" since the recirculators were unable to pump the gas. The data on the 4kw helium run is being reduced. The 13kw run was not obtained due to electrode failure. (See subsequent discussion).

Series VI.

Two attempts to obtain xenon spectra resulted in failure. Xenon gas is presently on order and will be run when the mass spectrometer is available for gas analysis.

Plasma Stability and Electrodes

Argon plasma is very stable at various inputs and the electrode lifetime is relatively good. Neon plasmas, while quite stable, drastically reduces the cathode

lifetime. The helium plasma was not stable in that a kink is present in the plasma arc itself. This resulted in anode failure after a brief period at the higher input power levels. These factors, among others, determine the maximum plasma current levels permitted for moderate electrode lifetime.

80kw Arc

The 80kw arc is nearing completion at Spectrolab and should be delivered in the near future.

Most of these results have been presented at JPL at the Pasadena conference on coating and solar simulation.

CONCLUSION

The mixture of various gases and the increased power levels are two promising approaches for spectral tailoring.

The problem of electrode lifetimes requires increased attention.

3.3 FLIGHT EXPERIMENT 6

6 John Flemming
J. J. Webb 8

ABSTRACT

An experiment has been jointly undertaken with the Thermodynamics Branch of T&E Division to measure the solar radiant flux and solar spectral irradiance from a NASA research aircraft in an effort to improve on the data presently available, most of which have been obtained from ground-based measurements. This report describes the progress made on the project during the fourth quarter. The instruments to be used by the Thermal Systems Branch, a Leiss Monochromator and an Electronic Scanning Spectrometer, are presently being set up in the laboratory for intensity and wavelength calibration. Supporting equipment has been selected and ordered. Calibration techniques have been devised using quartz-iodine and mercury lamps, An elliptical flight path has tentatively been chosen. A study of possible sources of error has been made, and correction factors for mirror reflections, window transmissions, and other uncertainties have been considered. An 8% RMS error in spectral irradiance has been estimated. Modifications to the equipment to adapt it to the aircraft environment have been detailed.

INTRODUCTION

An aircraft flying at an altitude of 40,000 feet is above 80% of the atmosphere. It is this fact which has prompted the current interest in determining the solar constant and wavelength distribution of solar energy at air mass zero from aboard NASA's Convair 990.

In all fairness it should be recognized that there is no clear evidence that the atmosphere was the cause of the wide divergences among the results obtained by the various experimenters. These earlier workers were well aware of the variability of the atmosphere and were scrupulous to discard observations which did not extrapolate smoothly to air mass zero. It is consequently somewhat improbable that the atmosphere was entirely to blame for the wide range of values thus far reported. In many respects, the electronic instrumentation they used and the radiometric standards which were then available bear little resemblance to those available today. Even the measuring techniques have been improved as various sources of error have been uncovered.

In the proposed experiment nearly all circumstances appear to favor a significant contribution to the body of work already recorded in this field. Not only will the electronic instrumentation be of the most advanced type, but the spectroradiometric standard employed will be of a type not available to the older and oft-quoted workers. Moreover, the measurement will take place at a minimum air mass of about 0.22. There is an obvious inherent advantage in extrapolating from 0.22 to zero rather than from 1.00 to zero.

On the negative side the aircraft environment introduces complicating factors such as uncertainty in location, a somewhat unstable platform, and the necessity to view the sun through a window of uncertain transmission. There are increased chances for stray reflections to enter the optical system. Measurement time, and therefore the number of observations, will be restricted by aircraft flight time.

At this time it appears that half of the anticipated uncertainty in this experiment is attributable to the use of an aircraft platform. The advantage to be gained cannot so easily be anticipated, but will depend largely upon how well scatter in the observations can be minimized.

The uncertainty (for the shortest wavelengths) to be expected appears to be about ±17% (arithmetic sum), or about ±8% (rms sum). This does not sound very different from the accuracies claimed by prior investigators, but the fact remains that these investigators were unable to agree with one another to within the claimed accuracies, and in fact differed by as much as 40%.

The following paragraphs detail the progress and current status of the various phases of the project.

ELECTRONICS

Leiss

Since the Leiss Monochromator is an optical system only, all its electronic instrumentation must be externally supplied.

The amplifier chosen was a Brower Laboratories Model 130 B synchronous type. This is a new state-of-the-art instrument having unique advantages for the flight experiment. It is insensitive to power frequency variation from less than 50 hertz to 400 hertz. A tachometer chopper will be supplied so there is no possibility of detuning due to line frequency drift. Accuracy and sensitivity have been improved over the old model 130 (which we now have) along with dynamic range capabilities and frequency range.

A Power Designs Model 1565 high voltage power supply will be used to drive the photomultiplier detector. Since the EMI 9558QA is an eleven stage tube, a power supply stability of better than ±.05% is needed in order to prevent signal variations of ±.5%. Well regulated six and twelve volt power supply modules will supply the PbS cell.

A strip chart recorder will record the detector signal from the Brower. The chart speed will be ten inches per minute, so as to accommodate the Leiss' 1/2 rpm drum speed. A capillary inking system will be used.

Electronic Scanning Spectrometer

The Electronic Scanning Spectrometer (ESS) is a self contained unit except for external power and read-out equipment.

A Kepco model CK36-1.5M will be used to energize the system. The ESS has its own internal regulator so that the supply is not critical.

A definite decision has not been made as yet whether to use an analog tape recorder from T&E or a strip chart recorder for the output signals. The tape recorder would be perferred since the standard scan rates of the ESS are 100 and 1000 scans per second. If a strip chart recorder is used, the scan rate will obviously have to be slowed to a compatible rate, such as 1 scan every 5 or 10 seconds.

DETECTORS

Leiss

Two detectors will be required to cover the wavelength range of the Leiss. The two detectors, an S-20 response photomultiplier tube and a PbS cell, will be mounted in a single housing for ease of operation. Extensive pre-flight testing should be done to determine the stability of the detectors, and the need if any to temperature stabilize the detector housing.

An EMI 9558QA (chosen for low NEP) has been selected over the Ascop 541E-05M-14 largely for its substantial price advantage. The EMI tube has the disadvantage of being a 2 inch diameter tube as compared with the 1-1/4 inch diameter Ascop tube. Its specifications are also not as good as the Ascop, but the application should not require the more expensive tube.

No specific PbS cell has as yet been chosen. The choice depends somewhat on the design for a detector housing.

ESS

The ESS uses an image dissector tube, similar in design to a photomultiplier. It has an S-21 response characteristic which sets its useful range at 2500 Å to 5300 Å. Cut-off or band-pass filters may be needed to eliminate second-order effects and scattered radiation. These will cut down the useful wavelength range to 2500 Å—4300 Å. Ozone absorption will reduce the range even further—to roughly 3000 Å—4300 Å.

CALIBRATION

Calibration for spectral response can be accomplished on each of the projected eastward legs of the flight plan. This will be done by covering the integrating sphere entrance port used for solar radiation, and allowing radiation from a 1000 watt quartz-iodine standard of spectral irradiance to enter the sphere via a second port conveniently located on the side. This approach has been adopted since there is no way for standard lamp radiation to traverse the optical system in exactly the same way as did the solar radiation. It requires careful evaluation of the mirror reflection coefficients and the window transmission.

A check on the wavelength calibration can easily be accomplished by use of a small mercury vapor discharge tube.

ENTRANCE OPTICS

In any radiometric work, it is an advantage to minimize the number of optical elements involved. Each element used in the present case will affect the radiation from the standard lamp differently from the radiation from the sun, if only because the entrance optics will sub-tend a much larger solid angle at the standard lamp than at the sun. Therefore a correction must be made to the data for the effect of each optical element used, and an uncertainty recognized which is the uncertainty of that correction.

It would be possible to use no optical elements at all, except the observation window, by mounting the spectrometers with their integrating spheres very close to the window. In this case it would only be necessary to correct for the solar aspect angle with respect to the integrating sphere port, and for the observation window transmission (including reflection losses). A fairly large correction, on the order of 10%, would have to be made for the light scattered into the sphere by the atmosphere, since the sphere's field of view would have to be about 60°.

An alternative approach is to severely restrict the field of view (to ±1/2° for example) and to introduce a servo-driven heliostat to maintain the image of the sun in the spectrometer aperture. In this case sky brightness would not require a correction, but the additional optics required would. Moreover, it is doubtful that these optics could be used with the standard lamp. Furthermore, development and/or procurement of a suitable heliostat appears to be unacceptable within the current time schedule.

The approach adopted is to restrict the field of view to ±5°. Two turning flats, one of them fixed and one having two degrees of rotational freedom, will be used to transfer sunlight into the integrating sphere, whose view angle will be limited by stops. The advantage of this approach is that no servo-driven heliostat is required (adjustments will be made by hand), and the sky-brightness contribution is restricted to ±5° of sky.

The disadvantage here is that both optical and sky-brightness corrections must be made instead of one or the other.

SOLAR ASPECT ANGLE

The solar aspect angle is equal to the great circle distance in degrees between the point of observation and the sub-point on the earth's surface of the sun.

If α is the solar aspect angle, then

$$\cos \alpha = \sin L_1 \sin L_2 + \cos L_1 \cos L_2 \cos (\lambda_2 - \lambda_1)$$

where

L_1 = latitude of point of observation

L_2 = solar declination

λ_1 = longitude of point of observation

λ_2 = longitude of solar sub-point (Longitudes are negative if West, positive if East.)

The Air Almanac gives L_2 and λ_2 at ten minute intervals.

Therefore, the experimenters need only know their latitude and longitude as a function of Greenwich time to determine the sun's position with respect to the plane.

FLIGHT PLAN

It has been generally decided that the plane should fly a race-track-type course over the Pacific Ocean. The actual time of measurement has not been set, but a ten minute measuring leg flying away from the sun and a twenty minute leg flying into the sun seems reasonable. This procedure will permit the greatest variation in the optical air mass while allowing ample time on each measurement leg for all experiments. In the course of about three hours and ten minutes, the procedure provides for seven measurement legs and a solar aspect angle variation of approximately 55°. The procedure also concludes with the airplane only about one hour's flying time from home base. It will not be necessary for the pilot to fly perpendicular to the sun-plane azimuth.

The time of day of the flights may be fixed by the zenith angle of the sun. It may be necessary to make all flights at midday when the zenith angle is small. Since the air mass determination depends on the secant of this angle, it is essential to know the precise position of the plane at the time of measurement in order to determine the angle accurately. The secant changes considerably at angles above 60°. At 80°, for example, the change is approximately 10% per degree. At this angle, the plane's position must be known to within six minutes

of arc (six nautical miles) in order to maintain an air mass uncertainty of 1%. It is not known at this time whether or not the aircraft's position can be fixed this accurately. This factor will determine how great a zenith angle can be tolerated.

INSTRUMENT MODIFICATIONS

Leiss

The general intention is to assemble the Leiss instrumentation in such a way as to require a minimum of manipulation by the operator while in flight. Reliability and mechanical and thermal stability are also to be stressed. The following is a list of modifications thought desirable:

1. The Leiss should be shock-mounted to dampen the normal shock and vibration occasionally experienced aboard jets.

2. The detector support bracket, and also the integrating sphere support bracket, should be strengthened and made more rigid so as not to introduce varying strains into the casting on which the optical components are mounted.

3. The prisms should be potted into their cages so as to futher inhibit misalignment due to shock and vibration. A quantity of GE RTV-11 is on hand for this job. This compound should be pigmented black if possible.

4. A lightweight, thermally insulated cover should be constructed. This will reduce the structural requirements and will aid in temperature stabilizing the Leiss.

5. A thermostatic control for the heaters should be installed inside the Leiss. One heater will have to be moved to make room for a chopper.

6. The miniaturized chopper should be installed inside the Leiss just in front of the intermediate slit. A Brower chopper will be used, and Brower has agreed to furnish a template or drawing for their required mounting holes and cable feed-throughs.

7. The wavelength drive motor and electric clutch should be permanently attached to the spectrometer casting. The speed selected for the wavelength drum is 1/2 rpm. About 7 or 8 minutes will be required for the entire spectrum (Photomultiplier and PbS cell).

8. A trigger commutator consisting of a uniquely coded wheel and a wiper which is to serve as the contact closure for the strip chart recorder event marker. The wheel should be unsymmetrically coded so as to provide positive and unique identification of wavelength (drum position) on the strip chart. Additional circuitry may be desirable to reduce the event width on the chart. This would improve precision.

ESS

At the present time, no modifications are necessary except for special shock mounts similar to those required for the Leiss.

ERROR ANALYSIS

Below are listed uncertainties which will be encountered and their sources. The list may not be complete, and it may include items which will ultimately be circumvented.

±6%	This is the uncertainty associated with the standard of spectral irradiance at about 300 nm.
±1%	This is probably somewhat larger than the error associated with setting the standard lamp current.
±1%	This is uncertainty associated with the read-out of the data.
±1%	This is uncertainty associated with the linearity of detection and amplification.
±2%	This is uncertainty of the reflectance of the first turning flat.
±2%	This is uncertainty of the reflectance of the second turning flat.
±1%	This is uncertainty of the window transmittance. This figure assumes no contamination of the window by the atmosphere encountered in flight or on the ground.
±1%	This is uncertainty of the air mass. Actually this uncertainty depends on the angular distance

	of the sun from the zenith and the accuracy with which the plane's position can be determined.
±2%	This is the uncertainty added by the sky-brightness connection. At this stage, the figure is little more than a guess.

A direct summation of these uncertainties yields a total value of ±17%. If the uncertainties are summed in an RMS fashion, the total RMS uncertainty is about ±8%.

CONCLUSIONS AND RECOMMENDATIONS

The experiment may perhaps be best characterized as still in the analytical stage. Much more analysis appears to be needed, particularly in the areas of the entrance optics, the flight plan, and navigation.

A particularly urgent need exists to positively define the flight plan including the location, time on station, and accuracy of location. This is important since it has an influence on other areas of design.

Referring to the performance schedule given in the experiment proposal; it is readily apparent that the work is already 2 to 3 months behind schedule as regards instrumentation integration and checkout. Some essential items having long lead times have not yet been ordered. Nor has work begun on the design of the mounting structures for the spectrometers. Even more serious than the present delays in these areas is the fact that there is no end in sight for the delay. Unless action is initiated very soon, the experiment may be seriously compromised, and it may be advisable to re-schedule the program for the following summer.

43 COATINGS QUALIFICATION 6

6 Alfred Hobbs and Ben Seidenberg 8

ABSTRACT

DEGRADATION EQUIPMENT

Eight vacuum-irradiation degradation cells were improved.

Eight ULTEK pumps were ordered for December 27, 1966.

Lamp ripple reduction equipment was ordered and lamp housing designed.

A unique coatings degradation tool will be built from an Electronic Scanner obtained from Dr. Frankel's group (provided enough space is available).

A patent disclosure was filed for a method for detection and analysis of coatings changes.

For degradation detection, tests showed resistivity measurements of coatings can be made.

COATINGS R&D

An analytical coatings chart was prepared listing coatings used on satellites.

Our group prepared a good methyl-silicone white paint.

Our group is developing a promising black metallic-oxide coating for vacuum-chamber shrouds.

Beckman DK-2A indicates electron-bombardment in air did not optically damage Boeing specimens.

Our group is studying the volatiles from Boeing specimens.

Our group is developing large-area thermocouples for paint substrates.

Thermal shock T&E test of Boeing specimens is stalled for lack of proper authorization.

INTRODUCTION

Our group, The Coatings Quality Assurance Group, is a recent addition to the unofficial Radiometry Section which is part of the Thermal Physics Systems Branch. We are charged with the task of creating and performing tasks that will insure an effective area and working team consistent with good fundamental quality control practices. These tasks are in direct support of passive, thermal control coatings designed for application or possible application to satellites at GSFC. These efforts not only take in the areas of procuring, designing, etc. equipment that will meaningfully degrade and measure these coatings but also the area of coatings R&D as well as Quality Control SOP's, library of retained coatings, retained paints, etc. (latter outlined in memos to Mr. M. Schach dated 10/14/66 and 6/22/66).

DISCUSSION

Degradation Equipment

Modification of electromagnetic radiation degradation chambers.

The chambers were redesigned to give us greater pump down speed. The new design also allows us to check the vacuum directly in the chamber and not as line current at the pumps as is the case with similar chambers now in use in our Branch. This design also increases the possibilities of achieving an optical in situ degradation reading. Four of the eight chambers are being modified with push-pull systems which are extremely inexpensive with hopes that it will enable us to accomplish our measurements in the 10^{-6} torr, range. One chamber has been fitted with an expensive magnetic rotational feedthrough. This feedthrough was given to us gratis and we had it modified and installed so that it translates rotary motion into linear motion enabling us to move the specimen holder up to the measurement port. This method and feedthrough can be utilized at much greater vacuum than the cheap feedthroughs (10^{-8} and greater torr). Only the insertion of the four cheap feedthroughs remain to be achieved in this area of our endeavors.

Getter-Ion/Titanium sublimation pumps (8) were ordered from Ultek Corp. after much negotiation and delay on the part of Ultek, approval of design, etc., the systems are now scheduled for completion and check-out at Ultek's plant by December 27, 1966. A. J. Hobbs will check the performance as to specifications at plant site.

These systems are designed to allow our degradation chambers to achieve a 10^{-8} torr vacuum (vacuum measured inside the chamber) in a "clean" empty condition in approximately one hour.

Chokes and condensers have been ordered from Westinghouse Electric to be utilized in connection with our relatively inexpensive power supplies (Westinghouse). We have taken this step in our effort to reduce ripple from its present 10-12% down to a possible 1-3%. We believe that this will materially increase the life span of the lamps that we will be operating with these power supplies. The lamps will be the 2.5kw Osram Xenon lamp and the 5.5kw Hanovia Xenon lamp. These lamps were chosen in order to obtain a range of solar constants of from 1-3 or possibly 4 solar constants.

Also as an additional aspect of our degradation effort we have had designed lamp housings that will accommodate interchangeability both types of lamps. These housings should allow us to use two chambers at a time using only one lamp, thereby conserving room and at the same time giving us a relatively safe, convenient and easy to get to ultra-violet degradation system.

We have obtained, on indefinite loan, an Electron Microscope capable of generating energy levels of from 50 kev to 150 kev electrons utilizing a range of rates. We have signed this equipment out of storage after gaining permission from Dr. Frankel's group. Our group hopes to initially set up the instrument and familiarize itself with its use and then alter its design so that we can irradiate coatings specimens in vacuum and measure this specimen in situ. We have obtained from T. Sciacca pertinent literature and advice.

A patent disclosure has been filed with the office of the patent counsel and a patent search completed concerning the use of harmonic vibratory motion (tuning fork principle) to detect changes in coatings due to degradation. It is theorized that these changes can be sensitively detected either under terrestrial (air) or under spatial conditions (vacuum). We are in the process of reviewing a few pertinent patents. Some basic, inexpensive equipment has already been ordered.

Our group and John Flemming have been approached by Mr. M. Schach with the possibility of using Resistivity on Dielectric Constant measurements as a sensitive, rapid means of detecting degradation in a meaningful context. After completion of a feasibility study undertaken by J. Flemming and R. Bernstein it was determined that between the two only Resistivity measurements offered the best approach for in situ degradation study. Special rigid feedthroughs have already been obtained and preliminary plans have been drawn concerning the use of coating specimen, vacuum chamber (G.E.) and an electrometer.

Coatings R&D

A chart was prepared by our group in which we have gathered information showing the vehicle, pigmentation and manufacturer of various paints in use by R. Sheehy's applications group. This is included as Appendix I.

Our group prepared a white paint (coded P in the Boeing series and B-1 at GSFC) which utilizes an additional type of methyl silicone from Dow Corning and a silica corticated type of rutile TiO_2 pigment manufactured by Dupont. Our examination and an x report by Joseph Haynos of GSFC (X-716-65-369), on unpigmented adhesives for solar cells, confirms that this coating, P, is superior to most pigmented methyl silicones in use at GSFC in that it possesses greater film integrity and toughness as well as the least shrinkage. This last characteristic is important particularly as loss of adhesion, under certain conditions, could occur due to poor shrinkage characteristics. To date the coating has demonstrated excellent temperature resistance. Shrinkage and optical discoloration (in the visible spectrum) have not taken place while in a vacuum oven set at 220-230°F for a period of 64 hours. We have also immersed one coating specimen briefly (approximately 30 seconds) in liquid nitrogen with no harmful effects, however, much investigation must take place in this area prior to any certification. The coating, because of its relatively tough, glasslike surface can more easily be cleansed than most other pigmented methyl silicones. An important aspect concerning this coating is that it can be cured by air drying. Data sheets produced by Dow Corning claim 48 hours, however, an additional 30 minutes at a low temperature, 150°F, is sufficient to insure a full cure and thereby avoidance of volatile matter as well as the achievement of optimum in physical properties. We have forwarded the specimens with utmost haste to Boeing for testing but it may be some time before results can be derived from that source. We have, also, some 3 weeks ago, modified a P specimen so as to be suitable for ultraviolet irradiance and in situ measurement. This specimen was forwarded to EMR for inclusion in one of the planned degradation tests. They have not carried out this test to date.

We have, however, with our efforts initiated a program with F. Gordon's (Jules Hirschfield) whereby many of our white coatings (P included) will be exposed in vacuum to a 400 kev electron source. However, optical measurements will be taken in air some time (perhaps 5-10 minutes) after irradiation so that annealing will probably take place.

Black coatings for shrouds in vacuum chambers are for the most part either alkyds, thermosetting type polyesters or epoxies pigmented with carbon black. These paints are used mostly because of their convenience, their jet black optical properties (absorptances of 95-98%) etc. However, they also have serious drawbacks such as; only fair resistance to ultra-violet (fair when

temperatures together with slight vacuum (vacuum oven). We have therefore selected the white coatings in the Boeing Project together with a vacuum deposited aluminum coating undercoated with a thermo-setting lacquer much in use at GSFC. C. Nicoletta, who is monitoring the test, placed the coatings in a desiccator and weighed them periodically over a period of several days (laboratory Mettler balance - to 4th place) to weight constancy. The specimens were then subjected to the vacuum oven. The work is still in progress.

Our group has already initiated in this period a program that may lead to the development of inexpensive, convenient large area, thin section thermocouples for use as paint substrates in our coatings degradation work. We are at present in a stage of accumulating suitable material and hope to have a prototype ready for testing by December 19, 1966.

Thermal shock experiment - the test was brought to our attention in the early part of this year and a project was initiated by our group in May of this year to expose the Boeing specimens A through M (excluding D, E and F) because of possible cross contamination) to this environment. We found ourselves blocked from facilities, labor availability and space in our area and therefore approached the T&E Division with an informal written proposal outlining our goals, purpose etc. requesting their cooperation and aid (facilities, etc.) to carry this program to a conclusion. To date we have with their kind cooperation obtained some concomittant exposure to ultra-violet/vacuum/thermal shock for our coatings specimens. We are presently stalled at T&E as regards this experiment due to a lack of priority. We have communicated this problem to Branch Management via conferences and the attached written report. It appears that little additional headway, in spite of all our efforts, can be made without support from this latter area. Please see attached report.

CONCLUSIONS AND RECOMMENDATIONS

We have pointed out that equipment designed to be used as tools for coatings degradation studies have been ordered and will be arriving shortly. This equipment includes "clean" vacuum systems, chambers equipped with push-pull feedthroughs, etc. We would also point out that little or no space exists for their accommodation. Also we feel improvement or progress should be made towards intersectional communication as well as support for vital degradation study efforts. In our memo to Mr. Schach dated 10/14/66 we pointed out specifically the steps we feel to be essential in achieving a fundamental and meaningful Quality Control effort as concerns thermal coatings.

compared to some metals and some ceramics) and are fair at best to extremes in temperature. Some possess only fair mar and scratch resistance while others such as the black alkali silicates after a period of time simply lose adhesion in certain areas (C. Duncan's G.E. Vacuum Chamber) and fall into the chamber.

This problem has interested our group and we are progressing in our attempt to achieve a black metallic oxide (Titanium Oxide) coating that will answer some or all of the above objections or problems. To date a preliminary "run" has shown excellent results. We have immersed the coating, which is .010" thick on a steel substrate into liquid nitrogen, exposed it to Hg-Xe light source for a minimum of 2 uv solar constants (below 400 ma) for a period of 3 weeks with no change in either the integrated absorptance (90.2%) or it's adhesion to the substrate. We have already pointed out that it will withstand great extremes in temperature and it is obviously superior to paints as regards mar and scratch resistance. Also, it appears that it is possible to conveniently repair areas that might be damaged, but this appears remote in view of the great toughness and strength of the coating. We have forwarded a specimen on a copper block some 4 weeks ago to EMR and hope to obtain an emissivity soon. I have been informed that the equipment to spray this material is on base.

Mr. M. Schach initiated, with C. Duncan and W. Gdula of EMR (using F. Gordon's Radiation Effects Group) a project to expose, with the lowest, uniform electron energy level available, the Boeing specimens in air. Our group was to coordinate the supply of these coatings between the groups doing the degradation work and that performing the measurement. This effort was needed, it was thought, to minimize the effect of annealing. The test showed that under the above conditions (and 400 kev electrons and a total integrated dose of 5×10^{15} p/cm^2) no changes could be measured optically. We believe that constant annealing due air exposure as well as energy absorptance within the bulk (and not at the surface) may have been responsible for the lack of optically detectable surface change. Our group has therefore initiated, and work is in progress with J. Hirschfield, a program to irradiate some of our white coatings in vacuum (10^{-6} torr) at a 400 kev electron level for a total integrated dosage of approximately 10^{15} p/cm^2. It should be noted that lack of a Faraday probe makes the determination inexact but the inaccuracy is between 15-20% and does not destroy the purpose of the test. However, in many cases the lack of an in situ optical measurement may prove misleading as regards degradation (no change).

Please see photo showing an alkali silicate paint prior to and after electron exposure.

Our group also initiated in this period a test to investigate the possible evaluation of volatiles emanating under the influence of a range of elevated

We are also concerned with the length of time taken by Boeing as regards their part in degradation studies (NASA contract #NAS-5-9650) and we are keeping a watchful eye on that situation. Please find enclosed R. Brown's* work statement given to us on his visit to our installation on 11/21/66.

It appears decidedly risky to use materials such as black alkali silicates for use as shroud coatings without further development and more testing. Also, where the cleansing or treatment of metallic or other surfaces appears limited adhesion of the white silicate paints to the various substrates would be highly suspect.

We have prepared a white thermal control coating that uses a vehicle deemed superior from various physical properties standpoints to the RTV 602 (G.E. product) and some other white pigmented methyl silicones in use by R. Sheehy's group today.

We strongly recommend that the suggestions we made and incorporated in a request for a meaningful Q.C. effort be adopted (see memo to Mr. Schach dated 10/14/66).

We recommend that prior to the usage of a new paint or coating by another section within our Branch that our group be notified and consulted.

We also urge that degradation work be more centralized in the future in order to conserve funds, space, equipment and the most efficient usage of manpower.

*Mr. Brown is chief project man for Boeing as regards above contract.

5. BOEING WORK STATEMENT

PREPARATION OF CETC FOR COMBINED EFFECTS TESTS

I. Vacuum System

A. Under Vacuum

1. U.V. bake out
2. Check out of pressure at 10 U.V. sun rate
3. Influence of wheel and wall temperature
4. Design improvements for wall temperature
5. Design improvements on the booster system

B. Open to Air

1. Modify the booster pump system
2. Thorough cleaning of the chamber
3. Improve the wall temperature

C. Back under Vacuum

1. Test sustained (50 hr.) vacuum at 10 U.V. sun rate

II. Temperature Control System

A. Under Vacuum

1. Temperature control (-70°C, -40°C, 10°C, 60°C, 100°C) undecided on coolant to be used
2. Ability to rapidly compensate for U.V. lamp temperature rise

B. Open to Air

1. Improve coolant system

C. Back under Vacuum

1. Control temperature at -70°C for sustained run

2. Determine energies 10 kev to 100 kev
3. Map electron scattering

V. In situ Reflectance

A. Under Vacuum

1. Analysis preliminary calibration data
2. Plan and prepare for system checkout (calibration and indexing)

B. Open to Air

1. Check out possible mirror degradation
2. Calibrate against NBS standards (vitrolite)
3. Check out indexing procedure
4. Determine time to align and measure samples
5. Establish measurement test plan (scans and range)

C. Back under Vacuum

1. Air vs vacuum measurements (Al and Paint)
2. Measurements for the contamination test

VI. Contamination Test

A. Under Vacuum

1. Consider potential problems
   a. Self contain
   b. X contain
   c. Troubles w/or 80 0 contains of or 80 in sphere by warm specimens

B. In Air

1. Improve wall cooling

C. Back under Vacuum

1. Al + Paint samples together vs Al separately under long term vacuum at -70°C
2. Test of Al + Paint samples together vs Al separately under 8 hours of U.V. at -70°C and 8 hours U.V. at +90°C (use baffled control as well)

III. Ultraviolet

A. Under Vacuum

1. Determine lamp switching time
2. U.V. bake out and vacuum check
3. U.V. mapping with photodiode

B. Open to Air

1. Radiometer remapping of U.V. to determine possible lamp degradation
2. Replacement of lamps if necessary and remap
3. Install U.V. baffles and hour meters

C. Back under Vacuum

1. Photodiode mapping
2. Vacuum tests for cross contamination

D. In Air Again

1. Radiometer recheck of the lamps

IV. Electrons

A. Under Vacuum

1. Determine beam alignment
2. Check focus adjust
3. Check voltage range
4. Check monitoring system
5. Bias cup to observe spot on quartz
6. Design electron deflection plates and Helmholtz coils for field compensation
7. Prepare particle detector (calibrate) and fabricate its mount

B. Open to Air

1. Map the magnetic field in the chamber
2. Adjust the compensating field coils
3. Mount the particle detector
4. Provide bucking voltage

C. Back under Vacuum

1. Align the beam with deflection plates

6. THERMAL CONTROL COATINGS—THERMAL SHOCK EXPERIMENT

ABSTRACT

This test which began 5/25/66 and compiled a total of 79 hours of concomitant electromagnetic radiation (approximately 1 solar constant) and 264 hours of cryogenic temp./vacuum* failed to show loss of adhesion on the 15/16" diameter coated specimens. Significant temperature rises due to degradation have also failed to appear to date. This test was carried out with the aid and facilities of the T&E Division.** We had hoped to continue the test but a priority is needed at present in T&E to conclude this work. The matter has been brought to the attention of the Branch Coordinator and Branch Management, in general, some weeks ago.

*Genarco Carbon Arc.

**We are indebted to W. Peterson, K. Rosette, F. Cuzzolina, H. Sipe of T&E for their aid.

D. Back to Air

1. Immediately check vacuum vs air readings as a function of time

VII. Sample Preparation

A. Under Vacuum (Now)

1. "Mic" the samples
2. Remove strippable coating sample type L
3. Complete cover plate design (thermal contact)
4. Complete cover plate fabrication

B. In Air

1. Install cover plates
2. Mount preliminary test samples
3. Determine data readout for computer analysis
4. Measure all samples in air (pre-irradiation)

PURPOSE

To investigate physical properties such as adhesion, film integrity, vacuum/UV/thermal shock resistance of various coatings in usage at GSFC (Boeing specimens A through M, excluding alkali silicate paints).

Prior to the initiation of this project by this group little information pertaining to this area existed as a GSFC effort. It was deemed necessary to obtain this information in view of the fact that many of these coatings had been and were being used on satellites for passive thermal control on near space efforts.

DISCUSSION

Our group issued an informal written proposal to the cognizant branch personnel at T&E, requesting the use of certain facilities and their cooperation in carrying out a thermal shock experiment concerning some thermal control coatings in use at GSFC (coatings frequently used on satellites at GSFC such as; IMP, OGO, etc.). It was necessary for us to approach T&E on the matter due to a lack of available facilities, equipment and support to carry out or even initiate this test in a reasonable amount of time.

The Coatings Quality Assurance group upon receipt of T&E approval immediately planned; fabricated and executed most of the work necessary to have the test array ready for insertion into a designated T&E vacuum chamber on schedule. Table 1 lists the samples used in this work.

Test Set-Up and Operating Procedure

The ultimate of irradiance is shown in Figure 2. The specimens rest securely on 3 extremely small vycor glass detents with a .010" (cross sectional area) copper-constant on thermocouple cemented to the aluminum surface of the specimen.* (See Figure 1). A statistical quantity of 3 specimens per coating tape was selected because of the array geometry. The temperature data was fed to Data Control and temperature readings were recorded every 5 minutes along with graphical data on some white paints. Figure 3 represents some of these. In addition each specimen was photographed prior to test under magnification as an additional diagnostic tool. The Genarco

*Leafing aluminum powder stirred into various epoxy cements recommended for vacuum use.

carbon arc was set so as to achieve an average of 1 solar constant. A uniformity scan was used to verify this last factor. The shroud, towards which the specimens radiated their heat, was set at -100°C by a combination of LN_2 vapor and liquid. Controls were set to maintain this shroud temperature. The average vacuum (diffusion pump) was approximately 10^{-7} torr with the carbon arc on for 1/2 hour and off for 1 hour. The first half of the test was accomplished using an 8 hour day. During the remaining 16 hours per day only vacuum was maintained. The last part of the test was run "around the clock." Table 2 shows some of the temperatures experienced by the samples.

CONCLUSION

It can readily be seen that the temperature ranges are severe, as they are meant to be, in order to accelerate changes in physical properties. Changes of sufficient magnitude make it easy to check different aspects of these physical changes such as; adhesion, discoloration (optical degradation). To date neither loss in adhesion nor optical degradation have been rated. However, we may not expect more since our exposure time has been limited. Annealing may have taken place as well since the test was interrupted and the array has been outside the chamber more often than inside it.

Table 1

Series of Coatings for Testing as a Joint Effort Between Thermal Systems and T&E

(a)	105 - 107.	Epoxy white substrate with methyl silicone/TiO_2 top coat.
(b)	105 - 107.	Primed Al substrate top coat, S-13 methyl silicone.
(c)	105 - 107.	Epoxy white substrate; methyl silicone/zinc oxide.
(g)	105 - 107.	Vacuum deposited Al oxide on buffed Al.
(h)	105 - 107.	Vacuum deposited SiO_2 on buffed Al.
(i)	105 - 107.	Leafing Al paint.
(j)	105 - 107.	Vacuum deposited Al on lacquer substrate.
(k)	105 - 107.	Buffed Al
(l)	72 - 74.	Epoxy white substrate/methyl silicone TiO_2 (heavier than Al)
LS	105 - 107.	Same as L except that strippable had been applied.
(m)	172 - 174.	S13G methyl silicone.

Table 2

Boeing Code		5/26/66 Start of Test °C °C	6/15/66 °C
A	Epoxy white subtrate, TiO_2/ methyl silicone Q92-0090	91.87(112.34)108.67	93.76(115.39)110.14
B	S-13	68.62(63.64)54.54	68.39(65.96)51.34
C	Q92-016 Dow Corning	64.79(68.85)78.01	51.93(60.51)76.40
G	Haas Coating	108.15(94.60)82.53	106.26(87.67)65.50
H	Vac. depos. SiO_2 (GSFC)	69.67(68.85)79.06	55.06(57.37)68.39
I	Leafing Al/phenylated silicone (NRL)	126(116.65)110.25	133.03(101.95)93.87
J	Vac Deposits Al on Logo lacquer	99.21(105.20)99.32	78.01(85.04)81.68
K	Buffed Aluminum at GSFC	173.45(150.04)129.25	158.29(136.28)107.62
L	Epoxy white substrate as per spec. A Q92-0090 but thicker than Spec. A	105(105.20)108.98	113.07(107.09)120.32
L_s	Same as L but strippable treat.	106.89(89.04)78.48	120.43(105.53)91.35
M	S-13G	52.04(56.45)57.37	47.53(55.06)48.45

APPENDIX I

DESCRIPTION OF THERMAL CONTROL COATINGS

Manufacturer	Product Name	Vehicle	Pigment	Remarks
DOW Corning	Q 92-0090	Condensation type Methyl Silicone—evolves acetic acid	Anatose TiO_2 - Titanox AMO	Pigmentation approx. 40% of total solids
DOW Corning	Q 92-016	Condensation type Methyl Silicone supposedly an oxime	NJ Zinc's SP 500	Experimental we understand from Sheehy's group that it cannot be obtained
DOW Corning	Q 92-007	Condensation type Methyl Silicone Oxime	Rutile TiO_2 Titanox RANC	Pigmented to 48% of total solids. Rutile TiO_2 made from sulfate process.
GSFC	Joe Colony's	Condensation type of Methyl Silicone with use of solid amine at 130°C. Vehicle is Gen. Elect. RTV 602.	Rutile TiO_2 R960-Dupont	Pigmented 2 parts pigment 1 part vehicle TiO_2 made from chloride process & is silica corticated. Fair to good film integrity. The same for adhesion.
IITRI (Zerlaut)	Z-93	Potassium silicate an alkali silicate of an electronic grade made by Sylvania Electric - PS-7	NJ Zinc's SP 500	Pigment incorp. 1.5 or 2 to 1 vehicle
Minn. Mining (3M)	Velvet Black & White White = 401-A-10 Black = 401-C-10	A polyester type thermoset therefore cannot be linear type, (thermoplastic)	White paint utilizes - Rutile TiO_2 & spherical glass beads. Black utilizes carbon black & spherical glass beads.	2 part system. Utilizes cellosolve acetate & xylol for solvent 65% total solids after conversion, spherical glass beading 60% of total volume based on dry paint .3 pts paint/1 pt catalyst.

Manufacturer	Product Name	Vehicle	Pigment	Remarks
Finch & Co.	Cat-a-Lac white	A one package epoxy—We understand heat unnecessary for conversion	probably TiO_2	
GSFC B-1	B. Seidenberg & A. J. Hobbs	An optically clear methyl silicon. An additional type polymer. Vehicle is DOW Corning XR 6-3488. Will cure at room temp. 48 hrs. or with nominal heat (150°F) for 30 min.	Rutile TiO_2 R-960-Dupont	Pigmented 1.5 parts TiO_2/1 part vehicle. High gloss surface. Good film integrity. Good adhesion.
IITRI (Zerlaut)	S-13	A condensation type methyl silicone oxime? Uses a GE catalyst & GE primer SS 4044 catalyst is alkaline	N.J. Zinc's SP 500	Appearance varies from gloss to dull flat appearance. Adhesion can be extremely poor if not properly primed. Cures at room temp. but some temp. may be needed to drive off solvent poor film integrity.
IITRI (Zerlaut)	S-13G	A condensation type methyl silicone oxime? Uses a GE catalyst & GE primer SS 4044 catalyst is alkaline	N.J. Zinc's SP 500	Uses a small percentage of an alkali silicate like pot. silicate Sylvania PS-7 no shelf stability

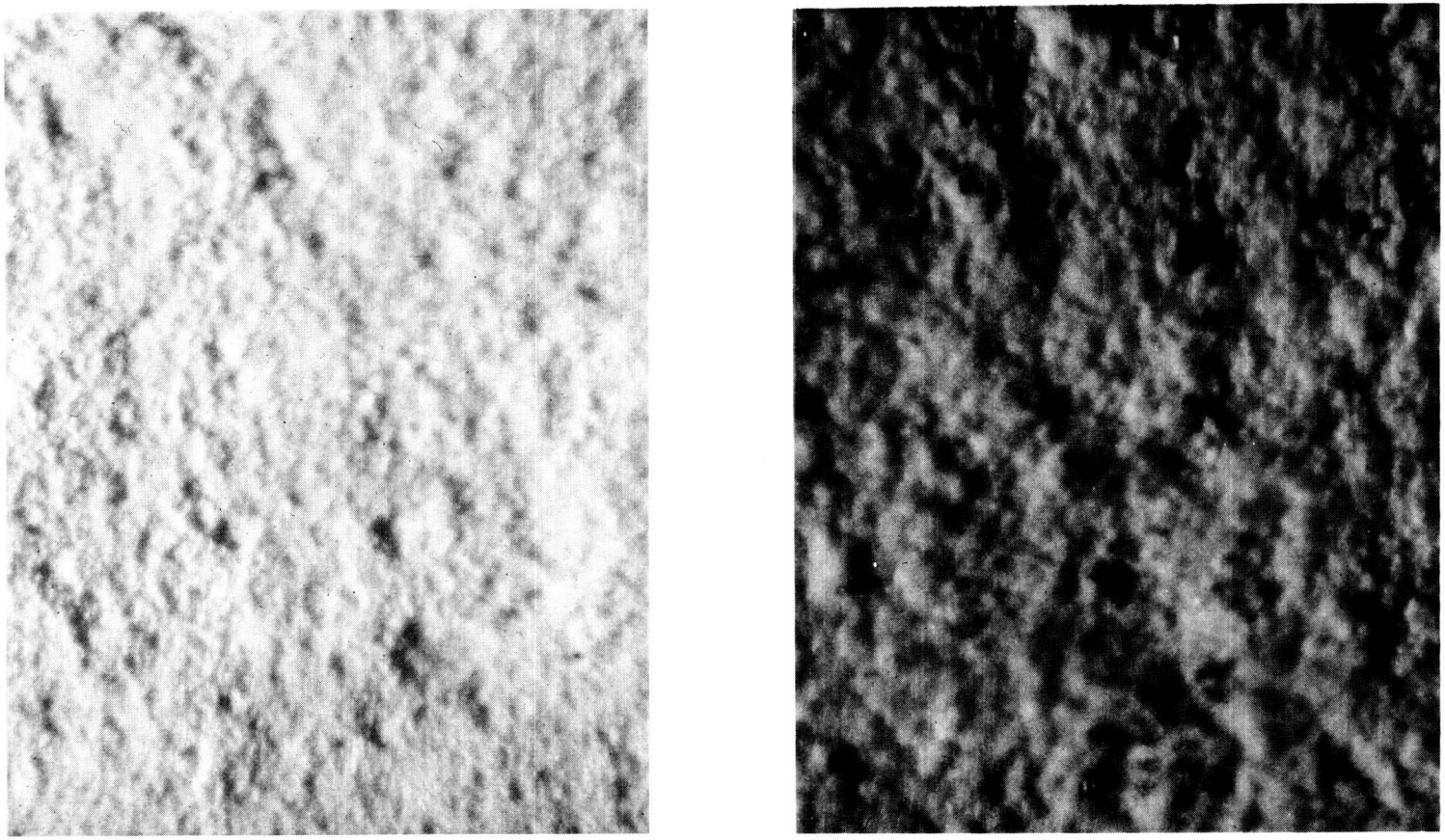

Not Irradiated

Irradiated $E_3 72$

Figure 1. Paint Samples Exposed to 400 kev Electrons

SOLAR INTENSITY DISTRIBUTION

USE INK

Date 8.8.66 Before / After

Hour 1000 J.O. (PROGRAM) T.A.R.

Taken by BAKER Distance CENTER CHAMBER DIA 12"

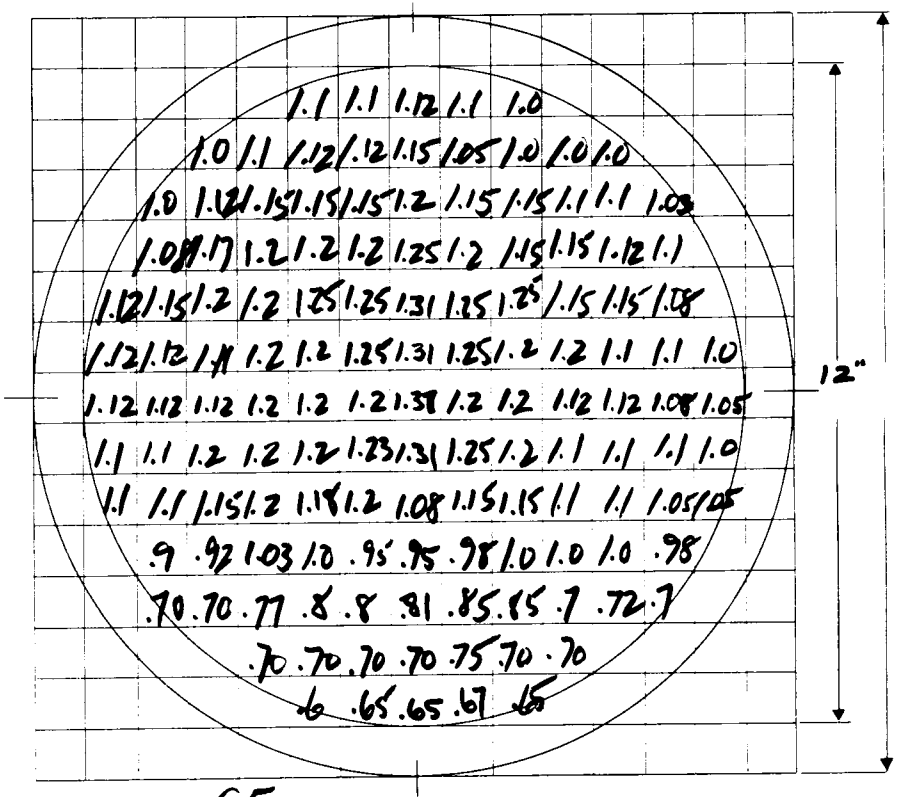

Focus Adjustments

L. H. ———

R. H. ———

Detector Used GE

Temperature AMBIENT

Chopped ———

Average Value = ——— ÷ ——— (TOTAL MV) (NO POINTS)

= ——— MV ——— S.C.

320-92 A (11/64)

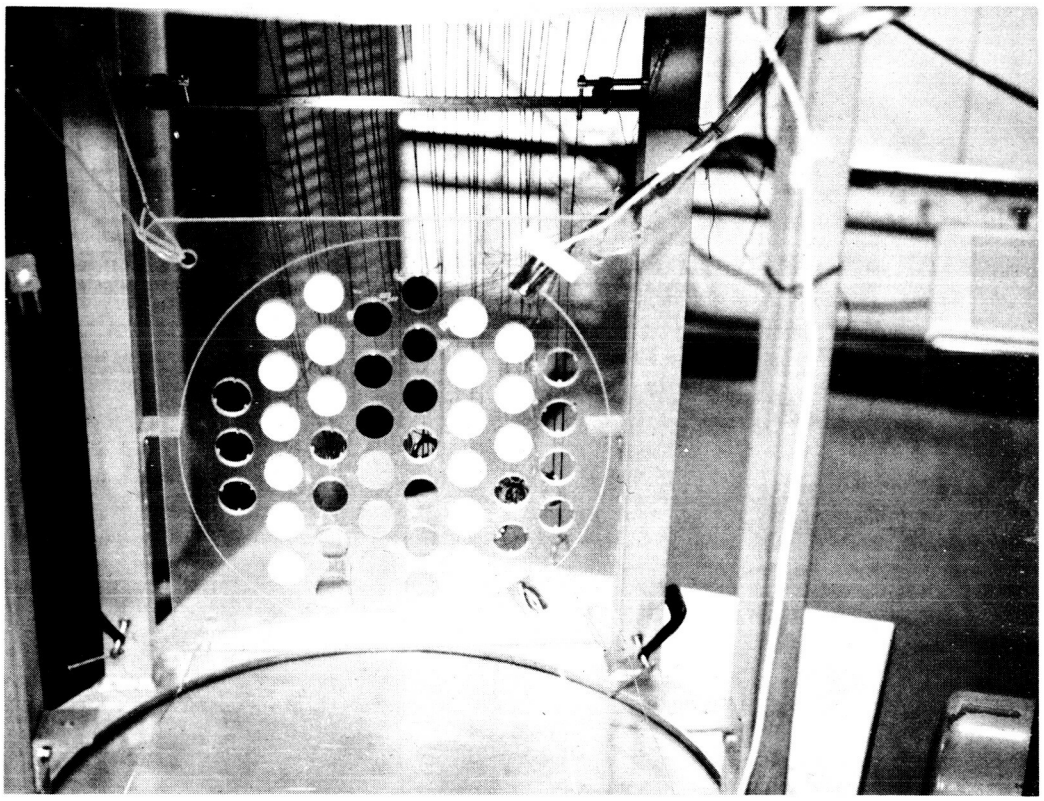

Figure 3. Thermal Shock Array

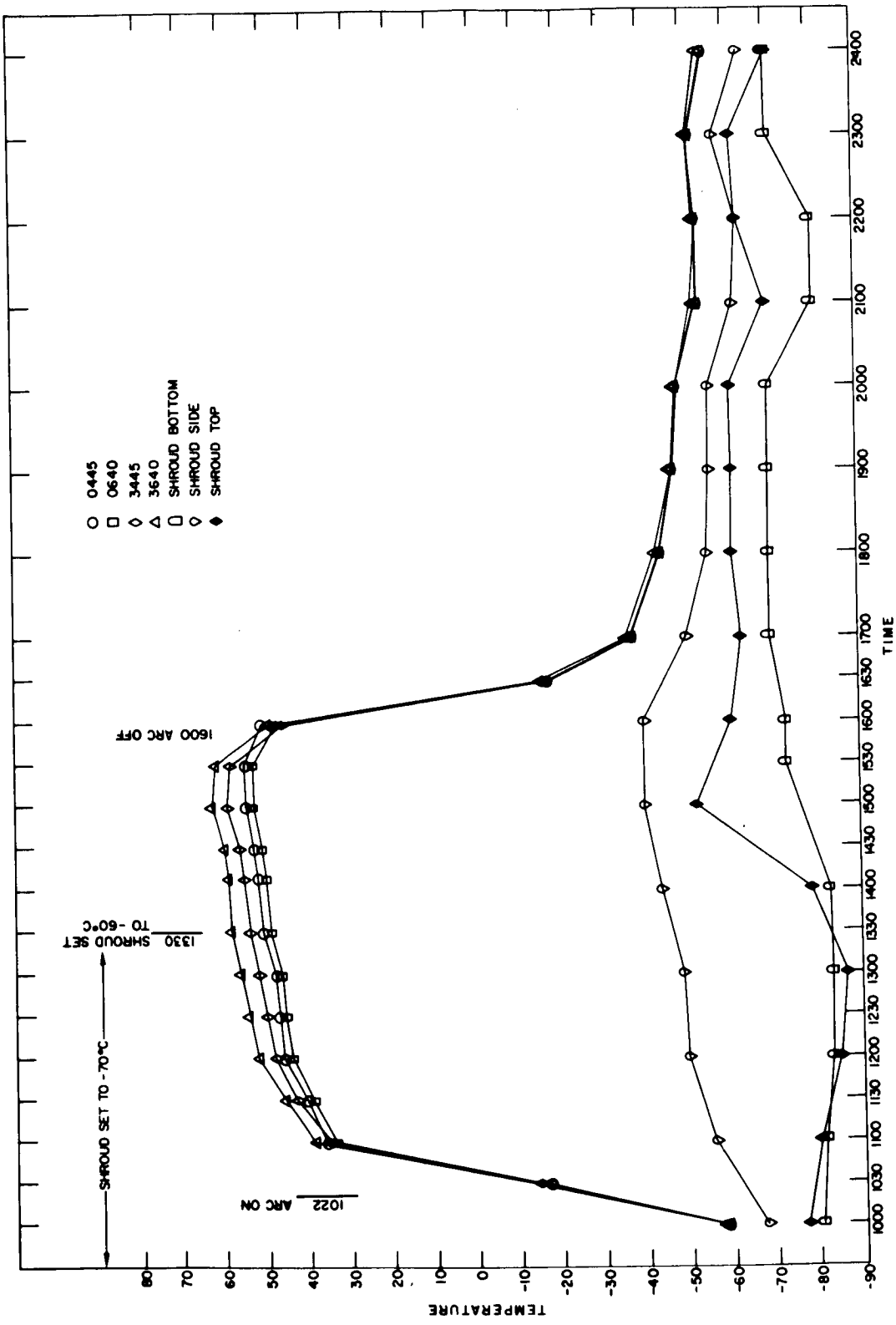

Figure 4. Temperature-Time Curve

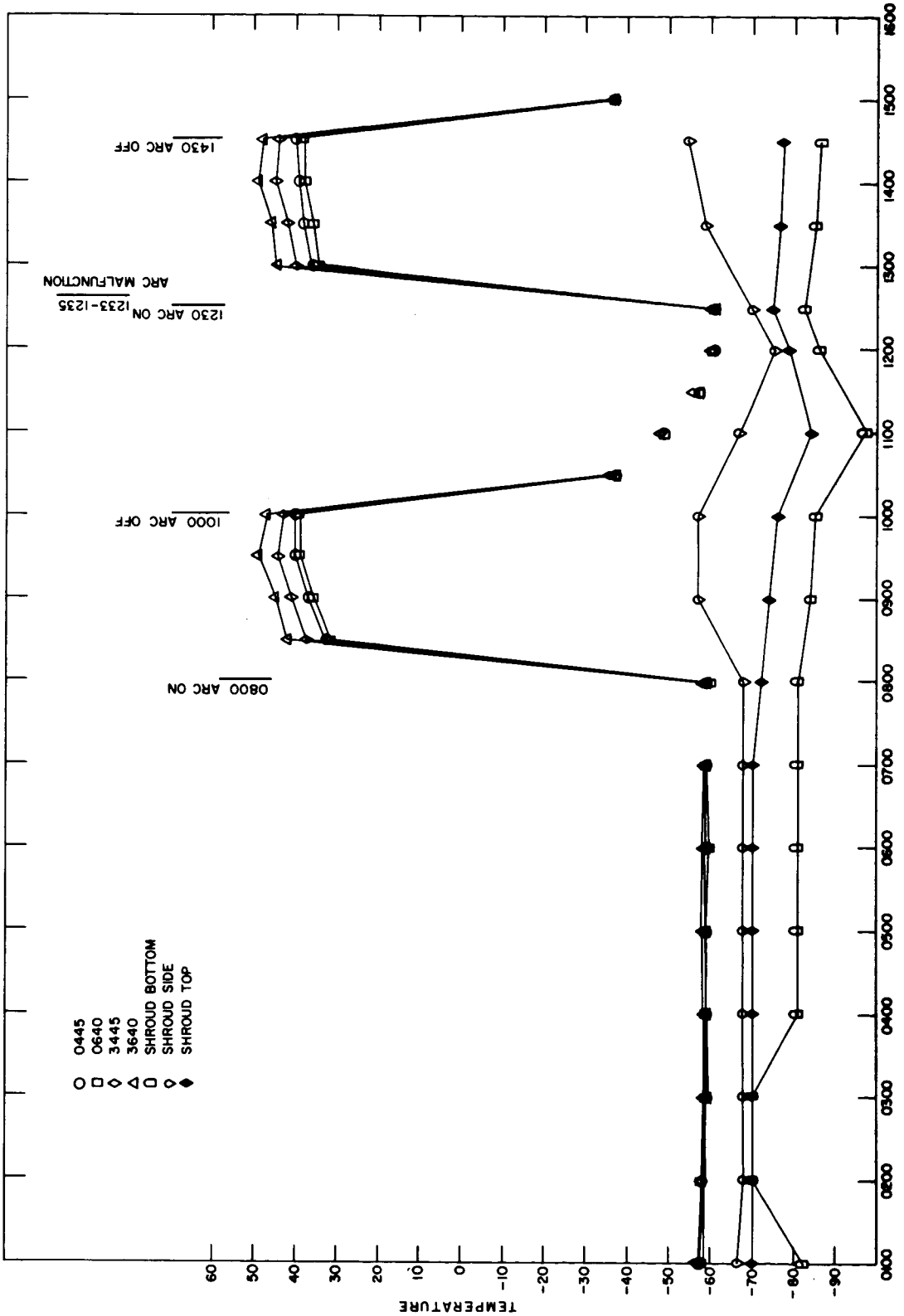

Figure 5. Temperature-Time Curve

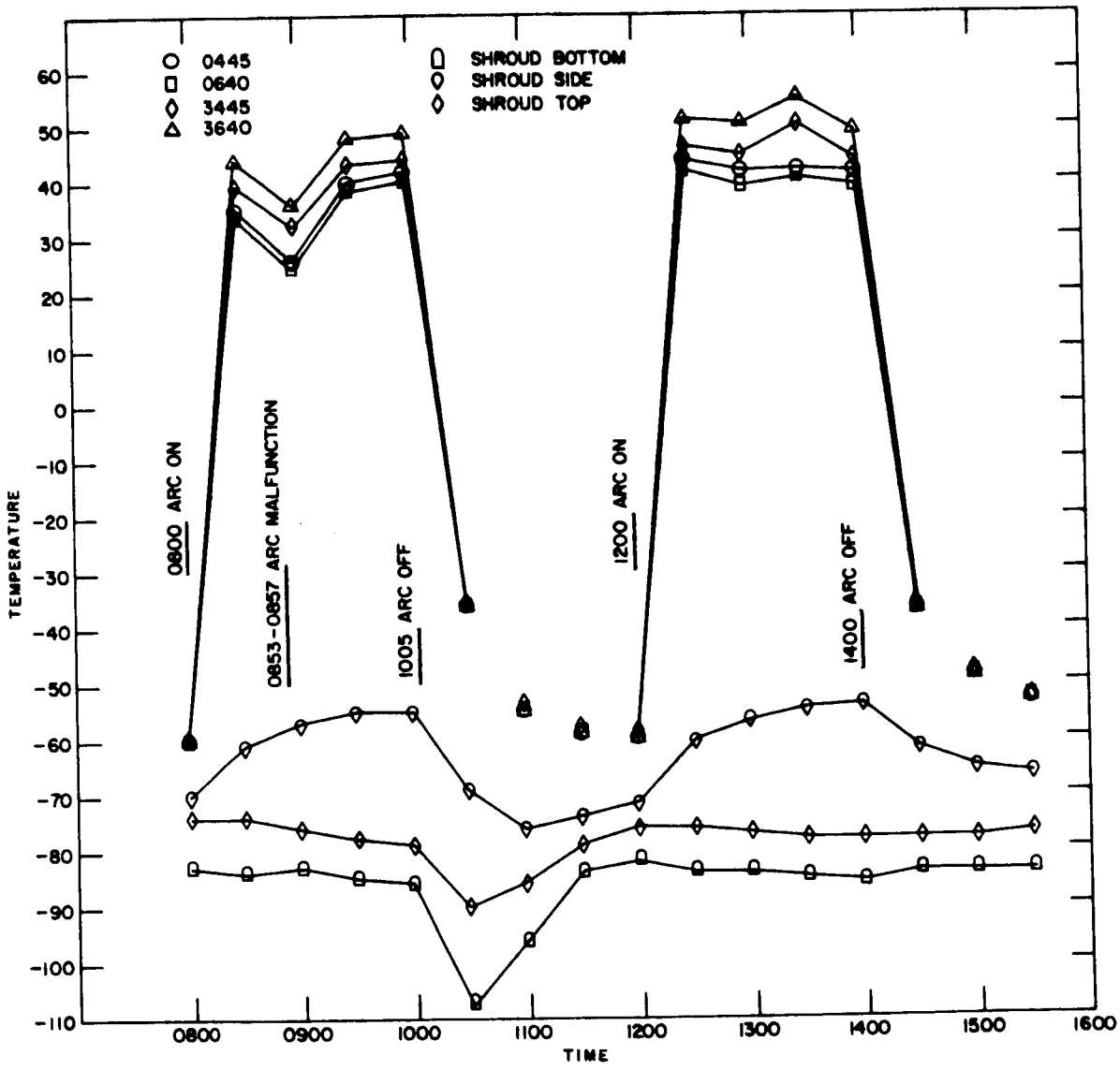

Figure 6. Temperature-Time Curve

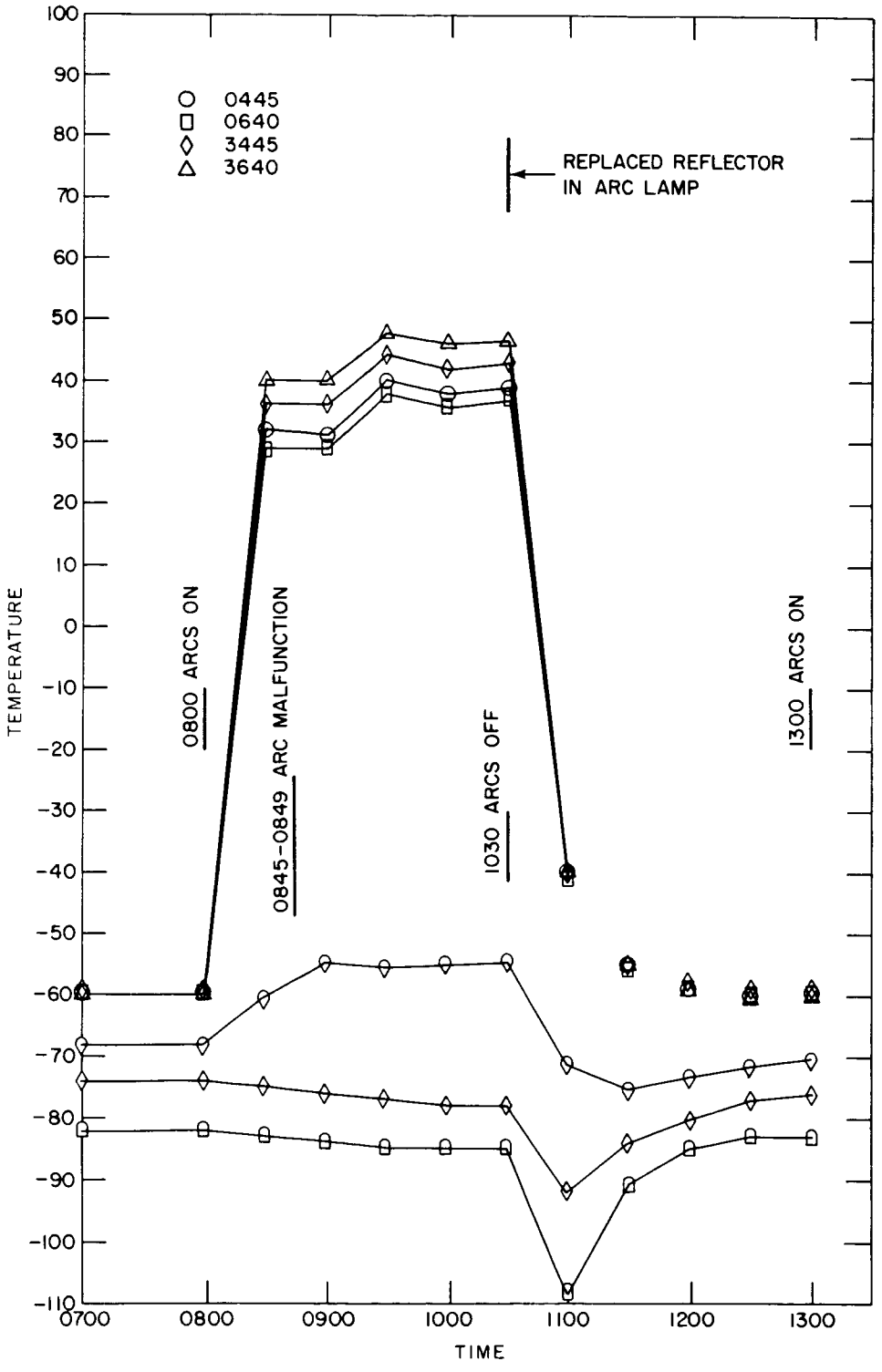

Figure 7. Temperature-Time Curve

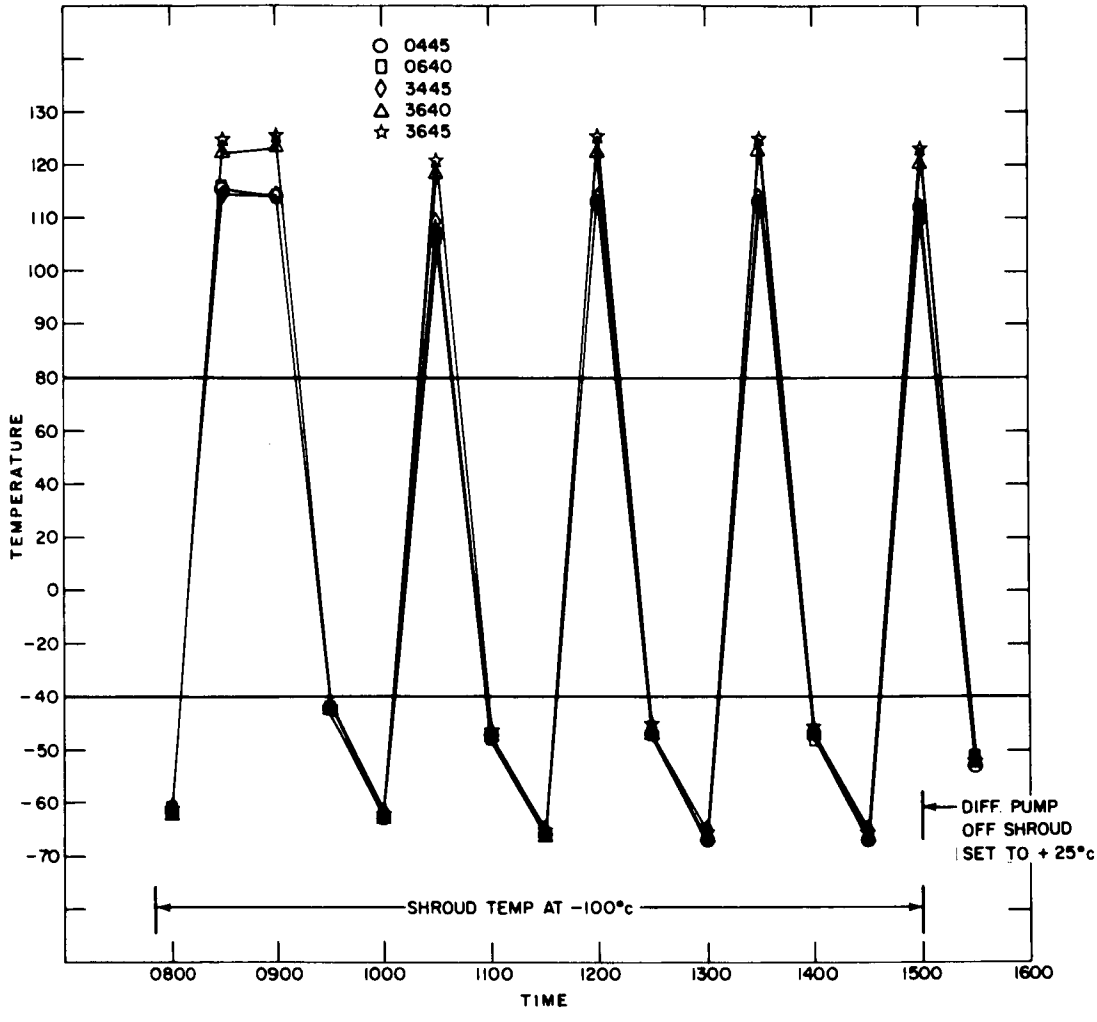

Figure 8. Temperature-Time Curve

PART II

Section 1

THERMAL LABORATORY REPORT

Contract No. NAS 5-9244

Prepared By

M. Lillywhite
Electro-Mechanical Research, Inc.
5012 College Avenue
College Park, Maryland

Work Performed By

K. Kishinchand
O. Olesen
Dan Lester
M. Goldenberg
G. Enos
L. Hallman

CONTENTS

ILLUSTRATIONS

TABLES

APPENDICES

3 THERMAL LABORATORY REPORT 6

6 M. Lillywhite 8

ABSTRACT

Recent developments in solar simulation techniques are discussed. These developments include uniformity filtering, spectral filtering, and improved spectral matching using krypton and xenon lamps. The problems involved in using these components are discussed along with the consequent modifications necessary to the A 1200 solar simulator. Early results are presented from a study that evaluates solar simulation anomalies experienced when different sources and techniques are used. Spectral irradiance data of various sources are given and coatings degradation data using these different sources are compared. The general problem of maintaining the spectral and total irradiance of a solar simulation system during coatings testing is discussed.

INTRODUCTION

This document reports on the activities of the thermal laboratory starting November, 1965. The emphasis will be concentrated on results obtained after September 1, 1966, and only a general discussion of work performed before this date will be given. The principal effort has been concentrated on solar simulation research and development. Much of this effort has been devoted to the study of some solar simulation anomalies which are manifested in coating degradation testing. This anomalies study has as its principal interest the determination of the type and magnitude of errors that are involved when data obtained from different types of solar simulation testing are compared. The test planning and presentation of the data were both designed to study primarily the solar simulation problems, not coatings problems. These data may still be used to evaluate the specific coatings if the evaluation is made with discretion.

The solar simulation research and development work has been concerned with developing optical components (e.g., uniformity filters, aluminum surfaces and lamps) that were temporally stable, and, more recently, modifications of existing A1200 solar simulator for one-to-two solar constant irradiance operation when these new optical components are employed. The problem faced by this laboratory at present probably represents a new phase of development in the solar environmental field; i.e., maintaining the performance of a given simulation system for a reasonable length of testing time. This is more difficult to control as simulation requirements become more demanding. The requirements themselves depend greatly on the material being tested and intended accuracy and use of data obtained. Sufficient criteria is not available to determine conclusively the requirements that should be imposed for all types of solar simulation tests; however, early work indicates a solar simulated environment differing from outer space conditions can cause large errors in test results. The new phase of solar simulation development should be concerned with determining system performance limits for various types of materials now being tested and for systems presently being used. These limits should be used as design criteria for future systems.

The solar simulation anomalies studies (coating degradation testing) represents some early work done in studying this problem. The immediate concern was to evaluate the various sources used by the Thermal Systems Branch, GSFC, for thermal testing and coatings degradation work. This has been done in terms of the temporal stability of various systems and changes in absorptance of coatings (e.g., white paints) resulting from different spectral irradiance and the temporal characteristics of the systems used. The results represent a preliminary effort from which precise conclusions should not be drawn, but, nevertheless, they yield quite clear data for comparison of absorptance changes resulting from the

use of different sources. If accurate solar simulation testing, particularly coatings degradation testing, is to yield meaningful data, a close match of the solar environment must be obtained.

SOLAR SIMULATION RESEARCH AND DEVELOPMENT HARDWARE

The optical components in the A1200 solar simulation systems that have been of greatest concern during the past year are: (1) uniformity filters, (2) aluminum surfaces, (3) lamps, and (4) spectral filters. The uniformity filters used in the A1200 solar simulator have gone through three general stages of development. The outcome of each of these stages in terms of ultimate uniformity attainable in the test volume can be seen in Figures 1 through 3. The first and most basic step was developing a technique to fabricate one large filter (8" diameter) to be employed in the single lens system originally used with the A1200 solar simulator. A simple vacuum coating process using platinum was developed and the results can be seen in Figure 1. The lenticular system was installed and did not improve the inherent uniformity as expected (See Figure 2). This was due to poor design of the lenticular array which limited the collection efficiency and uniformity. It was necessary to extend the techniques of prescribing and fabricating the filters to obtain a smaller and more sophisticated filter to perform in the lenticule system. This was accomplished in two steps: (1) prescribing filters for each of seven lenticules, each filtering for uniformity of that one lenticule, and (2) prescribing one filter for one lenticule that compensates for the nonuniformity of all the lenticules. The approach described in (1) above was successful and the results are shown in Figure 3; however, the use of up to seven quartz blanks reduces the efficiency of the system and taxes the electronic and thermal capability of the system when one solar constant total irradiance is required. For this reason the attempt described in (2) was made. This represents our most successful attempt in uniformity and efficiency (see Figure 4). A uniformity filter of this type also compensates for any imperfections in the optical elements. If a lenticular system with a different design was being used such filtering might not be necessary, but in order to obtain desired uniformity with the existing system filtering was required. As a result a stable neutral density filter of variable transmission which is stable under high irradiance is now used.

Maintaining reflectance characteristics of the aluminum surfaces is a continuing problem that contributes to more than half of the long term temporal variation in the ultraviolet portion of the spectra of the A1200 solar simulator.

Tests have been conducted to study degradation that occurs over a period of time and the portion of this degradation resulting from changes in the aluminum surfaces. It is difficult to discriminate between lamp and mirror surface degradation in this system, but enough is known about the type of lamps used and the test environment to allow compilation of Table 1. This table shows the spectral irradiance of the X-25L solar simulator as it degrades through normal use over a 310 hour period. This change is attributed almost entirely to the aluminum surface degradation. The spectral irradiance curves of runs M-21, M-22 and M-25 are shown in Figures 4A, 4B, 4C, 4D. Table 2 shows how such degradation can change the effective absorptance and therefore the equilibrium temperatures (during thermal testing) of some commonly used coatings. Degradation of this type probably occurs in the A1200 solar simulator. A test to check this has not been conducted; however, this type of degradation is inherent, to some degree, in all solar simulation systems.

The approach taken to resolve this problem has been to minimize the rate of degradation. Several approaches are being tried. Among these, and perhaps the most promising, is to lower the temperature of the aluminum substrate. Also, covering the aluminum surface with SiO_x has been tried. The problems of contamination from atmospheric debris and high temperature resulting in burning holes in the surfaces seem to be the most severe because these surfaces are used at atmospheric pressure. A satisfactory solution has yet to be developed.

The spectral filters used in both the A1200 and the X-25L systems have been checked for degradation during the past six months. The filters have accumulated approximately 1000 hours under normal test conditions and show no change in transmission characteristics. Figures 5 and 6 show the transmission curves of filters from both systems at zero hours and $\approx$1000 hours. The discrepancy seen in Figure 6 results from using a different instrument to measure transmission in each case. Results of attempts to obtain a spectral match in the A1200 solar simulator using different numbers of these filters on xenon lamps are shown in Figures 7 and 8.

The A1200 solar simulator was designed to operate at 2.5kw per module for as many as nineteen modules or about 50kw total power. The desired total irradiance in the test volume of the original system could be achieved by choosing the proper number of modules and making slight power input adjustment on the console. The efficiency (irradiant output/electrical input) of the system was $\approx$9.5% with the original single lens optical system and could obtain one solar constant with twelve lamps. The introduction of the lenticular system, the necessary uniformity filters (25 to 40% filtration), and the spectral filters ($\approx$35% filtration), reduces the efficiency of the system to $\approx$3%, requiring operation at an "overload" condition to obtain one solar constant total irradiance. This loss is

Table 1

Spectral Irradiance—Ratio of X-25L to Solar Energy
for Various Stages of Degradation

Wavelength	New lamp and Collector— 0 hours	New lamp and Collector— 45 hours	New lamp and Collector— 95 hours	New lamp and Collector— 310 hours	New Collector and Al surface and clean optics-old lamp 0 hours	Dirty optics and old lamp	Cleaned optics and new lamp
	M-21	M-22	M-23	M-25	M-27	M-12	M-13
255						0.30	1.09
265	0.77	0.65	0.44	0.30	0.80	0.27	0.90
275	1.40	1.24	0.89	0.56	1.31	0.45	1.43
285	1.23	1.08	0.84	0.49	1.08	0.39	1.14
295	0.83	0.76	0.58	0.34	0.71	0.28	0.76
305	0.54	0.52	0.39	0.23	0.46	0.19	0.53
315	0.40	0.39	0.29	0.17	0.37	0.15	0.36
325	0.63	0.55	0.46	0.26	0.57	0.22	0.46
335	0.95	0.89	0.77	0.44	0.87	0.41	0.78
345	1.11	0.98	0.88	0.53	0.98	0.51	0.92
355	1.18	1.00	0.95	0.58	1.05	0.60	0.99
365	1.19	0.99	0.98	0.60	1.11	0.64	0.01
375	1.21	1.00	1.03	0.64	1.16	0.71	1.08
385	1.38	1.10	1.17	0.74	1.30	0.84	1.22
395	1.34	1.05	1.16	0.74	1.28	0.83	1.20
405	0.96	0.76	0.84	0.54	0.89	0.60	0.87
415	0.93	0.72	0.81	0.53	0.84	0.60	0.85
425	0.98	0.79	0.88	0.59	0.89	0.64	0.91
435	1.03	0.84	0.93	0.63	0.91	0.68	0.96
445	0.91	0.77	0.85	0.58	0.79	0.62	0.86
455	0.94	0.80	0.86	0.62	0.83	0.65	0.89
465	1.12	0.90	0.71	0.76	1.01	0.81	1.04
475	1.02	0.87	0.85	0.71	0.91	0.72	0.99
485	1.08	0.88	1.00	0.77	0.94	0.76	1.07
495	1.03	0.86	0.96	0.77	0.89	0.76	1.00
505	1.03	0.90	1.00	0.80	0.88	0.75	1.00
515	1.03	0.85	0.95	0.78	0.88	0.76	1.00
525	1.02	0.84	0.94	0.78	0.87	0.76	0.99

Table 1 (Continued)

Wavelength	New lamp and Collector— 0 hours	New lamp and Collector— 45 hours	New lamp and Collector— 95 hours	New lamp and Collector— 310 hours	New Collector and Al surface and clean optics-old lamp 0 hours	Dirty optics and old lamp	Cleaned optics and new lamp
	M-21	M-22	M-23	M-25	M-27	M-12	M-13
535	1.01	0.83	0.92	0.78	0.85	0.75	0.97
545	1.01	0.83	0.93	0.80	0.84	0.77	0.97
555	1.03	0.86	0.95	0.82	0.87	0.79	0.97
565	1.05	0.88	0.97	0.84	0.91	0.82	0.99
575	1.03	0.89	0.94	0.83	0.89	0.83	0.97
585	1.02	0.95	0.94	0.85	0.86	0.86	0.96
595	1.00	0.96	0.94	0.88	0.87	0.88	0.93
605	1.05	1.06	0.98	0.95	0.94	0.95	0.95
615	1.06	1.09	1.00	0.99	0.98	1.00	0.99
625	1.07	1.05	1.01	0.99	0.98	1.02	1.03
635	1.05	1.05	1.04	1.04	0.97	1.00	1.08
645	1.06	1.04	1.06	1.05	0.99	1.00	1.09
655	1.09	1.08	1.08	1.07	1.02	1.01	1.09
665	1.13	1.10	1.10	1.10	1.05	1.02	1.03
675	1.11	1.11	0.98	1.09	1.00	1.08	1.05
685	1.05	1.05	1.01	1.03	1.00	1.18	1.08
695	1.10	1.08	1.07	1.10	1.07	1.08	1.07
705	1.06	1.06	1.04	1.07	1.03	1.07	0.99
715	1.16	1.13	1.12	1.16	1.11	1.10	1.02
725	1.13	1.12	1.09	1.14	1.10	1.13	1.03
735	1.08	1.11	1.06	1.11	1.09	1.18	1.02
745	1.15	1.14	1.11	1.15	1.15	1.16	1.06
755	0.92	0.98	0.91	0.96	0.99	1.15	1.05
765	0.74	0.80	0.71	0.79	0.78	1.20	0.93
775	0.63	0.68	0.63	0.75	0.70	0.83	0.63
785	0.59	0.62	0.63	0.78	0.71	0.70	0.57
795	0.62	0.77	0.70	0.80	0.70	0.65	0.54
805	0.99	0.95	0.95	1.03	1.05	0.69	0.67
815	1.27	1.19	1.12	1.30	1.25	1.19	0.98
825	0.87	0.82	0.83	0.97	0.99	1.59	1.01
835	0.56	0.85	0.82	0.84	0.84	1.14	1.06

Table 1 (Continued)

Wavelength	New lamp and Collector— 0 hours	New lamp and Collector— 45 hours	New lamp and Collector— 95 hours	New lamp and Collector— 310 hours	New Collector and Al surface and clean optics-old lamp 0 hours	Dirty optics and old lamp	Cleaned optics and new lamp
	M-21	M-22	M-23	M-25	M-27	M-12	M-13
845	0.30	0.57	0.29	0.64	0.50	0.60	0.41
855	0.51	0.66	0.65	0.66	0.70	0.40	0.39
865	0.71	0.72	0.66	0.86	0.76	0.58	0.38
875	0.88	0.81	0.86	1.15	0.80	1.07	0.83
885	1.03	1.11	1.01	1.15	1.18	1.44	0.93
895	0.99	1.09	0.98	1.14	1.11	1.46	1.10
905	0.99	1.06	0.94	1.09	1.11	1.43	1.10
915	0.87	0.99	0.86	1.00	1.02	1.34	0.94
925	0.81	0.90	0.82	0.94	0.93	1.11	0.92
935	0.88	0.95	0.89	1.03	1.00	1.24	0.88
945	0.87	0.96	0.89	1.00	1.02	1.28	0.92
955	0.85	0.92	0.82	0.93	0.97	1.09	0.89
965	0.95	1.05	1.02	1.17	1.04	1.36	1.11
975	1.01	1.14	1.22	1.32	1.27	1.71	1.11
985	1.17	1.41	1.25	1.46	1.48	1.92	1.20
995	1.06	1.26	1.17	1.06	1.22	1.74	1.16
1005	0.97	0.99	1.21	1.10	1.27	1.31	1.20
1015	0.99	1.01	0.78	1.12	1.12	1.19	1.22
1025	0.67	0.88	0.73	0.94	0.76	0.96	1.25
1035	0.66	0.68	0.66	0.73	0.72	0.75	0.76
1045	0.72	0.74	0.73	0.80	0.80	0.85	0.73
1055	0.81	0.77	0.83	0.86	0.87	0.93	0.73
1065	0.89	0.84	0.94	0.99	0.93	1.14	0.83
1075	1.06	1.00	1.07	1.22	1.14	1.33	0.93
1085	1.21	1.14	1.32	1.30	1.26	1.34	1.10
1095	1.22	1.24	1.41	1.38	1.33	1.60	1.24
1150	1.17	1.35	1.32	1.50	1.29	1.47	1.29
1250	0.71	0.97	0.97	1.12	0.95	1.04	0.92
1350	0.84	0.96	1.00	1.13	0.92	1.02	0.70
1450	1.54	1.72	1.88	2.01	1.63	2.30	1.85
1550	1.20	1.46	1.42	1.94	1.39	1.49	1.44

Table 1 (Continued)

Wavelength	New lamp and Collector— 0 hours	New lamp and Collector— 45 hours	New lamp and Collector— 95 hours	New lamp and Collector— 310 hours	New Collector and Al surface and clean optics-old lamp 0 hours	Dirty optics and old lamp	Cleaned optics and new lamp
	M-21	M-22	M-23	M-25	M-27	M-12	M-13
1650	1.10	1.31	1.33	1.61	1.21	1.45	1.18
1750	0.95	1.17	1.18	1.37	1.04	1.16	1.16
1850	0.90	1.06	1.11	1.23	0.96	0.99	0.80
1950	1.05	1.15	1.29	1.46	1.05	1.01	1.88
2050	1.22	1.54	1.54	1.93	1.35	1.48	1.28
2150	1.19	1.41	1.47	1.80	1.29	1.44	1.24
2250	1.16	1.66	1.59	2.02	1.42	1.76	1.51
2350	1.32	1.93	1.85	2.84	1.62	1.88	1.61
2450	1.15	2.21	2.14	3.16	1.98	2.00	1.84

Table 2

Absorptance Values of Some Coatings for X-25L Solar Simulator at Various Stages of Degradation

	Run Number						
	M-21	M-22	M-23	M-25	M-27	M-12	M-13
Name of Coating	0 Hrs.	45 Hrs.	95 Hrs.	310 Hrs.	New Optics at 0 hours	Dirty Optics	Clean Optics
Silver	4.284	3.931	3.547	2.673	3.969	2.595	3.996
Aluminum	7.566	7.352	7.274	7.110	7.42	7.304	7.405
J. Colony white 78—two coats over G. E. primer—Methyl silicon—TiO_2 (R960)	18.186	17.797	17.460	15.783	18.017		
3M White—eight coats over G. E. primer (Polyester)	21.118	20.561	20.283	18.44	20.841		
Cat-a-lac White—eight coats (Epoxy)	21.650	21.568	21.258	19.976	21.739		
Dow Corning Q007 over Cat-a-lac White—Methyl silicon—TiO_2 (Rutile)	16.675	15.941	15.613	13.504	16.319		
Dow Corning Q090 over Cat-a-lac White—Methyl silicon—TiO_2 (Anatase)	16.402	16.199	15.726	14.435	16.263		
S-13 over G. E. Primer—Methyl silicon—ZnO (SP500)	19.183	19.039	18.605	17.248	19.165		
Gold	19.951	17.036	17.403	13.235	18.027	13.526	18.615
Cat-a-lac Black—epoxy	94.784	94.791	94.794	94.819	94.792	94.840	94.792
3M Velvet Black	97.204	97.221	97.220	97.243	97.214	97.234	97.211

further complicated by the power loss in the cables and lamp starter mechanism. The power transfer between power supply and lamp operation at 100 amps is 86% and at 110 amps 84%. The power supply manuals specify that operation at 100 amps is permissible. This was found to be satisfactory and the criticality of operation in the overload condition was discovered during a five day test employing the system under these conditions. Since that time major modifications of the system have been underway.

These modifications include electrical and thermal design changes. The thermal design changes include increased cooling capacity with water cooled collectors and air flow modification. The electrical design changes include design of new chokes and transformers for 5kw operation of the power supplies, modification of the starter mechanism, and replacement of #4 power cable with #"0" to reduce power losses. These modifications should be completed during the next quarter.

A1200 Solar Simulation Electronic Modifications

During a five day test in the month of November, 1966, using the A1200 solar simulator, numerous malfunctions occurred. Many of these failures have been traced back to under-rated electronics components. In order to achieve a one solar constant total irradiance with the filters presently used in the system, each unit has to be operated at 103 amperes or 3.1kw generated power. Literature distributed by the manufacturers stated that "the system is capable of operating at 110 amperes," however, it was found that some of the filter chokes in the power supplies were saturating as early as 93 amperes, causing loss of regulation, and unstable operation. Another problem found was loss of power transfer between power supplies and lamps, cable loss in monitoring system as well as reference systems. All of these problems created a very unstable operation. Corrective action has been taken to eliminate the problems mentioned above and modifications for an overall improvement in performance of the system has been accomplished in the following manner.

A new filter choke with the same amount of inductive reactance but capable of handling a 150 ampere nominal current has been designed and fabricated. Endurance tests are presently being performed on two engineering models of this type.

Power cables for interconnecting power supplies and arc lamps are being changed from No. "4" to Vulkene cable size "0". Two pairs of these cables have been installed and will be tested during our next experiment with the system to see if they will withstand the environment within our system.

Starter transformers are hooked in series with the arc lamp, and these consume some of the power being generated from the power supplies. In order to eliminate this power loss a circuit has been designed to by-pass the transformer in the starter unit automatically after the lamp is ignited.

The control console that operates the system has been relocated. During this move the methods for monitoring the systems' performance has been changed and a remote control instrumentation panel has been designed and installed. This panel enables one man to execute start-up and alignment procedures; previously, three people were necessary for electronics alignment. The panel features conveniences such as current-to-light mode switching, solar cell performance monitoring, current output monitoring and level of operation adjustments.

A cathode ray tube oscilloscope with a 1-1/2" x 3" display pattern has been designed and is being fabricated to present the purpose of applying a visual continuous monitor for each module. Twenty of these units will be incorporated into the new control console.

For the purpose of a single unit operation a new control unit has been designed and fabricated. A unique design feature of this unit is a calibrated dial for output current; prior to this electronics instrumentation was necessary to monitor the exact current output of the power supply. This new unit can be set up to operate at any desired level without instrumentation monitoring.

Experimental Lamps

Various types of new lamps have been tested during the past year. These include Kr, Ar, H-Xe and HgXe. The spectral irradiance curves of these sources are shown in Figures 9 through 11 and Figure 52, Section 2. These lamps were tested with the hope of finding a source that could be combined with zenon lamps in the A1200 solar simulator array along with spectral filters to improve the ultraviolet continuum of the system. Some of the results can be seen in Figures 12 and 13.* Figure 13 represents a considerable improvement in the ultraviolet region; however, the krypton line emission shows through at 765 nm indicating that the spectral filters were not designed for krypton. This can be corrected by using modified spectral filters.

*Lillywhite, M. A., McIntosh, R., Lester, D. "Operational Characteristics" and Development of a Thermal Vacuum Solar Simulator Used for Spacecraft Thermal Design AIAA Log #1897, September 1966.

SOLAR SIMULATION ANOMALIES STUDIES

The sources and techniques for thermal coatings testing used by experimenters in the field and the Radiometry Section, GSFC differ considerably. The data obtained from these tests are used as criteria to evaluate experimental coatings, and in most cases data are compared disregarding the test conditions (e.g., spectral irradiance of source). This results primarily because there is no easy way to relate such tests except in terms of equivalent sun hours (ESH). This employs a reciprocity rule which implies that a linear relationship exists between total radiation dosage and time. Proof of this rule has not been documented. It is the purpose of the solar simulation anomalies studies to evaluate this method of testing as well as other anomalies experienced in solar simulation in terms of the errors that can result in final data and conclusions when such anomalies are not considered. Several tests have been conducted and a limited amount of data is available. The remaining portion of this report will describe what has been accomplished to date, looking first at a group of sources that are commonly used for testing.

The lamps studied consisted of three basic types of sources; (1) high pressure compact short arc lamps, (2) a medium pressure mercury vapor lamp, and (3) a carbon arc. Each of these types has different operational characteristics and each source has different spectral irradiance characteristics. A comparison of the relative spectral irradiance of several sources is given in Table 3, "Ratio of Test Lamp Energy to Solar Irradiance." Columns 2, 3, 4, 7, 8, and 9 of Table 3 are representative of a 2.5kw compact arc lamp of the type indicated. Column 5 is a typical experimental arc, Column 6 is a mercury vapor lamp, and Column 10 is a typical carbon arc. It should be pointed out that each column contains spectral irradiance data chosen from many sets of measurements in order to be representative of a typical new source of that type without optics ($\approx$0 hours). This data, therefore, may not agree with identical lamps of different ages and/or used in different optical systems. The last column of the table gives the percentage of the solar irradiance in a 10 nm bandwidth whose center wavelength is indicated in Column 1, "Interval Wavelength." The irradiance is calculated for 10 nm intervals over the entire range (250 nm to 2500 nm); the energy is averaged over 100 nm bandwidths over the range 1100—2500 nm. The actual solar irradiance, $I_{s\lambda}$, may be obtained by multipling a value in Column 11 (% Solar Irradiance) by the solar total irradiance (250 nm to 2600 nm). The other nine columns contain data displayed in fractions of a solar constant for the bandwidth indicated in Column 1 when all sources are considered to have a total irradiance of one solar constant. The total irradiance of a specific bandwidth for a specific source is obtained from the product of the indicated value in the source column, the value in the percent solar irradiance column, and the total solar irradiance value. This table gives direct comparison of the energy per

Table 3

Ratio of Test Lamp Energy to Solar Irradiance

#1	#2	#3	#4	#5	#6	#7	#8	#9	#10	#11
nm Interval Wavelength	Xe	M-13 Filtered Xe X-25L	M-20 HgXe	V-3 Exper. Source	Medium Pressure Hg	M-5 Kr	M-11 Ar	M-9 H-Xe	M-14 Carbon Arc	% Energy Solar
255	0.56	1.09	5.02	13.25		6.18	2.54	4.59		0.072
265	0.45	0.90	1.62	6.34	34.64	3.06	1.29	2.31		0.166
275	0.83	1.43	5.39	6.81	13.64	3.39	1.45	2.60		0.166
285	0.80	1.14	4.55	3.96	5.97	2.06	0.88	1.63		0.290
295	0.71	0.76	4.78	2.65	6.79	1.37	0.58	1.12	0.31	0.456
305	0.85	0.53	7.65	2.53	10.95	1.43	0.59	1.13	0.48	0.476
315	0.78	0.36	5.89	2.04	18.97	1.22	0.49	0.96	0.53	0.590
325	0.72	0.46	0.70	1.65	1.09	0.99	0.40	0.80	0.53	0.746
335	0.72	0.78	1.31	1.54	1.98	0.92	0.37	0.76	0.58	0.828
345	0.79	0.92	0.37	1.56	0.44	0.90	0.35	0.76	0.57	0.870
355	0.83	0.99	0.55	1.62	0.35	0.89	0.37	0.80	0.54	0.870
365	0.73	1.01	6.78	1.41	11.21	0.83	0.36	0.78	0.70	0.922
375	0.73	1.08	1.23	1.36	0.22	0.77	0.34	0.78	1.12	0.942
385	0.92	1.22	0.58	1.45	0.26	0.78	0.37	0.87	1.57	0.859
395	0.89	1.20	0.47	1.28	0.23	0.68	0.35	0.83	1.47	0.942
405	0.63	0.87	1.77	0.88	3.25	0.46	0.25	0.57	1.02	1.346
415	0.59	0.85	0.37	0.93	0.12	0.43	0.29	0.55	0.98	1.429
425	0.63	0.91	0.33	0.98	0.27	0.45	0.29	0.57	0.98	1.357
435	0.64	0.96	2.86	0.96	4.95	0.47	0.26	0.58	0.91	1.336
445	0.56	0.86	0.35	0.69	0.13	0.39	0.20	0.51	0.74	1.564
455	0.60	0.89	0.20	0.65	0.07	0.36	0.20	0.53	0.74	1.615
465	0.66	1.04	0.18	0.67	0.06	0.34	0.19	0.61	0.77	1.605
475	0.73	0.99	0.18	0.67	0.06	0.34	0.19	0.57	0.77	1.595
485	0.66	1.07	0.21	0.69	0.10	0.34	0.20	0.59	0.79	1.522
495	0.67	1.00	0.27	0.67	0.13	0.33	0.20	0.55	0.81	1.522
505	0.67	1.00	0.18	0.68	0.12	0.34	0.21	0.54	0.87	1.450
515	0.66	1.00	0.17	0.64	0.06	0.36	0.21	0.54	0.90	1.429
525	0.65	0.99	0.17	0.60	0.06	0.36	0.21	0.54	0.88	1.439
535	0.63	0.97	0.55	0.57	0.51	0.37	0.19	0.52	0.84	1.470
545	0.59	0.97	2.25	0.54	4.47	0.39	0.20	0.51	0.83	1.460
555	0.60	0.97	0.49	0.54	1.03	0.43	0.20	0.52	0.84	1.439
565	0.62	0.99	0.59	0.56	0.60	0.47	0.20	0.53	0.84	1.408
575	0.61	0.97	3.16	0.53	5.28	0.48	0.19	0.52	0.81	1.429
585	0.62	0.96	1.68	0.54	0.83	0.52	0.20	0.53	0.81	1.408
595	0.63	0.93	0.62	0.56	0.08	0.55	0.22	0.53	0.80	1.398
605	0.66	0.95	0.23	0.56	0.08	0.56	0.23	0.55	0.81	1.336
615	0.67	0.99	0.23	0.53	0.08	0.50	0.22	0.56	0.81	1.305
625	0.69	1.03	0.24	0.53	0.08	0.49	0.21	0.57	0.83	1.284
635	0.69	1.08	0.24	0.54	0.08	0.52	0.22	0.58	0.87	1.253
645	0.68	1.09	0.25	0.57	0.09	0.56	0.22	0.61	0.92	1.232
655	0.68	1.09	0.26	0.58	0.09	0.56	0.23	0.67	0.96	1.212
665	0.68	1.03	0.27	0.57	0.11	0.52	0.24	0.66	0.96	1.201
675	0.71	1.05	0.28	0.65	0.15	0.51	0.25	0.62	0.96	1.170
685	0.75	1.08	0.33	0.74	0.13	0.52	0.29	0.66	0.95	1.139
695	0.78	1.07	0.38	0.87	0.11	0.53	0.43	0.66	0.94	1.108

Table 3 (Continued)

#1	#2	#3	#4	#5	#6	#7	#8	#9	#10	#11
nm Interval Wavelength	Xe	M-13 Filtered Xe X-25L	M-20 HgXe	V-3 Exper. Source	Medium Pressure Hg	M-5 Kr	M-11 Ar	M-9 H-Xe	M-14 Carbon Arc	% Energy Solar
705	0.71	0.99	0.34	0.89	0.11	0.50	0.48	0.62	0.90	1.118
715	0.76	1.02	0.35	0.89	0.10	0.52	0.40	0.66	0.91	1.067
725	0.76	1.03	0.35	0.96	0.10	0.56	0.41	0.66	0.89	1.056
735	0.78	1.02	0.36	1.27	0.10	0.57	0.60	0.70	0.89	1.036
745	0.82	1.06	0.34	1.71	0.11	0.80	0.94	0.71	0.90	1.004
755	0.79	1.05	0.33	1.97	0.11	1.07	0.97	0.71	0.88	1.004
765	0.85	0.93	0.36	1.90	0.12	2.06	1.25	0.77	0.91	0.963
775	0.87	0.81	0.37	1.77	0.12	1.77	0.76	0.73	0.92	0.932
785	0.69	0.57	0.37	1.75	0.12	1.30	0.66	0.65	0.92	0.922
795	0.67	0.54	0.38	2.02	0.11	1.25	1.12	0.67	0.93	0.901
805	0.72	0.67	0.39	2.54	0.12	1.48	1.72	0.73	0.94	0.880
815	0.89	0.98	0.48	2.86	0.12	2.65	1.89	1.31	0.95	0.859
825	1.71	1.01	0.72	2.76	0.12	3.12	1.22	1.98	0.93	0.849
835	2.25	1.06	0.66	2.46	0.13	2.77	1.44	2.06	0.92	0.818
845	1.81	0.41	0.53	2.22	0.13	2.02	1.65	1.37	0.90	0.797
855	1.16	0.39	0.46	1.79	0.14	1.42	1.11	0.75	0.88	0 777
865	0.97	0.38	0.49	0.94	0.14	1.12	1.13	0.47	0.86	0.756
875	1.17	0.83	0.70	0.75	0.14	1.11	0.57	1.28	0.86	0.746
885	1.94	0.93	0.90	0.87	0.14	1.59	0.55	2.31	0.86	0.735
895	2.44	1.10	0.94	0.91	0.15	1.81	0.54	2.73	0.87	0.715
905	3.19	1.10	0.86	0.75	0.16	1.59	0.78	2.58	0.91	0.683
915	3.12	0.94	0.88	0.71	0.16	1.06	1.11	2.30	0.91	0.673
925	2.88	0.92	0.77	0.70	0.17	0.85	1.06	2.15	0.92	0.663
935	2.73	0.88	0.68	0.66	0.18	0.83	0.77	1.91	0.93	0.652
945	2.55	0.92	0.69	0.59	0.18	0.86	0.72	1.78	0.95	0.632
955	2.79	0.89	0.68	0.58	0.17	0.88	0.79	1.75	0.96	0.611
965	2.64	1.11	0.70	0.53	0.77	0.89	0.83	1.65	0.97	0.601
975	2.47	1.11	0.86	0.51	1.13	1.01	0.84	2.07	0.96	0.601
985	2.94	1.20	1.04	0.54	1.19	1.15	0.84	2.32	1.01	0.570
995	3.42	1.16	1.09	0.52	1.22	1.08	0.78	1.92	1.03	0.559
1005	3.46	1.20	1.56	0.52	2.47	0.99	0.80	1.69	1.08	0.538
1015	2.92	1.22	1.82	0.55	2.08	0.92	0.83	1.72	1.11	0.528
1025	2.41	1.25	1.82	0.58	1.66	0.90	0.85	1.64	1.14	0.518
1035	1.73	0.76	1.34	0.59	1.69	0.90	0.90	0.93	1.15	0.507
1045	1.75	0.73	0.98	0.63	0.41	0.92	0.95	0.91	1.15	0.497
1055	1.07	0.73	0.73	0.65	0.20	0.94	1.08	0.93	1.16	0.487
1065	1.09	0.83	0.71	0.66	0.17	0.97	1.12	0.93	1.19	0.476
1075	1.09	0.93	0.70	0.65	0.17	0.98	1.13	0.95	1.19	0.466
1085	1.15	1.10	0.71	0.59	0.17	0.99	1.12	0.96	1.18	0.456
1095	1.21	1.24	0.74	0.53	0.29	0.98	1.05	1.00	1.21	0.445
1150	1.10	1.29	1.13	0.61	0.68	1.13	1.21	0.98	1.28	0.392
1250	0.97	0.92	1.08	1.12	0.24	1.57	1.81	1.03	1.35	0.314
1350	0.65	0.70	1.34	2.08	0.81	1.66	3.01	1.16	1.42	0.253
1450	0.92	1.85	1.34	0.94	0.35	1.87	2.76	1.52	1.49	0.205
1550	1.14	1.44	1.53	0.71	0.60	1.81	2.99	1.61	1.51	0.168
1650	0.95	1.18	1.79	0.60	0.84	2.10	3.11	1.70	1.58	0.139
1750	0.83	1.16	2.41	0.50	1.00	2.18	3.41	1.89	1.63	0.115
1850	0.84	0.80	1.69	0.54	0.60	2.17	4.02	2.07	1.56	0.096
1950		0.88	1.73	0.49	0.70	1.95	4.40	2.26	1.50	0.082
2050		1.28	1.88	0.54	0.74	2.03	4.66	2.33	1.51	0.069
2150		1.24	2.20	0.51	0.82	2.19	4.91	2.46	1.45	0.059
2250		1.51	2.52	0.51	1.72	2.15	5.89	2.81	1.41	0.051
2350		1.61	2.96	0.63	2.11	2.28	6.46	2.65	1.34	0.043
2450		1.84	3.05		1.76	2.26	7.35	1.75	1.21	0.038

bandwidth for several sources in terms of the air mass zero solar spectral irradiance or an equivalent solar dose/bandwidth which can be used to obtain equivalent sun hours of irradiation when these sources are used in degradation testing.

The ultraviolet region of the simulated solar spectrum is of greatest concern to the degradation of optical characteristics of thermal spacecraft coatings. This region is defined, for solar simulation purposes, as radiation having wavelengths between 250 nm and 400 nm; it comprises about 9% of the solar spectrum. The energy of this region (9%) is nearly wholly absorbed by most paint type coatings, and the absorptances of evaporated surfaces (Ag, Au, etc.) are determined largely by this portion. This radiation is a major factor in the change in absorptance of these coatings in testing and in space. The use of a solar spectral mismatch in the ultraviolet region can produce quite erroneous results in solar absorptance values and the rate of change in absorptance values or optical degradation. The use of extreme intensities in the ultraviolet region, possibly due to emission lines (e.g., Hg and HgXe sources), results in data that are very difficult to interpret in terms of the actual solar environment. The use of a source deficient in the ultraviolet is equally misleading because the change that might be normal in space would not occur or would occur at a different rate. The errors in absorptance due to the spectral mismatch can be corrected for when analytical calculations are used, but the errors resulting from a different degradation rate due to spectral mismatch cannot be eliminated.

Table 4 points out the criticality of this match for the sources being discussed in this report. This data shows the equivalent total solar irradiance

Table 4

Ratio of Test Lamp Energy to Solar Irradiance Below 405 nm

	Sources								
	A-1 Xe	M-13 Filtered Xe-X-25	M-20 HgXe	V-3 Experimental Source	Med. Pressure Hg	M-5 Kr	M-11 Ar	M-9 H-Xe	M-14 Carbon Arc
Ratio of test lamp energy to solar irradiance below 405 nm.	.79	.91	2.40	1.84	4.56	1.01	.44	.91	.80

dose in the ultraviolet region below 405 nm for a given total irradiance. Many experimenters use values similar to these to obtain equivalent sun hour doses (ESH) of solar irradiance when one of these sources is being used for irradiation in coating degradation testing. It can be seen from Table 3 that the distribution of spectral irradiance in this region is very different for many of these sources. It appears, then, that one might expect not only different absorptance values for different sources, which can be calculated, but different rates of degradation for which reciprocity may not hold and therefore these rates may not be linearly related. This is, in fact, the case and will be discussed later in this report.

Table 5 shows the effective absorptance values of different types of coatings commonly used on spacecraft for the group of sources studied. The effect of the solar spectral mismatch can be seen here by comparing the effective absorptance values in Table 5, Columns 2-10 to the solar absorptance values in Column 11. These are values the coatings have at zero hours of irradiation for a specific source and do not indicate that any degradation has occurred. It is extremely difficult to compare rates of degradation under similar test conditions for different sources; however, this will be discussed later.

Coatings were selected for these tests in order to demonstrate possible large differences in degradation dependent upon exposure environments. For this reason some coatings which are known to be highly unstable were included with some which have been used in space flight experiments and also some which look promising for the future.

The paint formulations tested employ zinc oxide and titanium dioxide pigments in a variety of vehicles including two types of silicone, an epoxy resin, potassium silicate, and a polyester resin. Table 7 is a list of white paint formulations.

Testing Methods

Two systems were used to obtain "in-situ" absorptance data of the coatings which were irradiated with different sources. One system utilized an ultra high vacuum system with a LN_2 shroud to determine steady state absorptance values from thermal equilibrium states, while the other method used a portable vacuum cell with a movable sample holder and a spectrophotometer to determine absorptance as a function of wavelength. The thermal method yields a total absorptance and the optical method yields both a spectral absorptance and total absorptance value. The changes in total absorptance obtained in these two methods are directly comparable. It is felt that the spectral and total absorptance data must be studied simultaneously in order to obtain useful information for mechanisms

Table 5

Effective Absorptance Values for Various Solar Simulation Sources

Name of Coating	Irradiance Sources									
	Xe	M-13 Filtered X-25L	M-20 HgXe	V-3 Ar 5KW	M-24 Hg	M-5 Kr	M-11 Ar	M-9 H-Xe	M-14 Carbon Arc	Solar Energy
Silver	4.05	3.99	13.42	10.09	28.53	6.00	3.16	5.17		4.96
Aluminum	7.97	7.41	6.54	8.45	7.09	7.32	5.53	7.21		7.64
J. Colony white 78 - 2 coats over G.E. primer-Methyl silicon-TiO_2 (R960)	14.52	17.63	33.20	24.43	49.36	20.90	22.21	19.82		18.18
3M white - 8 coats over G.E. primer (Polyester)	17.44	20.49	35.20	27.14	51.12	23.25	23.98	22.30		
Cat-a-lac white - 8 coats (Epoxy)	18.43	21.30	36.54	27.50	50.89	25.19	27.79	24.10		
Dow Corning Q007 over Cat-a-lac white-Methyl silicon - TiO_2 (Rutile)	13.22	15.96	31.05	23.29	48.39	18.37	17.89	17.40		16.24
Dow Corning Q090 over Cat-a-lac white-Methyl silicon - TiO_2 (Anatase)	14.03	15.98	30.26	23.06	46.49	19.33	19.49	18.16		16.30
S-13 over G.E. Primer-Methyl silicon - ZnO (SP500)	16.49	18.76	34.47	25.81	50.16	22.63	23.71	21.32		18.91
Gold	14.45	18.62	23.45	21.97	38.48	12.78	7.14	14.00		19.75
Cat-a-lac black-epoxy	94.88	94.79	94.55	94.69	94.26	94.74	94.69	94.77		94.79
3M Velvet black	97.20	97.21	97.19	97.20	97.10	97.26	97.32	97.24		97.21

Table 6

Ultraviolet Irradiance of X-25L Solar Simulator at Various Stages of Degradation

	M-12	M-13 Clean Optics New Collector	M-21 New Lamp New Collector	M-22 45 hrs. After M-21	M-23 95 hrs. After M-21	M-25 310 hrs. After M-21	M-27 New Collector & Al Surfaces Old Lamp
Ultraviolet total irradiance below 405 nm in fractions of a solar constant at one solar constant total irradiance	.53	.91	1.03	.87	.84	.52	.95
Test performed at time of measurement		- - - An - 2A - -			An - 2D		
	- - - - An - 2B - - - - - -		An - 2 - 1A				
	- - - - An - 2C - - - - - -			An - 2 - 1B			

Table 7

White Paint Formulations

Name	Pigment	Vehicle	Solvent
090	Anatase TiO_2-Titanox AMO	Condensation type methyl silicone	Xylene
007	Rutile TiO_2-Titanox RANC	Condensation type methyl silicone	Xylene
S-13	ZnO (SP500 from N.J. Zinc)	Condensation type methyl silicone (RTV 602 from GE)	Toluene
J.C. 78	Rutile TiO_2-Dupont's R960	Condensation type methyl silicone (RTV 602 from GE)	Toluene
Cat-a-lac White	Probably TiO_2	Epoxy	
3M White	Rutile TiO_2	Polyester type thermoset	Cellosolve acetate and xylol in 1:1 ratio
ZnO Silicate	ZnO (N.J. Zinc's SP500)	Potassium silicate (Sylvania's PS-7)	Water
TiO Silicate	Rutile TiO_2 (Dupont's RF-1)	Potassium silicate (Sylvania's PS-7)	Water

studies, employing rate of change of absorptance, ultimate degradation predictions and possible change in emittance values. This is particularly true when different sources are used because the change in calculated integrated total α_s, or effective absorptance, is different for different sources even though the magnitude of spectral change of the coating is the same. This is due to the variation in the spectral irradiance of the various sources.

The optical measurement is made using the ion pumped vacuum system shown in Figure 15.* This cell accommodates one sample which is irradiated in position A and moved to position B where reflectance measurements are made through the quartz port using a Beckman DK-2 Spectrophotometer. The sample is connected to a spring and is moved from position B to A using a magnet. The precision of the measurement is within ±1% and its absolute accuracy is better than 4%. The temperature of these samples with one solar constant irradiance ranges from +40°C to +60°C at initial equilibrium conditions. This technique allows measurements to be taken at virtually any time interval. The sample is measured in vacuum before irradiation and a number of times during irradiation to determine the change in rate of degradation, and after irradiation in vacuum and in air to determine whether the absorptance of the sample has experienced

any recovery. This measurement involves physically moving the cell system to a position in the integrating sphere port and takes about fifteen minutes.

The thermal measurement is accomplished using an ultra high vacuum system (10^{-9} Torr pressure) with a LN_2 shroud and a sample having well known radiative properties. Knowing these data, other heat "input" values, and the equilibrium temperature of the sample when irradiated with a known total and spectral irradiance, the ratio of absorptance to emittance can be computed. The assumption is made that there is no change in emittance due to degradation and that the total and spectral irradiance of the source is constant. If these assumptions hold true, the change in absorptance can be computed as a function of time using a steady state equilibrium calculation.

The assumptions mentioned above are reasonable in that the irradiance is monitored and the emittance values can be checked indirectly. The $\Delta\alpha$ computed can be compared to the $\Delta\alpha$ values obtained in the optical measurement under identical test conditions. This comparison enables calculation of the emittance which is compared with the previously obtained emittance values. The emittance values are known as a function of temperature and the appropriate corrections are made for samples tested using high intensity irradiance which run at high temperatures. The total and spectral irradiance values are monitored periodically during testing. The total irradiance is monitored "in-situ" with a razor blade detector and in air with a radiometer. Total irradiance measurements are taken at each sample before and after each test. The spectral irradiance is monitored with a filter radiometer device and with the Leiss system used for spectral irradiance measurements.

This thermal absorptance measurement is continuous in that the temperature is recorded every five seconds with a strip chart recorder (±1/4°C precision). It is possible then to study the rate of degradation for each sample after the sample reaches an equilibrium temperature. This presents a problem in that achieving an equilibrium temperature may take 2 hours for the sample used in this study, and the degradation that occurs during this period is not directly obtainable. This error can be checked in two ways: (1) the difference in calculated predicted equilibrium temperature and that measured equilibrium temperature may be used to compute a change in absorptance for this time period, and (2) comparison of optical measurement made at very short intervals of time early in the test. These methods have been partially successful in determining the magnitude of initial $\Delta\alpha$.

The results of coatings testing using different total irradiance levels with approximately the same spectral irradiance (thermal measurements) to obtain absorptance data are displayed in Tables 8-12. Several problems must be

Table 8
Degradation Data-Thermal "In-Situ" Measurement—Sheet #1

SUMMARY SHEET—1 DATE 8-20-66 to 8-28-66

Test Title: AN02A — 200 Hours at 1 Solar Constant for 200 ESH

Coating Description	°C T_1	°C T_2	α_1 Thermal in-situ initial	α_2 Thermal in-situ final	% change $\frac{\alpha_2-\alpha_1}{\alpha_1}$	Solar α_{A1} initial in air	Solar α_{A2} after in air	% change $\frac{\alpha_{A1}-\alpha_{A2}}{\alpha_{A1}}$	% change $\frac{\alpha_1-\alpha_{A1}}{\alpha_{A1}}$	% change $\frac{\alpha_2-\alpha_{A2}}{\alpha_{A2}}$	% change $\frac{\alpha_{A1}-\alpha_2}{\alpha_{A1}}$	α_s source integrated spectrum	% Δ $\frac{\alpha_1-\alpha_s}{\alpha_s}$	% Δ $\frac{\alpha_{A1}-\alpha_s}{\alpha_s}$
S-13/G. E. Primer	-14.5	-14.0	.182	.185	.94	19.8	17.86	-9.8	-8.1	3.6	6.6	18.91	3.8%	4.7
S-13/D. C. Primes	-8	-5	.20	.21	5.0	19.5	21.36	9.54	-2.6	1.7	7.7			
007/G. E. Primer	-12	-8	.188	.20	10.6		19.58			-2.1				
007/D. C. Primer	-16	-12	.191	.210	9.95	18.9	18.42	-2.5	-1.1	-14.0	11.1			
090/G. E. Primer	8	24	.256	.315	23.05		28.24			-11.5				
090/D. C. Primer	8.5	23	.256	.315	23.05	19.7	26.30	33.5	-29.9	-19.8	60.0			

FILTER DATA - Spectral Irradiance - UV cut-off filters

Filter Number	Corrected I_o below λ_{co} mw/cm²	λ_{co}	Solar I_o below λ_{co}	Fraction of solar constant	Comments
	Total Irradiance		Total Irradiance	At One Solar Constant	
No Filter	12.29	405mn	13.5 mw/cm²	.91	Obtained from Leiss Measurement

Name:

Table 9
Degradation Data-Thermal "In-Situ" Measurement—Sheet #2

SUMMARY SHEET—2 DATE 9-27-66 to 10-2-66

Test Title: AN-2B — 100 Hours at 2 Solar Constants for 200 ESH

Coating Description	°C T_1	°C T_2	α_1 Thermal in-situ initial	α_2 Thermal in-situ final	% change $\frac{\alpha_2-\alpha_1}{\alpha_1}$	Solar α_{A1} initial in air	Solar α_{A2} after in air	% change $\frac{\alpha_{A1}-\alpha_{A2}}{\alpha_{A1}}$	% change $\frac{\alpha_1-\alpha_{A1}}{\alpha_{A1}}$	% change $\frac{\alpha_2-\alpha_{A2}}{\alpha_{A2}}$	% change $\frac{\alpha_{A1}-\alpha_2}{\alpha_{A1}}$	α_s source integrated spectrum	% Δ $\frac{\alpha_1-\alpha_s}{\alpha_s}$	% Δ $\frac{\alpha_{A1}-\alpha_s}{\alpha_s}$
S-13/G. E. Primer	20	22	.15	.16	06.7	19.5	19.68		-23.1	-18.7	17.9			
S-13/D. C. Primer	31	38	.18	.19	05.6	19.5	21.32	09.3	-07.7	-10.9	2.6			
007/G. E. Primer	29.5	36	.17	.19	11.8		19.12			-.63				
007/D. C. Primer	19	22	.17	.18	05.9	18.9	18.6		-10.1	-3.2	4.8			
090/G. E. Primer	81	84	.31	.32	03.23		28.12			13.8				
090/D. C. Primer	81	84	.31	.32	03.23	19.7	28.02	42.2	-57.4	14.2	-62.4			

FILTER DATA - Spectral Irradiance - UV cut-off filters

Filter Number	Corrected I_o below λ_{co} mw/cm² Total Irradiance	λ_{co} nm	Solar I_o below λ_{co} Total Irradiance	Fraction of solar constant At One Solar Constant	Comments
No Filter	21.6 mw/cm²	405nm	13.5 mw/cm²	.80	Obtained with Leiss Measurement

Name:

Table 10
Degradation Data-Thermal "In-Situ" Measurement—Sheet #3

SUMMARY SHEET —3 DATE 10-13-66 to 10-16-66

Test Title: AN-2C — 50 Hours at 4 Solar Constants for 200 ESH

Coating Description	°C T_1	°C T_2	α_1 Thermal in-situ initial	α_2 Thermal in-situ final	% change $\frac{\alpha_2-\alpha_1}{\alpha_1}$	Solar α_{A1} initial in air	Solar α_{A2} after in air	% change $\frac{\alpha_{A1}-\alpha_{A2}}{\alpha_{A1}}$	% change $\frac{\alpha_1-\alpha_{A1}}{\alpha_{A1}}$	% change $\frac{\alpha_2-\alpha_{A2}}{\alpha_{A2}}$	% change $\frac{\alpha_{A1}-\alpha_2}{\alpha_{A1}}$	α_s source integrated spectrum	% Δ $\frac{\alpha_1-\alpha_s}{\alpha_s}$	% Δ $\frac{\alpha_{A1}-\alpha_s}{\alpha_s}$
ϵ = .90 S-13/G. E. Primer	85	86	16.6	16.8	12.04	19.8	20.1	-1.5	-14.1	-16.5	15.2			
ϵ = .91 S-13/D. C. Primer	127	130	22.1	23.4	05.88	19.5	24.58	26.0	13.3	-4.8	-20.0			
ϵ = .90 007/G. E. Primer	98	103	16.3	17.2	05.52		20.52			-16.2				
ϵ = .89 007/D. C. Primer	52	56	16.4	17.3	05.49	18.9	19.24	1.8	-13.2	-10.08	8.5			
ϵ = .92 090/G. E. Primer	154	154	32.8	32.8	0		31.22			5.1				
ϵ = .91 090/D. C. Primer	123	123	31.2	31.2	0	19.7	30.9	56.8	58.4		-58.4			

FILTER DATA - Spectral Irradiance - UV cut-off filters

Filter Number	Corrected I_o below λ_{co} mw/cm²	λ_{co}	Solar I_o below λ_{co}	Fraction of solar constant	Comments
	Total Irradiance	nm	Total Irradiance	At One Solar Constant	
No Filter	42.1 mw/cm²	405	13.5	.78	Leiss Measurement

Name:

Table 11A
Degradation Data-Thermal "In-Situ" Measurement—Sheet #4

SUMMARY SHEET —4

DATE 10-18-66 to 10-27-66

Test Title: AN-2-1A — 200 Hours at 1 Solar Constant for 200 ESH

Coating Description	°C T_1	°C T_2	α_1 Thermal in-situ initial	α_2 Thermal in-situ final	% change $\frac{\alpha_2-\alpha_1}{\alpha_1}$	Solar α_{A1} initial in air	Solar α_{A2} after in air	% change $\frac{\alpha_{A1}-\alpha_{A2}}{\alpha_{A1}}$	% change $\frac{\alpha_1-\alpha_{A1}}{\alpha_{A1}}$	% change $\frac{\alpha_2-\alpha_{A2}}{\alpha_{A2}}$	% change $\frac{\alpha_{A1}-\alpha_2}{\alpha_{A1}}$	α_s source integrated spectrum	% Δ $\frac{\alpha_1-\alpha_s}{\alpha_s}$	% Δ $\frac{\alpha_{A1}-\alpha_s}{\alpha_s}$
8c. cat-a-lac White	-10	+19	19.1	29.5	54.5	23.14	28.52	23.3	49	3.44	27.5			
5c. 3M White 1c. G. E. Primer	-11	+2	19.1	23.2	21.5	22.08	26.26	18.9	37.5	-11.7	-5.1			
090+ 2c. Cat-a-lac	+2½°C	+22.5	21.4	29.6	38.3	17.26	25.92	50	21.1	4.2	-71.5			
J. C.-78-2 over G. E. Primer	-20	-18.5	17.3	17.9	3.4	19.5	19.72	1.1	13.98	-9.3	8.2	18.18	-4.8	-7.3

FILTER DATA - Spectral Irradiance - UV cut-off filters

Filter Number	Corrected I_o below λ_{co} mw/cm² Total Irradiance	λ_{co} nm	Solar I_o below λ_{co} Total Irradiance	Fraction of solar constant At One Solar Constant	Comments
No Filter	13.9 mw/cm²	405	13.5	1.03	Leiss Measurement

Name:

Table 11B
Degradation Data-Thermal "In-Situ" Measurement—Sheet #4

SUMMARY SHEET —4 DATE 11-15-66 to 11-23-66

Test Title: AN 2D — 200 Hours at 1 Solar Constant for 200 ESH

Coating Description	^{o}C T_1	^{o}C T_2	α_1 Thermal in-situ initial	α_2 Thermal in-situ final	% change $\frac{\alpha_2-\alpha_1}{\alpha_1}$	Solar α_{A1} initial in air	Solar α_{A2} after in air	% change $\frac{\alpha_{A1}-\alpha_{A2}}{\alpha_{A1}}$	% change $\frac{\alpha_1-\alpha_{A1}}{\alpha_{A1}}$	% change $\frac{\alpha_2-\alpha_{A2}}{\alpha_{A2}}$	% change $\frac{\alpha_{A1}-\alpha_2}{\alpha_{A1}}$	α_s source integrated soectrum	% Δ $\frac{\alpha_1-\alpha_s}{\alpha_s}$	% Δ $\frac{\alpha_{A1}-\alpha_s}{\alpha_s}$
1 coat G. E. Primer 6 coats 007	-8.0	-7.5	21.8	23.24	6.6		19.82			16.8				
8 coats Cat White	*14.5	49.5	29.18	49.2	68.88		29.62			66.1				
2 coats Cat-a-lac White 6c. Q90-090	*13.5	41.0	29.18	45.15	54.73		28.22			59.99				
1c. G. E. Primer 6 c. Q90-090	*18.5	38.5	31.5	42.9	36.19		26.74			60.4		16.3	93.25	
1c. G. E. Primer 6c. (old) S-13	-6.5	-2.5	21.76	24.83	14.11	19.8	20.64	-4.2	9.9	20.3	-25.4	18.91	15.07	4.7
1c. Dow Corning 6c. Q92-090	*18.5	39.5	30.55	43.45	42.23		27.64			57.2				

*After 6 hours irradiance

FILTER DATA - Spectral Irradiance - UV cut-off filters

Filter Number	Corrected I_o below λ_{co} mw/cm^2	λ_{co}	Solar I_o below λ_{co}	Fraction of solar constant	Comments
	Total Irradiance	nm	Total Irradiance	At One Solar Constant	
No Filter	11.2 mw/cm^2	405	13.5 mw/cm^2	.83	Leiss Measurement

Name:

Table 12
Degradation Data-Thermal "In-Situ" Measurement—Sheet #5

SUMMARY SHEET —5 DATE 11-8-66 to 11-10-66

Test Title: AN-2-1B — Test 50 Hours at 4 Solar Constants for 200 ESH

Coating Description	^{o}C T_1	^{o}C T_2	α_1 Thermal in-situ initial	α_2 Thermal in-situ final	% change $\frac{\alpha_2-\alpha_1}{\alpha_1}$	Solar α_{A1} initial in air	Solar α_{A2} after in air	% change $\frac{\alpha_{A1}-\alpha_{A2}}{\alpha_{A1}}$	% change $\frac{\alpha_1-\alpha_{A1}}{\alpha_{A1}}$	% change $\frac{\alpha_2-\alpha_{A2}}{\alpha_{A2}}$	% change $\frac{\alpha_{A1}-\alpha_2}{\alpha_{A1}}$	α_s source integrated spectrum	% Δ $\frac{\alpha_1-\alpha_s}{\alpha_s}$	% Δ $\frac{\alpha_{A1}-\alpha_s}{\alpha_s}$
ϵ = .92 8c. Cat-a-lac White	146	175	32.79	42.85	30.6	23.14	50.9	1.20	42.6	-15.8	-85.1			
ϵ = .93 5c. 3M White G. E. Primer		179	22.08 Air valve	39.83	82.30	22.08	48.66	1.20	0	-18.2	-80.4			
ϵ = .92 090+ Cat-a-lac Primer	152.5	152.5	32.9	32.9	0	17.26	29.58	.714	90.6	-11.2	-90.6			
ϵ = .89 J. C.-78-2	83.5	89	18.15	19.56	+7.8	19.5	21.1	.0820	7.8	-07.3		18.18		7.3

FILTER DATA - Spectral Irradiance - UV cut-off filters

Filter Number	Corrected I_o below λ_{co} mw/cm²	λ_{co}	Solar I_o below λ_{co}	Fraction of solar constant	Comments
	Total Irradiance	nm	Total Irradiance	At One Solar Constant	
No Filter	47.0 mw/cm²	405	13.5	.87	Leiss Measurement

Name:

considered when evaluating this data. The temperatures of the samples for each of the tests are different due to the measurement technique. This makes it difficult to distinguish between temperature and irradiance effect for some coatings. The value of the port input is different for each level of irradiance and is not known accurately for each sample. The spectral irradiance of the X-25L source degraded during this series of tests. This was monitored and the results can be seen in Tables 1, 2, and 6. The ultraviolet total irradiance of the X-25L for a particular test is given on the bottom of the data sheets (Tables 8-12). It is necessary to consider this parameter when comparing this data. The magnitude of degradation is enough to affect the absorptance of the coating but does not compare to the differences experienced when other sources are used (See Table 3 and 5). These data can be expressed in terms of rates of degradation as a function of ultraviolet equivalent sun hours. This information becomes more directly comparable and can be used to determine the validity of a reciprocity rule for various circumstances. This is being done now and the complete data is not available for this report. Despite these problems it is still true that each test was conducted using approximately identical parameters with the exception of total irradiance levels; therefore, several conclusions can be drawn from the data.

This thermal data indicates that 090, Cat-a-lac white and 3M white paints degrade very rapidly initially. This rapid rate is attributed to surface degradation. The rate of this initial change seems to be highly dependent upon total and spectral irradiance or temperature but the magnitude of change is independent of these factors. Several primers were used in this series of tests (e.g., G. E. primer, Dow Corning, Cat-a-lac primer) and no difference in degradation characteristics could be attributed to primers. The optical degradation data supports and explains some of the observations made from the thermal "in-situ" data and will be discussed later.

A summary of the optical "in-situ" data obtained using four of the sources and some of the coatings discussed herein is shown in Table 13. The absorptance values are absolute integrated or total absorptance values. The "α" before and the "α" after values are made at the beginning and end of the time indicated in the "Time Irradiated" column. The "Intermediate Measurements" are absorptance values taken a short time after irradiation started (as indicated in "Time of Intermediate Measurement"). This data as well as the thermal data indicates that there are two types of degradation observed, long and short term.

The very rapid initial reflectance changes noted for Cat-a-lac white and Q92-090 provide confirmation of the large initial temperature changes for these materials in the thermal tests before equilibrium was reached. This has been discussed previously. It was noted that the magnitude of this very rapid initial

Table 13

Results of Degradation Testing With Various Sources Using Optical "In-Situ" Measurements

Coatings Tested	α Before	α After	% Change	Total Irradiance mw/cm	Time Irradiated	Source Used	Time of Intermediate Measurement	α Intermediate Measurement	Equivalent UV Sun Hours
Dow Corning Q-090 over Cat-a-lac white - methyl silicone-TiO_2 (Anatase)	14.90	39.84	167.38	140 mw/cm^2	140 hours	HgXe	10 minutes	25.27	336
	16.03	39.96	149.3	140 mw/cm^2	140 hours	Xe	10 minutes	25.47	110
	16.4	41.22	151.3	70 mw/cm^2	280 hours	Hg			638.4
Cat-a-lac white eight coats (Epoxy)	17.39	27.66	59.06	140 mw/cm^2	36 minutes	HgXe			1.24
	17.56	28.14	60.25	140 mw/cm^2	3½ hours	Xe			8.40
	16.98	21.73	27.97	140 mw/cm^2	30 min.	Carbon Arc			2.28
J. Colony 88-S. Same composition as S-13 ZnO SP500 + methyl silicone	17.25	27.49	59.36	140 mw/cm^2	140 hours	HgXe	24 hours	24.18	336
	16.49	28.57	73.26	140 mw/cm^2	140 hours	Xe			110
	13.81	41.93	203.62	70 mw/cm^2	140 hours	Hg	24 hours	23.64	319.2
Dow Corning Q007 over G. E. Primer - methyl silicone - TiO_2 (Rutile)	15.47	24.05	55.46	140 mw/cm^2	140 hours	HgXe	24 hours	23.27	336
	16.75	25.22	50.57	140 mw/cm^2	140 hours	Xe		23.65	110.6
	15.81	31.54		70 mw/cm^2	140 hours	Hg	24 hours	26.38	319.2
J. Colony 78-5B, 2 coats over G.E. primer - methyl Silicone - TiO_2 (R960)	16.83	23.42		140 mw/cm^2	140 hours	HgXe	24 hours	19.33	336
	15.71	22.82		140 mw/cm^2	140 hours	Xe	24 hours	18.83	110
	17.67	29.04		70 mw/cm^2	140 hours	Hg	24 hours	25.17	319

change in Q92-090 and 88S is nearly independent of spectrum while the rate is increased by increased short (<400 nm) ultraviolet irradiance, spectral and total.

The long range degradation which can be considered separately from the rapid initial changes noted above is characteristically most severe in the blue region of the visible spectrum (causing yellowing). This type of degradation has been noted to some degree with all of the white coatings tested by the thermal laboratory group. The magnitude of this degradation is directly related to the intensity of the short wavelength or ultraviolet region (high-energy photon). In order to appreciate this dependence on wavelength it is necessary to consider the rate of reflectance change in the visible rather than the change in integrated α. This is because the effect can be largely masked by the initial fast degradation in the red and infrared wavelength regions.

"In-situ" reflectance measurements, then, seem to indicate that the effect of spectral distribution is minimal with respect to rapid initial reflectance changes due to surface reactions of pigment and maximal with respect to the long range diffusion controlled bulk reactions of the crystals. Thus the choice of irradiance source is most important when the effect of rapid surface reactions on reflectance or total α is small and bulk crystal degradation has the prime effect.

The last column in Table 4 gives the equivalent sun hour dose for the ultraviolet region assuming a constant total irradiance (one solar constant). It can be seen that, generally, the magnitude of degradation is greater when the equivalent sun hour values are greater, but there is certainly not a linear relationship between total ultraviolet irradiance and time. Therefore a reciprocity rule may not be employed to obtain ultraviolet equivalent sun hours when the entire ultraviolet irradiance is used (wavelengths <400 nm). Additional complications arise when different sources are used because the coating temperatures are different in this type of testing. Even if the substrate temperature is kept constant a problem still exists in determining the actual difference between substrate temperature and coating surface temperature. The substrate temperatures measured during these tests were as high as 70°C.

The temporal spectral stability of the system supplying the simulated solar irradiance is a factor which must be considered when evaluating data obtained from long term degradation testing. Degradation of this type is inherent with all solar simulation systems and it is true that this can affect the change in absorptance of a coating being irradiated. Such degradation of the ultraviolet total irradiance generally does not approach an order of magnitude in comparison with the effects from values of the different sources shown in Table 2, but for

comparable results the spectral irradiance should be monitored periodically. If periodic spectral and total irradiance measurements are taken and degradation does occur, an average value of irradiance may be obtained for the time interval and used to obtain ultraviolet equivalent sun hours. This is the method used by the authors to obtain the data in the last column of Table 4 ("Equivalent Ultraviolet Sun Hours").

It is the opinion of this Thermal Laboratory Group that testing with different sources and, consequently, with different spectra may produce errors in short term surface degradation and will produce errors in long term degradation. This degradation is highly dependent upon the coating formulation. It was observed that many different rates and magnitudes of degradation occurred for various values of (1) spectral irradiance, (2) total irradiance, and (3) temperature. It is proposed, therefore, that valid comparison of coatings optical degradation characteristics may be done only when test conditions (e.g., spectral and total irradiance, temperature and coating formulation, and application) are approximately the same; moreover, environmental testing of thermal coatings materials should be conducted using the same conditions that will be experienced in space, with emphasis on spectral and total irradiance and temperature.

CONCLUSION

Many of the basic development problems in solar simulation have been resolved and/or defined in a manner that permits an experimenter to be aware of the limitations of a particular solar simulation system when it is used for a specific purpose. Considerable improvements in solar simulation systems will be necessary in the future; however, existing systems must be used in present testing despite their deficiencies. The immediate problem, then, is to evaluate present systems and techniques used comprehensively with particular emphasis placed upon the type of material tested, the use of the material in the actual solar environment, and how well the simulated conditions meet the actual environmental conditions, in order to gain a better understanding of the test results.

A series of tests concerned with solar simulation anomalies has been conducted using white paints (thermal coatings). These tests were designed to evaluate the effect of solar spectral mismatch on these materials. The data indicates that the change in absorptance of such coatings depends upon the type and formulation (chemically) of the material, the spectrum of the source, and the total irradiance (or temperature). These data have shown that direct comparison of absorptance values of the same coating irradiated with equal total irradiance, but different spectral irradiance is not valid. It has been observed that degradation of some coatings occurs in two forms: rapid initial changes, which may be

associated with surface phenomenon; and long term changes, which may be a near-surface or bulk property. The rapid initial absorptance changes of some coatings ultimately obtain an absorptance value independent of spectral irradiance and long term absorptance changes are highly dependent upon the spectral irradiance. These observations are profound but do not represent sufficient evidence for complete evaluation of solar simulation testing when there is a solar spectral mismatch. A good spectral match is difficult to obtain, expensive, and may not be critical for certain types of test specimens. For this reason additional work of this type is needed. The follow up work should be quantitative in nature in order to set testing limits for, various types of materials, accurate simulation of specific missions, and future system experimentation goals.

PROGRAM FOR NEXT REPORTING INTERVAL

1. The modifications to the A1200 solar simulator will be completed.

2. Work will be continued on the 24 hour/day unmanned coating degradation studies using optical "in-situ" measurements in cooperation with J. Colony, GSFC.

3. Work will continue on the thermal "in-situ" coatings degradation testing if overtime allows.

4. A detector calibration effort in conjunction with the T&E division, GSFC, will be completed. The next step will be planned in an effort to explain discrepancies between thermal and radiometric measurements of total irradiance that arise when a test is being conducted in the T&E Space Environmental Simulator.

5. The "in-situ" uniformity scanner will be installed in the large vacuum system used with the A1200 solar simulator.

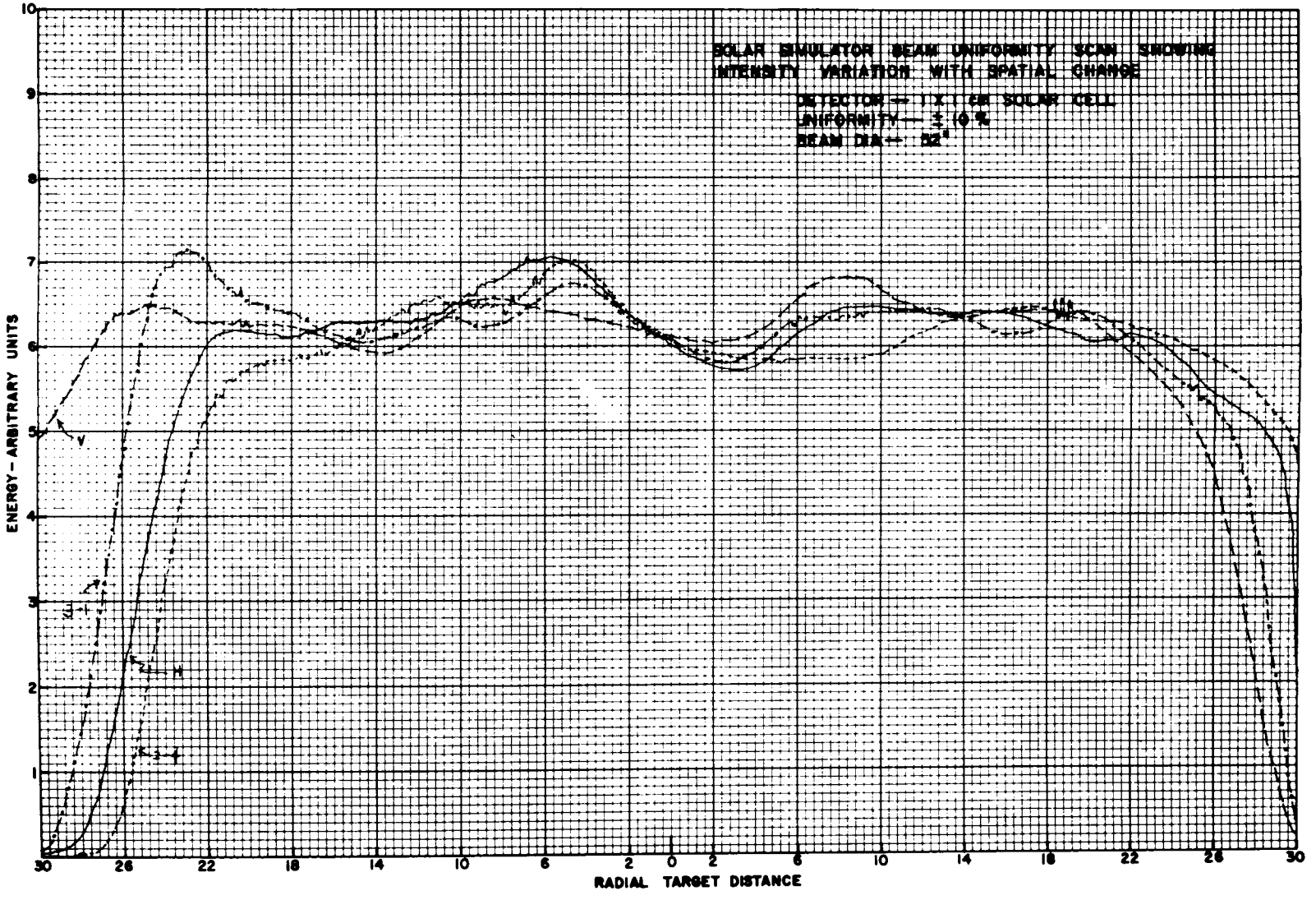

Figure 1. Uniformity Scan—Old System

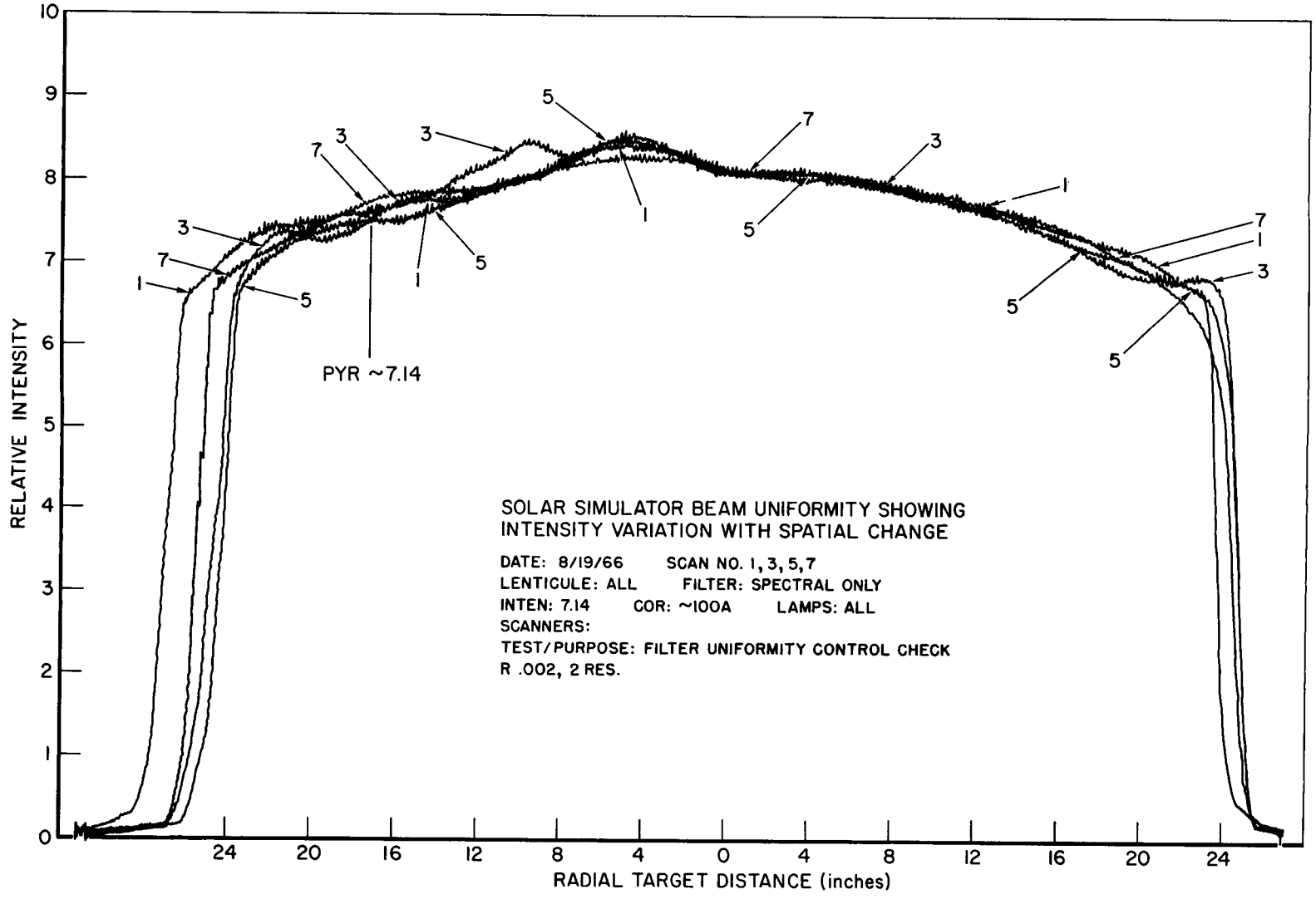

Figure 2. Uniformity Scan—Lenticule System (no filters)

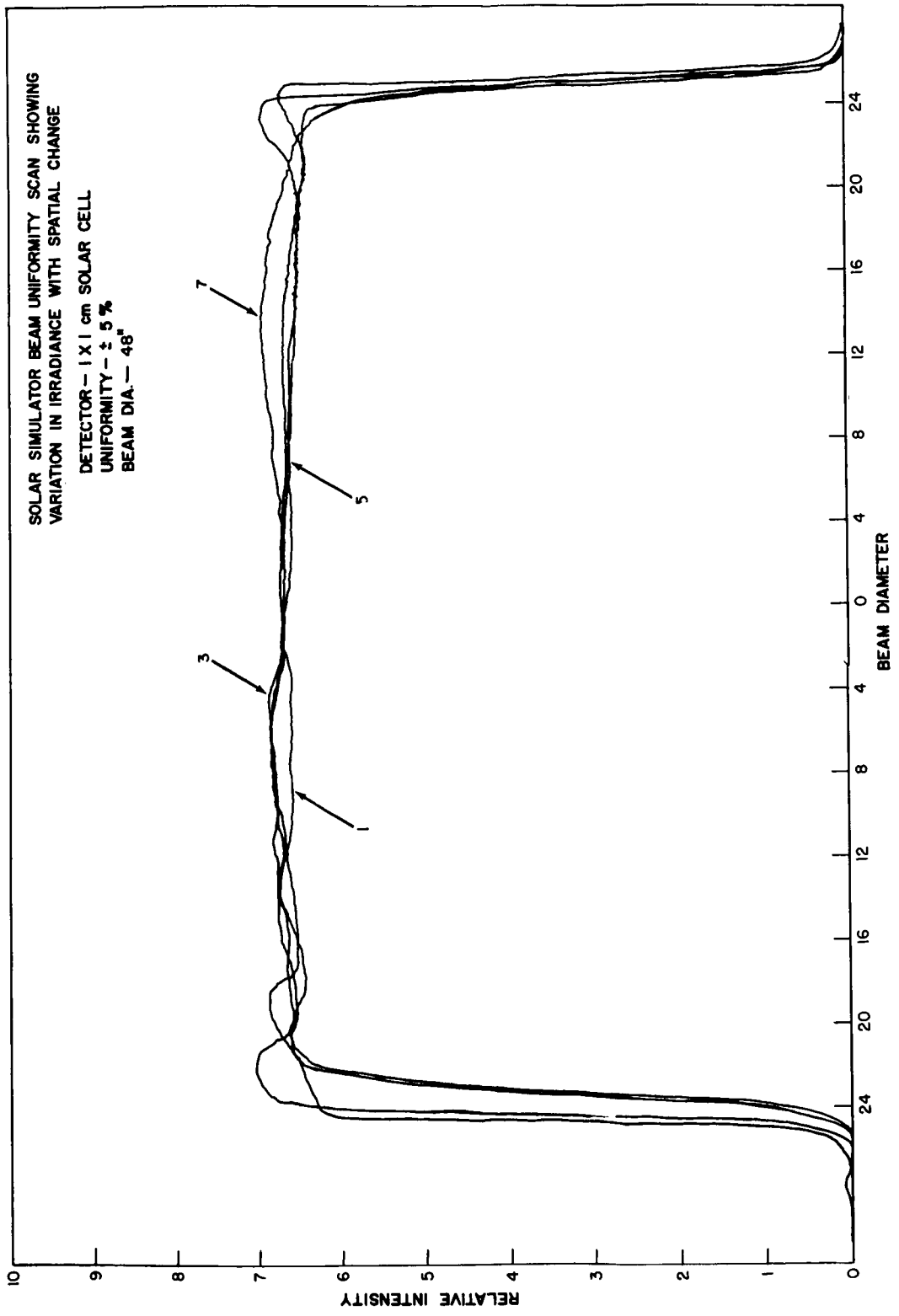

Figure 3. Uniformity Scan—Lenticule System (filters)

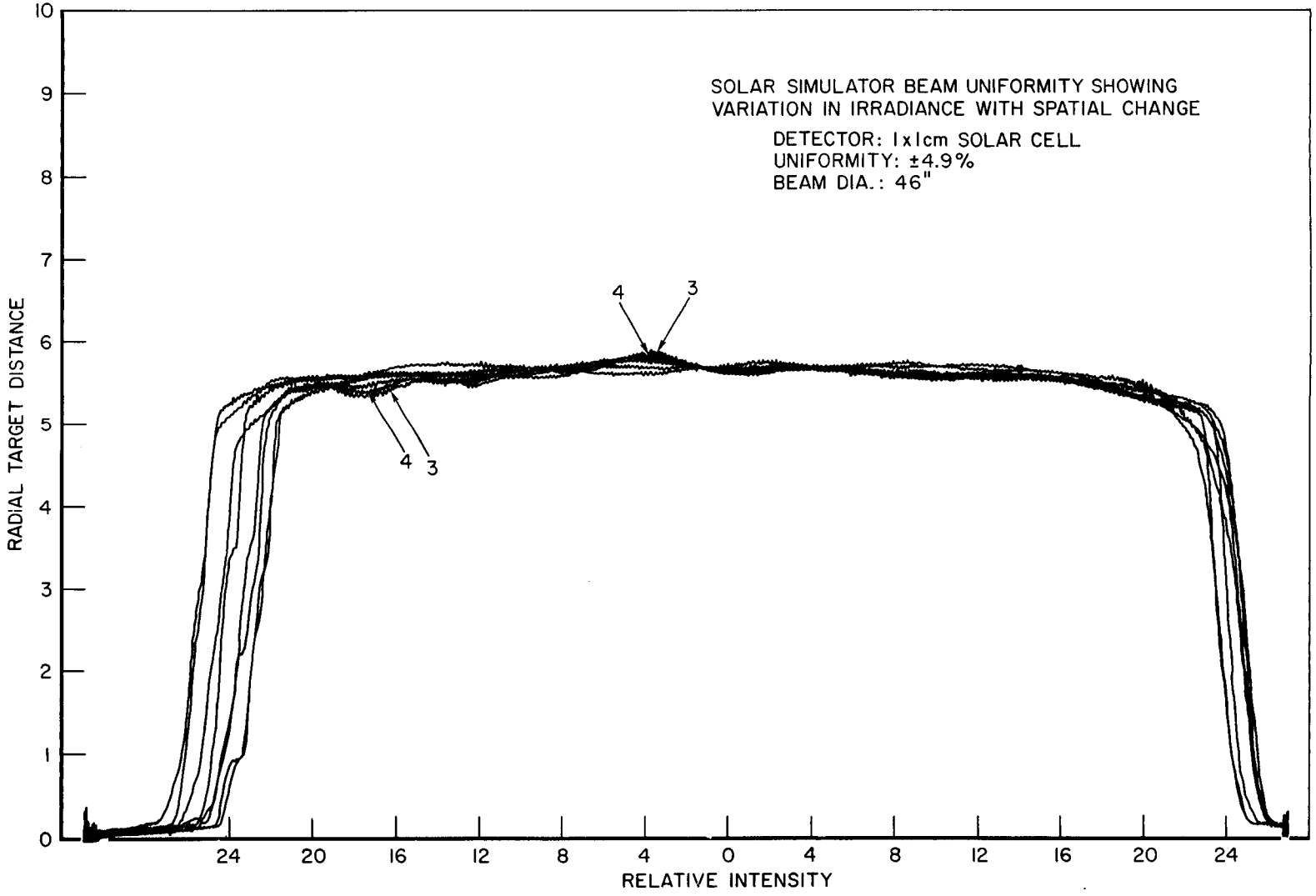

Figure 4. Uniformity Scan—Lenticule System (one filter)

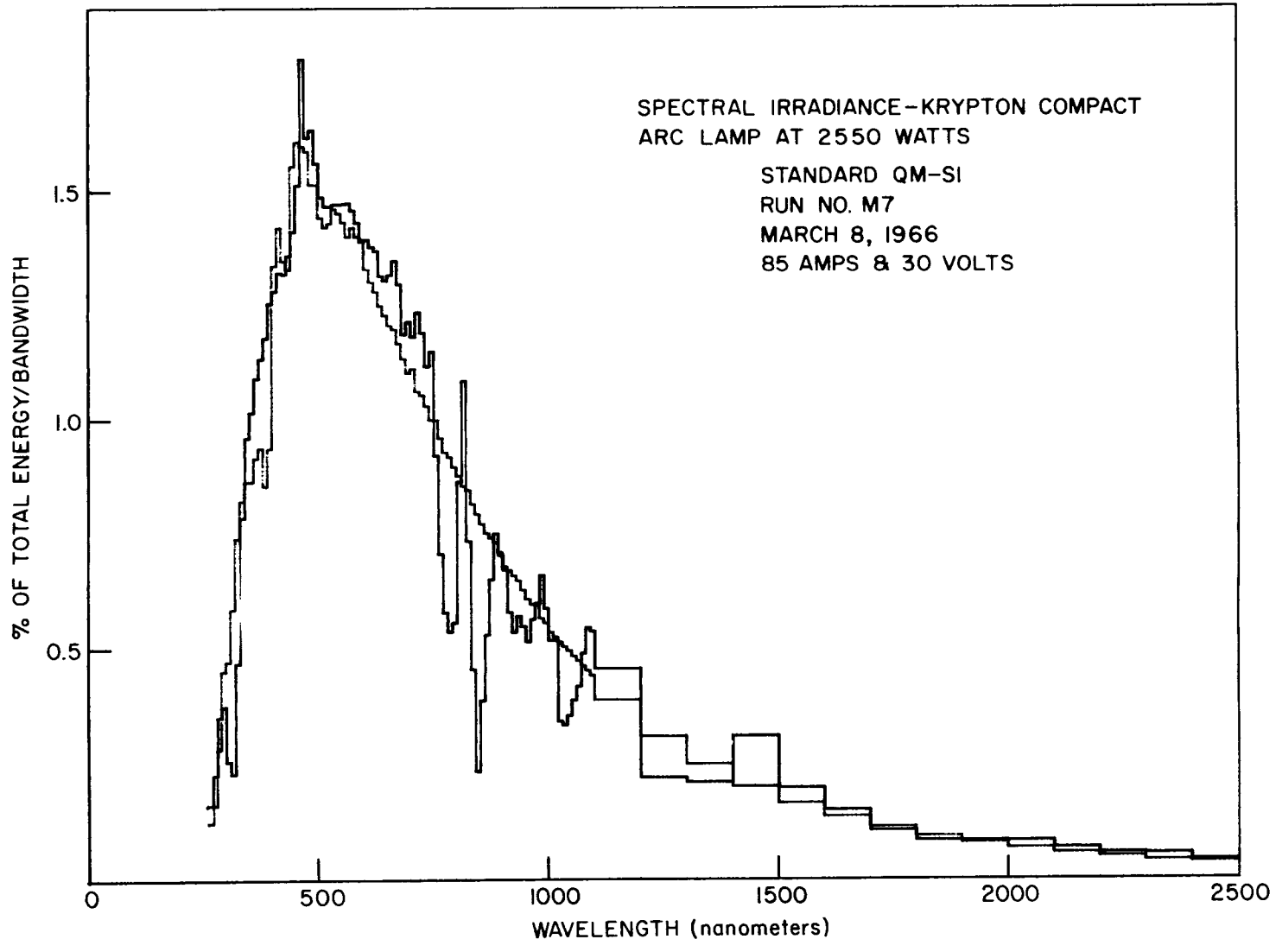

Figure 4A. Spectral Irradiance—X-25L Solar Simulator—0 hours

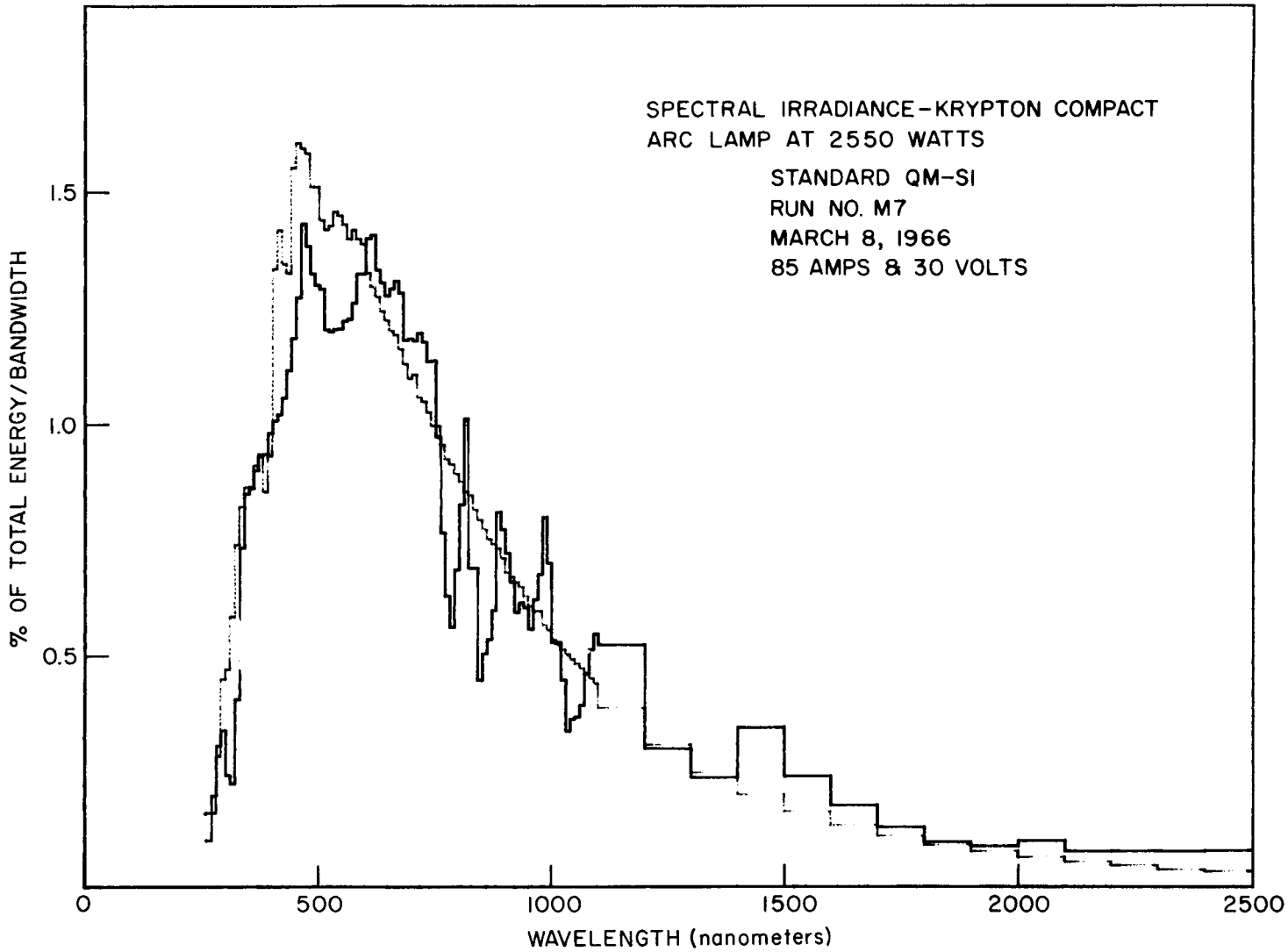

Figure 4B. Spectral Irradiance—X-25L Solar Simulator—45 hours

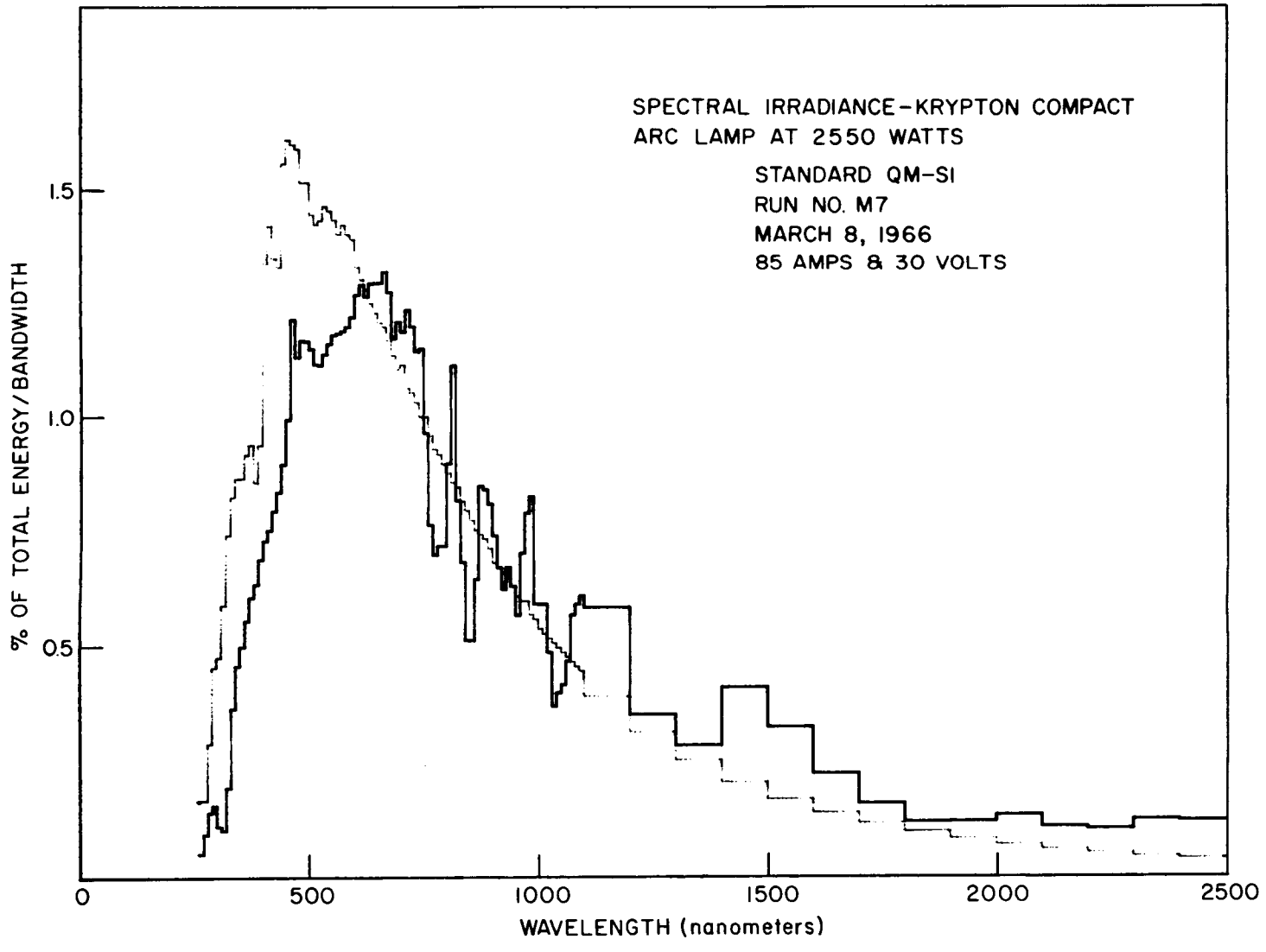

Figure 4C. Spectral Irradiance—X-25L Solar Simulator—310 hours

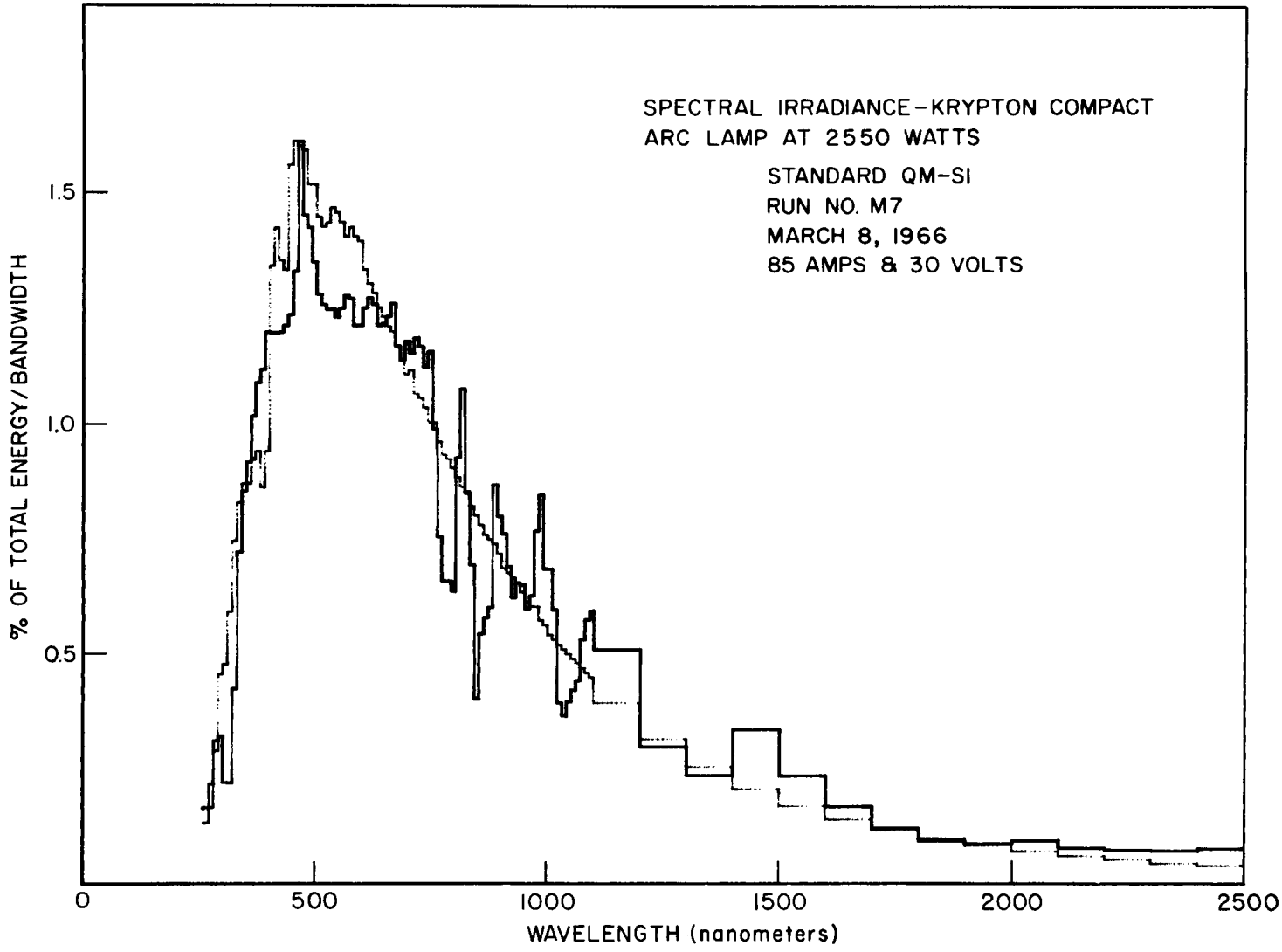

Figure 4D. Spectral Irradiance—X-25L Solar Simulator—New Optics—320 hours Lamp

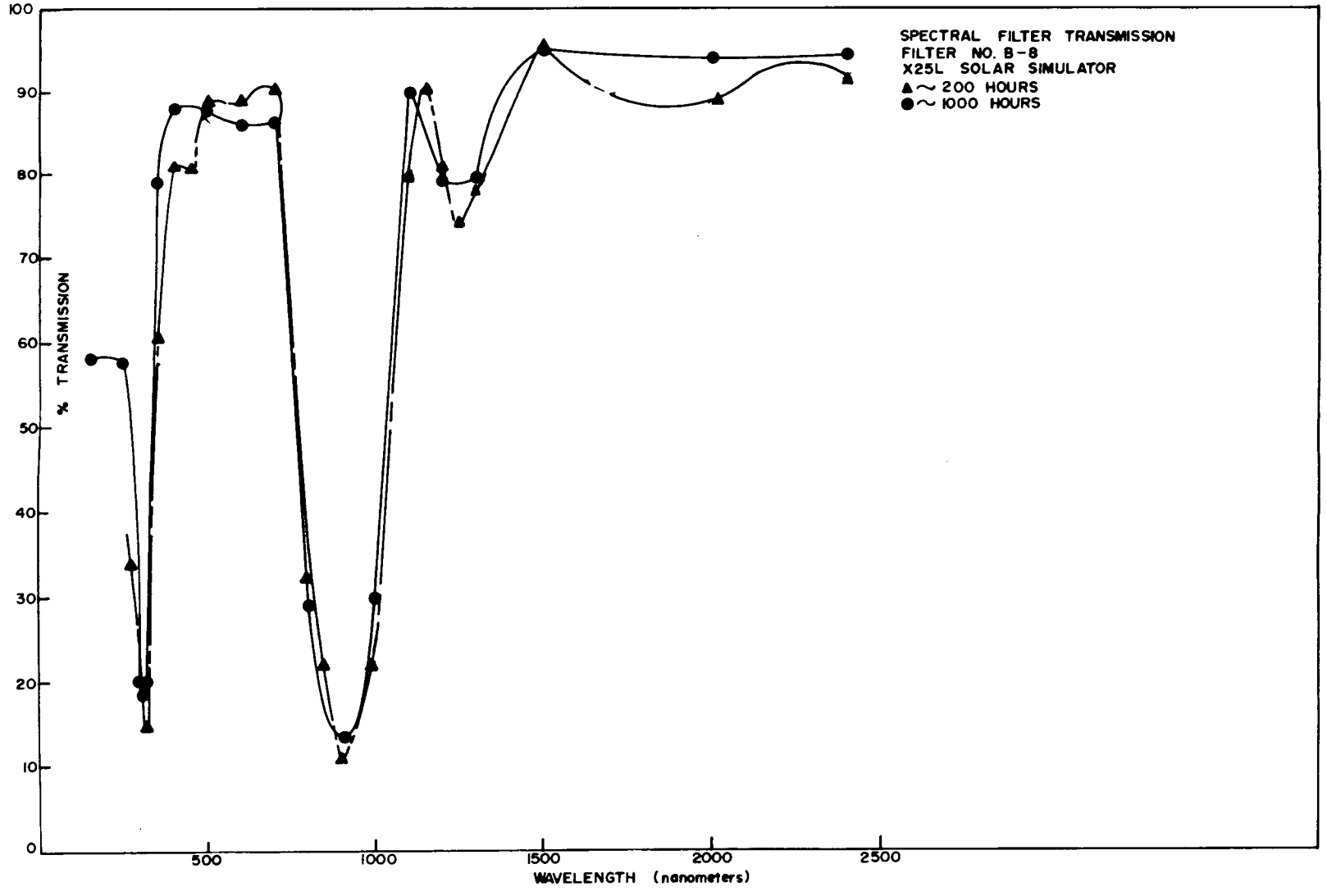

Figure 5. Transmission Curve of Spectral Filter—X-25L

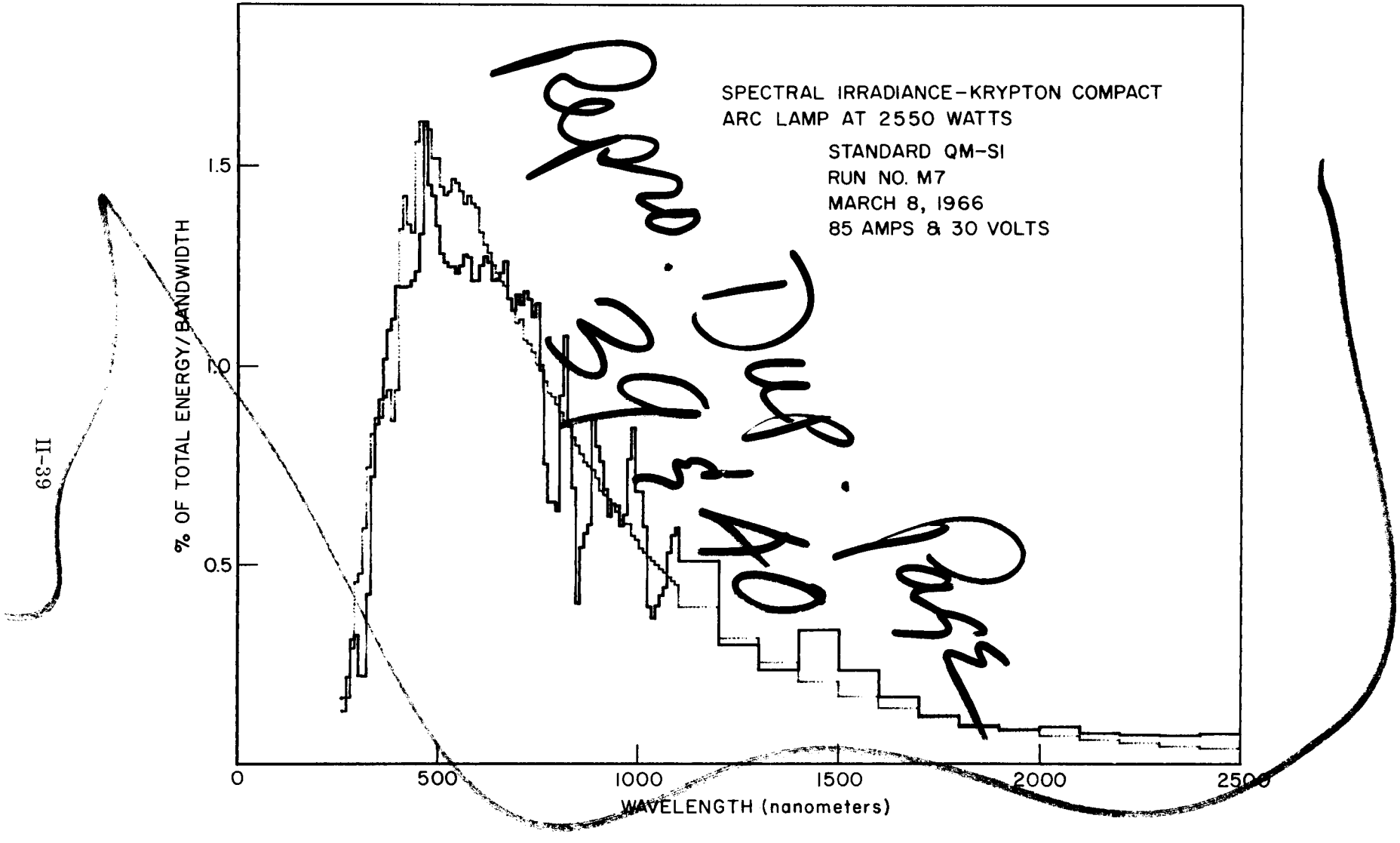

Figure 4D. Spectral Irradiance—X-25L Solar Simulator—New Optics—320 hours Lamp

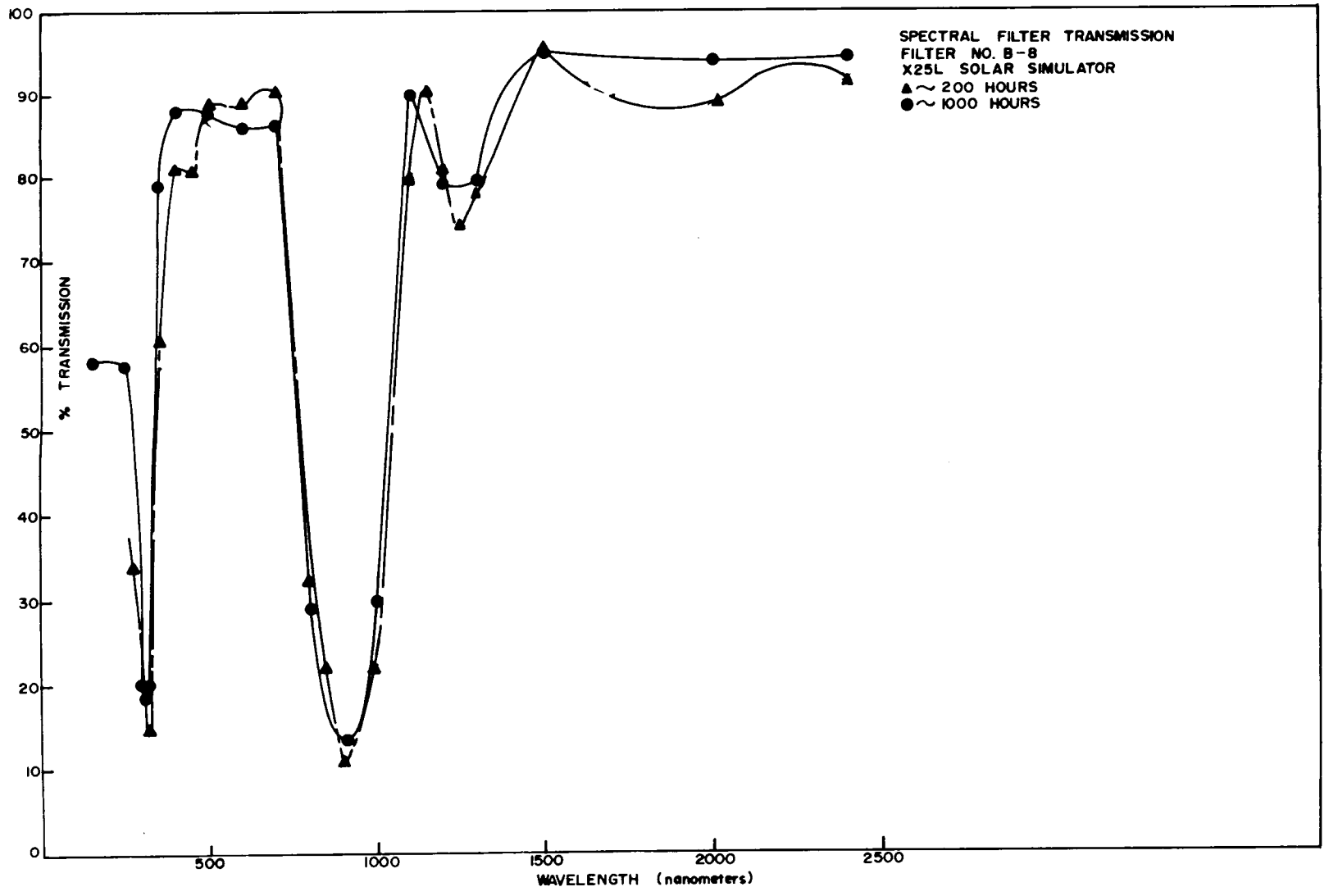

Figure 5. Transmission Curve of Spectral Filter—X-25L

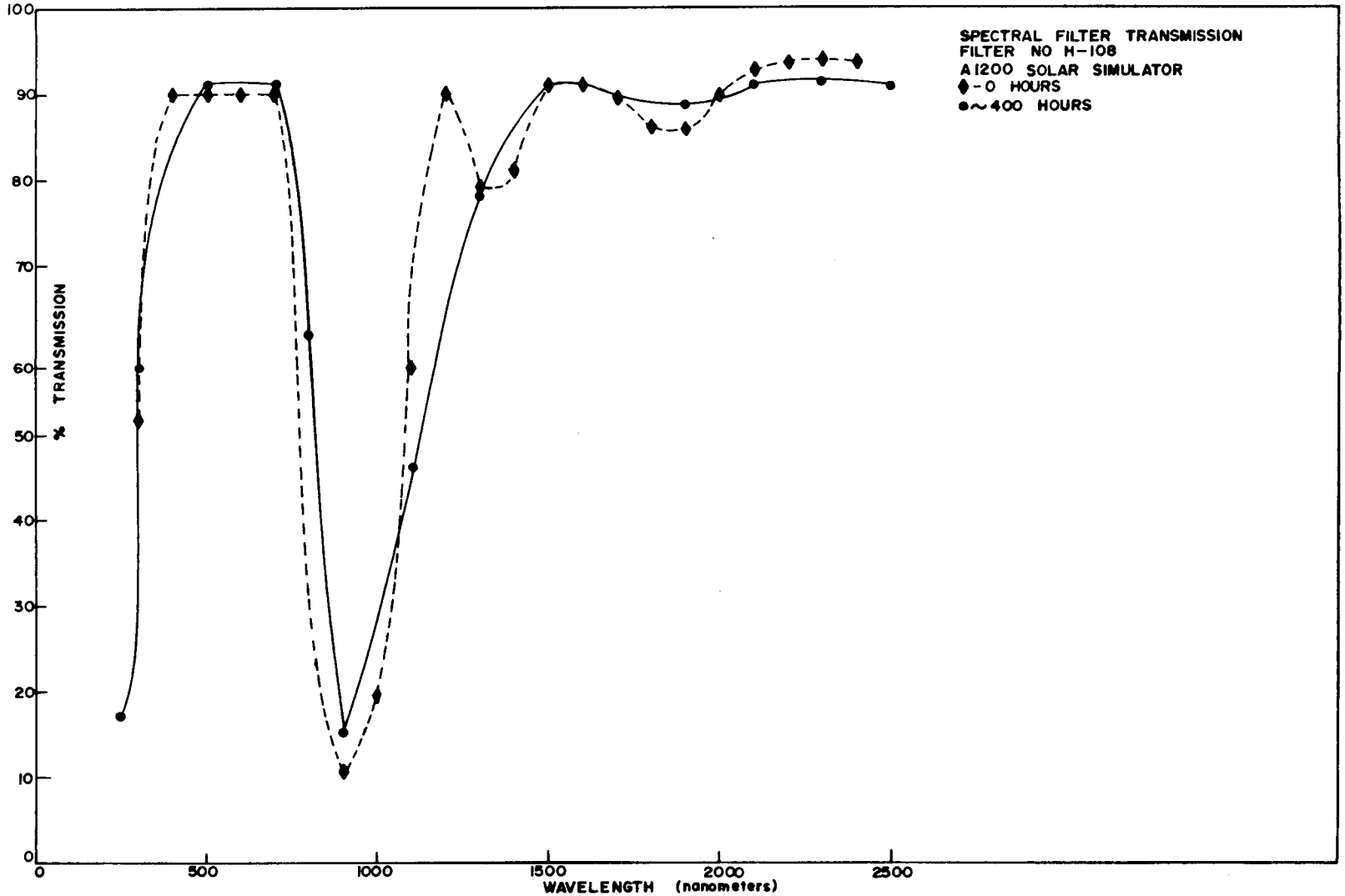

Figure 6. Transmission Curve of Spectral Filter—A1200 Solar Simulator

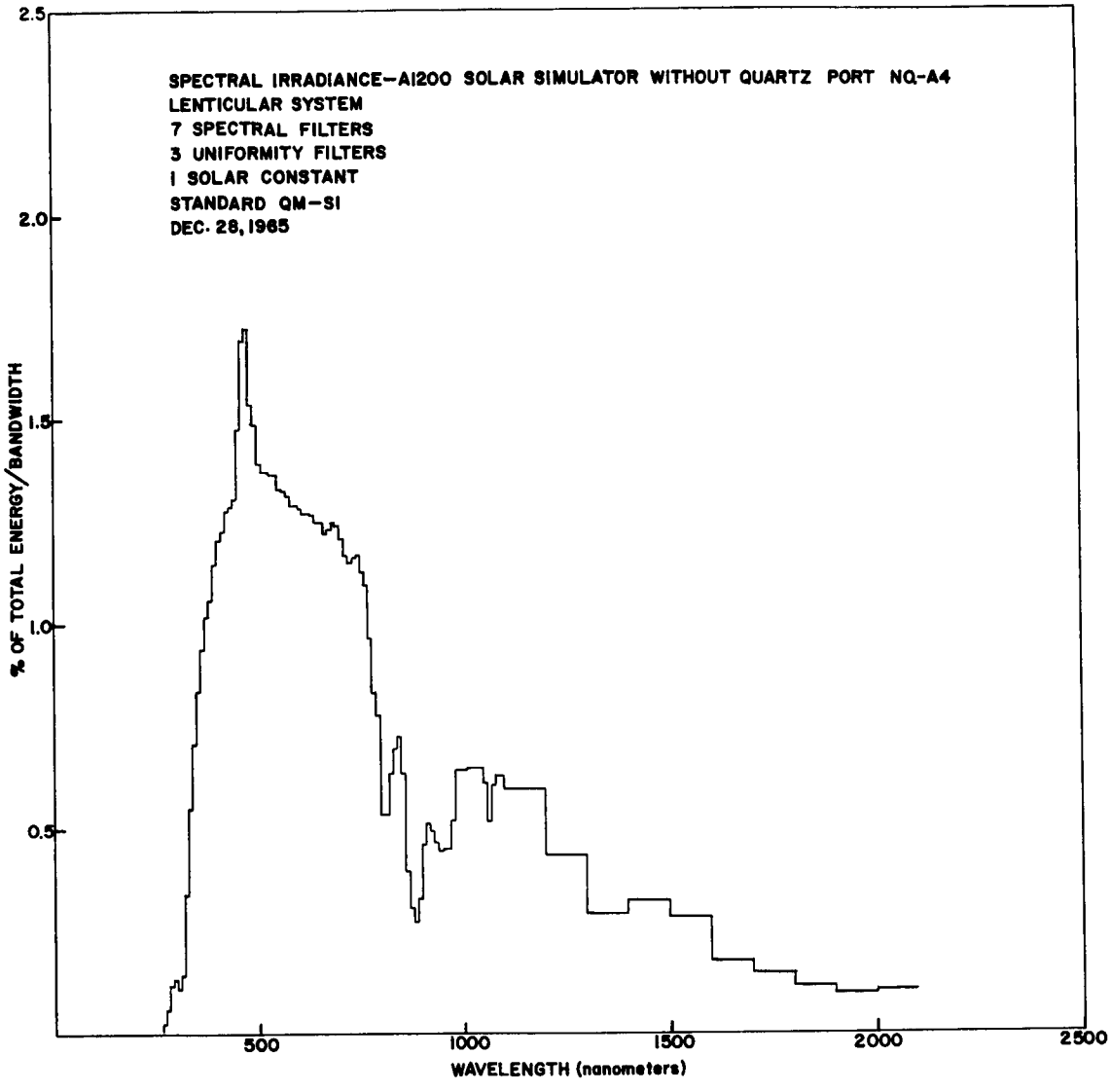

Figure 7. A1200 Spectral Irradiance—7 spectral filters

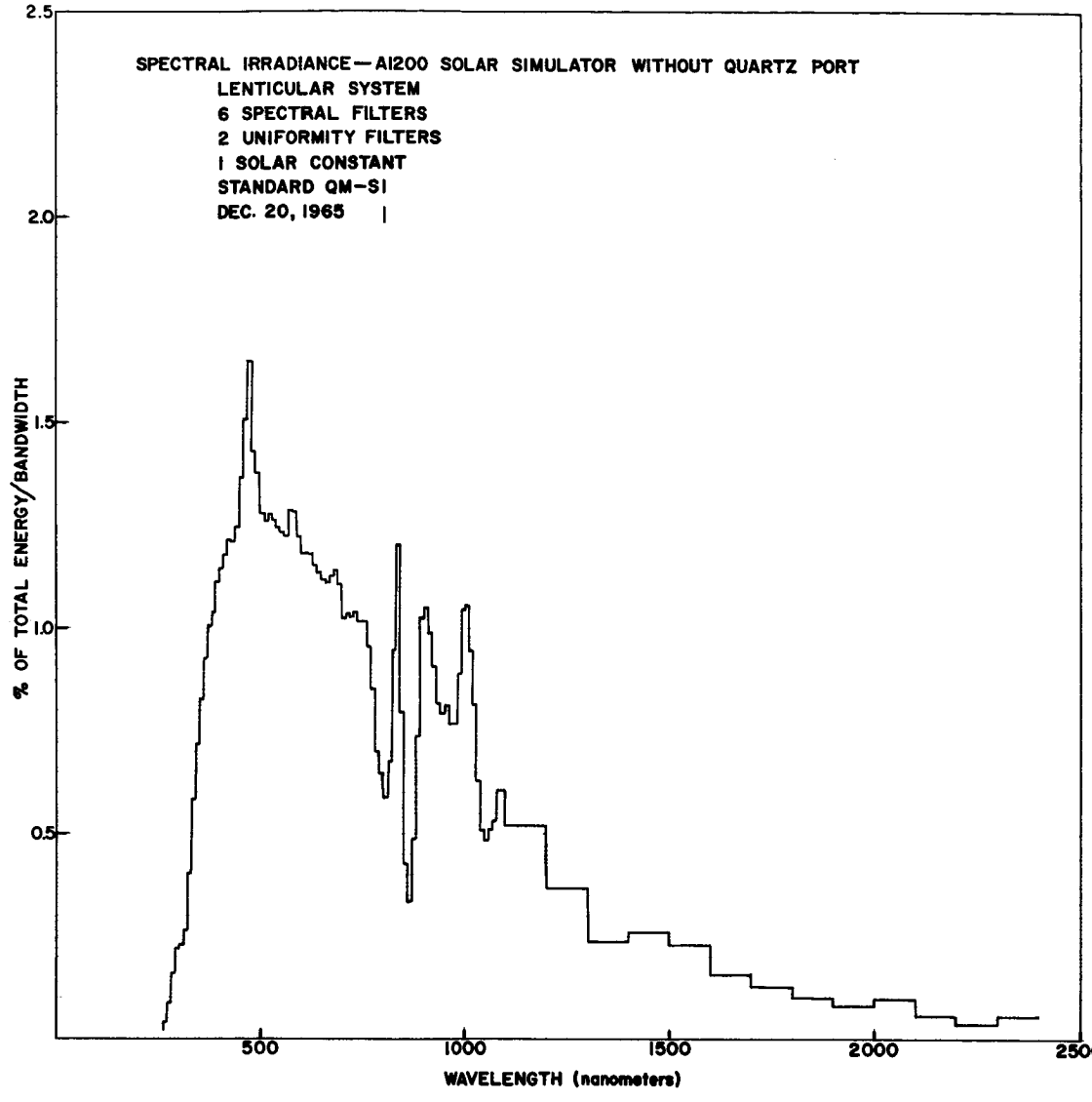

Figure 8. A1200 Spectral Irradiance—6 spectral filters

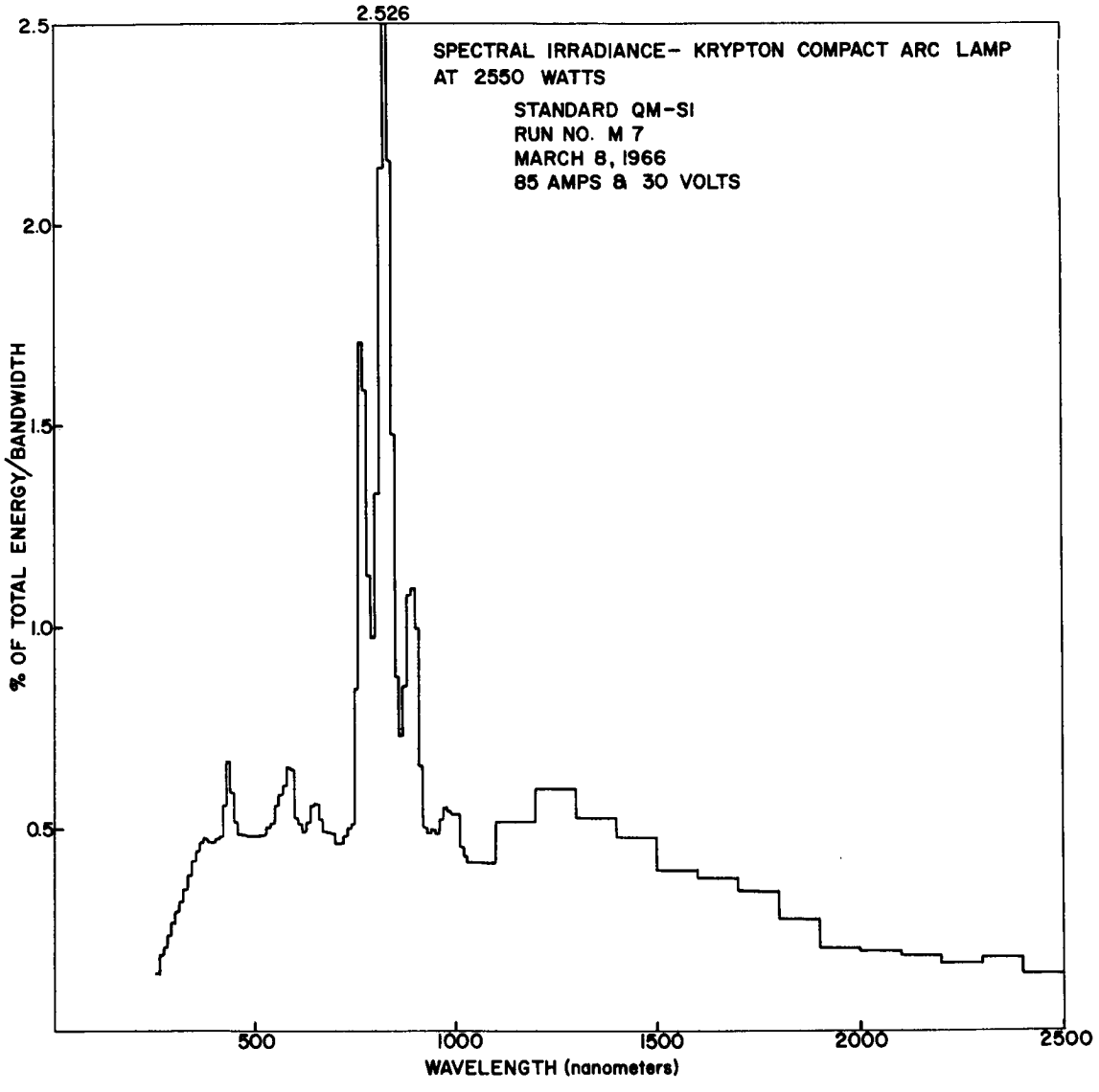

Figure 9. Spectral Irradiance—Krypton Arc Lamp

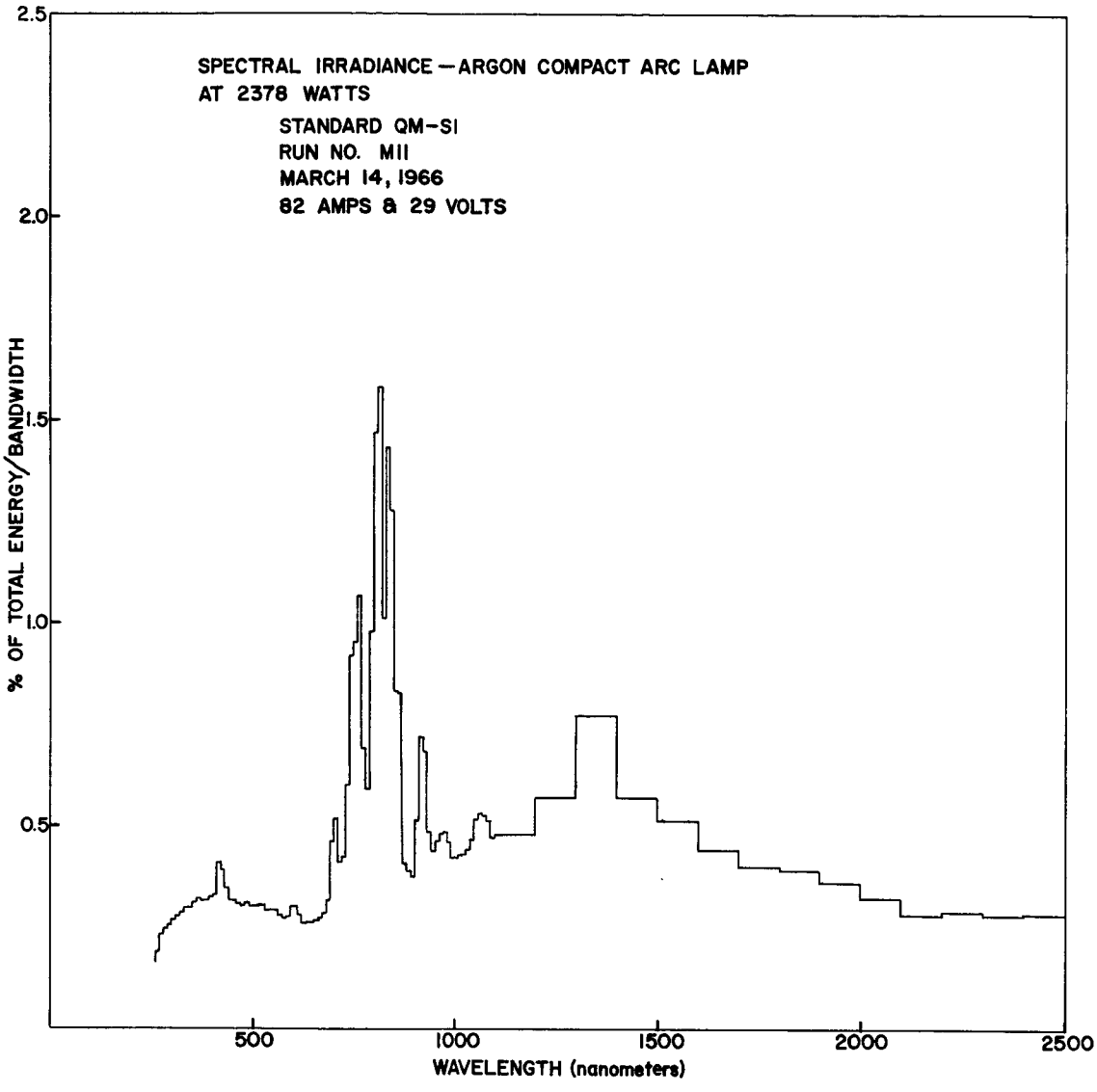

Figure 10. Spectral Irradiance—Argon Arc Lamp

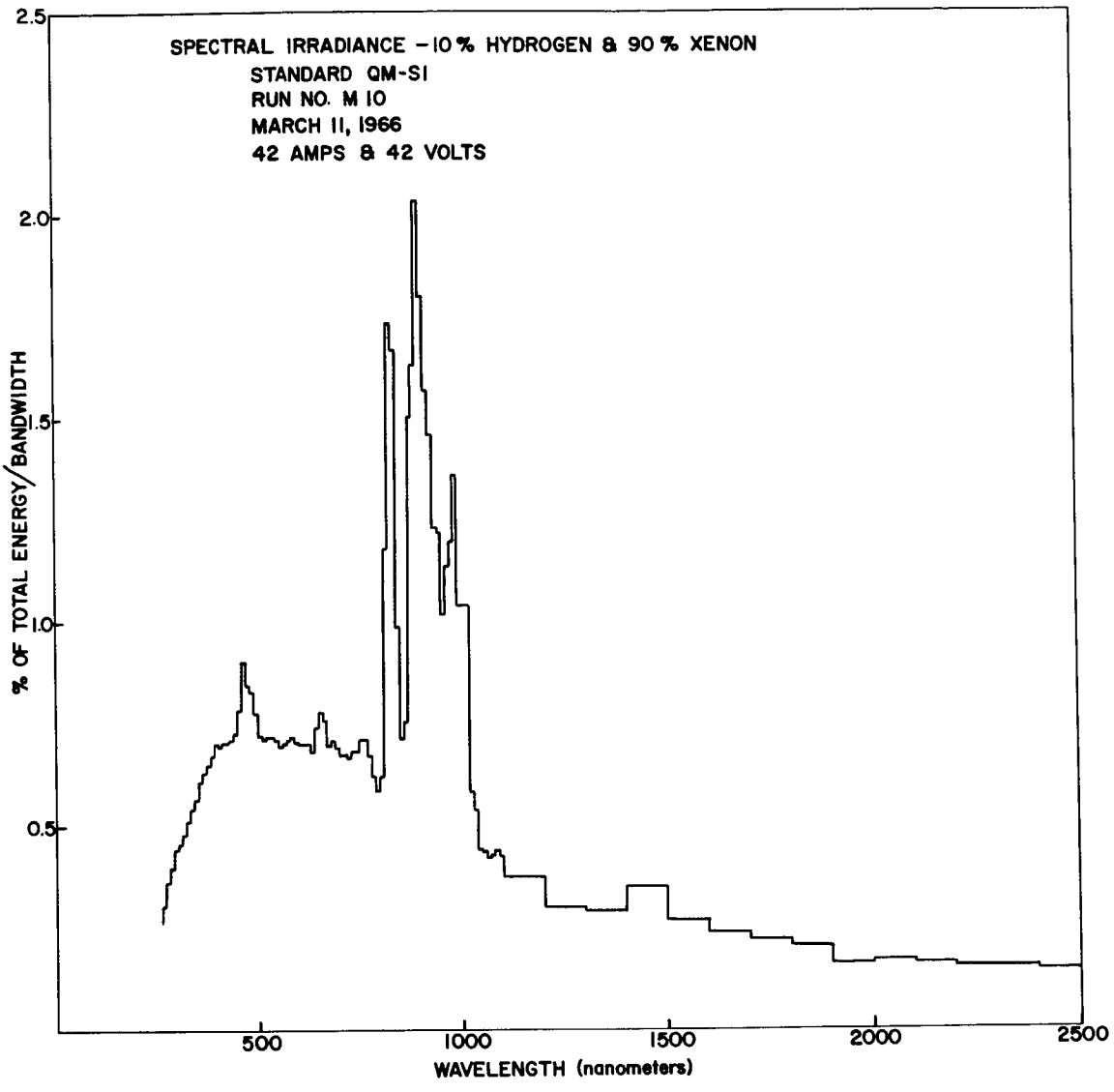

Figure 11. Spectral Irradiance—H-Xe Arc Lamp

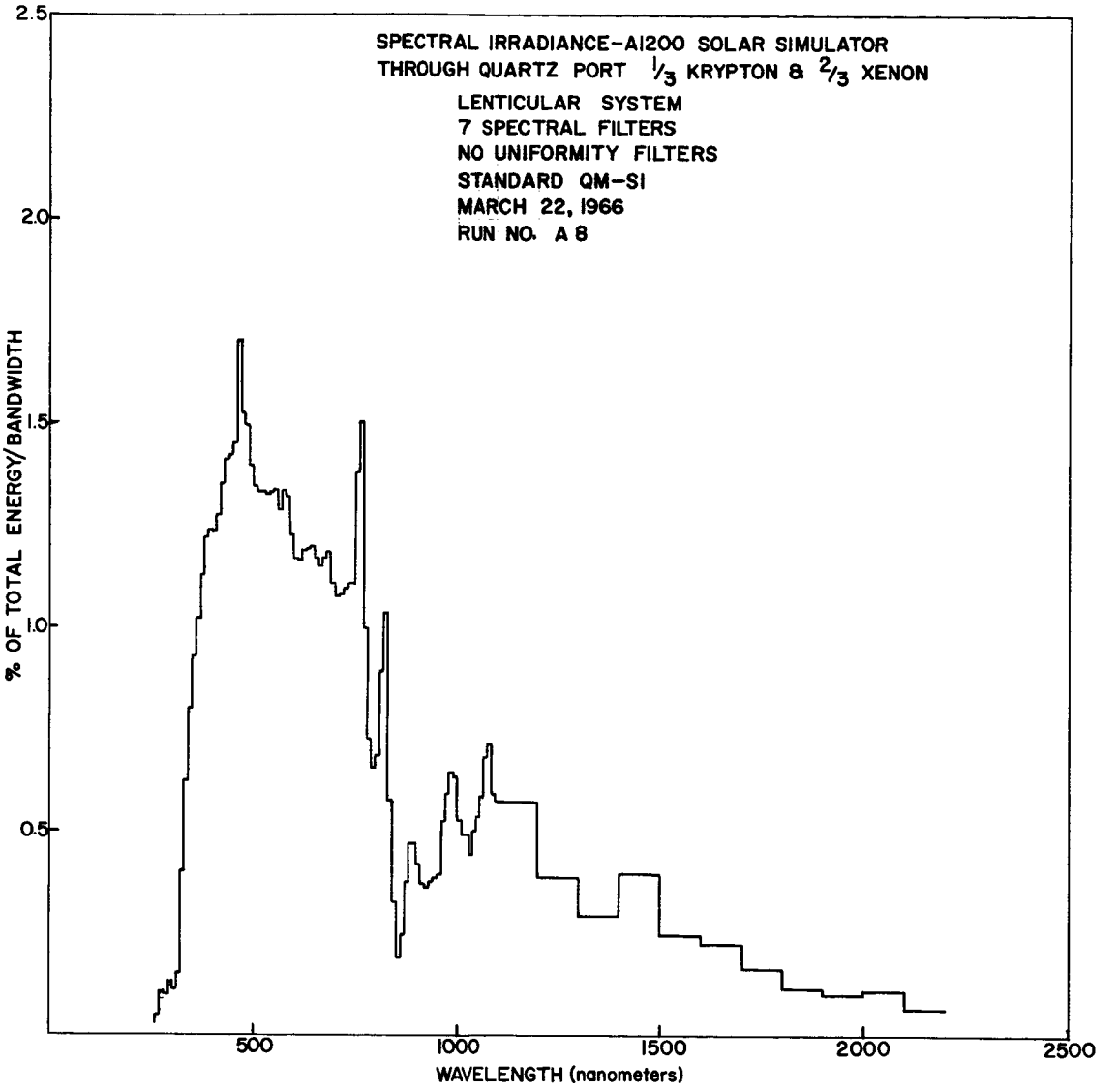

Figure 12. A1200 Spectral Irradiance—1/3 Krypton 2/3 Xenon

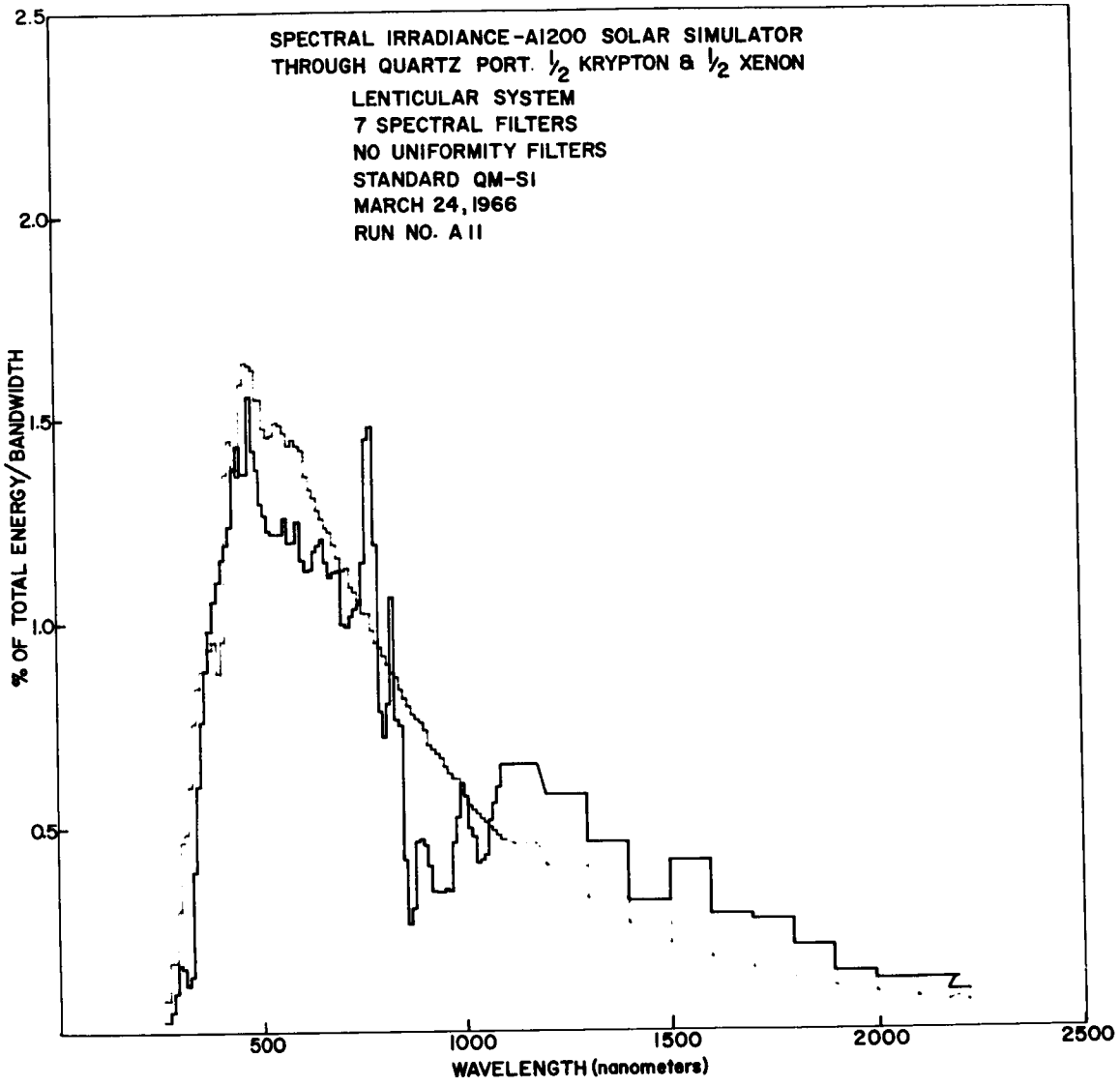

Figure 13. A1200 Spectral Irradiance—1/2 Krypton 1/2 Xenon

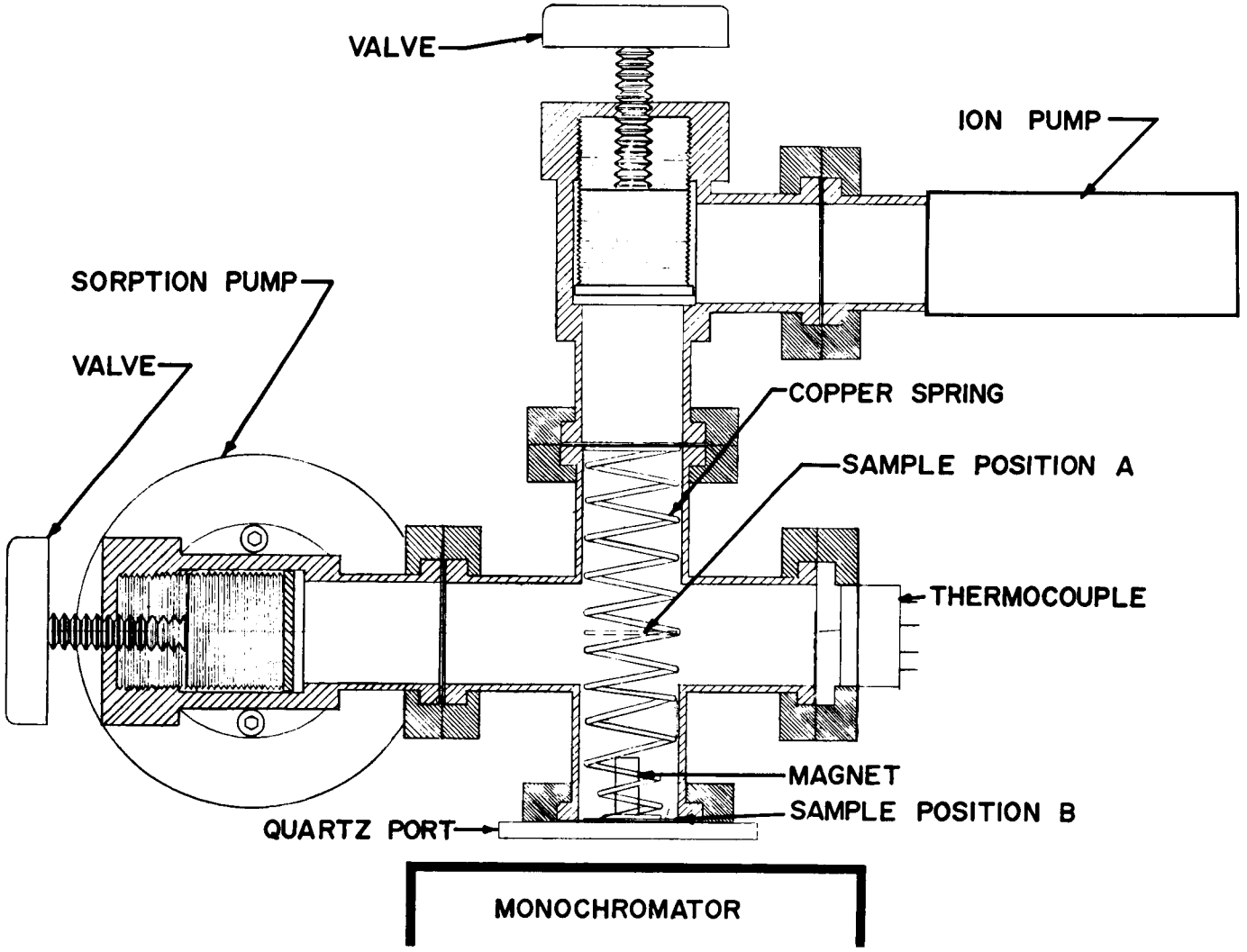

Figure 14. Vacuum Cell—Optical "In-Situ" Measurements System

APPENDIX I

SPECTRAL IRRADIANCE DATA—F-7

A 4 17XE7SPEC3UNIF LNO.1 S1

WAVELENGTH	TEST LAMP ENERGY PER 10NM WAVELENGTH INTERVAL	SOLAR ENERGY	RATIO	TESTLAMP/SOLAR
255.	0.008	0.074	0.11	
265.	0.022	0.169	0.13	
275.	0.059	0.169	0.35	
285.	0.120	0.296	0.41	
295.	0.134	0.465	0.29	
305.	0.109	0.486	0.23	
315.	0.144	0.602	0.24	
325.	0.348	0.760	0.46	
335.	0.565	0.845	0.67	
345.	0.724	0.887	0.82	
355.	0.853	0.887	0.96	
365.	0.959	0.940	1.02	
375.	1.032	0.961	1.07	
385.	1.064	0.876	1.21	
395.	1.148	0.961	1.19	
405.	1.201	1.372	0.88	
415.	1.224	1.457	0.84	
425.	1.272	1.383	0.92	
435.	1.278	1.362	0.94	
445.	1.295	1.594	0.81	
455.	1.467	1.647	0.89	
465.	1.677	1.636	1.02	
475.	1.707	1.626	1.05	
485.	1.520	1.552	0.98	
495.	1.470	1.552	0.95	
505.	1.366	1.478	0.92	
515.	1.335	1.457	0.92	
525.	1.330	1.467	0.91	
535.	1.322	1.499	0.88	
545.	1.318	1.489	0.89	
555.	1.300	1.467	0.89	
565.	1.297	1.436	0.90	
575.	1.297	1.457	0.89	
585.	1.295	1.436	0.90	
595.	1.295	1.425	0.91	
605.	1.294	1.362	0.95	
615.	1.293	1.330	0.97	
625.	1.293	1.309	0.99	
635.	1.288	1.277	1.01	
645.	1.271	1.256	1.01	
655.	1.271	1.235	1.03	
665.	1.247	1.225	1.02	
675.	1.256	1.193	1.05	
685.	1.274	1.161	1.10	
695.	1.269	1.130	1.12	
705.	1.236	1.140	1.08	
715.	1.196	1.087	1.10	
725.	1.175	1.077	1.09	
735.	1.184	1.056	1.12	
745.	1.188	1.024	1.16	
755.	1.150	1.024	1.12	
765.	1.120	0.982	1.14	
775.	0.985	0.950	1.04	
785.	0.849	0.940	0.90	
795.	0.792	0.918	0.86	
805.	0.542	0.897	0.60	
815.	0.542	0.876	0.62	
825.	0.646	0.866	0.75	
835.	0.710	0.834	0.85	
845.	0.744	0.813	0.92	
855.	0.646	0.792	0.82	
865.	0.405	0.771	0.53	
875.	0.364	0.760	0.48	
885.	0.277	0.750	0.37	
895.	0.336	0.728	0.46	
905.	0.471	0.697	0.68	
915.	0.523	0.686	0.76	
925.	0.506	0.676	0.75	
935.	0.478	0.665	0.72	
945.	0.454	0.644	0.70	
955.	0.459	0.623	0.74	
965.	0.460	0.612	0.75	
975.	0.529	0.612	0.86	
985.	0.656	0.581	1.13	
995.	0.656	0.570	1.15	
1005.	0.656	0.549	1.20	
1015.	0.655	0.538	1.22	
1025.	0.655	0.528	1.24	
1035.	0.655	0.517	1.27	
1045.	0.655	0.507	1.29	
1055.	0.616	0.496	1.24	
1065.	0.512	0.486	1.05	
1075.	0.597	0.475	1.26	
1085.	0.622	0.465	1.34	
1095.	0.622	0.454	1.37	
1150.	0.585	0.400	1.46	
1250.	0.426	0.320	1.33	
1350.	0.283	0.258	1.10	
1450.	0.321	0.209	1.54	
1550.	0.272	0.171	1.59	
1650.	0.173	0.141	1.22	
1750.	0.144	0.117	1.23	
1850.	0.110	0.098	1.12	
1950.	0.097	0.083	1.16	
2050.	0.106	0.071	1.49	

APPENDIX II

SPECTRAL IRRADIANCE DATA—F-8

A 3 17XE6SPEC3UNIF LNC.: S1

WAVELENGTH	TEST LAMP ENERGY PER 10NM WAVELENGTH INTERVAL	SOLAR ENERGY	RATIO	TESTLAMP/SOLAR
255.	0.016	0.073	0.23	
265.	0.037	0.166	0.22	
275.	0.085	0.166	0.51	
285.	0.162	0.291	0.56	
295.	0.223	0.457	0.49	
305.	0.233	0.478	0.49	
315.	0.267	0.593	0.45	
325.	0.411	0.748	0.55	
335.	0.596	0.832	0.72	
345.	0.732	0.873	0.84	
355.	0.846	0.873	0.97	
365.	0.944	0.925	1.02	
375.	1.017	0.946	1.07	
385.	1.045	0.863	1.21	
395.	1.112	0.946	1.18	
405.	1.143	1.351	0.85	
415.	1.174	1.435	0.82	
425.	1.209	1.362	0.89	
435.	1.203	1.341	0.90	
445.	1.234	1.570	0.79	
455.	1.351	1.622	0.83	
465.	1.490	1.611	0.92	
475.	1.633	1.601	1.02	
485.	1.414	1.528	0.93	
495.	1.357	1.528	0.89	
505.	1.256	1.455	0.86	
515.	1.228	1.435	0.86	
525.	1.238	1.445	0.86	
535.	1.217	1.476	0.82	
545.	1.201	1.466	0.82	
555.	1.197	1.445	0.83	
565.	1.201	1.414	0.85	
575.	1.277	1.435	0.89	
585.	1.283	1.414	0.91	
595.	1.232	1.403	0.88	
605.	1.198	1.341	0.89	
615.	1.201	1.310	0.92	
625.	1.207	1.289	0.94	
635.	1.176	1.258	0.94	
645.	1.158	1.237	0.94	
655.	1.140	1.216	0.94	
665.	1.133	1.206	0.94	
675.	1.151	1.175	0.98	
685.	1.166	1.143	1.02	
695.	1.132	1.112	1.02	
705.	1.047	1.123	0.93	
715.	1.058	1.071	0.99	
725.	1.048	1.060	0.99	
735.	1.060	1.040	1.02	
745.	1.034	1.008	1.03	
755.	1.032	1.008	1.02	
765.	0.972	0.967	1.01	
775.	0.869	0.936	0.93	
785.	0.713	0.925	0.77	
795.	0.658	0.904	0.73	
805.	0.597	0.884	0.68	
815.	0.689	0.863	0.80	
825.	0.964	0.852	1.13	
835.	1.228	0.821	1.49	
845.	0.809	0.800	1.01	
855.	0.435	0.780	0.56	
865.	0.338	0.759	0.45	
875.	0.494	0.748	0.66	
885.	0.752	0.738	1.02	
895.	1.047	0.717	1.46	
905.	1.072	0.686	1.56	
915.	1.005	0.676	1.49	
925.	0.923	0.665	1.39	
935.	0.830	0.655	1.27	
945.	0.807	0.634	1.27	
955.	0.829	0.613	1.35	
965.	0.782	0.603	1.30	
975.	0.785	0.603	1.30	
985.	0.907	0.572	1.59	
995.	1.064	0.561	1.90	
1005.	1.073	0.541	1.98	
1015.	0.959	0.530	1.81	
1025.	0.824	0.520	1.59	
1035.	0.634	0.509	1.25	
1045.	0.507	0.499	1.02	
1055.	0.483	0.489	0.99	
1065.	0.508	0.478	1.06	
1075.	0.527	0.468	1.13	
1085.	0.594	0.457	1.30	
1095.	0.594	0.447	1.33	
1150.	0.511	0.394	1.30	
1250.	0.357	0.315	1.13	
1350.	0.228	0.254	0.90	
1450.	0.239	0.206	1.16	
1550.	0.224	0.168	1.33	
1650.	0.152	0.139	1.09	
1750.	0.125	0.115	1.08	
1850.	0.097	0.097	1.01	
1950.	0.078	0.082	0.95	
2050.	0.094	0.070	1.35	
2150.	0.059	0.059	1.00	
2250.	0.035	0.051	0.68	
2350.	0.053	0.044	1.22	

APPENDIX III

SPECTRAL IRRADIANCE DATA—F-13

A B 10XE 5KR7SPECOUNIFHC3.6 LNO.1 S1

WAVELENGTH	TEST LAMP ENERGY PER 10NM WAVELENGTH INTERVAL	SOLAR ENERGY	RATIO TESTLAMP/SOLAR
255.	0.022	0.073	0.30
265.	0.049	0.168	0.29
275.	0.104	0.168	0.62
285.	0.099	0.294	0.34
295.	0.131	0.462	0.28
305.	0.113	0.483	0.23
315.	0.151	0.598	0.25
325.	0.399	0.756	0.53
335.	0.623	0.840	0.74
345.	0.800	0.882	0.91
355.	0.928	0.882	1.05
365.	1.022	0.934	1.09
375.	1.127	0.955	1.18
385.	1.220	0.871	1.40
395.	1.237	0.955	1.30
405.	1.236	1.364	0.91
415.	1.273	1.448	0.88
425.	1.350	1.375	0.98
435.	1.407	1.354	1.04
445.	1.421	1.585	0.90
455.	1.450	1.637	0.89
465.	1.702	1.627	1.05
475.	1.523	1.616	0.94
485.	1.492	1.543	0.97
495.	1.394	1.543	0.90
505.	1.342	1.469	0.91
515.	1.331	1.448	0.92
525.	1.331	1.459	0.91
535.	1.325	1.490	0.89
545.	1.330	1.480	0.90
555.	1.334	1.459	0.91
565.	1.284	1.427	0.90
575.	1.332	1.448	0.92
585.	1.319	1.427	0.92
595.	1.222	1.417	0.86
605.	1.167	1.354	0.86
615.	1.163	1.322	0.88
625.	1.184	1.301	0.91
635.	1.191	1.270	0.94
645.	1.196	1.249	0.96
655.	1.168	1.228	0.95
665.	1.149	1.217	0.94
675.	1.168	1.186	0.99
685.	1.184	1.154	1.03
695.	1.106	1.123	0.98
705.	1.075	1.133	0.95
715.	1.080	1.081	1.00
725.	1.096	1.070	1.02
735.	1.106	1.049	1.05
745.	1.103	1.018	1.08
755.	1.377	1.018	1.35
765.	1.504	0.976	1.54
775.	0.996	0.944	1.05
785.	0.724	0.934	0.78
795.	0.653	0.913	0.71
805.	0.683	0.892	0.77
815.	0.893	0.871	1.03
825.	1.037	0.861	1.21
835.	0.573	0.829	0.69
845.	0.325	0.808	0.40
855.	0.189	0.787	0.24
865.	0.245	0.766	0.32
875.	0.376	0.756	0.50
885.	0.470	0.745	0.63
895.	0.470	0.724	0.65
905.	0.419	0.693	0.60
915.	0.368	0.682	0.54
925.	0.360	0.672	0.54
935.	0.376	0.661	0.57
945.	0.383	0.640	0.60
955.	0.393	0.619	0.63
965.	0.522	0.609	0.86
975.	0.591	0.609	0.97
985.	0.644	0.577	1.12
995.	0.634	0.567	1.12
1005.	0.529	0.546	0.97
1015.	0.491	0.535	0.92
1025.	0.491	0.525	0.94
1035.	0.441	0.514	0.86
1045.	0.500	0.504	0.99
1055.	0.534	0.493	1.08
1065.	0.586	0.483	1.21
1075.	0.683	0.472	1.45
1085.	0.718	0.462	1.55
1095.	0.590	0.451	1.31
1150.	0.574	0.398	1.44
1250.	0.388	0.318	1.22
1350.	0.292	0.256	1.14
1450.	0.391	0.208	1.88
1550.	0.244	0.170	1.43
1650.	0.225	0.141	1.60
1750.	0.169	0.116	1.45
1850.	0.116	0.098	1.19
1950.	0.100	0.083	1.21
2050.	0.104	0.070	1.48
2150.	0.063	0.060	1.06

APPENDIX IV

SPECTRAL IRRADIANCE DATA—F-14

All 5KE 5KR7SPEC.UNIFHC2.4 LNO.1 S1

WAVELENGTH	TEST LAMP ENERGY PER 10NM WAVELENGTH INTERVAL	SOLAR ENERGY	RATIO TESTLAMP/SOLAR
255.	0.021	0.073	0.28
265.	0.047	0.168	0.28
275.	0.094	0.168	0.56
285.	0.162	0.294	0.55
295.	0.148	0.462	0.32
305.	0.105	0.483	0.22
315.	0.135	0.598	0.23
325.	0.399	0.756	0.52
335.	0.598	0.840	0.71
345.	0.757	0.882	0.86
355.	0.862	0.882	1.00
365.	0.980	0.934	1.05
375.	1.053	0.955	1.10
385.	1.101	0.871	1.26
395.	1.155	0.955	1.21
405.	1.191	1.364	0.87
415.	1.235	1.448	0.85
425.	1.374	1.375	1.00
435.	1.433	1.354	1.06
445.	1.361	1.585	0.86
455.	1.361	1.637	0.83
465.	1.554	1.627	0.96
475.	1.416	1.616	0.88
485.	1.371	1.543	0.89
495.	1.286	1.543	0.83
505.	1.259	1.469	0.86
515.	1.219	1.448	0.84
525.	1.212	1.459	0.83
535.	1.211	1.490	0.81
545.	1.215	1.480	0.82
555.	1.255	1.459	0.86
565.	1.198	1.427	0.84
575.	1.196	1.448	0.83
585.	1.247	1.427	0.87
595.	1.148	1.417	0.81
605.	1.121	1.354	0.83
615.	1.129	1.322	0.85
625.	1.174	1.301	0.90
635.	1.189	1.270	0.94
645.	1.209	1.249	0.96
655.	1.143	1.228	0.93
665.	1.105	1.217	0.91
675.	1.122	1.186	0.95
685.	1.124	1.154	0.97
695.	0.991	1.123	0.88
705.	0.984	1.133	0.87
715.	1.014	1.081	0.94
725.	1.033	1.077	0.96
735.	1.044	1.049	0.99
745.	1.146	1.018	1.13
755.	1.449	1.018	1.42
(765)	1.478	0.976	1.51
775.	1.184	0.944	1.25
785.	.775	0.934	0.83
795.	0.713	0.913	0.78
805.	0.801	0.892	0.90
815.	1.061	0.871	1.22
825.	0.753	0.861	0.87
835.	0.738	0.829	0.89
845.	.411	0.804	0.51
855.	0.255	0.787	0.32
865.	0.297	0.766	0.39
875.	0.461	0.756	0.61
885.	.466	0.745	0.63
895.	0.448	0.724	0.62
905.	0.398	0.693	0.57
915.	0.334	0.682	0.49
925.	0.333	0.672	0.50
935.	0.333	0.661	0.50
945.	0.344	0.640	0.54
955.	0.336	0.619	0.54
965.	0.458	0.609	0.75
975.	0.521	0.609	0.85
985.	0.603	0.577	1.04
995.	0.567	0.567	1.00
1005.	0.489	0.546	0.90
1015.	0.468	0.535	0.88
1025.	0.405	0.525	0.77
1035.	0.415	0.514	0.81
1045.	0.428	0.504	0.85
1055.	0.513	0.493	1.04
1065.	0.556	0.483	1.15
1075.	0.594	0.472	1.26
1085.	0.649	0.462	1.40
1095.	0.649	0.451	1.44
1150.	0.577	0.398	1.43
1250.	0.455	0.318	1.43
1350.	0.309	0.256	1.21
1450.	0.414	0.208	1.99
1550.	0.279	0.170	1.63
1650.	0.264	0.141	1.87
1750.	0.199	0.116	1.71
1850.	0.134	0.098	1.37
1950.	0.114	0.083	1.37
2050.	0.122	0.070	1.73
2150.	0.085	0.060	1.42

PART II

Section 2

ELECTRO-MAGNETIC MEASUREMENTS GROUP

Electro-Mechanical Research, Inc.

Vortex Arc, High Pressure Arc and Miscellaneous Solar Simulation Sources and Support Equipment

NASA Contract 5-9244

Submitted by
Roy McIntosh

Work Performed by

R. Urschel
S. Hall
D. Mosier
R. Stair

CONTENTS (continued)

CONTENTS

ILLUSTRATIONS

TABLES

ELECTRO-MAGNETIC MEASUREMENTS GROUP

Roy McIntosh

ABSTRACT

This report describes the solar simulation effort of the Electro-Magnetic Measurements Group, Space Sciences Department of Electro-Mechanical Research, Inc., from 1 November, 1965 to 1 December, 1966. Subjects discussed are the Vortex Stabilized Arc, the Pressure Arc Facility, spectral irradiance measurements of various light sources, and the G.E. ultra high vacuum system used in support of simulation testing. The Computer programming techniques for this simulation effort are described. Included also are the goals for the next quarter's work.

INTRODUCTION

As the problem of satellite thermal control increases in importance, ground based testing has become more essential. Since the passive thermal control of these satellites depends upon the incident solar irradiance, the solar simulation phase of environmental testing takes on prime importance. With the requirements for this type of simulation becoming more demanding, new and more effective sources are required. Two experimental light sources presently under investigation by the Electro-Magnetic Measurements Group are the Vortex Stabilized Arc and the High Pressure Arc. This report discusses arc theory and advantages, improvements, problems encountered and measurements made during the past year.

In addition, the Electro-Magnetic Measurements Group is responsible for spectral irradiance measurements made on all other light sources in the Thermophysics Branch of the Spacecraft Technology Division, NASA-GSFC. This includes the A1200 solar simulator, X-25L solar simulator, carbon arc, xenon compact short arc lamps, etc. The results of significant measurements obtained during the year are included within this report.

The Electro-Magnetic Measurements group is also responsible for supervising the operation and maintenance of the General Electric ultra high vacuum system. The systems theory, experiments performed and operational problems are discussed.

Computer programming improvements and techniques are also covered in some detail.

This report outlines the work performed by the Electro-Magnetic Measurements Group during the period from 1 November 1965 to 1 December 1966. Since the period of time is extensive the report covers only the most interesting and important portions of this effort. Next quarter's goals for the arc studies, spectral measurements, the high vacuum system, data reduction along with flight experiment for measuring the solar spectrum from the NASA Convair 990 are lastly presented.

Since this is the first quarterly report, it covers all the work done since the inception of the program, a period of some 13 months. In the future, quarterly reports will cover only a three month period.

VORTEX ARC

Advantages

The vortex stabilized arc offers several potential advantages as a source for solar simulation. The arc lamp is very small (5 cm long by 3 cm in diameter) but it is capable of operating up to 25kw in its present configuration and at even higher powers with modifications. Therefore, its power to size ratio is very large when compared with the short arc lamp systems (e.g., Xe and Hg-Xe short arcs, carbon arcs, etc.) presently used for solar simulation.

Additionally, the vortex arc offers the advantage that various pressures and gas mixtures may be examined without elaborate modifications or reconstructions. This is accomplished by continuously recirculating the gas through a closed system into which gas may be added or removed as desired. This permits tailoring the spectral output of the lamp with a view towards a closer solar match.

Operating Features

Figure 1 illustrates the configuration of the vortex arc lamp. The working gas is fed under pressure into the lamp through the "gas in" tube into the space between the two concentric quartz tubes. The gas then passes through four (4) nearly tangential holes in the cathode. This imparts a spiral motion (vortex) to the gas inside the inner quartz tube. The gas is then evacuated through a central bore in the anode into a water cooled heat exchanger. The arc chamber itself is approximately 5-1/2 cm long x 3 cm in diameter. Both the cathode and anode are made of high purity tungsten. The quartz tubes are General Electric type 208 or 204 quartz.

During operation the cathode and anode are water cooled and the gas is recirculated. The pressure within the arc chamber can be varied between approximately 60 and 300 p.s.i.g. The arc power level can be varied between approximately 2 and 25kw depending upon the electrode spacing, arc gas, and desired power levels. The arc is initiated by a 75kv high frequency igniter. Once the arc has been ignited the pressure and power settings are adjusted to the desired point and the spectral and/or total irradiance measurement may be begun.

Instrumentation Methods

1. Present Spectral Irradiance Instrumentation - Since it is possible to change the spectral output characteristics of the vortex lamp, it is important to

measure its spectral irradiance with changes in gas composition, gas pressure, power, etc. Spectral irradiance measurements are made (see Figure 2) by directing the light from either the vortex arc or a 1000 watt NBS traceable standard of spectral irradiance through a chopper (chopped at 11.3 c.p.s. or 34 c.p.s.) as it enters an integrating sphere coated to a depth of ≈4 mm with smoked magnesium oxide. This sphere provides the illumination for the slit of the Leiss double prism monochromator. Three detectors are used to cover the spectral range from 250 nm to 2500 nm. These are the 1P28 photomultiplier, a 7102 photomultiplier, and a 2 mm x 10 mm lead sulphide cell. Suitable overlap regions minimize errors in the wavelength where detector sensitivities are changing rapidly. The signals from the photodetector are passed through a preamplifier and an amplifier (Brower Laboratories Model 130) to synchronize the chopper with the input signal minimizing electrical bandwidth and noise problems. The output from the amplifier is recorded on a strip chart recorder. The wavelength mechanism of the associated monochromator is driven by a synchronous motor. The data is taken from the strip chart recorder, punched onto IBM cards, and processed on a 7094 DCS computing system. The reduced data from these measurements are compared with Johnson's data* or the Handbook of Geophysics** data and presented as test lamp energy, ratio of test lamp to solar energy, and relative spectral distribution. The data are presented in tabular and graphical format.

2. Measurement Technique Improvements - When the work on the vortex arc was begun spectral radiance (rather than spectral irradiance) measurements were made creating several problems. The use of the standard of spectral radiance required that a very small area of the tungsten filament be viewed by the monochromator necessitating extreme care with mirror and monochromator adjustments. If the proper filament area were not viewed, large errors were introduced. These problems were overcome by using the standard of spectral irradiance. Other difficulties arose when the standard of spectral irradiance was used. The use of this standard required a diffusing surface to illuminate the slit of the monochromator; a magnesium oxide coated sphere was chosen for this purpose. When this sphere was used the energy incident on the entrance slit of the monochromator reduced by at least two orders of magnitude. This required that a very stable and high gain amplifier be used to obtain a suitable photodetector signal. Electronics previously used proved unsatisfactory since at the two wavelength extremes (250 nm and 2500 nm) the weak signals could not be distinguished from the noise. Therefore, a Brower Laboratories Model 130 synchronous rectifier amplifier was obtained. Recent improvements in this

*Johnson, F.S., J. Meteorol., 11(6):431-439, December 1954.

**United States Air Force Handbook of Geophysics, Revised edition, p. 16-16, 1961.

amplifier overcoming early synchronization difficulties have resulted in good signals down to 250 nm. The noise level in the far infrared region is still excessive because of the PbS cell characteristics. Several types and sizes of PbS cells have been tried; however, it appears the only good solution to this problem is to use a liquid nitrogen cooled PbS cell. This will be tried during the next two quarters. In addition to the good signal to noise ratio provided by this amplifier good accuracy (1%) and linearity (1%) are obtained.

Another innovation which improved the measurement system was the introduction of a multidetector housing which contained all three photodetectors. Previously three separate housings were used. The multidetector housing has saved approximately 15-20 minutes per measurement since the housings did not have to be changed during the measurements. This saving is especially important since at high power levels the vortex arc electrodes degrade rapidly.

Accuracy of spectral measurements was improved by the addition of a neutral screen filter and filter holder. This arrangement permitted insertion of a filter in the proper location in front of the sphere. The filter is used in the visible portion of the spectrum where the intensity of the vortex arc lamp is quite large, keeping amplifier signals within reasonable limits in this spectral region.

A new pressure measuring gauge has been installed in the gas recirculation system. This is a Heiss bourdon type gauge registering pressures from vacuum (30 in. of Hg) to 300 p.s.i.g. This was a significant improvement since the gauge supplied with the original equipment was difficult to read and improperly positioned.

A compressor and appropriate plumbing were added during the past year so that gases such as xenon and krypton which are expensive could be recovered from the system and reused for other measurements.

Quick disconnect couplings were added to the water cooled protective housing which surrounds the arc lamp. These fittings allow the housing to be removed and replaced quickly without flooding the working area.

The Leiss double prism monochromator, while quite adequate for the ordinary spectral irradiance measurements, did not provide the resolution needed to study certain fine spectral line structures because of its prismatic operation. To serve this function a Jarrell Ash 0.5 meter Ebert scanning spectrometer was obtained. Since this is a grating instrument its resolution is quite good ($\approx$.2 A from 180 nm to 910 nm). A complete description of its characteristics may be found in Appendix I.

This instrument was also used for calibrating the wavelength of the Leiss double prism monochromator. This provided a much better calibration than that obtained by using a number of discrete lines whose wavelength may or may not be known accurately and interpolating for wavelengths between these lines.

3. Data Reduction Techniques - The data from the spectral irradiance measurements is taken from the strip chart recordings and coded onto IBM cards. This data is then processed on an IBM 7094 DCS computing system. After comparing the test lamp energy with the energy from the NBS traceable standard of spectral irradiance, the computer further compares this information with Johnson's solar data.* The resultant information is presented in tabular form as relative spectral distribution, energy per 10 nm bandwidths, and ratio of test lamp energy to Johnson's data.

At the same time this table is generated, a magnetic tape is produced by the computer which can be used to graphically display the data on an EAI 3440 digital plotter. An explanation of the computer program together with samples of the Fortran IV program, the tabular information, and the graphs is contained in Appendix II.

The automatic plotting of the spectral data was the most important data reduction improvement made. The quality and accuracy of the plots generated by the EAI 3440 digital plotter were at least as good as those done by hand; the time taken by the automatic plotter was less than 1/10 that required by hand.

Spectral Irradiance Measurements

1. Argon: Power-Pressure Series - A series of nine spectral irradiance measurements was made in the vortex stabilized arc using argon to determine the effect of different power levels and pressures on the argon spectrum relative to improving the solar spectral match of the arc.

Three low power runs were made (at 5kw) with pressures of 4, 8, and 16 atm. (Figures 3, 4, and 5). There were almost no differences in the three runs and it would appear that at this low power an increase in pressure within the limitations of the vortex arc system does not affect the argon spectrum.

The types of electrodes used were then changed and the low pressure run at 4 atm repeated with the new style electrodes (see Figure 6) to determine

*Handbook of Geophysics, ibid. p. II-72

what effects these experimental electrodes had upon the spectrum. The new style cathode had a flat snout on the end, whereas the old style was pointed. The new anode had a recessed plate within the gas exit bore while the old one had only an open bore. The results showed an increase in infrared emission apparently because of a higher operating temperature at the anode. The arc ran at a lower voltage with the new electrodes necessitating a higher current to obtain the same power level.

Two runs with the new electrodes were made at 10kw with pressures of 4 and 16 atm (See Figures 7 and 8). There were very large and as yet unexplainable differences between the two spectra. Neither of the runs can be correlated with any of the other data taken on the arc. The low pressure results (Figure 7) showed a higher UV content than was evidenced with any other combination of parameters; the high pressure run (Figure 8) showed a lower UV content than any other combination of parameters. Therefore, data from these runs are disregarded for the present time. The low pressure run (Figure 9) was repeated at a later date and the data obtained was more in line with previous results.

Two measurements were made at high power level (20kw) using the old electrodes, one at 8 atm and one at 16 atm (see Figures 10 and 11). The only differences between the two spectra was an apparent increase in the UV in the high pressure run. This is a small shift and is not considered significant without more data to support it.

Looking at the effects of an increase in power for the runs at 5, 10, and 20kw there is a broadening and a shift to lower wavelengths in the UV band. This is true regardless of pressure. The emission lines around 800 nm are lower in intensity and the emission above 950 nm is raised in intensity. These effects tend to improve the solar spectral match.

2. Argon: Variable Flow Rate - Five runs were made with argon at the lowest power obtainable to determine whether flow rate affects spectral emission around 800 nm (see Figures 12 through 16). Measurements were made from 350 nm to 1050 nm which covered the region of interest. These runs had to be made in the open loop mode because the flow rate cannot be changed in a closed system. Measurement time was kept short to reduce the gas consumption. The first two of these measurements were made using worn electrodes and a gas proportioner as a flow meter. The lowest flow obtained with these electrodes while still maintaining arc stability was 1560 cc/min (see Figure 12); the highest flow obtained with the flow meter was 2106 cc/min (see Figure 13). Runs were made at these flow rates but it was felt that there was not a sufficiently large rate change to draw definite conclusions. Therefore, new electrodes were

installed and the experiment repeated. The 1560 cc/min run was repeated (see Figure 14) to see if the new electrodes gave the same spectrum because the new cathode was out of round and the arc gap was smaller resulting in different current-voltage characteristics.

The new electrode configuration permitted obtainment of a flow rate of 474 cc/min (Figure 15). No significant differences were obtained. Then the flow meter was removed and the flow rate increased to the maximum rate for safe operation of the arc. This rate was estimated to be 2500 cc/min (see Figure 16).

3. Neon Runs - Two runs were made with neon at 10 atm, one at 4kw (see Figure 17) and one at 16kw (see Figure 18). The spectrum beyond 1200 nm could not be measured on the low power run because the signal was too small for detection; the spectrum below 300 nm was lost on the high power run because of arc failures. Therefore, the effects of increased power can be studied only in the region from 300 nm to 1200 nm. In this region the spectrum is raised considerably below 550 nm and the emission band from 550 to 700 nm is raised slightly.

Comparison of the solar spectral match of the neon measurements with argon measurements at the same operating conditions indicated that neon tends to fill in areas where the argon spectrum is lacking and vice verse. The UV band extends farther into the visible in argon than in neon. Neon has an emission band extending approximately from 550 nm to 700 nm, and a sharp emission line at about 850 nm while argon has an emission band approximately from 750 nm to 850 nm. Above 1000 nm the argon emission peaks at about 1350 nm while the neon emission dips there. The neon emission peaks at about 1850 nm and the argon emission dips at this point. These complementary regions indicated a proper combination of neon and argon gases would provide an improved solar spectral match.

4. Neon-Argon Runs - A total of five measurements were made on mixtures of neon and argon. Two measurements were made on a mixture of 75% argon - 25% neon at 8kw and 13kw respectively (see Figures 19 and 20). These data appeared similar to 100% argon runs. Apparently neon did not contribute to the spectrum at this low a concentration even at a high power level. Three measurements were made over a short spectral range (350-1050 nm) on mixtures containing 90%, 80%, and 50% neon respectively. The 90% neon spectrum (see Figure 21) appeared like a neon spectrum except that some of the argon structure at 400 - 500 nm and at 700 - 800 nm can be seen. The 80% neon spectrum (see Figure 22) had generally more UV and less near IR that the 90%. The 350 nm peak and 600-700 nm band of neon was decreased somewhat and

there was considerably more energy from the 700-800 nm band of argon. The 50% neon mixture (see Figure 23) looks almost like pure argon but with a narrower and lower UV band. A little of the 600-700 nm band of neon was still present.

The 80% neon - 20% argon mixture offered a somewhat better solar spectral match than either argon or neon alone at the same power level and pressure. Assuming that this mixture will change in spectrum with increased power in the same manner as argon or neon alone, a good spectral match at a high power level will be obtained. The corroding effect of neon on the electrodes has to be overcome prior to obtaining any significant gain in power level.

Test Observations

From the foregoing results with the vortex arc it would appear that this source shows considerable promise for solar simulation. Future experiments should be directed towards finding mixtures of gases providing an even better solar spectral match then the neon-argon mixture. For example, it would be desirable to find a gas which provides considerable emission in the 400 nm to 600 nm region filling in the neon-argon mixture gap and not too much emission in the region around 880 nm. This should, of course, be a gas without too many sharp, strong emission lines.

From experience with neon-argon mixtures it appears that inert gases do not change their spectral characteristics in mixtures although it is difficult to tell the proper percentage of gas needed to obtain a certain spectral contribution because of unequal gas excitation. A mixture of three or more gases may provide the best match. Considerable effort should be directed towards obtaining higher power levels with all gases, especially those which tend to corrode electrodes at high power levels.

Increasing pressure or varying the gas flow do not improve spectral distribution unless very large increases are made. These two methods, therefore, do not show as much promise as increasing power or finding better gas mixtures.

PRESSURE ARC FACILITY

Advantages

The pressure arc facility (PAF) offers another interesting approach to the development of solar simulation sources. With the PAF it is possible to study arcs of various gases at pressures to 5000 p.s.i.g. and power levels up to 5kw. As the pressure at which a gas arc operates increases the line structure

broadens and the line to continuum ratio of the spectral output approaches unity. Therefore, a study of high pressure arcs should provide valuable data as to whether large increases in pressure will offer any significant advantages in terms of solar simulation possibilities.

Operational Difficulties and Improvements

Much of the EMR effort during this past year has been devoted to making the PAF and its related system components operational, maintaining the system, and obtaining and reducing spectral irradiance measurements.

Considerable difficulty was encountered in keeping the system running. Replacement seals around the quartz windows (see Figure 24) are not repeatable and leaked almost continually. Several suggestions were obtained during meetings with the vendor's technical staff on several occasions; however, despite improvements window seals still leak at pressures above 1500 p.s.i.g.

Boron nitride insulators used around the electrical feedthroughs have also leaked. During complete chamber dismantling it was found that these insulators had cracked. The insulators were then replaced but because of inadequate design there is high probability that the boron nitride cracked after installation.

During the past year the vacuum pumping system has been completely reworked. This improved the speed with which the system can be evacuated; however, because of system leaks the ultimate pressure was still quite high. As a result a deposit of several oxides of tungsten often appeared on the walls and quartz windows of the arc chambers. This deposit may reduce electrode life and reduces the accuracy and precision of the spectral measurements.

Data Reduction

A major area related to work on the pressure arc has been to develop a computer program to reduce data from the spectral irradiance measurements using a magnetic tape data logging system. This system records wavelength, detector output, and amplifier gain on three channels of a magnetic tape recorder for both the pressure arc and NBS traceable standard of spectral irradiance over the wavelength region of 250 - 2500 nm. This information is then fed into a computer and a spectral irradiance distribution calculated. Once the calculations are made, the results are programmed and stored on another magnetic tape used to graph the data in the same format as outlined in the data reduction section of the vortex stabilized arc. To accomplish this end it was necessary to generate a complete computer program. This program has just been completed and it appears to function quite well. While time has not permitted completion

of these graphs, the spectral irradiance data (energy per 10 nm bandwidths and ratios test lamp to solar) for eight measurements is presented in Tables 1 to 8.

Spectral Irradiance Measurements

1. Argon Measurements - Six of the spectral measurements made thus far have been with argon gas and various arc parameters. The spectral measurements were made using the same measuring instrumentation outlined for the vortex arc system. The results of these measurements are tabulated in Tables 1 through 5 and also Table 8.

The arc performed about as expected with the argon line structure in the regions of 400 - 450 nm, 800 - 850 nm etc., quite pronounced at low pressures and powers. As the pressure was increased, the line structure broadened and the continuum radiation became more prominent. The pressure arc operates much as a compact short arc lamp. The gas does not recirculate so that the arc is fairly broad, and at low pressures, triangularly shaped with the base located near the anode. It was interesting to note that as the pressure was increased, the arc became more and more stable and narrowed considerably.

2. Hydrogen-Doped Argon Runs - Two measurements were made on the pressure arc with hydrogen-doped argon gas (94% argon, 6% hydrogen). This small percentage of hydrogen was used because hydrogen alone would have corroded the electrodes very rapidly. It was hoped that the hydrogen structure could be observed with this small amount of hydrogen present. In both a low pressure (300 p.s.i.g.) measurement and a high pressure measurement (1500 p.s.i.g.) two lines of the Paschen series of hydrogen, 4861 and 6563 Å were prominent in the spectrum. The data from these measurements is tabulated in Tables 6 and 7 respectively.

3. General Observations - Measurements with argon at pressures above 1600 p.s.i.g. and also measurements with other gases or gas mixtures should provide important additional information as to the future potential of this system as a solar simulation source.

During the month of September the pressure arc facility and its associated measurements were moved to the EMR building at College Park, Maryland. This work will be continued under a separate contract and progress will be reported as a part of this new contract.

A1200 SOLAR SIMULATOR

The Electro-Magnetic Measurements Group is responsible for making all spectral irradiance measurements on the A1200 solar simulator. Table 9 lists the spectral irradiance measurements made during the past year. Since a detailed description of the A1200 system data is included in the Thermal Laboratory Quarterly Report* only the list of tests conducted is hereby presented.

MISCELLANEOUS SPECTRAL IRRADIANCE MEASUREMENTS

In addition to measurements of the vortex arc, pressure arc, and solar simulator, the Electro-Magnetic Measurements group has also made many additional spectral irradiance measurements on various types of light sources. Table 10 lists these measurements with the appropriate parameters.

Several spectral measurements were made on mercury-xenon lamps. It is very difficult to analyze the spectrum of this type of lamp because the spectrum appears to change from one measurement to the next (evidenced by M-3 and M-4, both taken on the same 2.5kw lamp) and also from lamp to lamp (evidenced by M-15 through M-20, taken on six different 3.5kw lamps made by two different companies, G.E. and Hanovia).

Measurements of krypton lamps are quite interesting because they show promise for solar simulation when used in conjunction with other lamps, such as xenon.

The measurements on the X-25L solar simulator reveal that this usually very stable source with a good solar spectral match changes spectrum drastically when the optics become contaminated during normal use. Measurement M-12 was a routine check of the spectrum and M-13 was run after the optics had been cleaned. The latter illustrates how the spectral match was restored by this simple remedy.

Further details of the measurements on the experimental lamps can be found in Reference 3.

*Lillywhite, M., McIntosh, R., Lester, D., Proceedings at the AIAA/ASTM/IEE Space Simulation Conference, AIAA Log. #A1897.

GENERAL ELECTRIC ULTRA HIGH VACUUM CHAMBER

Operating Features

The General Electric Ultra High Vacuum (UHV) system combines the capability of simultaneously obtaining an ultra high vacuum ($<10^{-8}$ Torr) with the ability to illuminate one or more samples from a light source such as a solar simulator. This feature makes it particularly adaptable to the study of proposed or existing spacecraft thermal control coatings.

The vacuum system is completely clean since no oils or greases are used anywhere in the system. The pumping system consists of molecular sieve sorption roughing pumps, a 500 liter/sec ion pump, and a titanium sublimation pump. The system also contains a shroud which may be filled with liquid nitrogen or silicone oil. When the oil is used it is recirculated through a heat exchanger so that the vacuum shroud temperature may be controlled to ±5°C over the range -50°C to +250°C.

Experiments Performed

Several experiments were made using the G.E. system during the past year including the following:

ATS-B Thermal Coatings Experiment - solar simulation tests - 4 tests
ATS-A Thermal Coatings Experiment - solar simulation tests - 2 tests
STL Particle determination experiment - 3 tests
Coatings Degradation Experiments - AN-2A, -2B, -2C, -2D, AN-2-1A, AN-2-1B

Problems Encountered

The system experienced an initial contamination from a green oily substance and one of the first problems was to determine the origin of the contamination and to remove it from the system. The material was analyzed by X-ray diffraction techniques and found to be a resin bonded pigment. The coating which had been used on the shroud was Cat-a-lac black, a resin bonded pigment, and analysis revealed that this coating had produced the contaminant. The system was subsequently disassembled, the Cat-a-lac coating removed, and a new black silicate coating applied to the shroud. The system was reassembled and while performance was improved, it still experienced ion pump contamination. After installation of a new ion pump, system performance was significantly improved.

Late in this reporting period a problem developed with the shroud coating. Frequent routine high temperature bakeouts of the shroud had degraded the

adhesion of the paint to the point where it began to flake off in large quantities. Investigations are underway to find a more stable paint and it is felt that definite progress will be made toward the solution of the problem during the next quarter.

CONVAIR 990 SOLAR IRRADIANCE EXPERIMENT

During the past several months there has been a continuing dialogue among several investigators connected with the various areas of solar simulation at NASA-GSFC as to the need for additional information regarding the total and spectral irradiance of the sun in the vicinity of the earth. The data which are presently available have been obtained by many experimentors under widely varying conditions, so that significant uncertainties exist throughout this data. The uncertainties in the spectral irradiance vary from ±10% to ±40% depending on the wavelength of interest (infrared, visible, or ultraviolet). Since it is impossible to simulate a phenomenon, in this case the sun's irradiance, whose characteristics are not accurately known, an experiment has been proposed to study the solar irradiance from the NASA Convair 990.

The Convair experiment offers two important advantages. First, several instruments will be flown by several experimentors to study both the total and spectral irradiance of the sun. These instruments will be as follows:

Spectral irradiance - Leiss Double Prism Monochromator - Thermophysics
Eppley Mark V-A, filter radiometer - Thermophysics
Block P-4 and I-4 interferometer - spectrometers - T&E
Perkin Elmer 112 U grating monochromator - T&E
Electronic Scanning Spectrometer - Thermophysics

Total Irradiance - Eppley Thermopiles - T&E
Eppley Angstrom Compensated pyrheliometer - T&E
Cone Radiometer - T&E

The second advantage is that these experiments will all be done at the same time and under similar conditions.

The Electro-Magnetic Measurements group is responsible for performing the experiments with the Leiss monochromator and the Eppley Mark V-A Radiometer. This effort has begun and both experiments are in the planning stage. Considerable thought has been given to the types of equipment to be used and the instrument mounting techniques.

During the next quarter most of the final plans should be made and a more complete idea of the overall experiment will be available.

GOALS FOR NEXT QUARTER

Vortex Arc

During the next quarter, the vortex arc measurements program will continue with measurements on other inert gases starting with helium. Also, a study of the effect of gap length on current-voltage characteristics is planned using different cathode adapters to obtain the different gap lengths. Preparation will be made for installation of the 85kw arc to be delivered in the near future. Recalibration of the working standard used for the spectral irradiance measurements will be necessary before many more measurements can be made.

A program will be initiated to improve the data reduction of the vortex arc measurements by having the EAI plotter put the legends on the graphs and plot the data with a reduced scale for peaks which are off scale with the present plotting routine.

Miscellaneous Spectral Measurements

During the next quarter in addition to continuance of the routine measurements, an experiment has been planned to study further the degradation of the X-25L solar simulator. Its spectral irradiance will be measured at 0, 50, 100, and 300 hours. This will provide more complete data on how well the system performs spectrally and, therefore, determine what modifications to testing procedures will have to be made when using this simulator.

A series of experiments has also been planned to study the spectral degradation of a xenon lamp over a period of 1000 hours. Further, an experiment to simulate conditions inside the A1200 is planned to determine how the spectrum of this system will degrade over a period of 1000 hours.

General Electric Vacuum System

Several more coatings degradation experiments are scheduled for this system during the next quarter. When these experiments have been completed the system will be dismantled and the shroud repainted. It is hoped that this will be completed by the end of the next quarter.

Miscellaneous

A trip is scheduled for the end of December to the Ultek Corporation in Sunnyvale, California to assist in the preliminary acceptance tests of the eight vacuum pump modules which are being purchased by the Thermo Physics Branch, NASA-GSFC, to support the coatings qualification effort. A report will be prepared detailing the results of these tests.

Convair 990 Experiment

During the next quarter a suitable design of modifications to the Leiss double prism monochromator will be made so that safety requirements of the aircraft may be met. A mount for the Leiss will also be designed so that the monochromator may be pointed toward the sun. The same techniques will be used to measure the spectral irradiance of the sun as used for similar measurements of the vortex arc, pressure arc, etc., described earlier in this report.

Final decisions on the electronics, photodetectors, recorder, and other related equipment will be made during the next quarter. Also, final decisions will be made as to the specific measuring technique, e.g., will the sphere of the monochromator be illuminated directly or by mirrors.

Design modifications of the Eppley filter radiometer should be complete by the end of the next quarter. A choice of filters for the Mark V filter radiometer will be made during the next quarter.

Finally, engineering mockups of the experimental configurations will be made to ensure that no major difficulties have been overlooked.

CONCLUSIONS

The foregoing paragraphs have presented a general overview of the work which the Electro-Magnetic Measurements Group has performed under NASA Contract No. NAS 5-9244 in support of the solar simulation studies effort. The relative progress of the various projects covered under this contract was presented. There have been several significant accomplishments to the overall effort in the area of solar simulation.

Especially good UV solar spectral match of certain neon-argon mixtures were obtained with the vortex arc. The possibilities of spectral tailoring with this arc now appears even more promising.

The pressure arc system has been dismantled and moved to the EMR facility at College Park. The system is again operational and it is expected that some very interesting data may be obtained in the near future.

Spectral irradiance measurements have been made on the A1200 solar simulator during every test run. Modifications to this system are basically complete and further studies to improve the spectral character of the system to obtain an even better solar spectral match should be obtained.

The miscellaneous lamp studies which have been done have proven quite valuable. It has been determined that when krypton short arc lamps are used with xenon lamps the spectral match of the A1200 can be improved. Plans are already underway to utilize this combination of lamps.

The studies of the spectral degradation of the X-25L solar simulator have shown that care must be exercised even with this highly stable and dependable source.

The General Electric Ultra High Vacuum system has been an invaluable tool for coatings studies as well as solar simulation and environmental testing of satellite experiments. Plans are currently being implemented to recoat the shroud and clean the entire system.

Lastly, work has begun to study the solar spectrum from the NASA Convair 990 aircraft at an altitude of 40,000 feet. This study offers an exciting opportunity to obtain a relatively large amount of data at a relatively minimal cost. It also provides a better basis from which to decide whether a satellite experiment to study the sun's spectrum is necessary or desirable. Work will certainly continue on this experiment during the coming months.

Table 1
Pressure Arc, Argon 1540psig, 38V, 41.5A, 1.6kw

P-1 RUN 25ARGON 1540PSI 38V 41.5A LNO.1 S1 TAPEX344C,TD2890

WAVELENGTH	TEST LAMP ENERGY PER 10NM WAVELENGTH INTERVAL	SOLAR ENERGY	RATIO TESTLAMP/SOLAR
255.	1.029	0.091	11.26
265.	1.151	0.209	5.51
275.	1.271	0.209	6.08
285.	1.376	0.366	3.76
295.	1.409	0.574	2.45
305.	1.492	0.601	2.48
315.	1.540	0.744	2.07
325.	1.593	0.940	1.69
335.	1.612	1.045	1.54
345.	1.659	1.097	1.51
355.	1.685	1.097	1.54
365.	1.669	1.162	1.44
375.	1.617	1.188	1.36
385.	1.574	1.084	1.45
395.	1.556	1.188	1.31
405.	1.524	1.697	0.90
415.	1.549	1.802	0.86
425.	1.658	1.710	0.97
435.	1.506	1.684	0.89
445.	1.342	1.972	0.68
455.	1.279	2.037	0.63
465.	1.257	2.024	0.62
475.	1.233	2.011	0.61
485.	1.199	1.919	0.62
495.	1.171	1.919	0.61
505.	1.157	1.828	0.63
515.	1.121	1.802	0.62
525.	1.115	1.815	0.61
535.	1.061	1.854	0.57
545.	0.994	1.841	0.54
555.	0.957	1.815	0.53
565.	0.955	1.776	0.54
575.	0.951	1.802	0.53
585.	0.944	1.776	0.53
595.	0.944	1.763	0.54
605.	0.939	1.684	0.56
615.	0.895	1.645	0.54
625.	0.831	1.619	0.51
635.	0.790	1.580	0.50
645.	0.795	1.554	0.51
655.	0.790	1.528	0.52
665.	0.785	1.515	0.52
675.	0.795	1.475	0.54
685.	0.804	1.436	0.56
695.	0.990	1.397	0.71
705.	1.302	1.410	0.92
715.	1.117	1.345	0.83
725.	0.912	1.332	0.68
735.	1.293	1.306	0.99
745.	1.572	1.266	1.24
755.	2.087	1.266	1.65
765.	2.452	1.214	2.02
775.	2.356	1.175	2.01
785.	1.772	1.162	1.53
795.	1.236	1.136	1.09
805.	2.037	1.110	1.84
815.	3.020	1.084	2.79
825.	2.703	1.071	2.52

Table 1 (Continued)
Pressure Arc, Argon 1540psig, 38V, 41.5A, 1.6kw

835.	1.886	1.031	1.83
845.	2.170	1.005	2.16
855.	2.335	0.979	2.39
865.	1.887	0.953	1.98
875.	0.876	0.940	0.93
885.	0.707	0.927	0.76
895.	0.607	0.901	0.67
905.	0.546	0.862	0.63
915.	0.862	0.849	1.02
925.	1.313	0.836	1.57
935.	0.879	0.823	1.07
945.	0.731	0.796	0.92
955.	0.490	0.770	0.64
965.	0.541	0.757	0.71
975.	0.675	0.757	0.89
985.	0.663	0.718	0.92
995.	0.536	0.705	0.76
1005.	0.485	0.679	0.71
1015.	0.422	0.666	0.63
1025.	0.404	0.653	0.62
1035.	0.404	0.640	0.63
1045.	0.404	0.627	0.65
1055.	0.438	0.614	0.71
1065.	0.438	0.601	0.73
1075.	0.437	0.588	0.74
1085.	0.437	0.574	0.76
1090.	-0.000	-0.000	-0.00

Table 2

Pressure Arc, Argon 1000psig, 133.5V, 107.6A, 3.6kw

P 3ARGON 1000PSI 33.5V 107.6A LNO.1 S1

WAVELENGTH	TEST LAMP ENERGY PER 10NM WAVELENGTH INTERVAL	SOLAR ENERGY	RATIO TESTLAMP/SOLAR
255.	0.845	0.091	9.24
265.	0.941	0.209	4.50
275.	1.026	0.209	4.91
285.	1.108	0.366	3.03
295.	1.130	0.574	1.97
305.	1.198	0.601	1.99
315.	1.245	0.744	1.67
325.	1.290	0.940	1.37
335.	1.328	1.045	1.27
345.	1.350	1.097	1.23
355.	1.385	1.097	1.26
365.	1.367	1.162	1.18
375.	1.342	1.188	1.13
385.	1.318	1.084	1.22
395.	1.310	1.188	1.10
405.	1.302	1.697	0.77
415.	1.345	1.802	0.75
425.	1.410	1.710	0.82
435.	1.279	1.684	0.76
445.	1.188	1.972	0.60
455.	1.173	2.037	0.58
465.	1.145	2.024	0.57
475.	1.116	2.011	0.56
485.	1.086	1.919	0.57
495.	1.076	1.919	0.56
505.	1.069	1.828	0.58
515.	1.074	1.802	0.60
525.	1.082	1.815	0.60
535.	1.086	1.854	0.59
545.	1.071	1.841	0.58
555.	1.043	1.815	0.57
565.	1.036	1.776	0.58
575.	1.038	1.802	0.58
585.	1.041	1.776	0.59
595.	1.041	1.763	0.59
605.	1.029	1.684	0.61
615.	1.006	1.645	0.61
625.	0.964	1.619	0.60
635.	0.956	1.580	0.61
645.	0.952	1.554	0.61
655.	0.952	1.528	0.62
665.	0.952	1.515	0.63
675.	0.957	1.475	0.65
685.	0.975	1.436	0.68
695.	1.167	1.397	0.84
705.	1.427	1.410	1.01
715.	1.301	1.345	0.97
725.	1.191	1.332	0.89
735.	1.421	1.306	1.09
745.	1.682	1.266	1.33
755.	2.103	1.266	1.66
765.	2.172	1.214	1.79
775.	2.286	1.175	1.95
785.	1.823	1.162	1.57
795.	1.572	1.136	1.38
805.	1.845	1.110	1.66
815.	2.612	1.084	2.41
825.	2.478	1.071	2.31

Table 2 (Continued)
Pressure Arc, Argon 1000psig, 133.5V, 107.6A, 3.6kw

835.	1.982	1.031	1.92
845.	1.897	1.005	1.89
855.	2.053	0.979	2.10
865.	1.763	0.953	1.85
875.	1.033	0.940	1.10
885.	1.033	0.927	1.11
895.	0.812	0.901	0.90
905.	0.796	0.862	0.92
915.	0.912	0.849	1.07
925.	1.173	0.836	1.40
935.	1.086	0.823	1.32
945.	0.999	0.796	1.25
955.	0.732	0.770	0.95
965.	0.713	0.757	0.94
975.	0.819	0.757	1.08
985.	0.737	0.718	1.03
995.	0.711	0.705	1.01
1005.	0.711	0.679	1.05
1015.	0.711	0.666	1.07
1025.	0.711	0.653	1.09
1035.	0.711	0.640	1.11
1045.	0.633	0.627	1.01
1055.	0.620	0.614	1.01
1065.	0.650	0.601	1.08
1075.	0.650	0.588	1.11
1085.	0.644	0.574	1.12
1090.	-0.000	-0.000	-0.00

Table 3
Pressure Arc, Argon 1540psig, 38.6V, 115A, 4.4kw

10.00.00.00.79.80.00.10.10.10.10.10

WAVELENGTH	TEST LAMP ENERGY	SOLAR ENERGY	RATIO TEST LAMP/SOLAR
253.	0.453	0.031	14.70
258.	0.479	0.060	7.98
263.	0.497	0.089	5.56
268.	0.507	0.104	4.88
273.	0.527	0.102	5.17
278.	0.540	0.118	4.57
283.	0.569	0.158	3.60
288.	0.564	0.210	2.69
293.	0.586	0.264	2.22
298.	0.550	0.292	1.89
303.	0.590	0.296	1.99
308.	0.621	0.312	1.99
313.	0.605	0.349	1.74
318.	0.628	0.395	1.59
323.	0.633	0.445	1.42
328.	0.647	0.484	1.34
333.	0.650	0.510	1.28
338.	0.653	0.528	1.24
343.	0.658	0.541	1.22
348.	0.679	0.546	1.24
353.	0.683	0.545	1.25
358.	0.673	0.552	1.22
363.	0.672	0.570	1.18
368.	0.658	0.585	1.13
373.	0.644	0.592	1.09
378.	0.634	0.577	1.10
383.	0.632	0.549	1.15
388.	0.625	0.538	1.16
393.	0.618	0.563	1.10
398.	0.625	0.651	0.96
403.	0.613	0.784	0.78
408.	0.611	0.872	0.70
413.	0.613	0.896	0.68
418.	0.656	0.889	0.74
423.	0.644	0.864	0.75
428.	0.631	0.839	0.75
433.	0.611	0.831	0.74
438.	0.573	0.869	0.66
443.	0.553	0.945	0.59
448.	0.546	0.996	0.55
453.	0.541	1.011	0.53
458.	0.533	1.013	0.53
463.	0.532	1.009	0.53
468.	0.531	1.006	0.53
473.	0.517	1.004	0.52
478.	0.514	0.989	0.52
483.	0.515	0.965	0.53
488.	0.503	0.954	0.53
493.	0.499	0.955	0.52
498.	0.505	0.944	0.54
503.	0.515	0.920	0.56
508.	0.524	0.903	0.58
513.	0.535	0.897	0.60
518.	0.557	0.896	0.62
523.	0.565	0.899	0.63
528.	0.587	0.908	0.65
533.	0.603	0.918	0.66
538.	0.607	0.922	0.66
543.	0.629	0.918	0.69

Table 3 (Continued)
Pressure Arc, Argon 1540psig, 38.6V, 115A, 4.4kw

548.	0.621	0.913	0.68
553.	0.609	0.906	0.67
558.	0.601	0.897	0.67
563.	0.590	0.886	0.67
568.	0.588	0.885	0.66
573.	0.600	0.893	0.67
578.	0.594	0.894	0.66
583.	0.575	0.887	0.65
588.	0.592	0.882	0.67
593.	0.586	0.880	0.67
598.	0.588	0.868	0.68
603.	0.580	0.847	0.68
608.	0.580	0.831	0.70
613.	0.573	0.822	0.70
618.	0.559	0.815	0.69
623.	0.560	0.808	0.69
628.	0.536	0.800	0.67
633.	0.529	0.790	0.67
638.	0.530	0.782	0.68
643.	0.527	0.776	0.68
648.	0.522	0.769	0.68
653.	0.516	0.763	0.68
658.	0.510	0.758	0.67
663.	0.509	0.755	0.67
668.	0.515	0.749	0.69
673.	0.523	0.739	0.71
678.	0.528	0.729	0.72
683.	0.539	0.719	0.75
688.	0.540	0.708	0.76
693.	0.636	0.698	0.91
698.	0.721	0.696	1.03
703.	0.764	0.701	1.09
708.	0.740	0.694	1.07
713.	0.644	0.677	0.95
718.	0.582	0.666	0.87
723.	0.576	0.663	0.87
728.	0.621	0.660	0.94
733.	0.696	0.653	1.07
738.	0.802	0.644	1.25
743.	0.891	0.634	1.41
748.	0.964	0.630	1.53
753.	1.040	0.630	1.65
758.	1.116	0.624	1.79
763.	1.174	0.611	1.92
768.	1.202	0.598	2.01
773.	1.137	0.588	1.93
778.	0.950	0.582	1.63
783.	0.739	0.579	1.28
788.	0.666	0.575	1.16
793.	0.764	0.568	1.34
798.	0.959	0.562	1.71
803.	1.123	0.555	2.02
808.	1.243	0.548	2.27
813.	1.262	0.542	2.33
818.	1.189	0.537	2.20
823.	1.039	0.534	1.94
828.	0.926	0.528	1.75
833.	0.891	0.518	1.72
838.	0.954	0.509	1.87
843.	1.027	0.503	2.04
848.	1.035	0.497	2.08
853.	0.921	0.490	1.88
858.	0.789	0.483	1.63
863.	0.655	0.477	1.37
868.	0.562	0.472	1.19
873.	0.496	0.469	1.06

Table 3 (Continued)
Pressure Arc, Argon 1540psig, 38.6V, 115A, 4.4kw

878.	0.454	0.466	0.97
883.	0.421	0.463	0.91
888.	0.400	0.458	0.87
893.	0.392	0.452	0.87
898.	0.393	0.443	0.89
903.	0.422	0.433	0.97
908.	0.501	0.426	1.17
913.	0.593	0.423	1.40
918.	0.638	0.420	1.52
923.	0.623	0.417	1.49
928.	0.557	0.414	1.34
933.	0.484	0.411	1.18
938.	0.422	0.406	1.04
943.	0.384	0.400	0.96
948.	0.362	0.393	0.92
953.	0.367	0.386	0.95
958.	0.388	0.381	1.02
963.	0.414	0.378	1.10
968.	0.426	0.377	1.13
973.	0.414	0.377	1.10
978.	0.386	0.372	1.04
983.	0.370	0.362	1.02
988.	0.348	0.355	0.98
993.	0.329	0.352	0.93
998.	0.322	0.347	0.93
1050.	0.301	0.308	0.98

Table 4

Pressure Arc, Argon 1540psig, 37.6V, 79.6A, 3kw

10.00.00.0%.79.80.Cu.10.10.10.10.10

WAVELENGTH	TEST LAMP ENERGY	SOLAR ENERGY	RATIO TEST LAMP/SOLAR
253.	0.367	0.031	11.90
258.	0.397	0.060	6.61
263.	0.421	0.089	4.71
268.	0.439	0.104	4.22
273.	0.457	0.102	4.49
278.	0.482	0.118	4.08
283.	0.493	0.158	3.12
288.	0.506	0.210	2.41
293.	0.516	0.264	1.96
298.	0.497	0.292	1.71
303.	0.543	0.296	1.84
308.	0.564	0.312	1.80
313.	0.552	0.349	1.58
318.	0.569	0.395	1.44
323.	0.566	0.445	1.27
328.	0.586	0.484	1.21
333.	0.589	0.510	1.16
338.	0.594	0.528	1.12
343.	0.594	0.541	1.10
348.	0.613	0.546	1.12
353.	0.617	0.545	1.13
358.	0.623	0.552	1.13
363.	0.609	0.570	1.07
368.	0.604	0.585	1.03
373.	0.593	0.592	1.00
378.	0.591	0.577	1.02
383.	0.579	0.549	1.06
388.	0.579	0.538	1.07
393.	0.578	0.563	1.03
398.	0.581	0.651	0.89
403.	0.574	0.784	0.73
408.	0.570	0.872	0.65
413.	0.567	0.896	0.63
418.	0.646	0.889	0.72
423.	0.628	0.864	0.73
428.	0.600	0.839	0.71
433.	0.574	0.831	0.69
438.	0.546	0.869	0.63
443.	0.515	0.945	0.55
448.	0.511	0.996	0.51
453.	0.510	1.011	0.50
458.	0.501	1.013	0.49
463.	0.503	1.009	0.50
468.	0.494	1.006	0.49
473.	0.490	1.004	0.49
478.	0.483	0.989	0.49
483.	0.484	0.965	0.50
488.	0.487	0.954	0.51
493.	0.482	0.955	0.50
498.	0.486	0.944	0.51
503.	0.498	0.920	0.54
508.	0.505	0.903	0.56
513.	0.530	0.897	0.59
518.	0.546	0.896	0.61
523.	0.567	0.899	0.63
528.	0.591	0.908	0.65
533.	0.607	0.918	0.66
538.	0.619	0.922	0.67
543.	0.643	0.918	0.70
548.	0.616	0.913	0.67
553.	0.596	0.906	0.66

Table 4 (Continued)
Pressure Arc, Argon 1540psig, 37.6V, 79.6A, 3kw

558.	0.596	0.897	0.66
563.	0.588	0.886	0.66
568.	0.587	0.885	0.66
573.	0.585	0.893	0.66
578.	0.584	0.894	0.65
583.	0.581	0.887	0.66
588.	0.590	0.882	0.67
593.	0.581	0.880	0.66
598.	0.566	0.868	0.65
603.	0.574	0.847	0.68
608.	0.581	0.831	0.70
613.	0.560	0.822	0.68
618.	0.543	0.815	0.67
623.	0.530	0.808	0.66
628.	0.522	0.800	0.65
633.	0.516	0.790	0.65
638.	0.515	0.782	0.66
643.	0.507	0.776	0.65
648.	0.509	0.769	0.66
653.	0.498	0.763	0.65
658.	0.498	0.758	0.66
663.	0.494	0.755	0.65
668.	0.489	0.749	0.65
673.	0.489	0.739	0.66
678.	0.519	0.729	0.70
683.	0.512	0.719	0.71
688.	0.533	0.708	0.75
693.	0.624	0.698	0.89
698.	0.743	0.696	1.07
703.	0.783	0.701	1.12
708.	0.754	0.694	1.09
713.	0.641	0.677	0.95
718.	0.565	0.666	0.85
723.	0.561	0.663	0.85
728.	0.605	0.660	0.92
733.	0.706	0.653	1.08
738.	0.854	0.644	1.33
743.	0.951	0.634	1.50
748.	1.037	0.630	1.65
753.	1.164	0.630	1.85
758.	1.236	0.624	1.98
763.	1.309	0.611	2.13
768.	1.375	0.598	2.30
773.	1.305	0.588	2.22
778.	1.034	0.582	1.78
783.	0.793	0.579	1.37
788.	0.690	0.575	1.20
793.	0.796	0.568	1.40
798.	1.051	0.562	1.87
803.	1.295	0.555	2.33
808.	1.434	0.548	2.62
813.	1.523	0.542	2.81
818.	1.396	0.537	2.60
823.	1.182	0.534	2.21
828.	1.007	0.528	1.91
833.	0.985	0.518	1.90
838.	1.080	0.509	2.12
843.	1.198	0.503	2.38
848.	1.222	0.497	2.46
853.	1.062	0.490	2.17
858.	0.863	0.483	1.79
863.	0.695	0.477	1.46
868.	0.574	0.472	1.22
873.	0.495	0.469	1.06
878.	0.446	0.466	0.96
883.	0.402	0.463	0.87

Table 4 (Continued)
Pressure Arc, Argon 1540psig, 37.6V, 79.6A, 3kw

888.	0.380	0.458	0.83
893.	0.366	0.452	0.81
898.	0.362	0.443	0.82
903.	0.402	0.433	0.93
908.	0.504	0.426	1.18
913.	0.620	0.423	1.46
918.	0.696	0.420	1.65
923.	0.673	0.417	1.61
928.	0.591	0.414	1.43
933.	0.490	0.411	1.19
938.	0.415	0.406	1.02
943.	0.373	0.400	0.93
948.	0.345	0.393	0.88
953.	0.351	0.386	0.91
958.	0.381	0.381	1.00
963.	0.408	0.378	1.08
968.	0.426	0.377	1.13
973.	0.415	0.377	1.10
978.	0.382	0.372	1.03
983.	0.359	0.362	0.99
988.	0.330	0.355	0.93
993.	0.303	0.352	0.86
998.	0.295	0.347	0.85
1050.	0.290	0.308	0.94

Table 5
Pressure Arc, Argon 1540psig, 38.7V, 51.6A, 2kw

WAVELENGTH	TEST LAMP ENERGY	SOLAR ENERGY	RATIO TEST LAMP/SOLAR
253.	.348	.031	11.28
258.	.381	.060	6.34
263.	.393	.089	4.4
268.	.413	.114	3.97
273.	.423	.102	4.15
278.	.448	.118	3.79
283.	.465	.158	2.94
288.	.473	.21	2.25
293.	.48	.264	1.82
298.	.463	.292	1.59
303.	.497	.296	1.68
308.	.52	.312	1.67
313.	.507	.349	1.46
318.	.524	.395	1.33
323.	.525	.445	1.18
328.	.541	.484	1.12
333.	.541	.51	1.06
338.	.547	.528	1.04
343.	.552	.541	1.02
348.	.567	.546	1.04
353.	.571	.545	1.05
358.	.581	.552	1.05
363.	.569	.571	1.0
368.	.562	.585	0.96
373.	.544	.592	0.92
378.	.552	.577	0.96
383.	.543	.549	0.99
388.	.54	.538	1.0
393.	.546	.563	0.97
398.	.546	.651	0.84
403.	.539	.784	0.69
408.	.54	.872	0.62
413.	.534	.896	0.6
418.	.619	.889	0.70
423.	.60	.864	0.69
428.	.57	.839	0.68
433.	.551	.831	0.66
438.	.52	.869	0.6
443.	.488	.945	0.52
448.	.484	.996	0.49
453.	.484	1.11	0.48
458.	.476	1.13	0.47
463.	.475	1.19	0.47
468.	.47	1.26	0.47
473.	.465	1.24	0.46
478.	.464	.989	0.47
483.	.457	.965	0.47
488.	.458	.954	0.48
493.	.462	.955	0.49
498.	.465	.944	0.49
503.	.473	.92	0.51
508.	.498	.913	0.55
513.	.511	.897	0.57
518.	.534	.896	0.6
523.	.557	.899	0.62
528.	.571	.918	0.62
533.	.587	.918	0.64
538.	.595	.922	0.65
543.	.615	.918	0.67
548.	.594	.913	0.65

Table 5 (Continued)
Pressure Arc, Argon 1540psig, 38.7V, 51.6A, 2kw

553.	.582	.946	.64
558.	.559	.897	.62
563.	.573	.886	.65
568.	.558	.885	.63
573.	.562	.892	.63
578.	.56[illegible]	.894	.63
583.	.565	.887	.64
588.	.557	.882	.63
593.	.573	.886	.65
598.	.556	.868	.64
603.	.557	.847	.66
608.	.554	.831	.67
613.	.544	.823	.66
618.	.531	.815	.65
623.	.515	.808	.64
628.	.5[illegible]6	.8[illegible]	.63
633.	.5[illegible]	.79[illegible]	.63
638.	.497	.782	.64
643.	.495	.776	.64
648.	.5[illegible]1	.769	.65
653.	.487	.763	.64
658.	.477	.758	.63
663.	.476	.755	.63
668.	.469	.749	.63
673.	.474	.739	.64
678.	.494	.729	.68
683.	.5[illegible]3	.719	.7[illegible]
688.	.5[illegible]2	.708	.71
693.	.6[illegible]5	.698	.87
698.	.752	.696	1.08
703.	.799	.701	1.14
708.	.777	.694	1.12
713.	.652	.677	.96
718.	.559	.666	.84
723.	.555	.663	.84
728.	.598	.6[illegible]	.91
733.	.711	.653	1.09
738.	.886	.644	1.38
743.	.982	.634	1.55
748.	1.093	.63[illegible]	1.74
753.	1.238	.63[illegible]	1.96
758.	1.337	.624	2.14
763.	1.431	.611	2.34
768.	1.518	.598	2.54
773.	1.431	.588	2.43
778.	1.11[illegible]	.582	1.91
783.	.81[illegible]	.579	1.4[illegible]
788.	.681	.575	1.18
793.	.829	.568	1.46
798.	1.114	.562	1.98
803.	1.398	.555	2.52
808.	1.669	.548	3.04
813.	1.779	.542	3.28
818.	1.634	.537	3.04
823.	1.334	.534	2.5[illegible]
828.	1.1[illegible]	.528	2.09
833.	1.[illegible]41	.518	2.41
838.	1.2[illegible]6	.5[illegible]9	2.37
843.	1.4[illegible]7	.5[illegible]3	2.8[illegible]
848.	1.428	.497	2.87
853.	1.19[illegible]	.49[illegible]	2.43
858.	.923	.483	1.91
863.	.718	.477	1.51
868.	.583	.472	1.23
873.	.487	.469	1.04
878	.42[illegible]	.466	.9[illegible]

Table 5 (Continued)
Pressure Arc, Argon 1540psig, 38.7V, 51.6A, 2kw

[illegible]	[illegible]	[illegible]	[illegible]
883.	.387	.463	.84
888.	.359	.458	.78
893.	.344	.452	.76
898.	.343	.443	.77
903.	.298	.433	.92
908.	.54	.426	1.27
913.	.661	.423	1.56
918.	.742	.42	1.77
923.	.717	.417	1.72
928.	.6[illegible]	.414	1.45
933.	.482	.411	1.17
938.	.41[illegible]	.4[illegible]6	.99
943.	.36	.4[illegible]	.9
948.	.31[illegible]	.393	.81
953.	.328	.386	.85
958.	.369	.381	.97
963.	.40[illegible]	.378	1.06
968.	.425	.377	1.13
973.	.413	.377	1.09
978.	.379	.378	1.[illegible]
983.	.356	.362	.98
988.	.326	.355	.92
993.	.297	.352	.84
998.	.291	.347	.84
1[illegible]	.27[illegible]	.3[illegible]	.89

Table 6

Pressure Arc, .94 Argon, .06 Hydrogen, 300psig, 29.2V, 86A, 2.5kw

TABLE 6 ARGON 1ATM 14V 100A WATTS

WAVELENGTH	TEST LAMP ENERGY PER 10NM WAVELENGTH INTERVAL	SOLAR ENERGY	RATIOTESTLAMP/SOLAR
305.	0.979	0.617	1.59
315.	1.056	0.764	1.38
325.	1.019	0.965	1.06
335.	1.095	1.078	1.02
345.	1.231	1.126	1.09
355.	1.647	1.126	1.46
365.	1.233	1.193	1.03
375.	1.306	1.320	0.99
385.	1.191	1.113	1.07
395.	1.167	1.220	0.96
405.	1.249	1.743	0.72
415.	1.452	1.850	0.78
425.	1.518	1.756	0.86
435.	1.588	1.729	0.92
445.	1.550	2.024	0.77
455.	1.235	2.091	0.59
465.	1.252	2.078	0.60
475.	1.220	2.065	0.59
485.	1.256	1.971	0.64
495.	1.160	1.971	0.59
505.	1.122	1.877	0.60
515.	1.166	1.850	0.63
525.	1.185	1.864	0.64
535.	1.146	1.904	0.60
545.	1.174	1.890	0.62
555.	1.277	1.864	0.69
565.	1.314	1.823	0.72
575.	1.353	1.850	0.73
585.	1.411	1.823	0.77
595.	1.543	1.810	0.85
605.	1.722	1.729	1.00
615.	1.651	1.669	0.98
625.	1.501	1.662	0.90
635.	1.443	1.622	0.89
645.	1.443	1.595	0.90
655.	1.443	1.569	0.92
665.	1.526	1.555	0.98
675.	1.544	1.515	1.02
685.	1.544	1.475	1.05
695.	2.101	1.435	1.46
705.	2.124	1.448	1.47
715.	2.093	1.581	1.32
725.	2.603	1.367	1.90
735.	2.602	1.341	1.94
745.	2.313	1.300	1.78
755.	2.190	1.300	1.68
765.	2.190	1.247	1.76
775.	1.232	1.207	1.02
785.	1.296	1.193	1.09
795.	1.432	1.166	1.23
805.	1.432	1.140	1.26
815.	0.992	1.113	0.89
825.	0.727	1.099	0.66
835.	0.603	1.059	0.57
845.	0.549	1.032	0.53
855.	0.511	1.005	0.51
865.	0.365	0.979	0.37
875.	0.167	0.965	0.17
885.	0.167	0.932	0.18
895.	0.219	0.925	0.24

Table 6 (Continued)
Pressure Arc, .94 Argon, .06 Hydrogen, 300psig,
29.2V, 86A, 2.5kw

905.	0.230	0.885	0.26
915.	0.230	0.871	0.26
925.	0.229	0.858	0.27
935.	0.233	0.845	0.28
945.	0.342	0.819	0.42
955.	0.849	0.791	1.07
965.	0.866	0.778	1.11
975.	1.335	0.778	1.72
985.	1.335	0.737	1.81
995.	1.148	0.724	1.59
1005.	1.032	0.697	1.48
1015.	1.032	0.684	1.51
1025.	1.032	0.670	1.54
1035.	1.686	0.657	2.57
1045.	2.492	0.644	3.87
1055.	2.797	0.630	4.44
1065.	3.595	0.617	5.83
1075.	-0.000	-0.000	-0.00
1085.	-0.000	-0.000	-0.00
1095.	-0.000	-0.000	-0.00

Table 7

Pressure Arc, .94 Argon, .06 Hydrogen, 1500psig, 50V, 50A, 2.5kw

H DOPED ARGON 300psig 29.2V 86A

WAVELENGTH	TEST LAMP ENERGY	SOLAR ENERGY	RATIO TEST LAMP/SOLAR
263.	.197	[illegible]	2.36
268.	[illegible].288	[illegible].111	2.59
273.	[illegible].314	[illegible].109	2.89
278.	[illegible].484	[illegible].126	3.85
283.	[illegible].394	[illegible].168	2.34
288.	[illegible].346	[illegible].224	1.54
293.	[illegible].362	[illegible].281	1.29
298.	[illegible].355	[illegible].311	1.14
303.	[illegible].396	[illegible].316	1.26
308.	[illegible].426	[illegible].333	1.28
313.	[illegible].428	[illegible].372	1.15
318.	[illegible].456	[illegible].421	1.08
323.	[illegible].466	[illegible].474	0.98
328.	[illegible].492	.516	0.95
333.	[illegible].513	.544	0.94
338.	[illegible].53[illegible]	[illegible].564	0.94
343.	[illegible].545	[illegible].577	0.94
348.	[illegible].57[illegible]	[illegible].582	0.98
353.	[illegible].591	[illegible].581	1.02
358.	.613	[illegible].589	1.04
363.	[illegible].637	[illegible].608	1.05
368.	[illegible].637	[illegible].624	1.02
373.	[illegible].6[illegible]5	[illegible].631	0.96
378.	[illegible].618	[illegible].616	1.00
383.	[illegible].623	[illegible].585	1.06
388.	.627	[illegible].574	1.09
393.	[illegible].637	[illegible].60[illegible]	1.06
398.	[illegible].643	[illegible].694	0.93
403.	[illegible].645	[illegible].836	0.77
408.	[illegible].649	[illegible].93[illegible]	0.70
413.	.647	.956	0.68
418.	[illegible].795	[illegible].948	0.84
423.	[illegible].75[illegible]	[illegible].922	0.81
428.	[illegible].742	[illegible].895	0.83
433.	[illegible].731	[illegible].886	[illegible].83
438.	.674	[illegible].927	[illegible].73
443.	[illegible].61[illegible]	1.[illegible]08	0.61
448.	[illegible].584	1.[illegible]63	0.55
453.	.587	1.[illegible]79	0.54
458.	.573	1.[illegible]81	[illegible].53
463.	[illegible].573	1.[illegible]77	0.53
468.	.572	1.[illegible]73	[illegible].53
473.	.586	1.[illegible]71	[illegible].55
478.	[illegible].635	1.[illegible]55	1.60
483.	[illegible].768	1.[illegible]29	[illegible].75
488.	[illegible].854	1.[illegible]17	[illegible].84
493.	.731	1.[illegible]19	0.72
498.	[illegible].62[illegible]	1.[illegible]7	0.62
503.	.566	[illegible].982	0.58
508.	[illegible].54	[illegible].963	[illegible].56
513.	[illegible].531	[illegible].957	[illegible].55
518.	.533	.956	0.56
523.	[illegible].53[illegible]	[illegible].959	[illegible].55
528.	[illegible].527	.968	[illegible].54
533.	[illegible].515	.979	[illegible].53
538.	[illegible].493	[illegible].984	[illegible].5[illegible]
543.	[illegible].492	[illegible].98[illegible]	[illegible].5[illegible]
548.	[illegible].491	.974	[illegible].5[illegible]
553.	[illegible].484	[illegible].967	[illegible].5[illegible]
558.	[illegible].487	[illegible].957	[illegible].5[illegible]

Table 7 (Continued)

Pressure Arc, .94 Argon, .06 Hydrogen, 1500psig, 50V, 50A, 2.5kw

563.	.489	.946	.52
568.	.463	.945	.49
573.	.485	.952	.51
578.	.461	.954	.48
583.	.478	.946	.51
588.	.49	.941	.52
593.	.497	.938	.53
598.	.488	.926	.53
603.	.500	.944	.56
608.	.524	.887	.59
613.	.496	.877	.57
618.	.485	.869	.56
623.	.476	.862	.55
628.	.451	.854	.53
633.	.475	.843	.56
638.	.473	.834	.57
643.	.521	.827	.63
648.	.615	.823	.74
653.	1.067	.813	1.31
658.	1.881	.859	2.33
663.	1.681	.856	2.09
668.	.947	.799	1.18
673.	.611	.788	.76
678.	.535	.777	.69
683.	.513	.767	.67
688.	.508	.756	.67
693.	.588	.745	.79
698.	.708	.743	.95
703.	.741	.747	.99
708.	.741	.741	1.00
713.	.645	.722	.89
718.	.534	.711	.75
723.	.52	.707	.74
728.	.563	.704	.80
733.	.639	.697	.92
738.	.862	.687	1.27
743.	.939	.676	1.39
748.	1.079	.672	1.51
753.	1.159	.673	1.72
758.	1.255	.666	1.88
763.	1.323	.652	2.02
768.	1.416	.638	2.21
773.	1.419	.628	2.25
778.	1.271	.621	1.78
783.	.756	.618	1.23
788.	.612	.613	1.00
793.	.72	.616	1.19
798.	1.029	.599	1.72
803.	1.312	.592	2.22
808.	1.649	.585	2.82
813.	1.917	.578	3.32
818.	1.824	.573	3.18
823.	1.396	.571	2.45
828.	1.041	.563	1.85
833.	.933	.553	1.69
838.	1.198	.543	2.13
843.	1.451	.536	2.71
848.	1.512	.53	2.85
853.	1.264	.523	2.42
858.	.925	.516	1.79
863.	.733	.509	1.44
868.	.587	.503	1.17
873.	.523	.504	1.04
878.	.478	.497	.96
883.	.448	.494	.91
888.	.42	.489	.86

Table 7 (Continued)
Pressure Arc, .94 Argon, .06 Hydrogen, 1500psig, 50V, 50A, 2.5kw

893.	.424	.482	[illegible]
898.	.428	.473	[illegible]
[illegible]	.449	.462	[illegible]
908.	.558	.455	1.23
913.	.687	.451	1.52
918.	.81[illegible]	.448	1.81
923.	.784	.445	1.76
928.	.7[illegible]	.442	1.58
933.	.59[illegible]	.438	1.35
938.	.488	.433	1.13
943.	.446	.426	1.05
948.	.426	.419	1.02
953.	.427	.412	1.04
958.	.459	.4[illegible]6	1.13
963.	.491	.4[illegible]3	1.22
968.	.51[illegible]	.4[illegible]2	1.27
973.	.514	.4[illegible]3	1.28
978.	.485	.397	1.22
983.	.477	.386	1.23
988.	.434	.379	1.15
993.	.42[illegible]	.376	1.12
998.	.4[illegible]2	.371	1.[illegible]8
[illegible]	[illegible]	.237	-[illegible]

Table 8
Pressure Arc, Argon, 15psig, 14V, 100A, 1.4kw

P-1(WAVELENGTH	RUN 38 HAR 1500 PSI 30V 50A LNO.1 5L TEST LAMP ENERGY PER 10NM WAVELENGTH INTERVAL	SOLAR ENERGY	RATIO	TESTLAMP/SOLAR
255.	1.002	0.097	10.34	
265.	1.130	0.221	5.10	
275.	1.200	0.221	5.42	
285.	1.303	0.387	3.36	
295.	1.308	0.609	2.15	
305.	1.353	0.637	2.12	
315.	1.384	0.789	1.75	
325.	1.417	0.996	1.42	
335.	1.442	1.107	1.30	
345.	1.492	1.162	1.28	
355.	1.527	1.162	1.31	
365.	1.503	1.231	1.22	
375.	1.464	1.259	1.16	
385.	1.431	1.148	1.25	
395.	1.423	1.259	1.13	
405.	1.415	1.799	0.79	
415.	1.467	1.910	0.77	
425.	1.559	1.813	0.86	
435.	1.457	1.785	0.82	
445.	1.292	2.089	0.62	
455.	1.224	2.159	0.57	
465.	1.207	2.145	0.56	
475.	1.238	2.131	0.58	
485.	1.443	2.034	0.71	
495.	1.385	2.034	0.68	
505.	1.176	1.937	0.61	
515.	1.077	1.910	0.56	
525.	1.046	1.923	0.54	
535.	0.980	1.965	0.50	
545.	0.919	1.951	0.47	
555.	0.902	1.923	0.47	
565.	0.894	1.882	0.48	
575.	0.895	1.910	0.47	
585.	0.896	1.882	0.48	
595.	0.894	1.868	0.48	
605.	0.886	1.785	0.50	
615.	0.875	1.743	0.50	
625.	0.858	1.716	0.50	
635.	0.899	1.674	0.54	
645.	1.469	1.647	0.89	
655.	2.614	1.619	1.61	
665.	2.251	1.605	1.40	
675.	1.139	1.564	0.73	
685.	0.946	1.522	0.62	
695.	1.156	1.481	0.78	
705.	1.266	1.494	0.85	
715.	1.023	1.425	0.72	
725.	0.976	1.411	0.69	
735.	1.289	1.384	0.93	
745.	2.129	1.342	1.59	
755.	2.195	1.342	1.64	
765.	2.298	1.287	1.79	
775.	2.178	1.245	1.75	
785.	1.553	1.231	1.26	
795.	1.686	1.204	1.40	
805.	2.461	1.176	2.09	

Table 8 (Continued)
Pressure Arc, Argon, 15psig, 14V, 100A, 1.4kw

815.	3.081	1.148	2.68
825.	2.512	1.135	2.21
835.	1.918	1.093	1.75
845.	2.387	1.065	2.24
855.	2.125	1.038	2.05
865.	1.390	1.010	1.38
875.	1.094	0.996	1.10
885.	0.811	0.982	0.83
895.	0.649	0.955	0.68
905.	0.695	0.913	0.76
915.	1.074	0.899	1.19
925.	1.232	0.886	1.39
935.	0.985	0.872	1.11
945.	0.754	0.844	0.89
955.	0.622	0.816	0.76
965.	0.701	0.803	0.87
975.	0.773	0.803	0.96
985.	0.697	0.761	0.92
995.	0.627	0.747	0.84
1000.	-0.000	-0.000	-0.00
1010.	-0.000	-0.000	-0.00
1020.	-0.000	-0.000	-0.00
1030.	-0.000	-0.000	-0.00
1040.	-0.000	-0.000	-0.00
1050.	-0.000	-0.000	-0.00
1060.	-0.000	-0.000	-0.00
1070.	-0.000	-0.000	-0.00
1080.	-0.000	-0.000	-0.00
1090.	-0.000	-0.000	-0.00

Table 9
Spectral Irradiance Measurements - A1200 Solar Simulator

A-1	11 Xenon lamps, no spectral filters, no uniformity filters, quartz port
A-2	17 Xenon lamps, 5 spectral filters, 2 uniformity filters, quartz port
A-3	17 Xenon lamps, 6 spectral filters, 3 uniformity filters, no quartz port
A-4	17 Xenon lamps, 7 spectral filters, 3 uniformity filters, no quartz port
A-5	17 Xenon lamps, 7 spectral filters, 3 uniformity filters, no quartz port
A-6	17 Xenon lamps, 7 spectral filters, 3 uniformity filters, quartz port
A-7	17 Xenon lamps, 7 spectral filters, 3 uniformity filters, quartz port
A-8	10 Xe lamps, 5 Kr lamps, 7 spectral filters, no uniformity filters, quartz port
A-9	10 Xe lamps, 5 Kr lamps, no spectral filters, no uniformity filters, quartz port
A-10	5 Xe lamps, 5 Kr lamps, no spectral filters, no uniformity filters, quartz port
A-11	5 Xe lamps, 5 Kr lamps, 7 spectral filters, no uniformity filters, quartz port
A-12	5 krypton lamps, 7 spectral filters, no uniformity filters, quartz port
A-13	14 lamps, 6 spectral filters, 6 uniformity filters, quartz port
A-14	19 lamps, 7 spectral filters, 3 uniformity filters, quartz port

NOTES:

A-1 was the first A1200 spectrum taken after Spectrolab added the lenticular system

A-2 through A-4 were run to determine the effects of various amounts of filtering in the A1200

A-5 was a repeatability run duplicating the parameters of A-4

A-6 was run during the IMP-D test

A-7 was run during the OGO test

A-8 through A-12 were run to test combinations of xenon and krypton lamps with and without spectral filters

A-13 was run during the ISIS-A test

A-14 was run during the fifth paint sample test

Table 10

Spectral Irradiance Measurements - Miscellaneous Light Sources

M-1	HgXe, Hanovia #929B-1, 2.5kw - N.G.
M-2	HgXe, Hanovia #929B-1, 2.5kw - N.G.
M-3	HgXe, Hanovia #929B-1, 2.5kw
M-4	HgXe, Hanovia #929B-1, 2.5kw
M-5	Krypton, Hanovia #513294, 30 volts, 85 amps, 1 or 2 hours
M-6	Krypton, Hanovia #513294, 30 volts, 85 amps, 3 or 4 hours
M-7	Krypton, Hanovia #513294, 30 volts, 85 amps, 100 hours
M-8*	Hydrogen doped xenon, PEK #01000, 40V, 50A, 0.5 hours, 1P28 only (exploded)
M-9	Hydrogen doped xenon, PEK #011024, 40V, 50A, 0.25 hours
M-10	Hydrogen doped xenon, PEK #011024, 42V, 42A, 3 hours
M-11	Argon, PEK #01025, 29V, 82A, 2.3 hours
M-12	X-25L solar simulator, dirty optics, no collimator
M-13	X-25L solar simulator, cleaned optics, no collimator
M-14	Carbon arc
M-15	HgXe, Hanovia #646356, 60.4V, 54A
M-16	HgXe, GE # T427, 53.3V, 65.5A
M-17	HgXe, GE # T971, 61V, 51A
M-18	HgXe, GE # T367, 66V, 47.5A
M-19	HgXe, GE # T710, 55.7V, 58A
M-20	HgXe, Hanovia #512524, 56.2V, 61A

*M-8 never reduced.

NOTES TO TABLE 10

M-3 and M-4 were spectra of a 2.5kw HgXe lamp

M-5 was done on a krypton experimental compact arc lamp

M-6 was done to determine repeatability from M-5

M-7 was done to determine degradation from M-5

M-8 was done on a hydrogen doped xenon experimental compact arc lamp, lamp exploded after 1-1/2 hours operation so that the spectral measurement could not be completed

M-9 was done on another Hg doped Xe lamp after the first one exploded

M-10 was done to check degradation from M-9

M-11 was the only spectrum obtained from an argon experimental compact arc lamp

M-12 and M-13 were done to check the spectrum of the X-25L; M-13 was run to see whether cleaning the optics would restore the solar spectral match

M-14 Carbon arc data

M-15 through M-20 were spectra on 6 different 3.5kw HgXe lamps supplied by the Testing and Evaluation Division

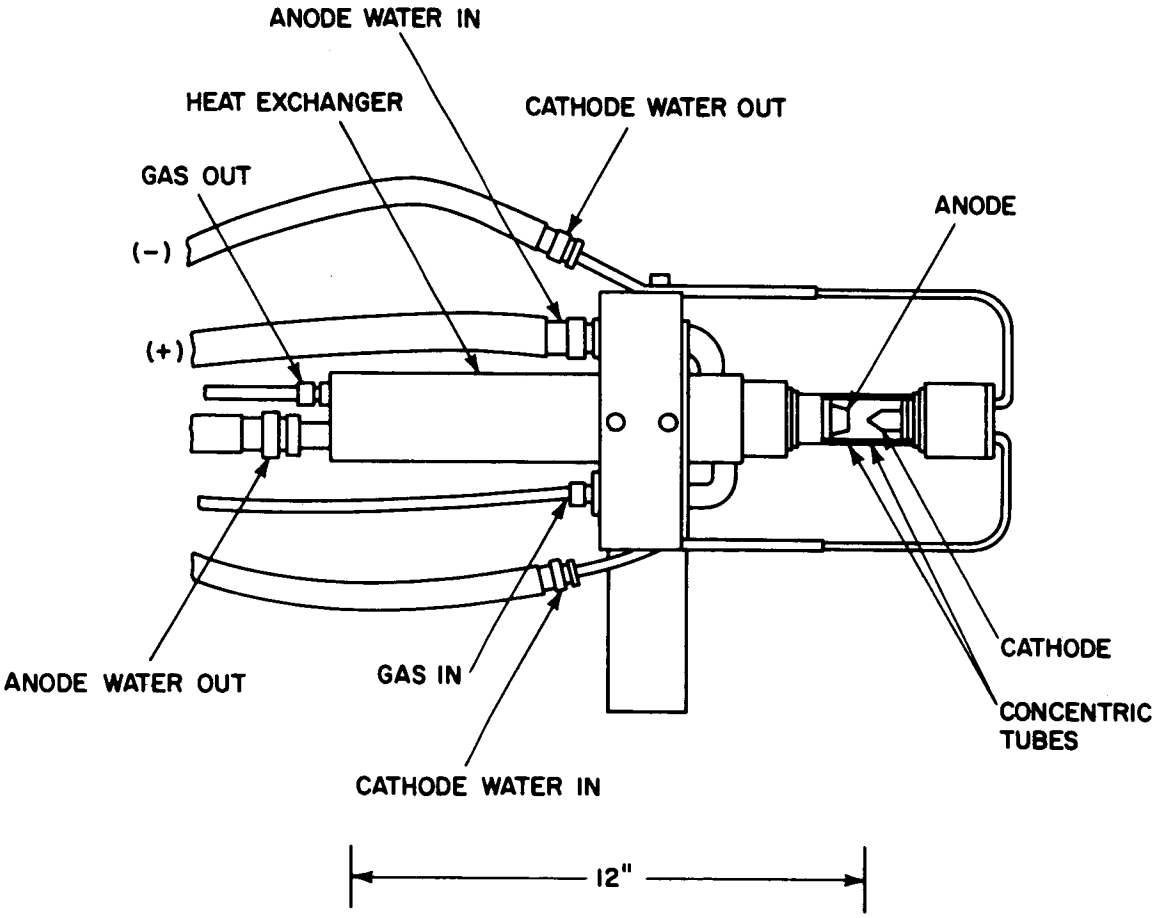

Figure 1. Vortex Arc Configuration

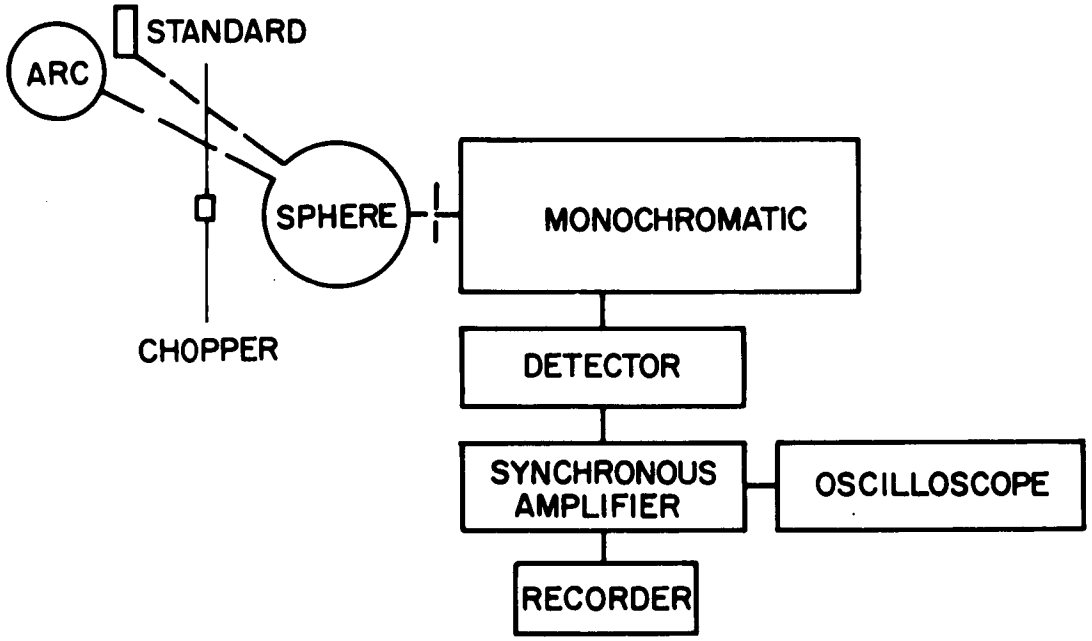

Figure 2. Spectral Irradiance Measuring Instrumentation

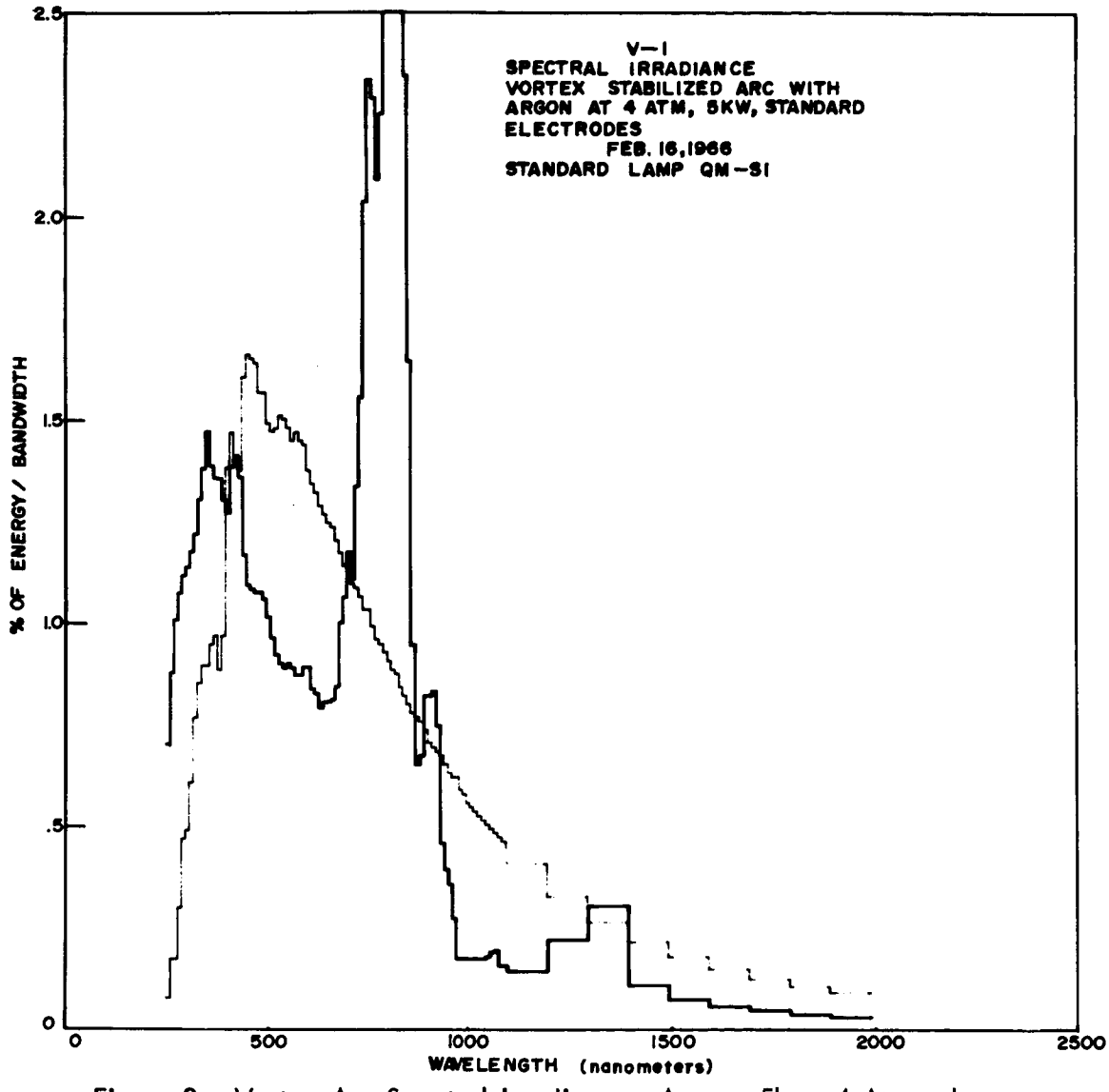

Figure 3. Vortex Arc Spectral Irradiance, Argon, 5kw, 4 Atmospheres

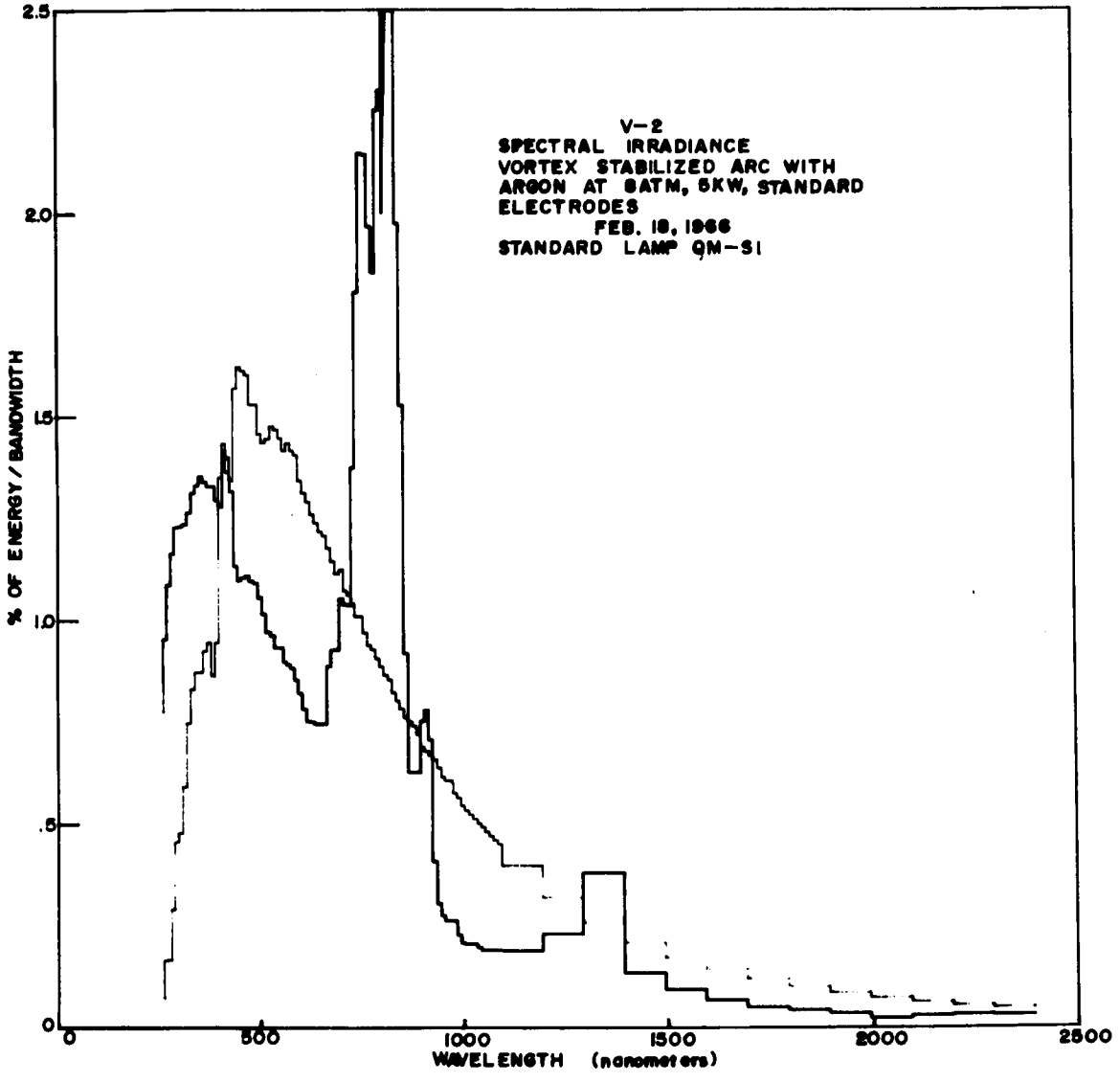

Figure 4. Vortex Arc Spectral Irradiance, Argon, 5kw, 8 Atmospheres

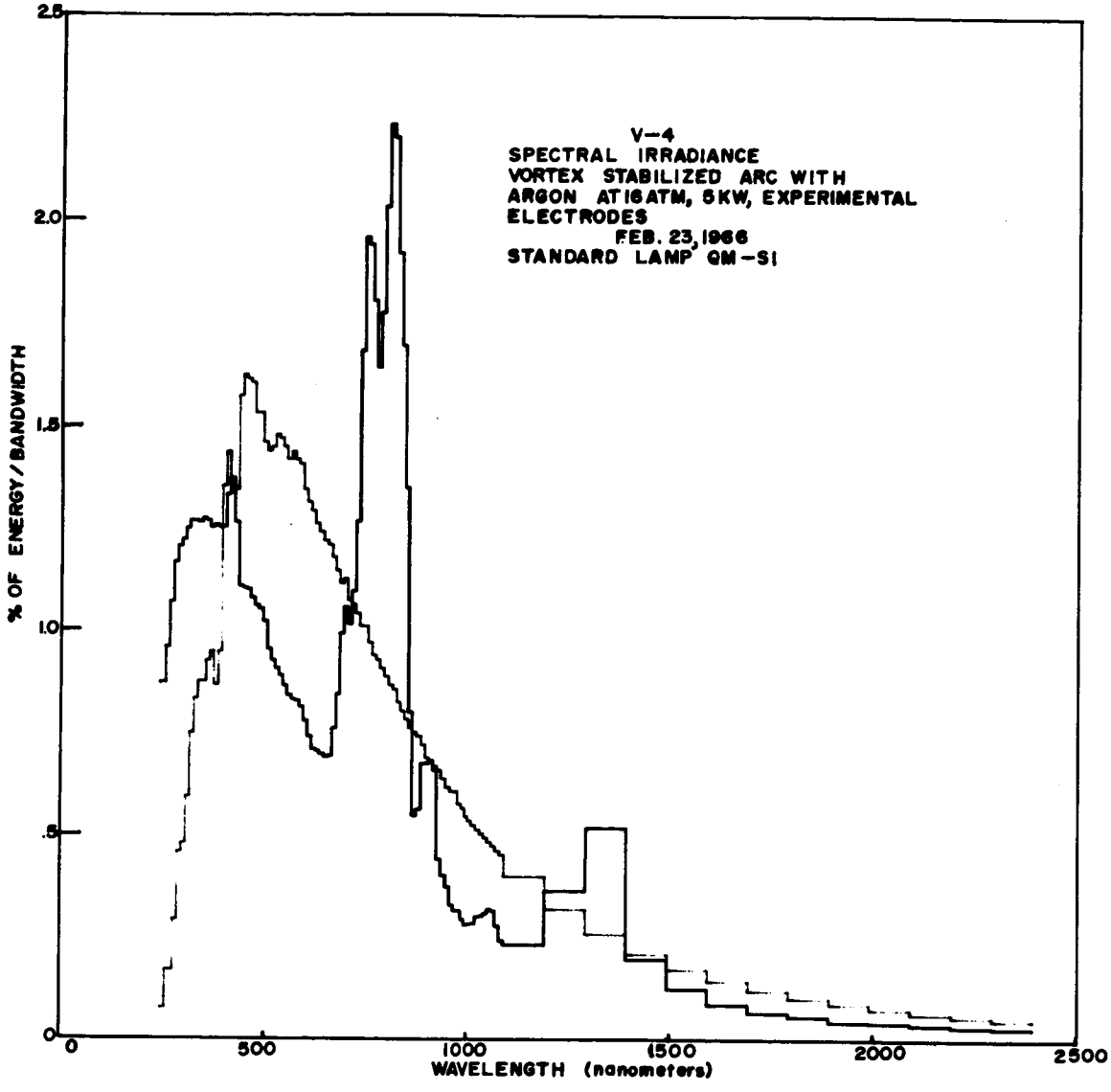

Figure 5. Vortex Arc Spectral Irradiance, Argon, 5kw, 16 Atmospheres

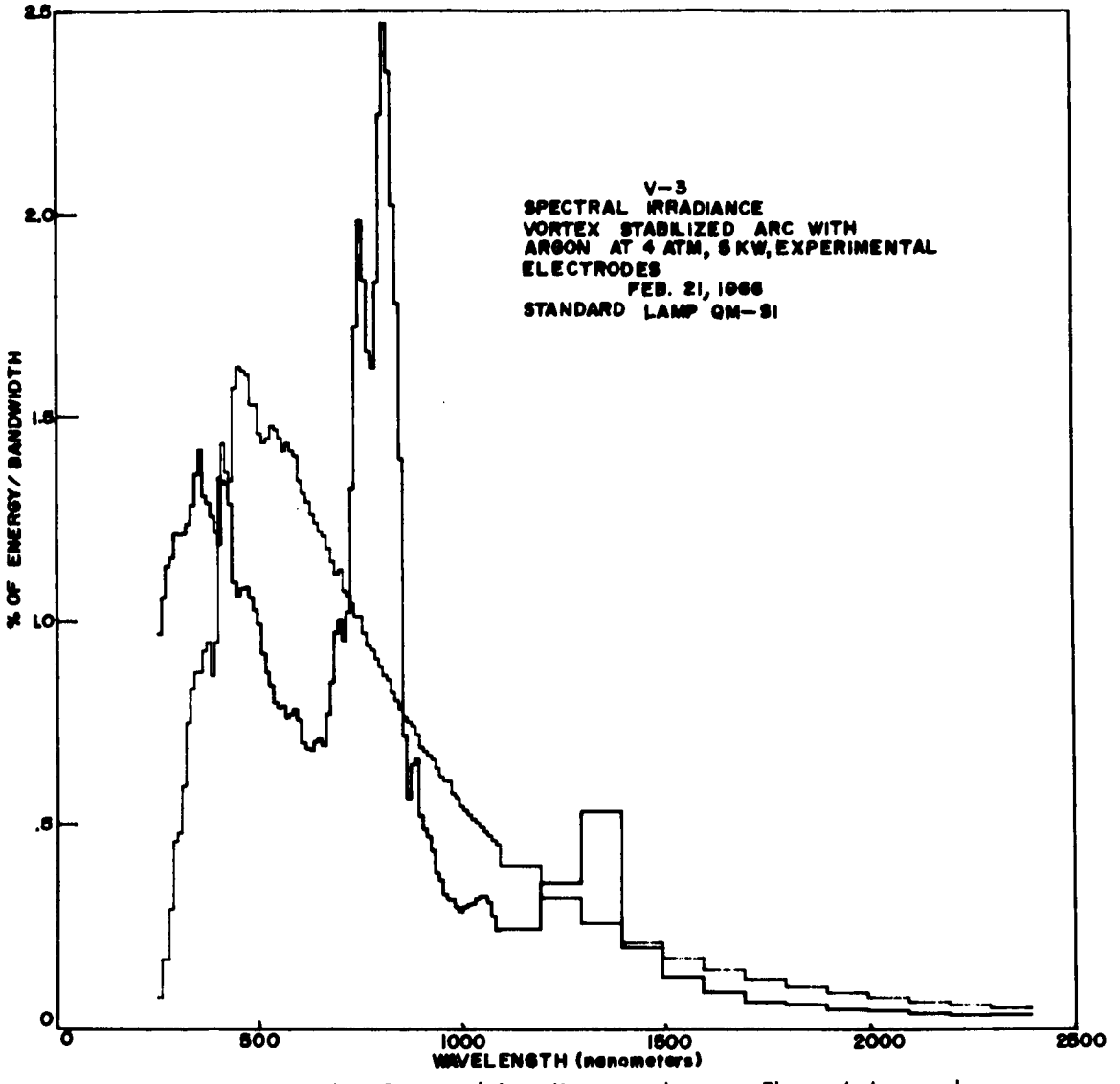

Figure 6. Vortex Arc Spectral Irradiance, Argon, 5kw, 4 Atmospheres, New Style Electrode

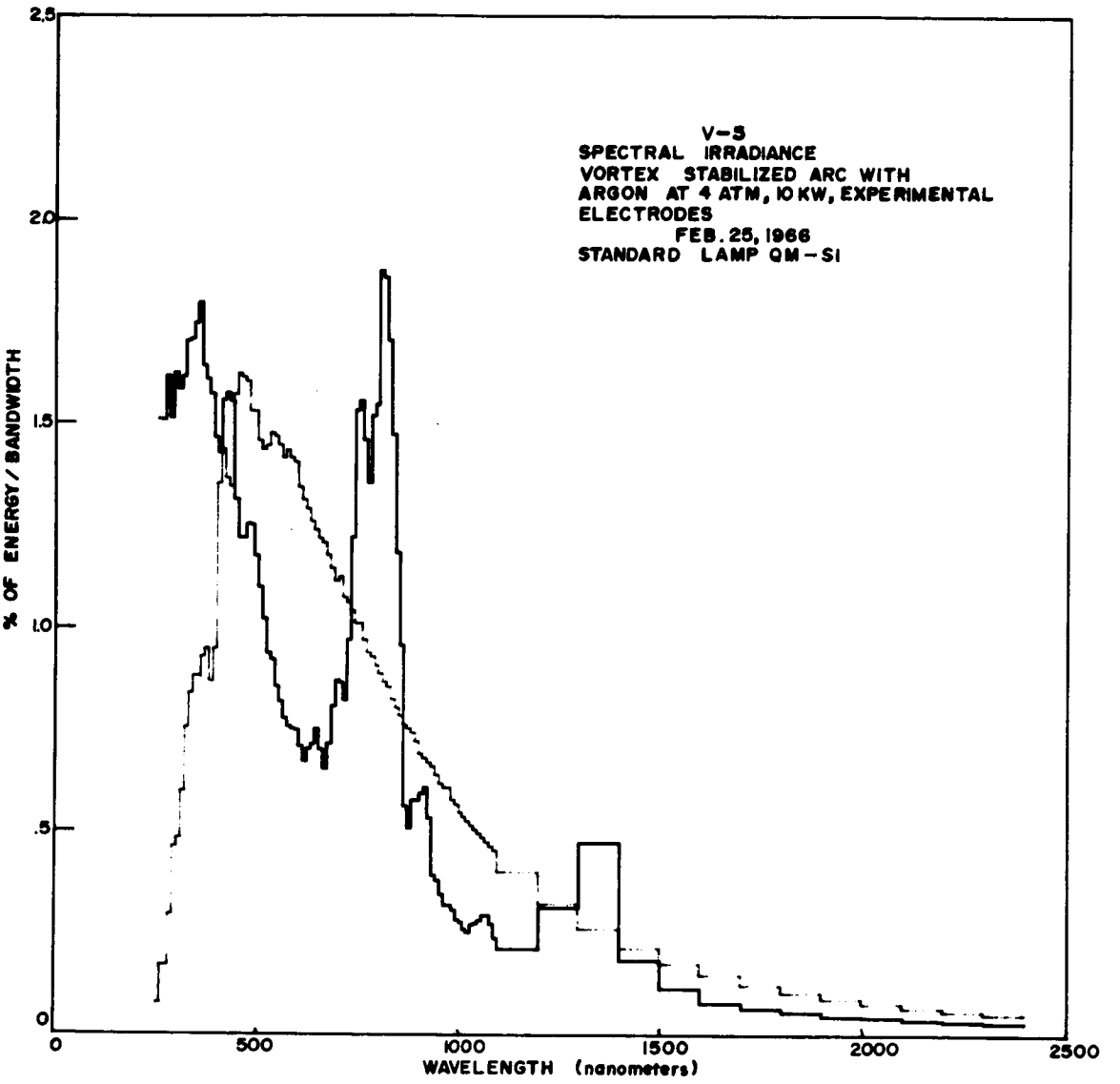

Figure 7. Vortex Arc Spectral Irradiance, Argon, 10kw, 4 Atmospheres, New Style Electrode

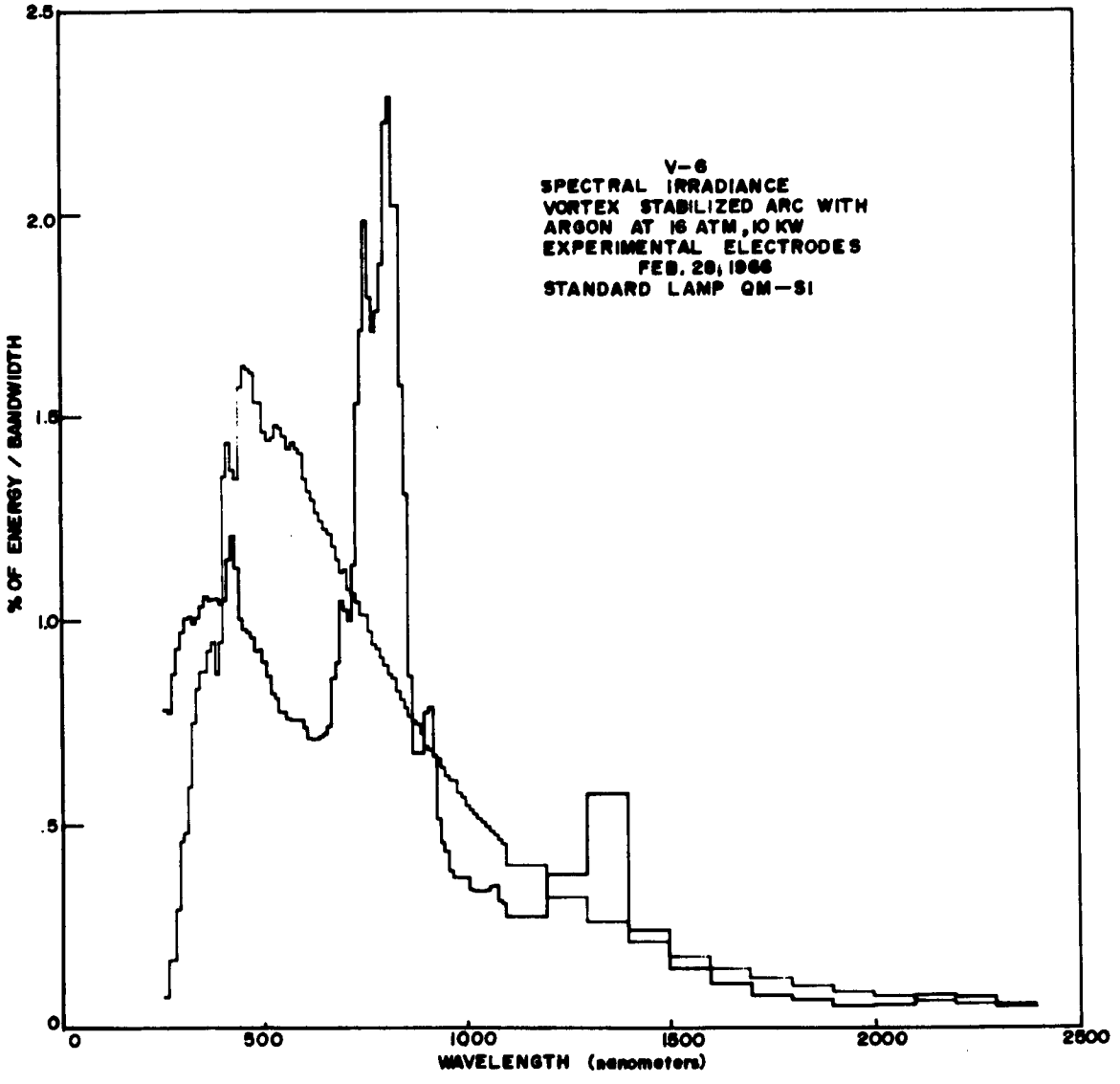

Figure 8. Vortex Arc Spectral Irradiance, Argon, 10kw, 16 Atmospheres, New Style Electrode

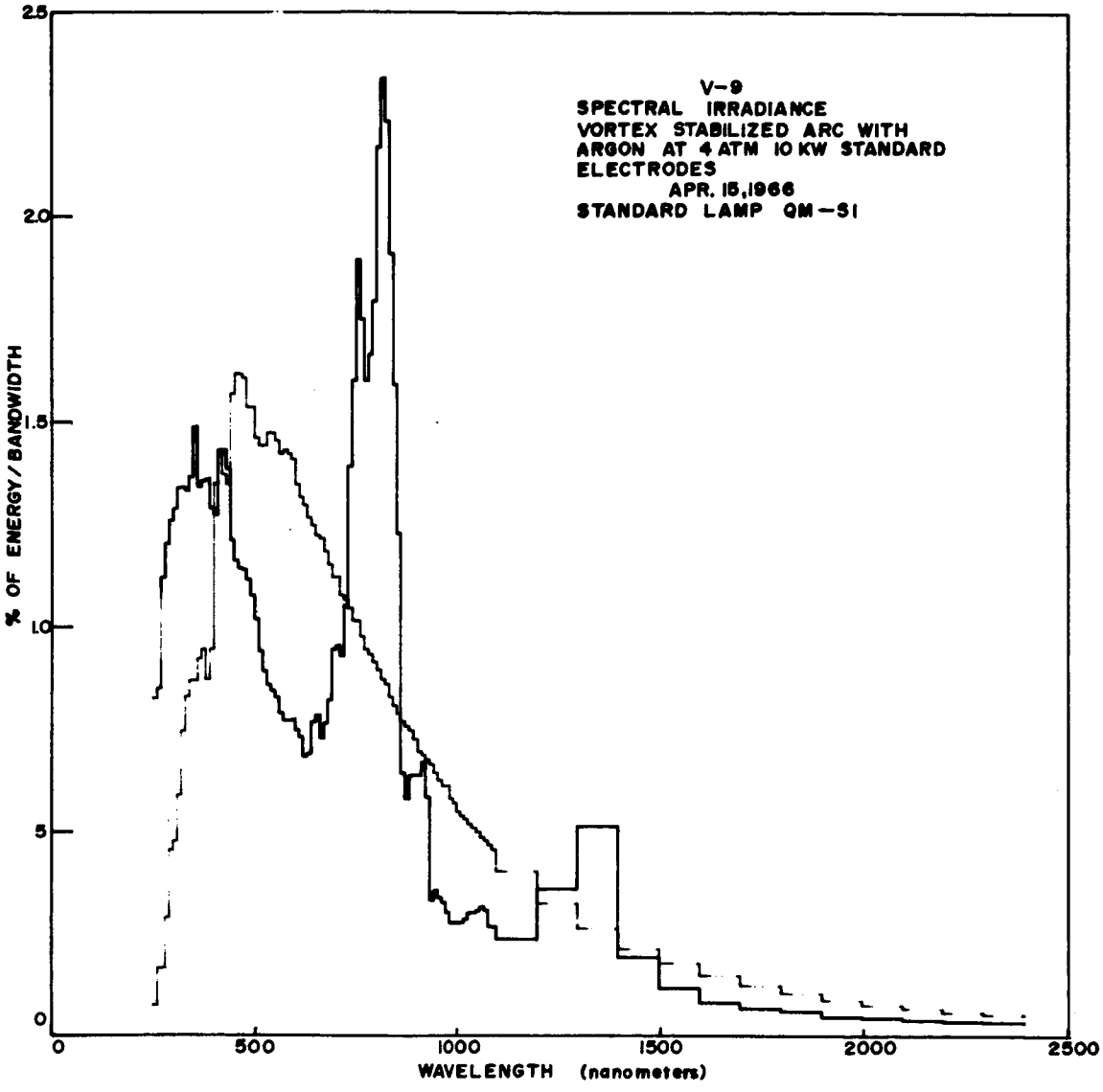

Figure 9. Vortex Arc Spectral Irradiance, Argon, 10kw, 4 Atmospheres, Old Style Electrode

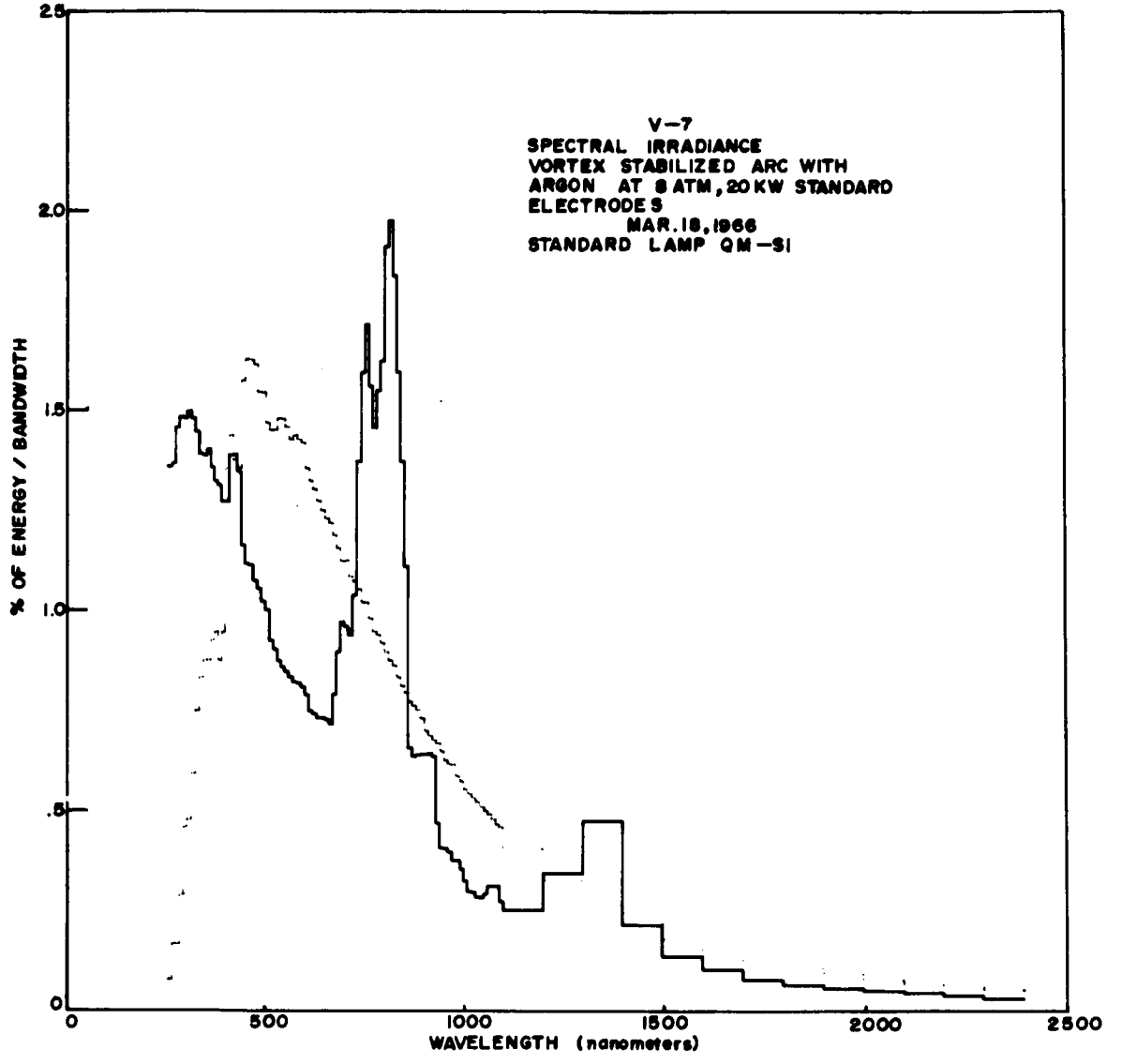

Figure 10. Vortex Arc Spectral Irradiance, Argon, 20kw, 8 Atmospheres, Old Style Electrode

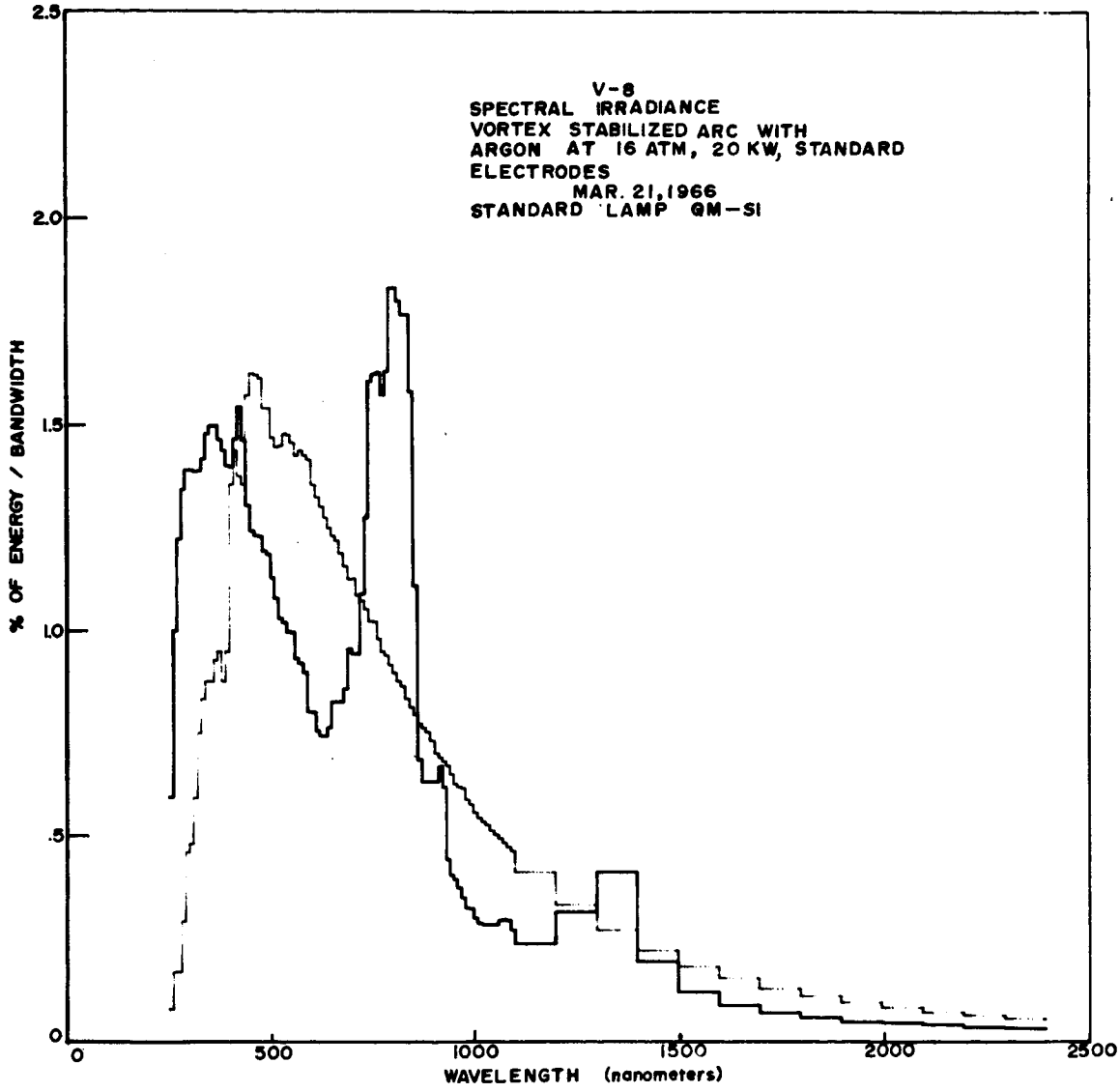

Figure 11. Vortex Arc Spectral Irradiance, Argon, 20kw, 16 Atmospheres, Old Style Electrode

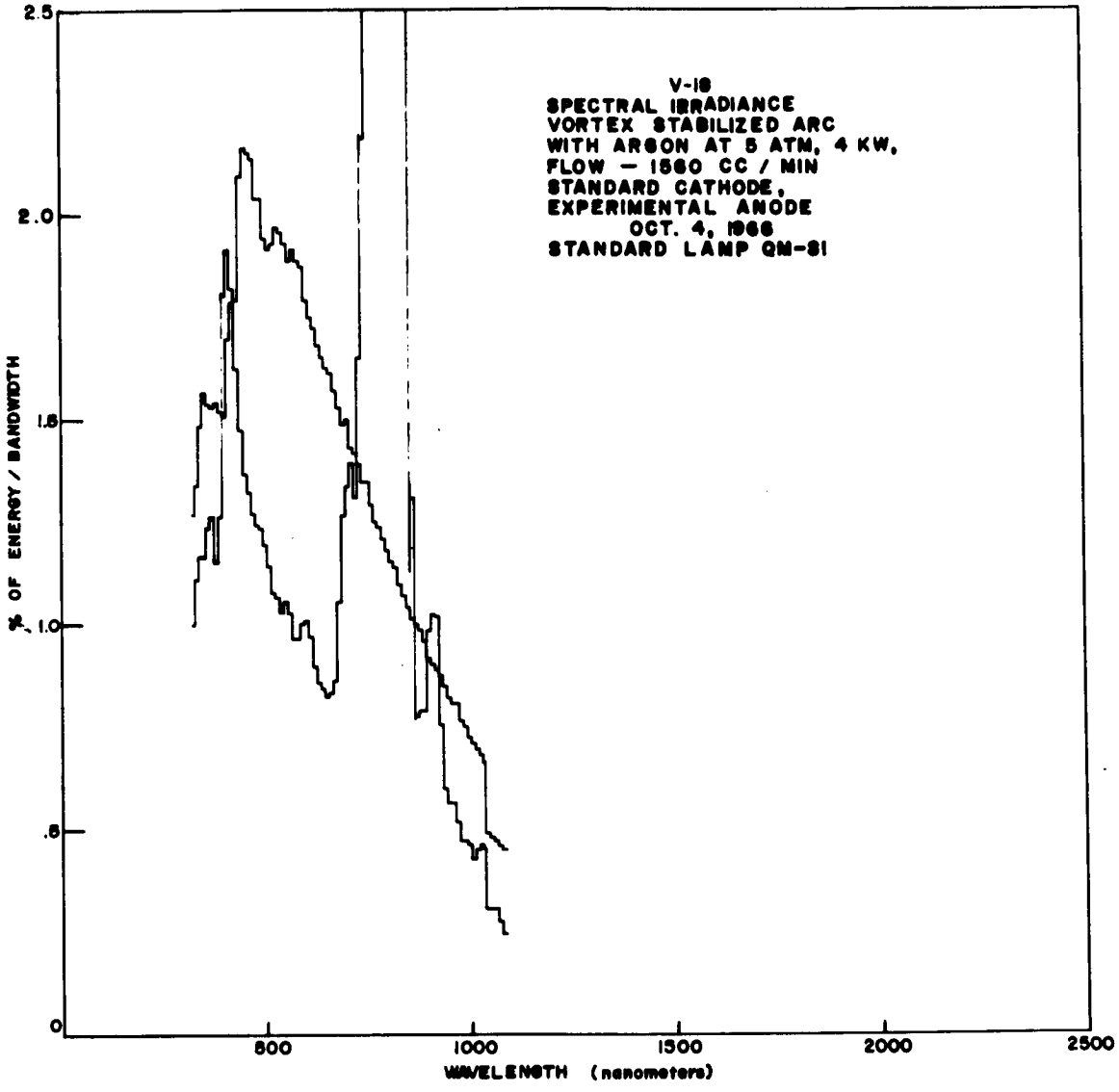

Figure 12. Vortex Arc Spectral Irradiance, 4kw, 5 Atmospheres, Gas Flow Rate 1560 cc/min

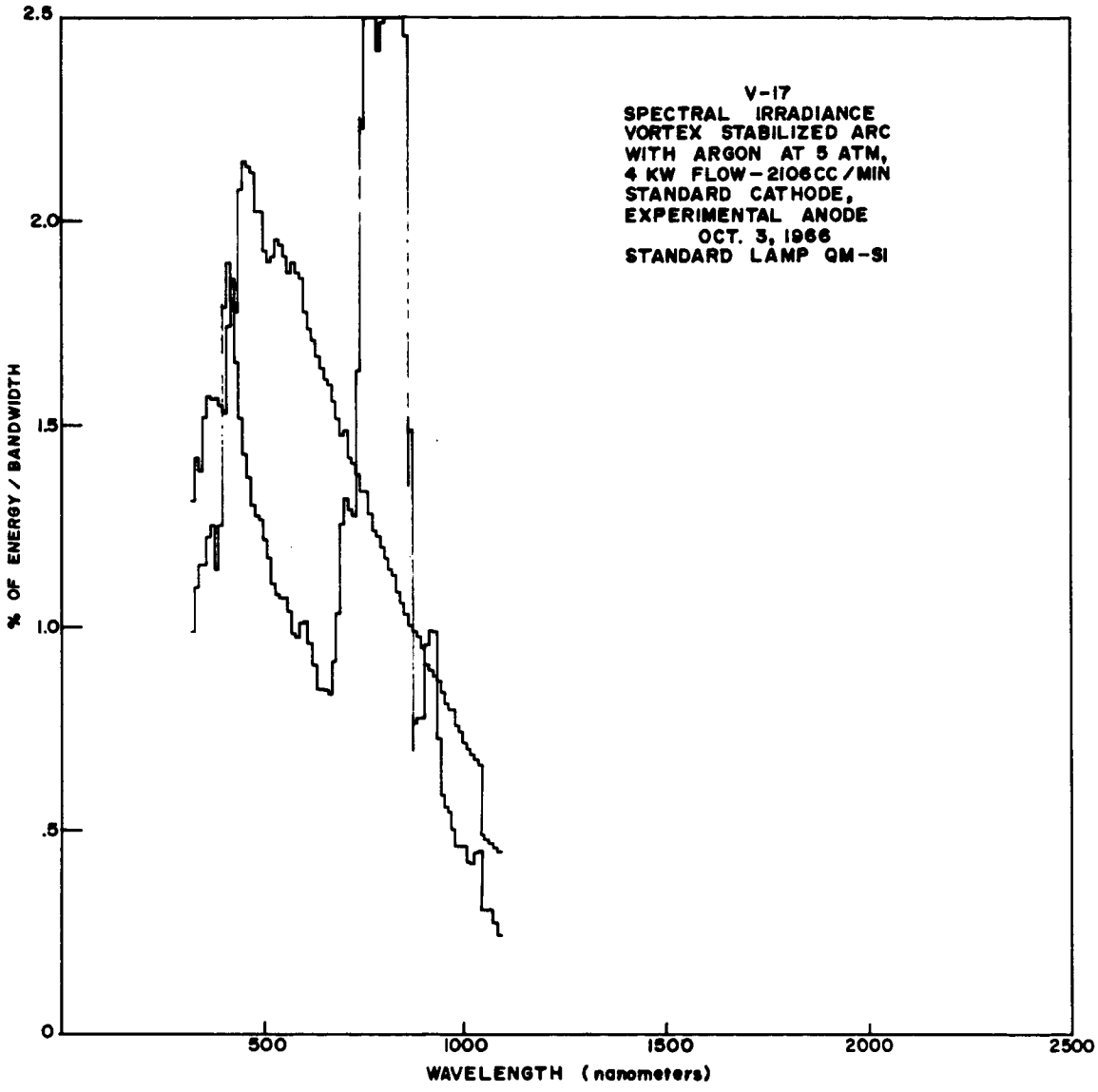

Figure 13. Vortex Arc Spectral Irradiance, 4kw, 5 Atmospheres, Gas Flow Rate 2106 cc/min

V-19 ARGON 5ATM 3KW 1200 CC/MIN LNO.2 S2 370-1000NM

WAVELENGTH	TEST LAMP ENERGY PER 10NM WAVELENGTH INTERVAL	SOLAR ENERGY	RATIOTESTLAMP/SOLAR
345.	1.811	1.198	1.51
355.	1.821	1.198	1.52
365.	1.815	1.269	1.43
375.	1.780	1.297	1.37
385.	1.782	1.183	1.51
395.	1.710	1.297	1.32
405.	1.674	1.853	0.90
415.	1.916	1.967	0.97
425.	1.922	1.868	1.03
435.	1.783	1.839	0.97
445.	1.514	2.153	0.70
455.	1.461	2.224	0.66
465.	1.436	2.210	0.65
475.	1.404	2.196	0.64
485.	1.359	2.096	0.65
495.	1.347	2.096	0.64
505.	1.302	1.996	0.65
515.	1.249	1.967	0.63
525.	1.186	1.982	0.60
535.	1.172	2.025	0.58
545.	1.128	2.010	0.56
555.	1.128	1.982	0.57
565.	1.086	1.939	0.56
575.	1.025	1.967	0.52
585.	1.025	1.939	0.53
595.	1.074	1.925	0.56
605.	1.078	1.839	0.59
615.	0.979	1.796	0.55
625.	0.959	1.768	0.54
635.	0.924	1.725	0.54
645.	0.923	1.697	0.54
655.	0.878	1.668	0.53
665.	0.874	1.654	0.53
675.	0.918	1.611	0.57
685.	1.050	1.568	0.67
695.	1.362	1.526	0.89
705.	1.557	1.540	1.01
715.	1.339	1.468	0.91
725.	1.134	1.454	0.78
735.	2.029	1.426	1.42
745.	2.510	1.383	1.81
755.	2.510	1.383	1.81
765.	2.395	1.326	1.81
775.	2.197	1.283	1.71
785.	2.050	1.269	1.62
795.	1.896	1.240	1.53
805.	3.604	1.212	2.97
815.	4.105	1.183	3.47
825.	3.771	1.169	3.23
835.	2.792	1.126	2.48
845.	3.261	1.098	2.97
855.	2.922	1.069	2.73
865.	1.341	1.041	1.29
875.	0.617	1.027	0.60
885.	0.771	1.012	0.76
895.	0.771	0.984	0.78
905.	1.194	0.941	1.27
915.	1.343	0.927	1.45
925.	1.136	0.912	1.24
935.	0.651	0.898	0.72
945.	0.667	0.870	0.77
955.	0.532	0.841	0.63
965.	0.488	0.827	0.59
975.	0.450	0.827	0.54
985.	0.411	0.784	0.52
995.	0.411	0.770	0.53
1005.	0.411	0.741	0.55
1015.	0.418	0.727	0.57
1025.	0.463	0.713	0.65
1030.	-0.000	-0.000	-0.00
1040.	-0.000	-0.000	-0.00
1050.	-0.000	-0.000	-0.00
1060.	-0.000	-0.000	-0.00
1070.	-0.000	-0.000	-0.00
1080.	-0.000	-0.000	-0.00
1090.	-0.000	-0.000	-0.00

Figure 14. Vortex Arc Spectral Irradiance, 3kw, 5 Atmospheres, Gas Flow Rate 1560 cc/min

V-20 ARGON 5ATM 2.5KW 364CC/MIN LNO.2 S1 370-1000NM

WAVELENGTH	TEST LAMP ENERGY PER 10NM WAVELENGTH INTERVAL	SOLAR ENERGY	RATIOTESTLAMP/SOLAR
345.	1.773	1.181	1.50
355.	1.795	1.181	1.52
365.	1.803	1.252	1.44
375.	1.769	1.280	1.38
385.	1.807	1.167	1.55
395.	1.756	1.280	1.37
405.	1.652	1.828	0.90
415.	1.845	1.941	0.95
425.	1.936	1.842	1.05
435.	1.745	1.814	0.96
445.	1.415	2.123	0.67
455.	1.378	2.194	0.63
465.	1.331	2.180	0.61
475.	1.296	2.166	0.60
485.	1.281	2.067	0.62
495.	1.277	2.067	0.62
505.	1.252	1.969	0.64
515.	1.226	1.941	0.63
525.	1.113	1.955	0.57
535.	1.074	1.997	0.54
545.	1.033	1.983	0.52
555.	1.047	1.955	0.54
565.	1.032	1.913	0.54
575.	0.932	1.941	0.48
585.	0.941	1.913	0.49
595.	0.983	1.898	0.52
605.	1.052	1.814	0.58
615.	0.926	1.772	0.52
625.	0.925	1.744	0.53
635.	0.837	1.702	0.49
645.	0.796	1.673	0.48
655.	0.785	1.645	0.48
665.	0.790	1.631	0.48
675.	0.828	1.589	0.52
685.	0.886	1.547	0.57
695.	1.199	1.505	0.80
705.	1.570	1.519	1.03
715.	1.422	1.448	0.98
725.	1.069	1.434	0.75
735.	1.677	1.406	1.19
745.	2.011	1.364	1.47
755.	3.011	1.364	2.21
765.	3.143	1.308	2.40
775.	3.249	1.266	2.57
785.	2.114	1.252	1.69
795.	1.838	1.223	1.50
805.	2.876	1.195	2.41
815.	3.708	1.167	3.18
825.	4.464	1.153	3.87
835.	3.551	1.111	3.20
845.	3.015	1.083	2.78
855.	3.183	1.055	3.02
865.	1.561	1.027	1.52
875.	0.554	1.013	0.55
885.	0.503	0.998	0.50
895.	0.712	0.970	0.73
905.	0.712	0.928	0.77
915.	1.167	0.914	1.28
925.	1.242	0.900	1.38
935.	0.664	0.886	0.75
945.	0.686	0.858	0.80
955.	0.616	0.830	0.74
965.	0.610	0.816	0.75
975.	0.467	0.816	0.57
985.	0.467	0.773	0.60
995.	0.439	0.759	0.58
1005.	0.423	0.731	0.58
1015.	0.419	0.717	0.58
1025.	0.418	0.703	0.60
1035.	0.460	0.689	0.67
1045.	0.466	0.675	0.69
1050.	-0.000	-0.000	-0.00
1060.	-0.000	-0.000	-0.00
1070.	-0.000	-0.000	-0.00
1080.	-0.000	-0.000	-0.00
1090.	-0.000	-0.000	-0.00

Figure 15. Vortex Arc Spectral Irradiance, 2kw, 5 Atmospheres, Gas Flow Rate 474 cc/min

V-21 ARGON 5ATM 3.6KW VERY HIGH FLOW RATE LNO.2 S1 370-1000NM

WAVELENGTH	TEST LAMP ENERGY PER 10NM WAVELENGTH INTERVAL	SOLAR ENERGY	RATIOTESTLAMP/SOLAR
345.	1.927	1.181	1.63
355.	1.913	1.181	1.62
365.	1.832	1.252	1.46
375.	1.955	1.280	1.53
385.	1.925	1.167	1.65
395.	1.791	1.280	1.40
405.	1.745	1.828	0.95
415.	1.876	1.941	0.97
425.	1.910	1.842	1.04
435.	1.723	1.814	0.95
445.	1.442	2.123	0.68
455.	1.396	2.194	0.64
465.	1.371	2.180	0.63
475.	1.342	2.166	0.62
485.	1.308	2.067	0.63
495.	1.298	2.067	0.63
505.	1.249	1.969	0.63
515.	1.201	1.941	0.62
525.	1.152	1.955	0.59
535.	1.141	1.997	0.57
545.	1.108	1.983	0.56
555.	1.108	1.955	0.57
565.	1.069	1.913	0.56
575.	1.063	1.941	0.55
585.	1.059	1.913	0.55
595.	1.043	1.898	0.55
605.	1.056	1.814	0.58
615.	0.980	1.772	0.55
625.	0.979	1.744	0.56
635.	0.925	1.702	0.54
645.	0.890	1.673	0.53
655.	0.866	1.645	0.53
665.	0.878	1.631	0.54
675.	0.907	1.589	0.57
685.	0.939	1.547	0.61
695.	1.250	1.505	0.83
705.	1.587	1.519	1.05
715.	1.343	1.448	0.93
725.	1.139	1.434	0.79
735.	1.895	1.406	1.35
745.	2.001	1.364	1.47
755.	2.435	1.364	1.79
765.	3.362	1.308	2.57
775.	2.593	1.266	2.05
785.	2.264	1.252	1.81
795.	1.610	1.223	1.32
805.	3.017	1.195	2.52
815.	4.187	1.167	3.59
825.	3.892	1.153	3.38
835.	2.959	1.111	2.66
845.	2.777	1.083	2.56
855.	2.884	1.055	2.73
865.	1.286	1.027	1.25
875.	0.527	1.013	0.52
885.	0.520	0.998	0.52
895.	0.725	0.970	0.75
905.	0.725	0.928	0.78
915.	1.119	0.914	1.22
925.	1.172	0.900	1.30
935.	0.745	0.886	0.84
945.	0.638	0.858	0.74
955.	0.550	0.830	0.66
965.	0.550	0.816	0.67
975.	0.550	0.816	0.67
985.	0.550	0.773	0.71
995.	0.550	0.759	0.72
1005.	0.492	0.731	0.67
1015.	0.414	0.717	0.58
1025.	0.414	0.703	0.59
1035.	0.451	0.689	0.65
1045.	0.456	0.675	0.68
1050.	-0.000	-0.000	-0.00
1060.	-0.000	-0.000	-0.00
1070.	-0.000	-0.000	-0.00
1080.	-0.000	-0.000	-0.00
1090.	-0.000	-0.000	-0.00

Figure 16. Vortex Arc Spectral Irradiance, 3.6kw, 5 Atmospheres, Gas Flow Rate 2500 cc/min

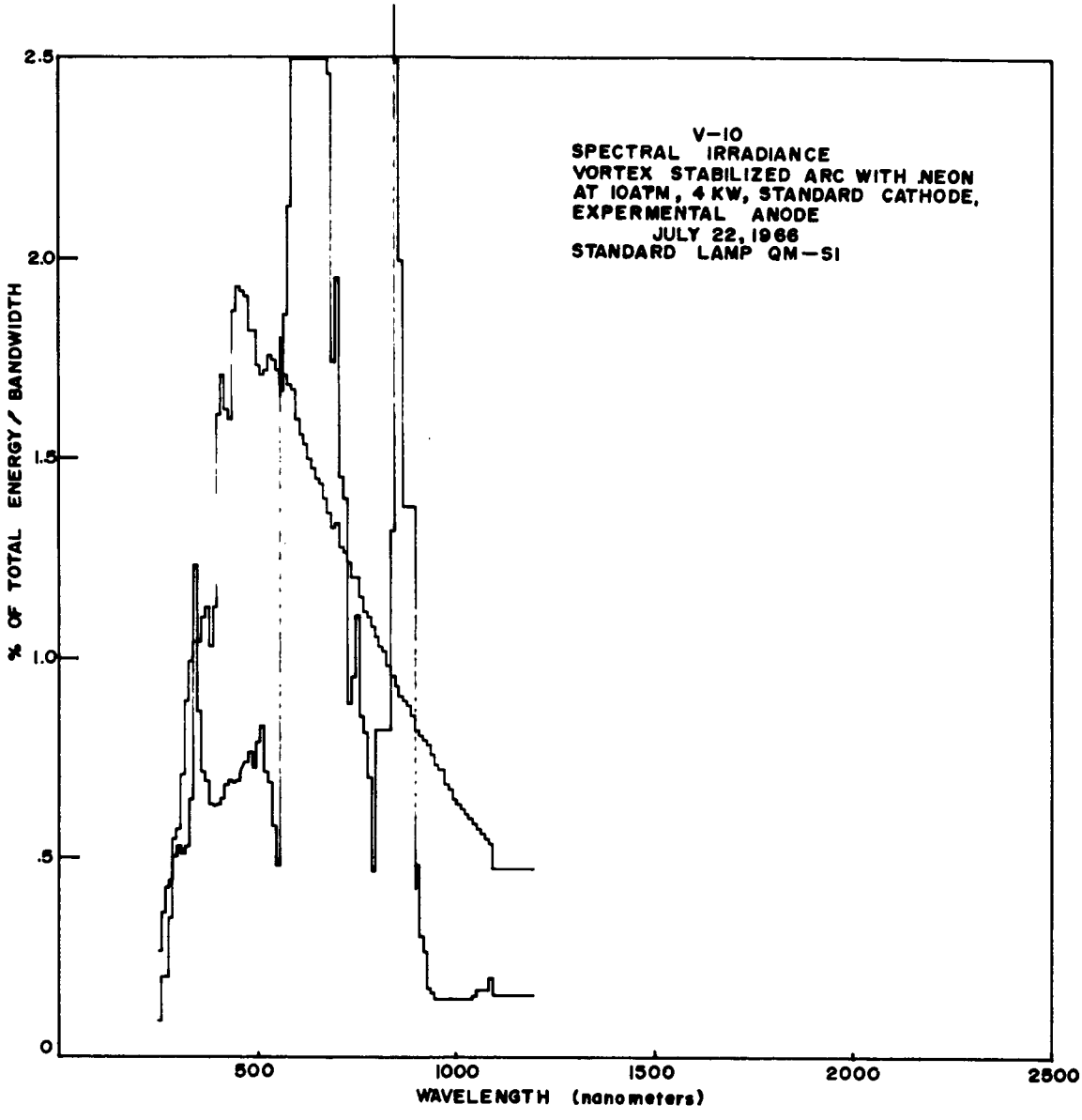

Figure 17. Vortex Arc Spectral Irradiance, Neon, 4kw, 10 Atmospheres

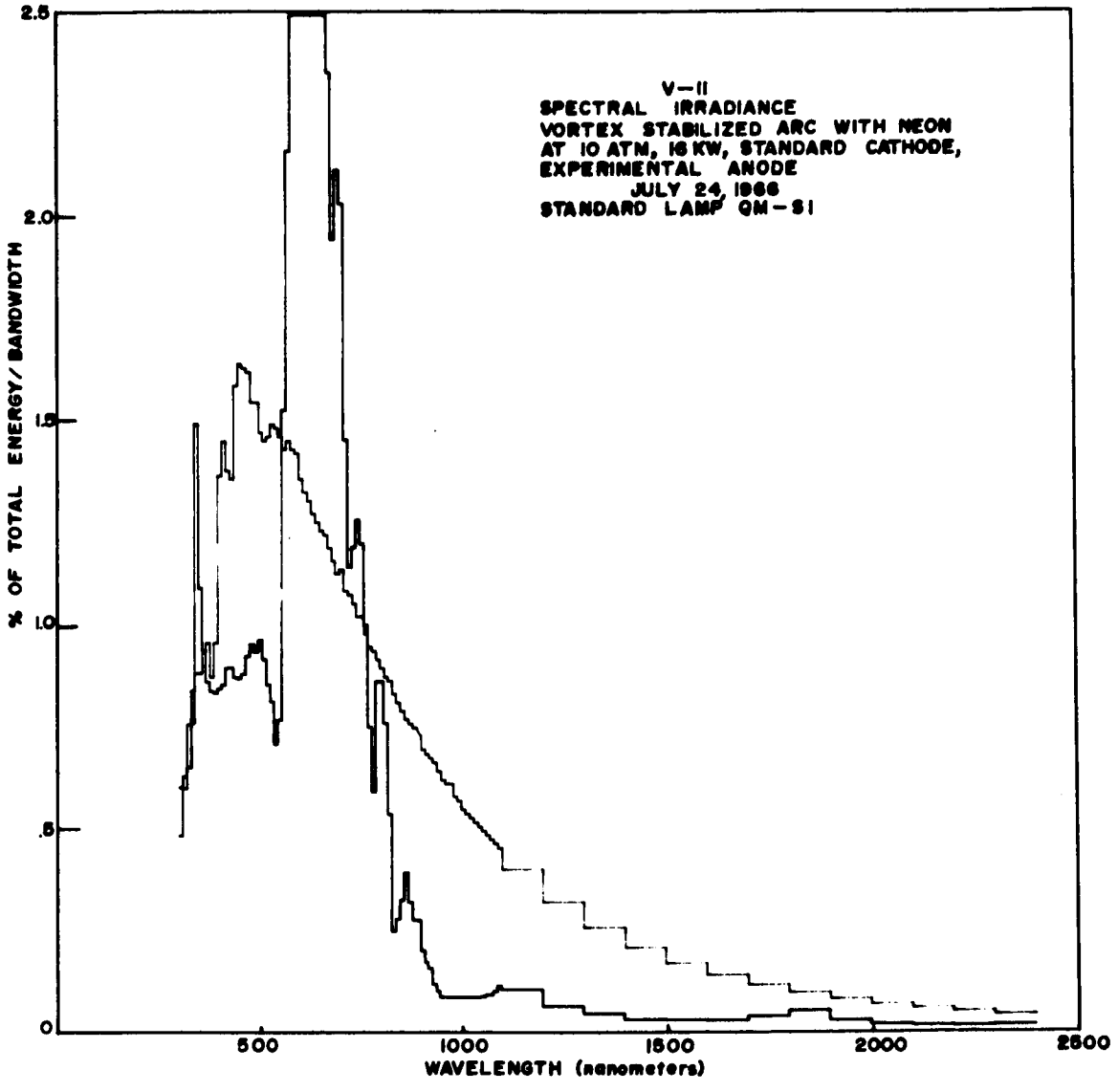

Figure 18. Vortex Arc Spectral Irradiance, Neon, 16kw, 10 Atmospheres

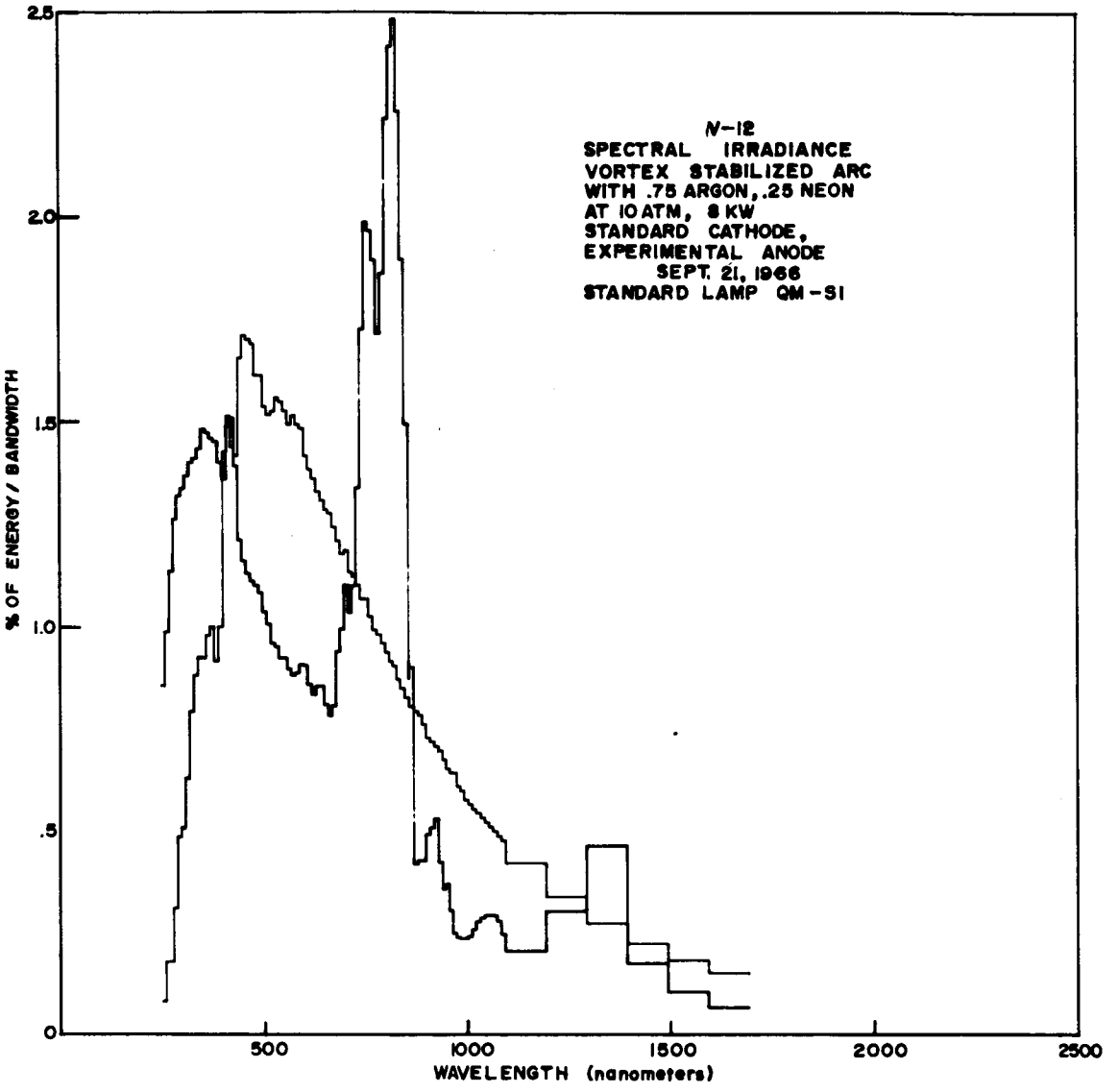

Figure 19. Vortex Arc Spectral Irradiance, 75% Argon-25% Neon, 8kw, 10 Atmospheres

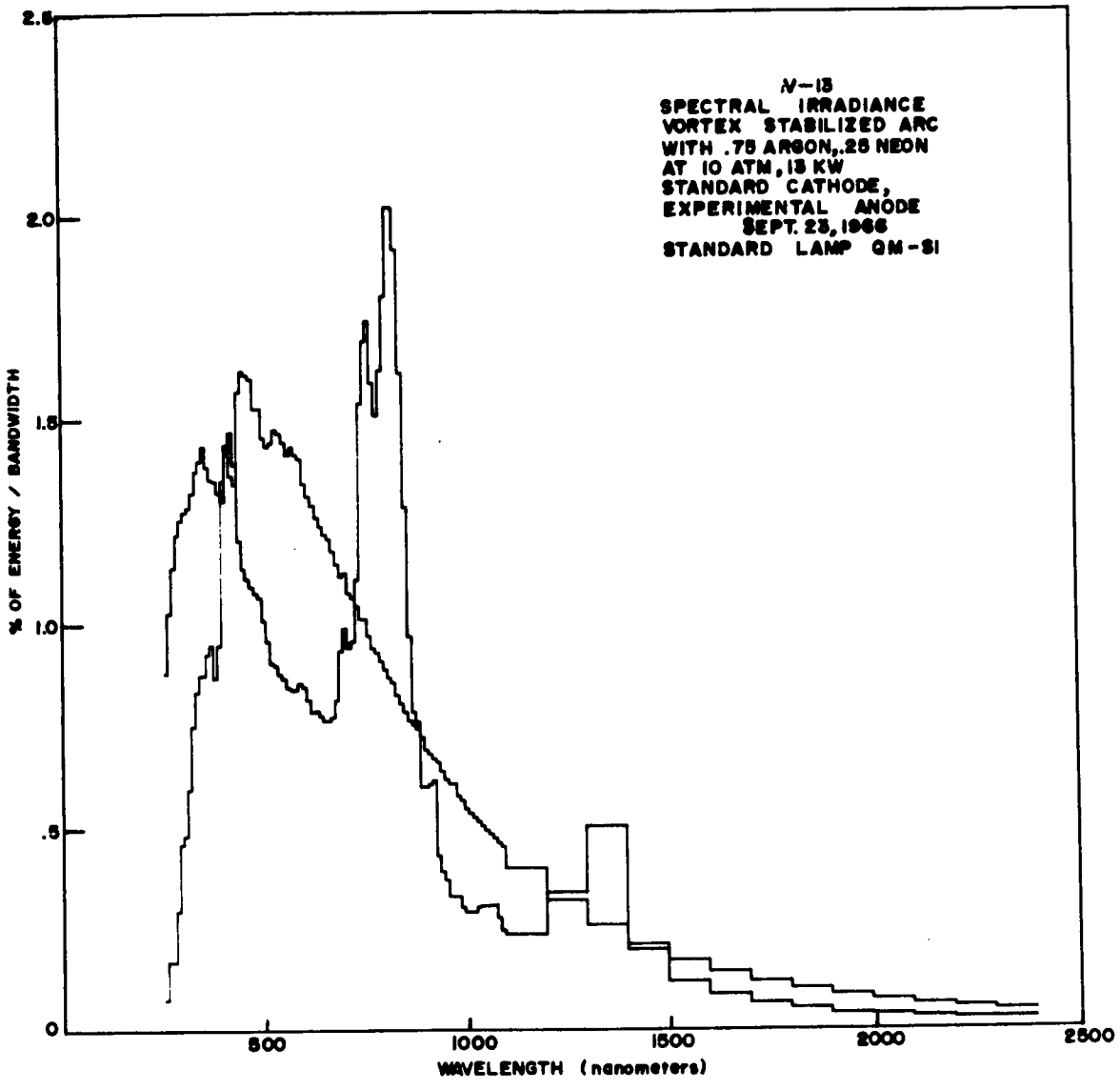

Figure 20. Vortex Arc Spectral Irradiance, 75% Argon-25% Neon, 13kw, 10 Atmospheres

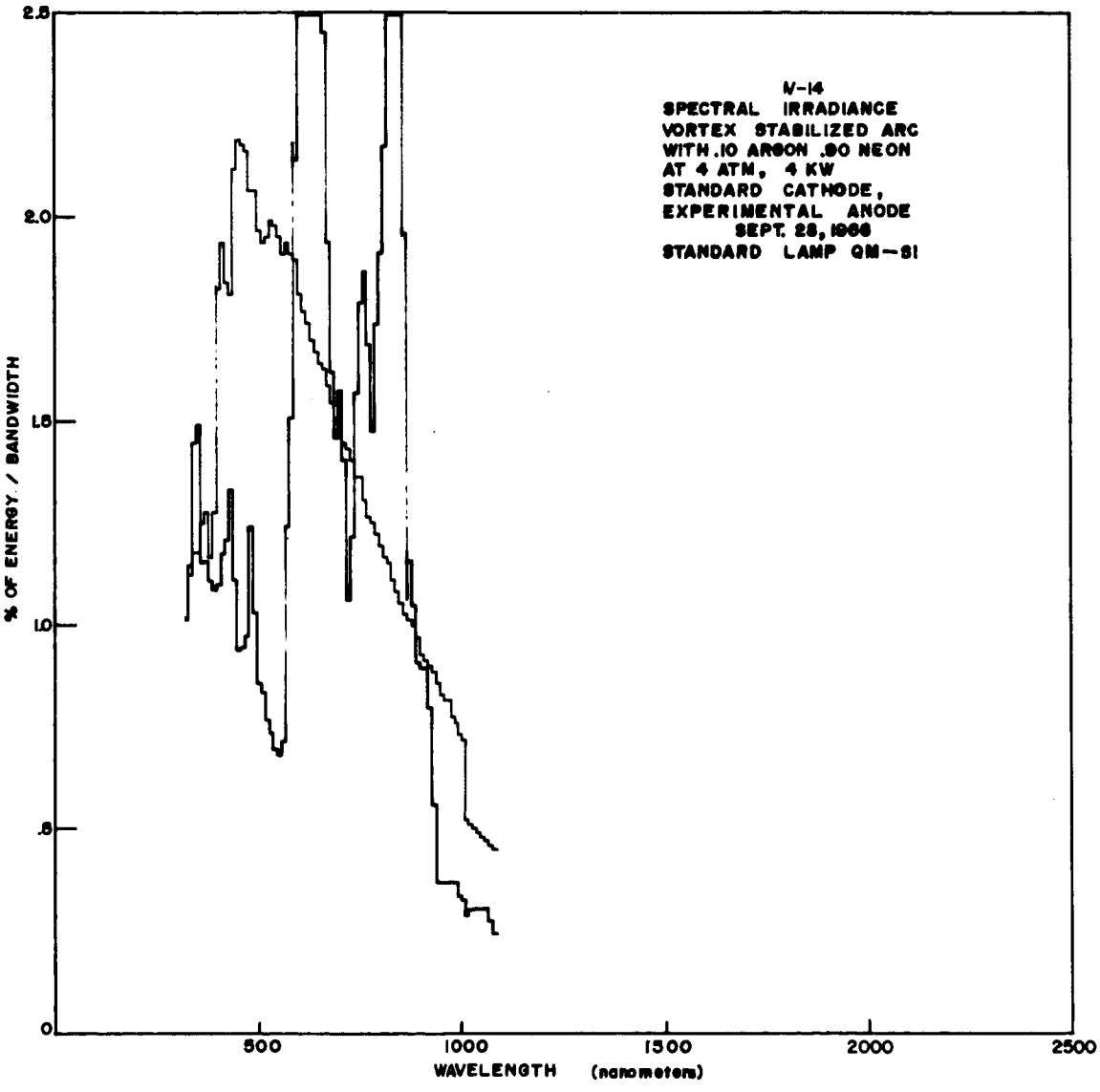

Figure 21. Vortex Arc Spectral Irradiance, 10% Argon-90% Neon, 4kw, 4 Atmospheres

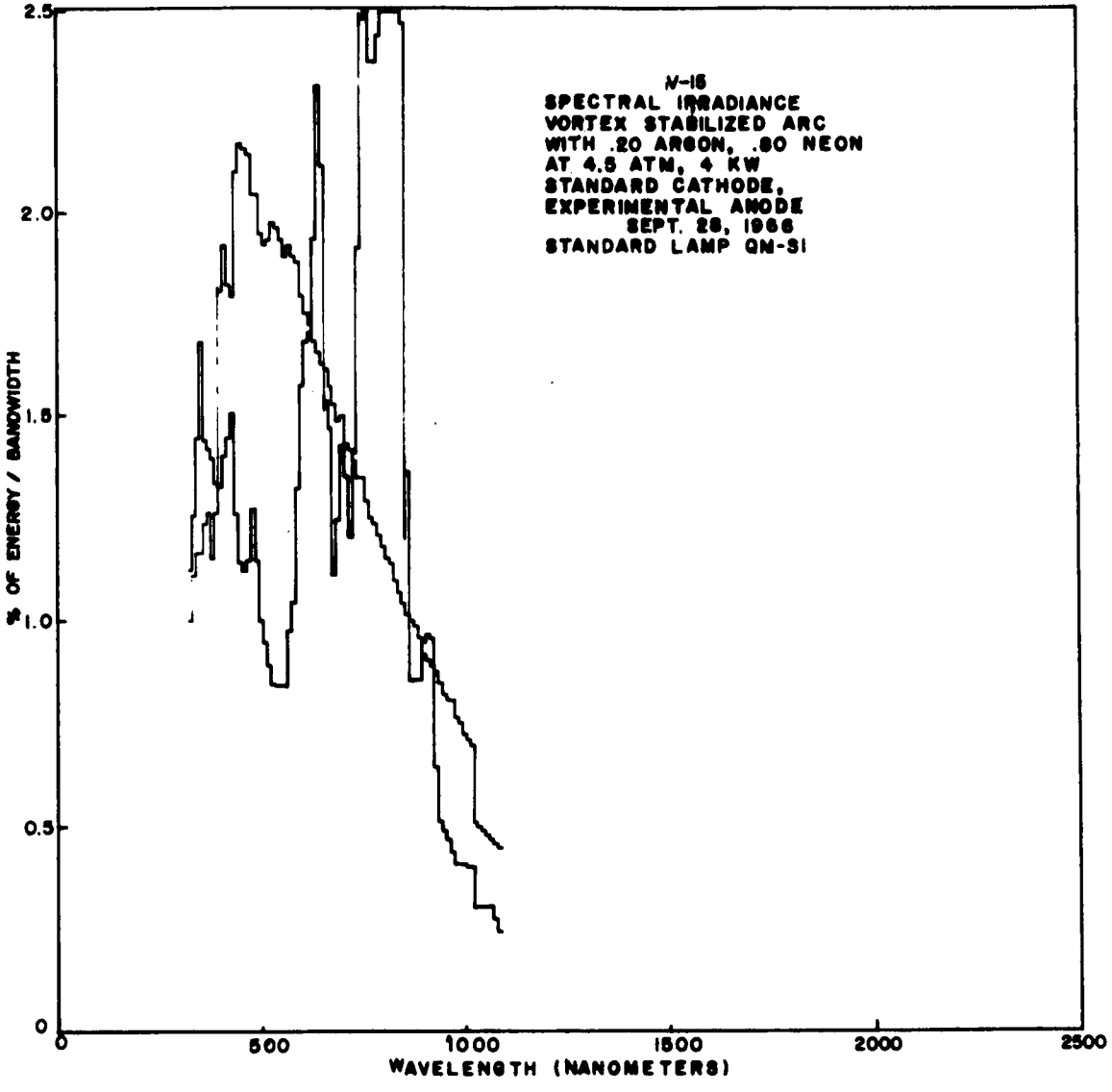

Figure 22. Vortex Arc Spectral Irradiance, 20% Argon-80% Neon, 4kw, 4.5 Atmospheres

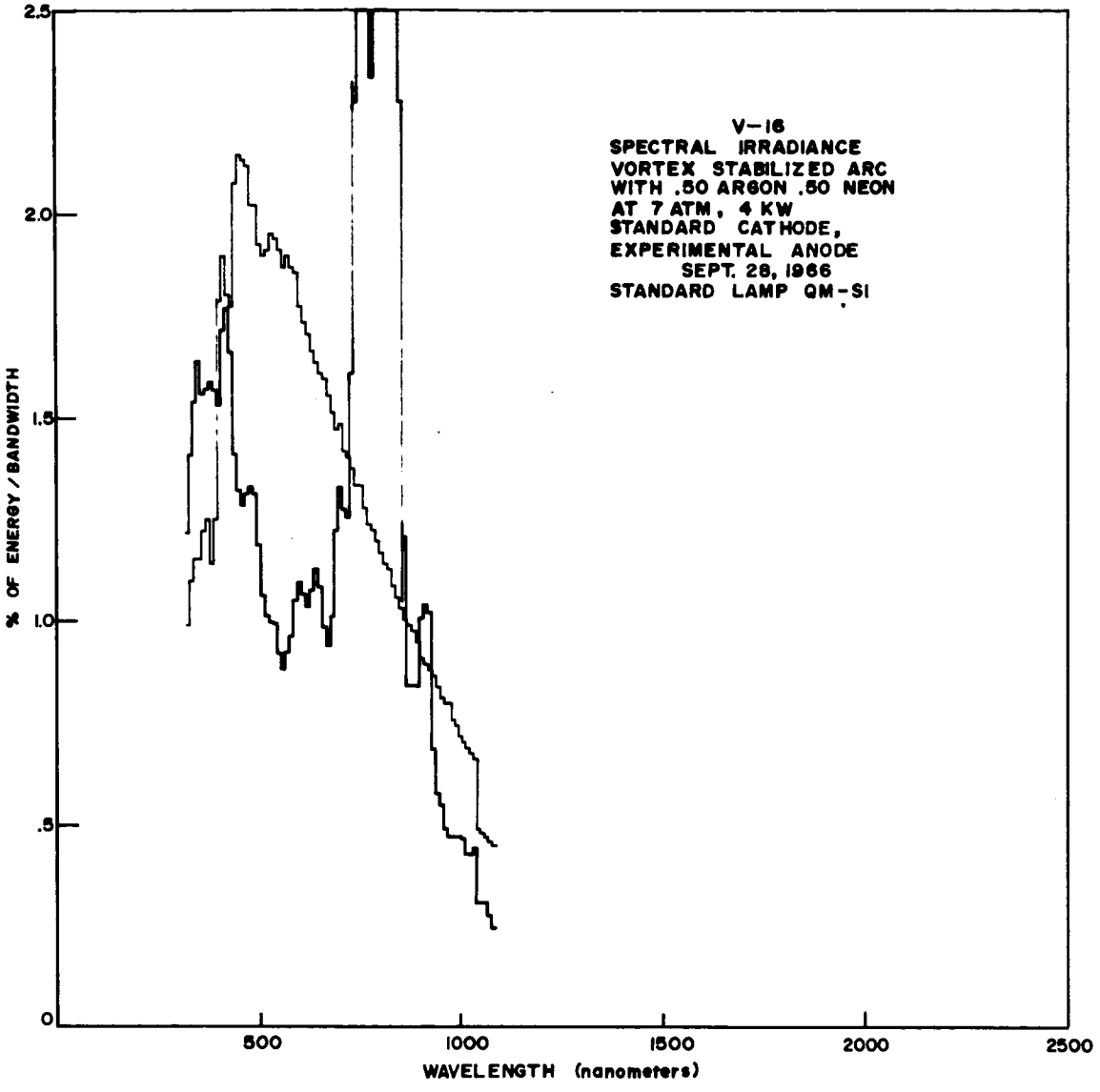

Figure 23. Vortex Arc Spectral Irradiance, 50% Argon-50% Neon, 4kw, 7 Atmospheres

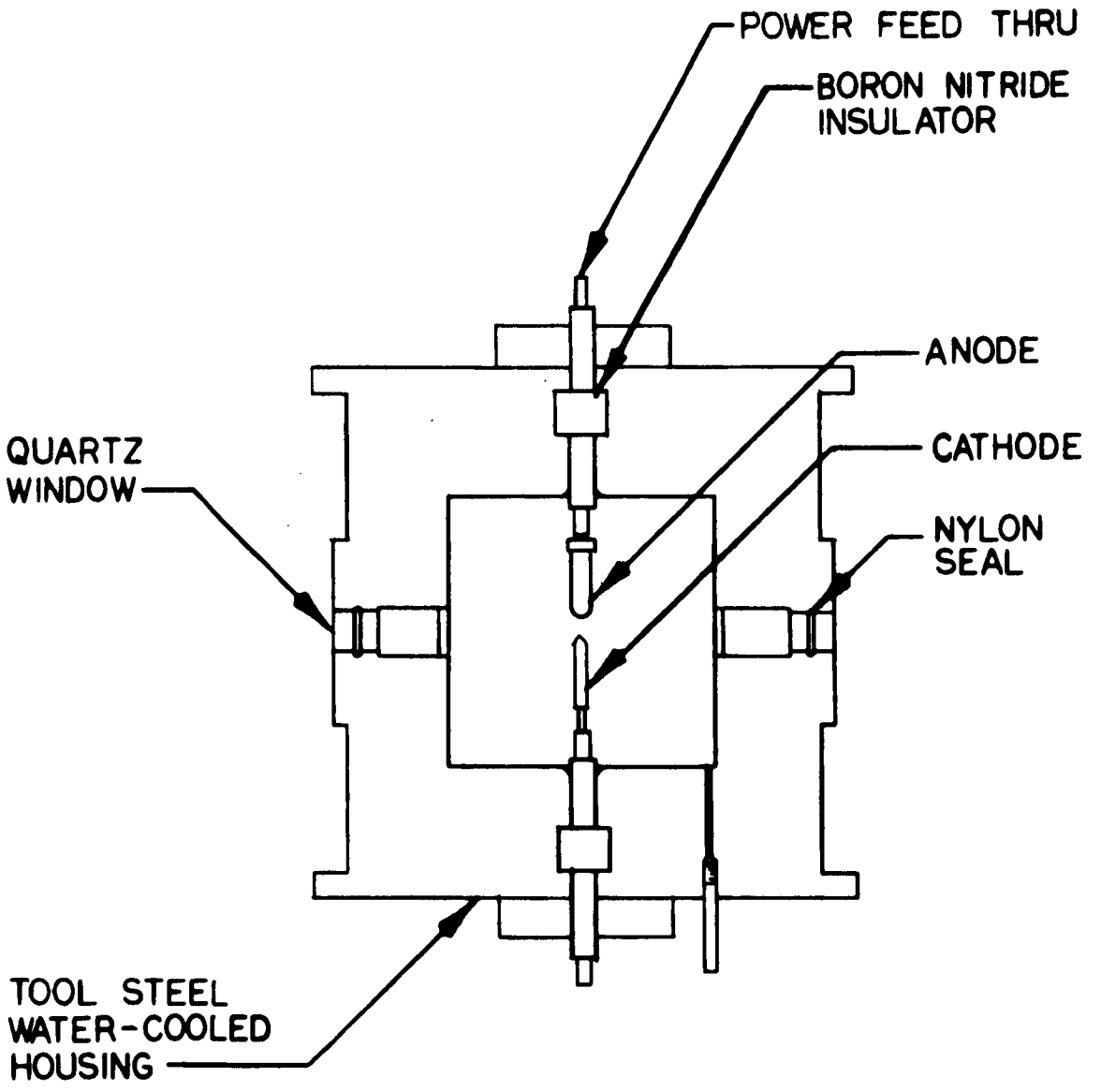

Figure 24. Pressure Arc Chamber

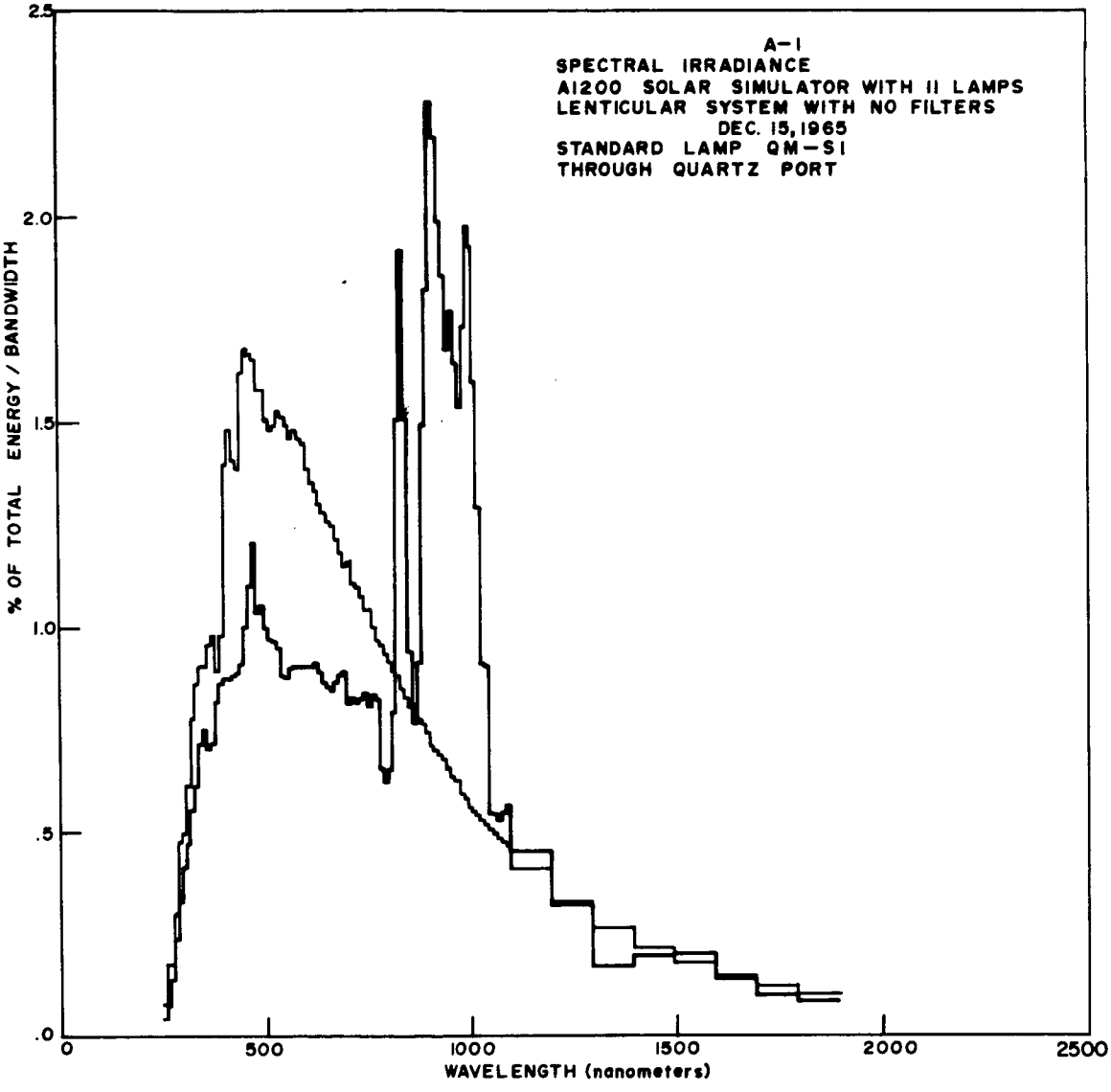

Figure 25. A1200 Spectral Irradiance, Xenon, 11 Lamps, No Filters

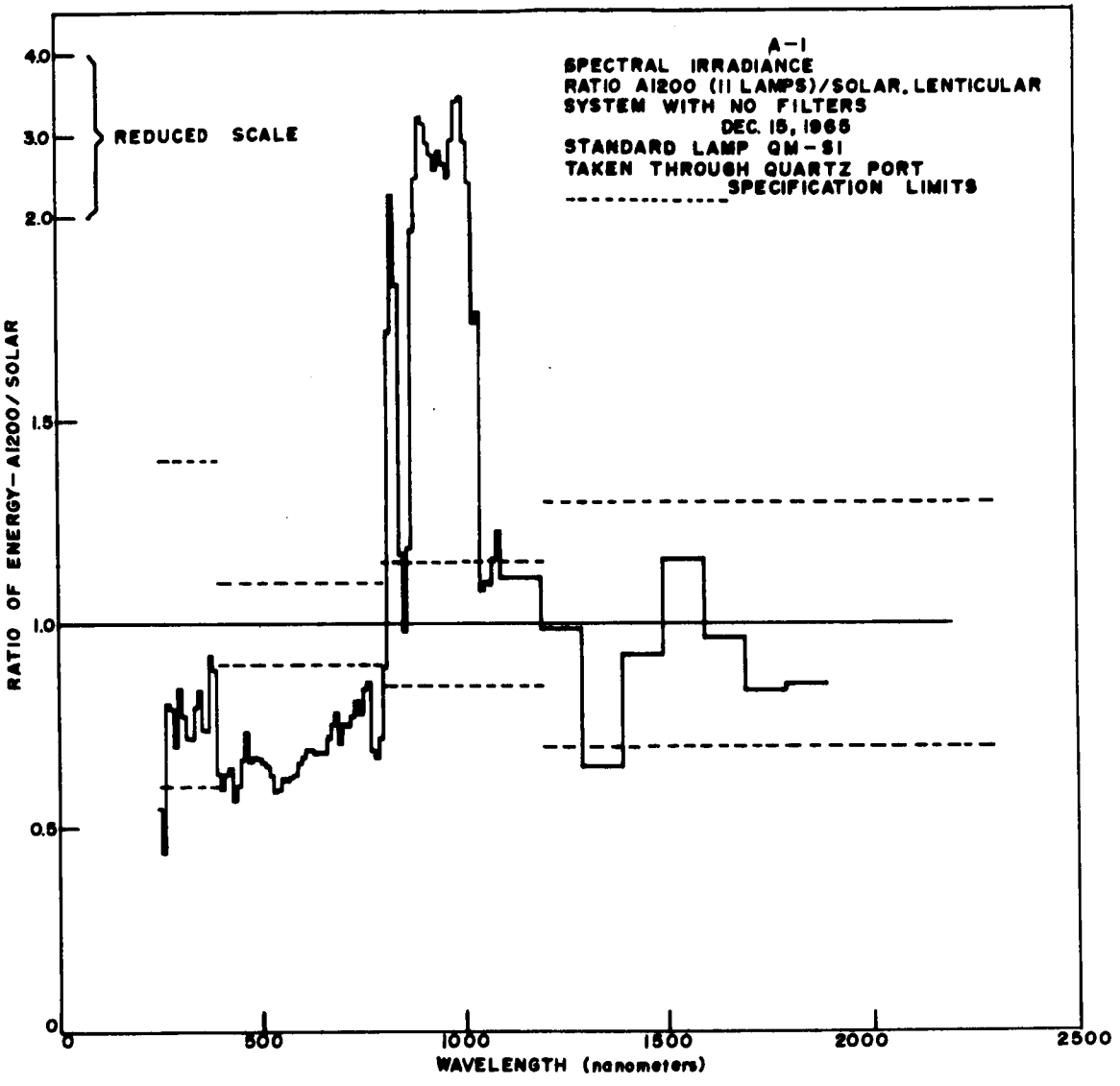

Figure 26. Ratio - A1200/Solar, Xenon, 11 Lamps, No Filters

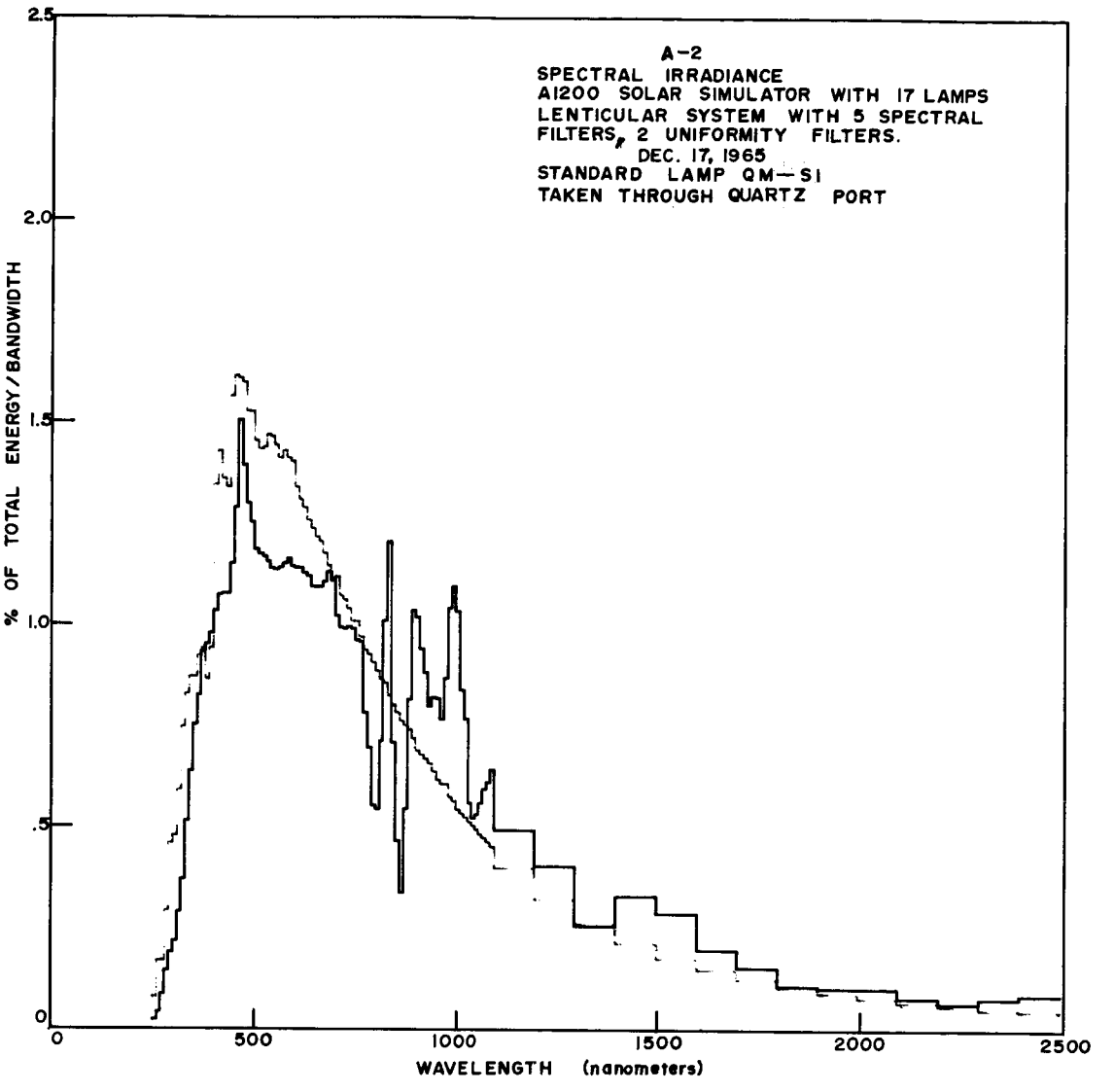

Figure 27. A1200 Spectral Irradiance, Xenon, 17 Lamps, 5 Spectral Filters, 3 Uniformity Filters

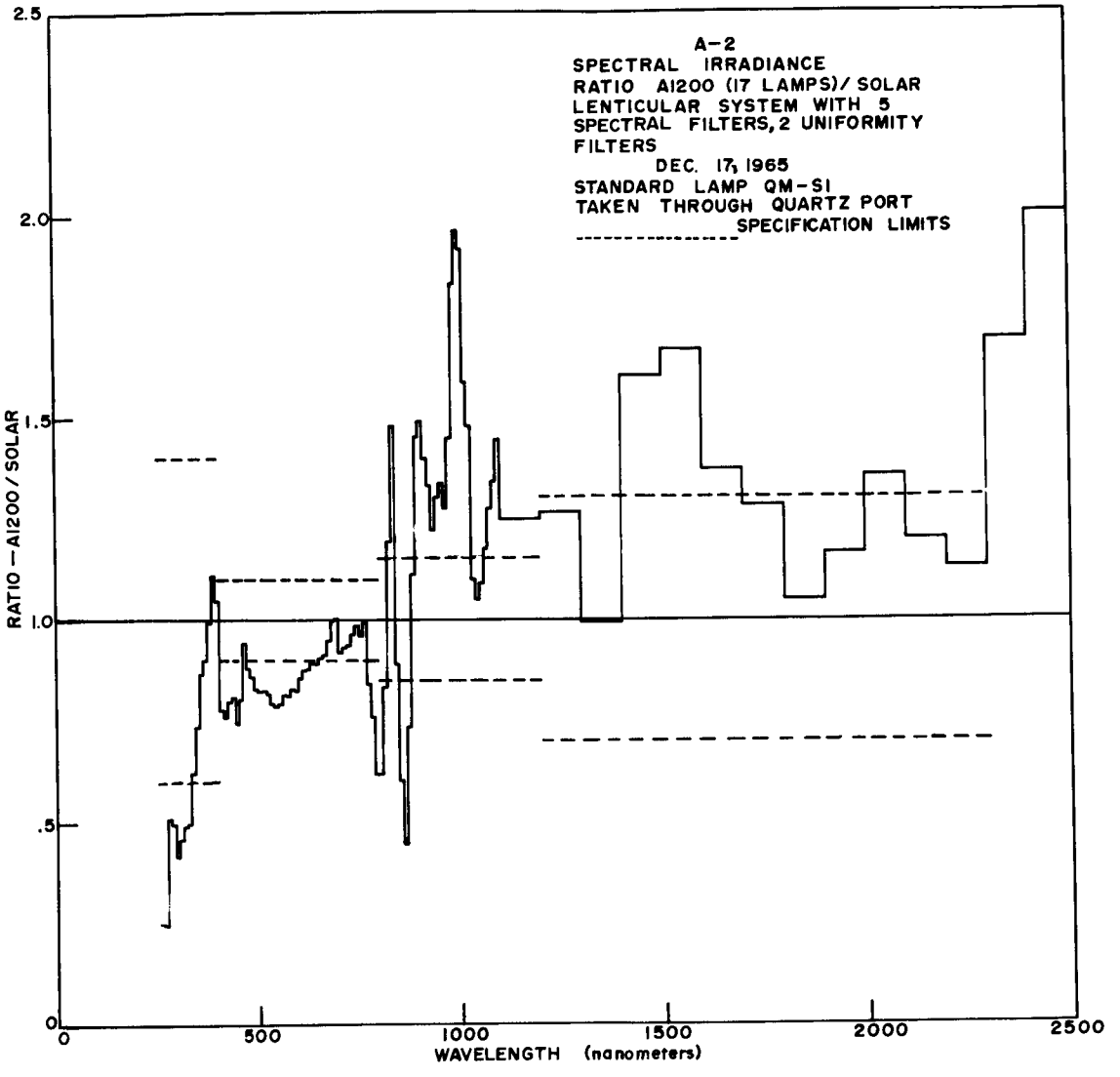

Figure 28. Ratio - A1200/Solar, Xenon, 17 Lamps, 5 Spectral Filters, 3 Uniformity Filters

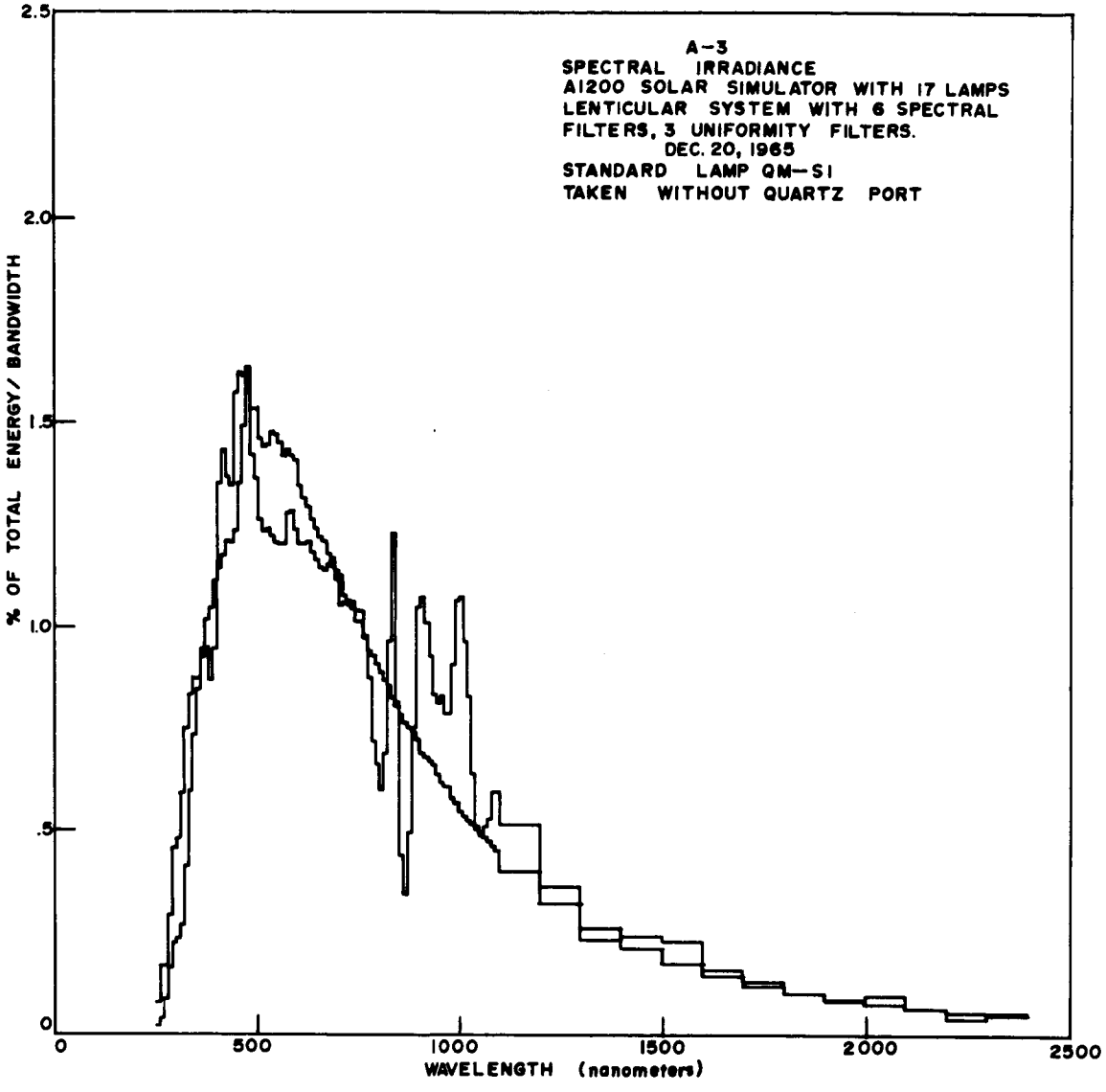

Figure 29. A1200 Spectral Irradiance, Xenon, 17 Lamps, 6 Spectral Filters, 3 Uniformity Filters

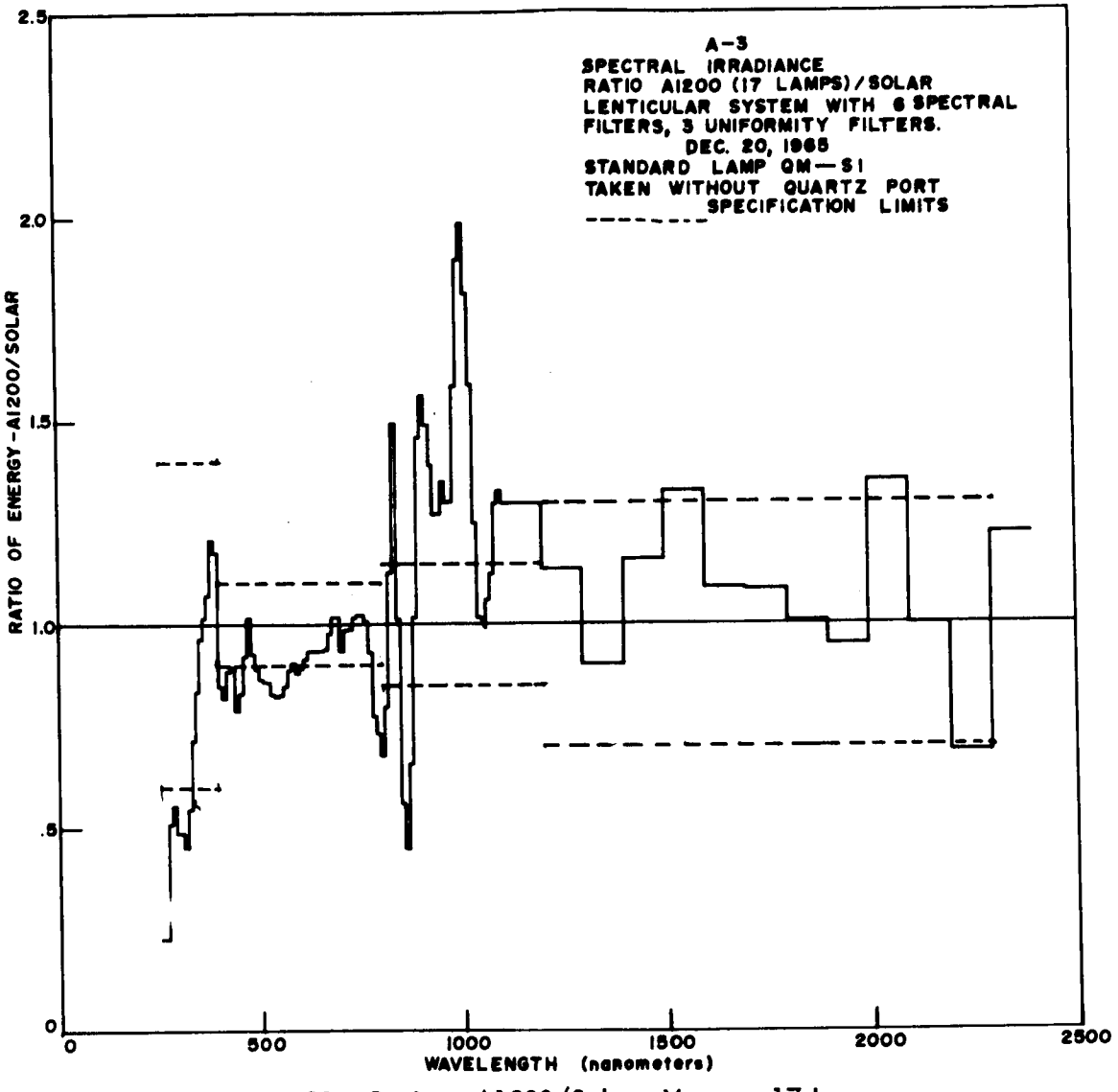

Figure 30. Ratio - A1200/Solar, Xenon, 17 Lamps, 6 Spectral Filters, 3 Uniformity Filters

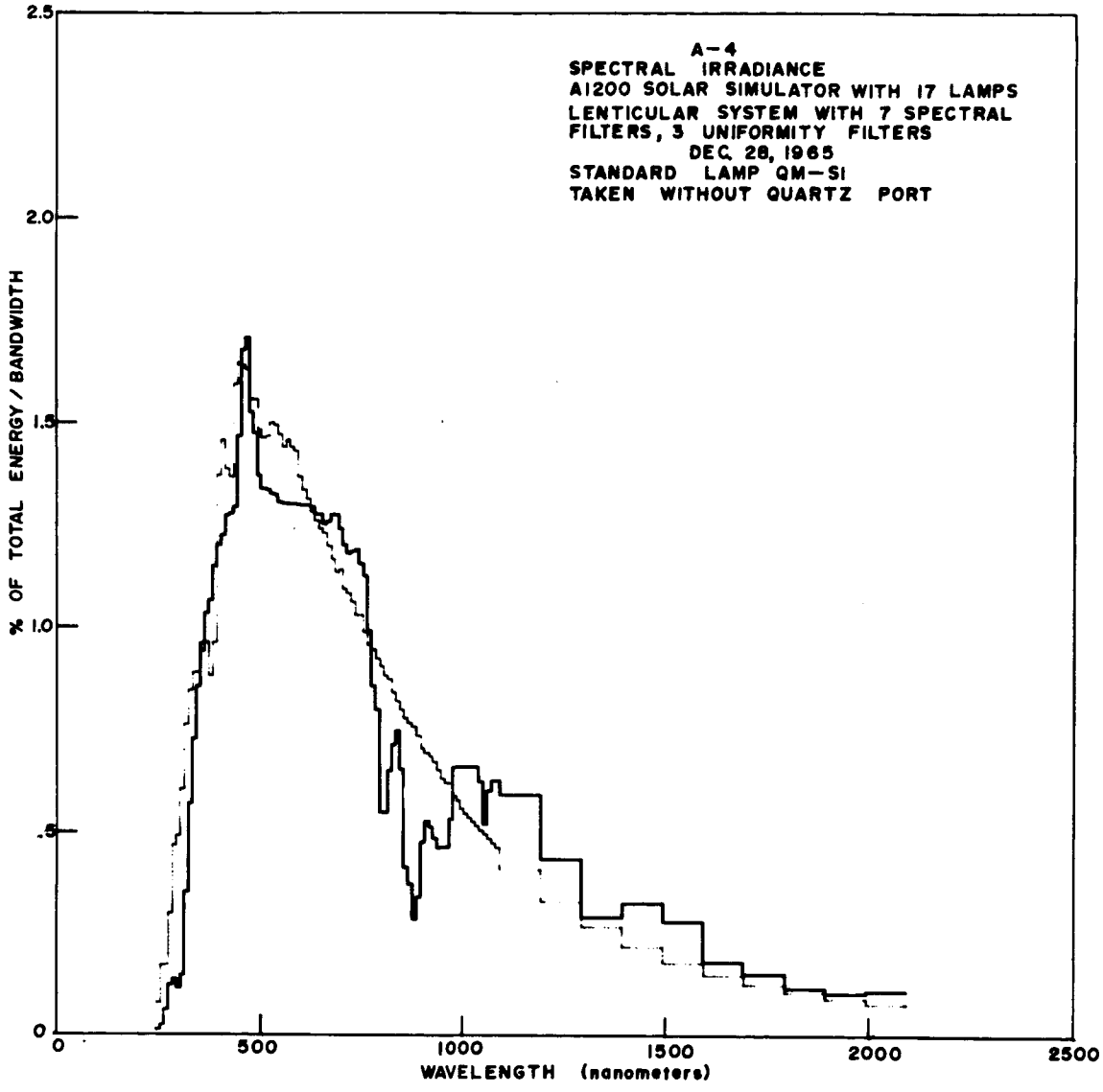

Figure 31. A1200 Spectral Irradiance, Xenon, 17 Lamps, 7 Spectral Filters, 3 Uniformity Filters

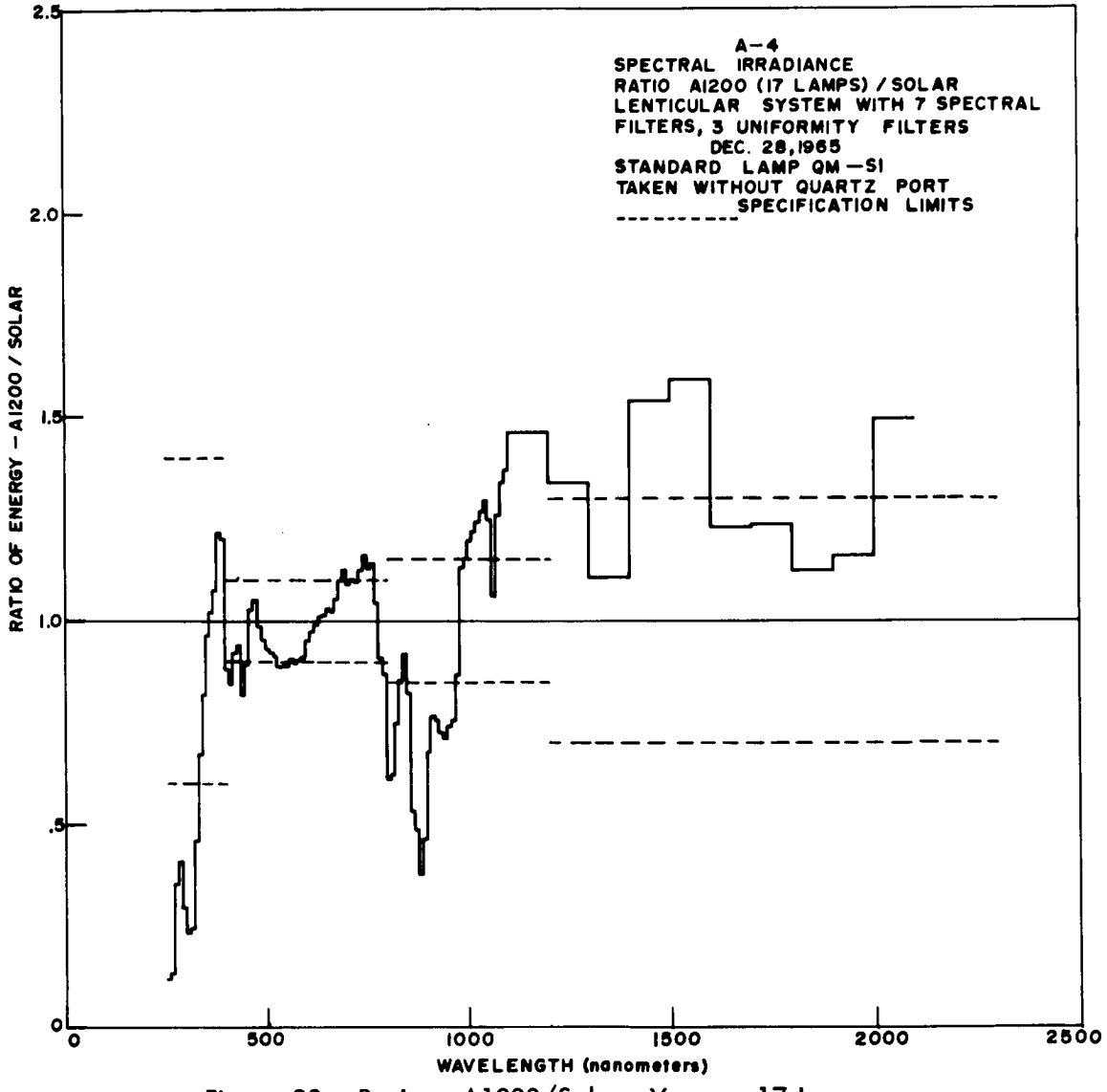

Figure 32. Ratio - A1200/Solar, Xenon, 17 Lamps
7 Spectral Filters, 3 Uniformity Filters

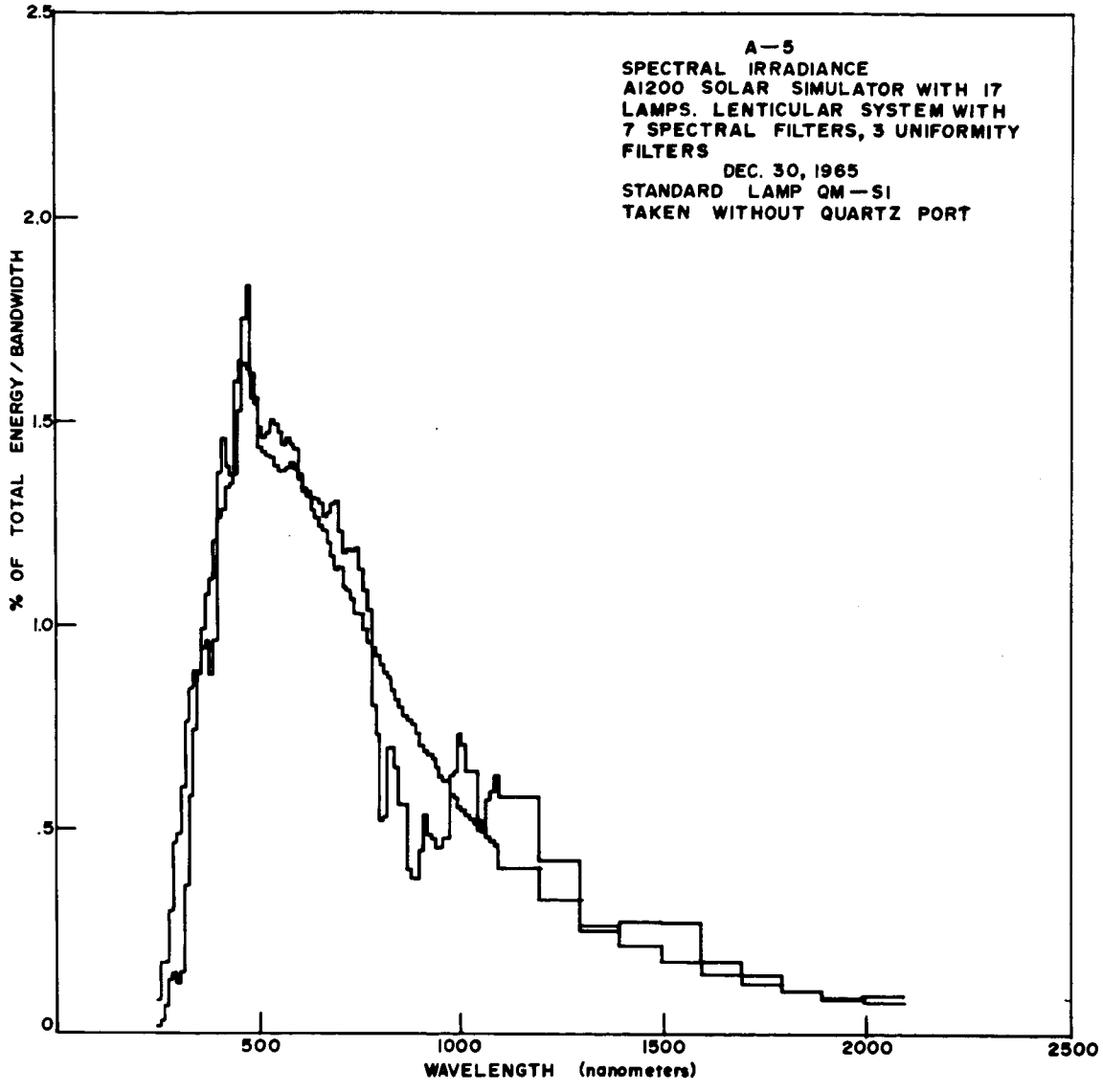

Figure 33. A1200 Spectral Irradiance, Xenon, 17 Lamps, 7 Spectral Filters, 3 Uniformity Filters

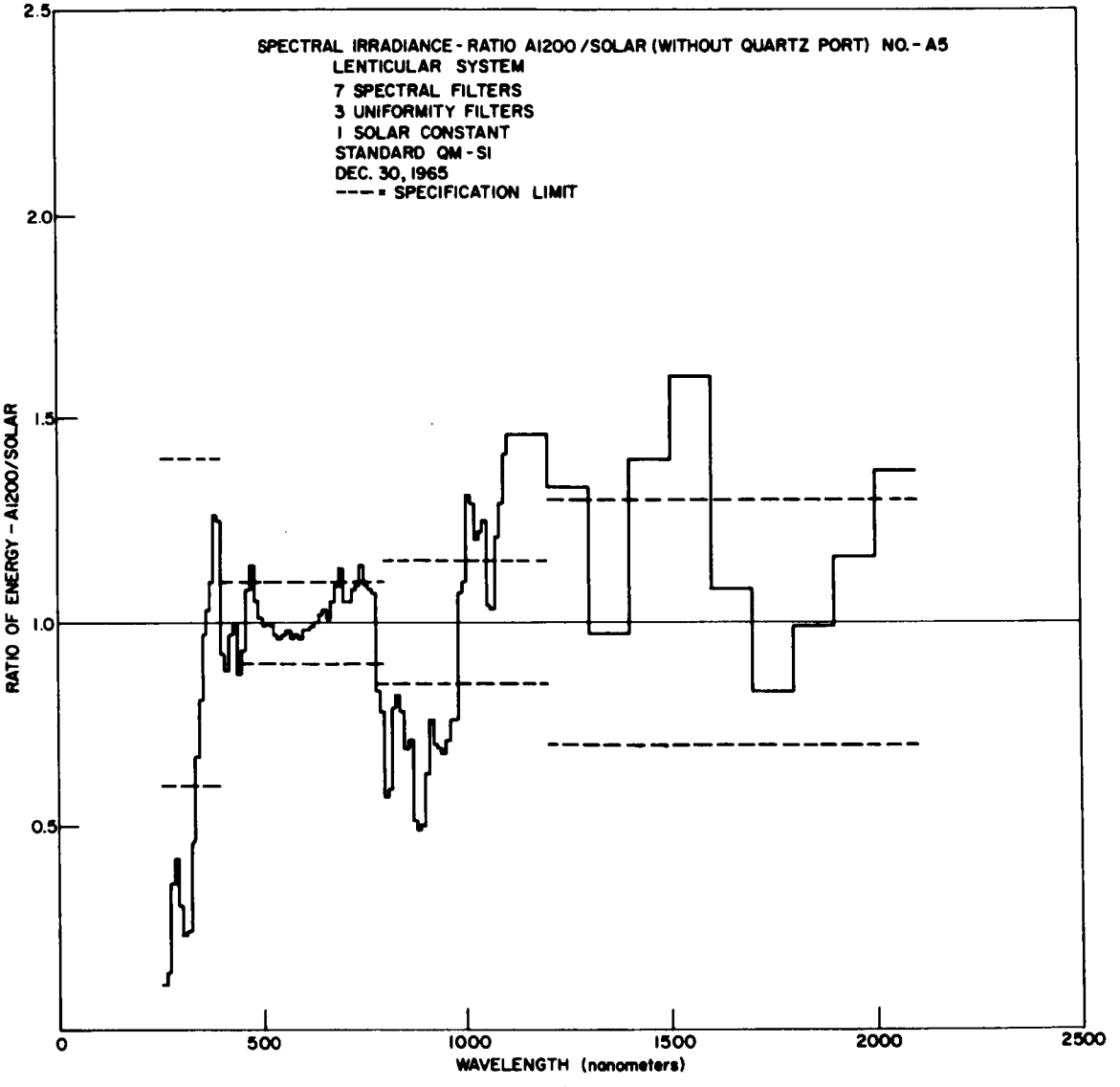

Figure 34. Ratio - A1200/Solar, Xenon, 17 Lamps, 7 Spectral Filters, 3 Uniformity Filters

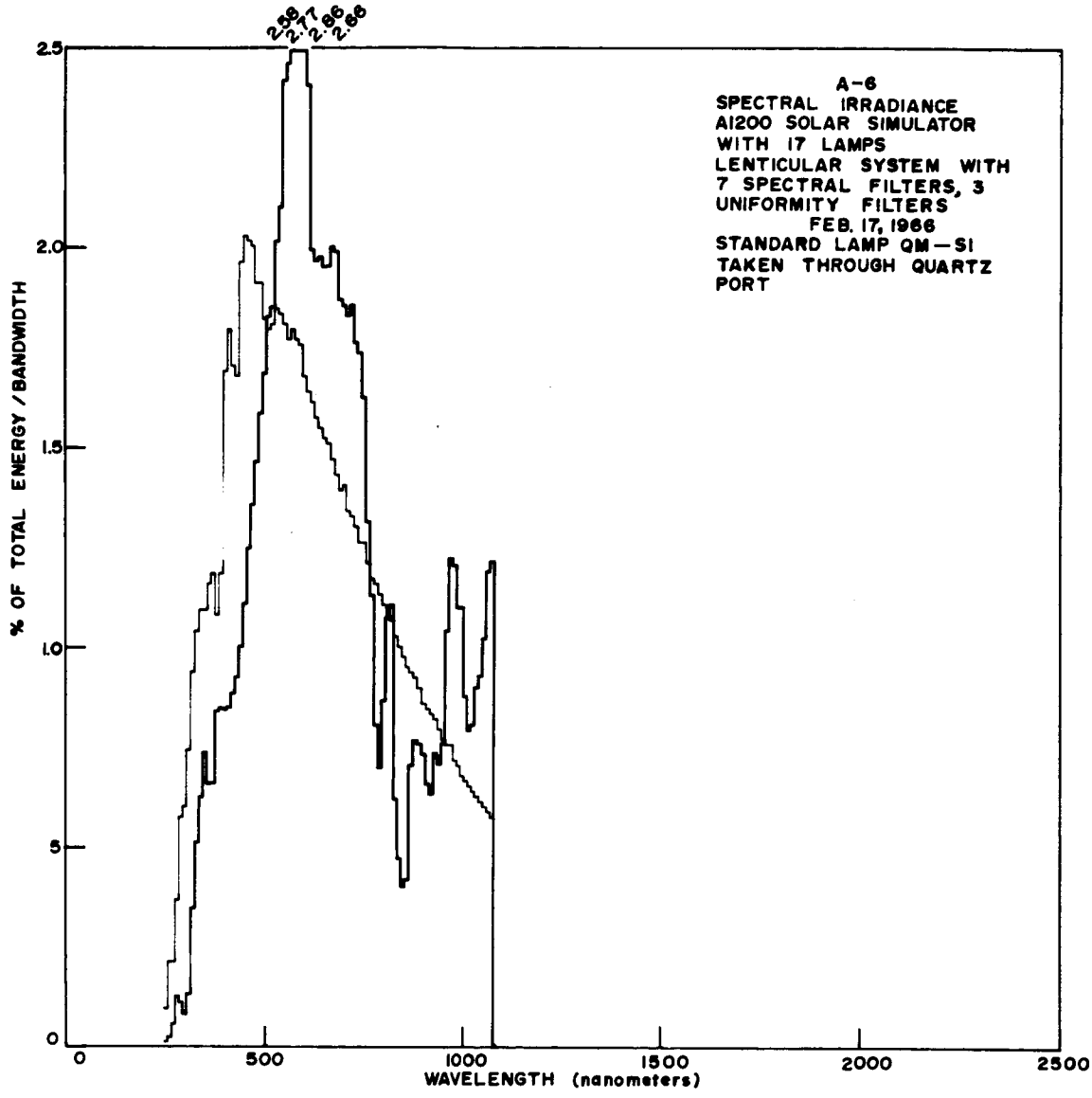

Figure 35. A1200 Spectral Irradiance, Xenon, 17 Lamps, 7 Spectral Filters, 3 Uniformity Filters

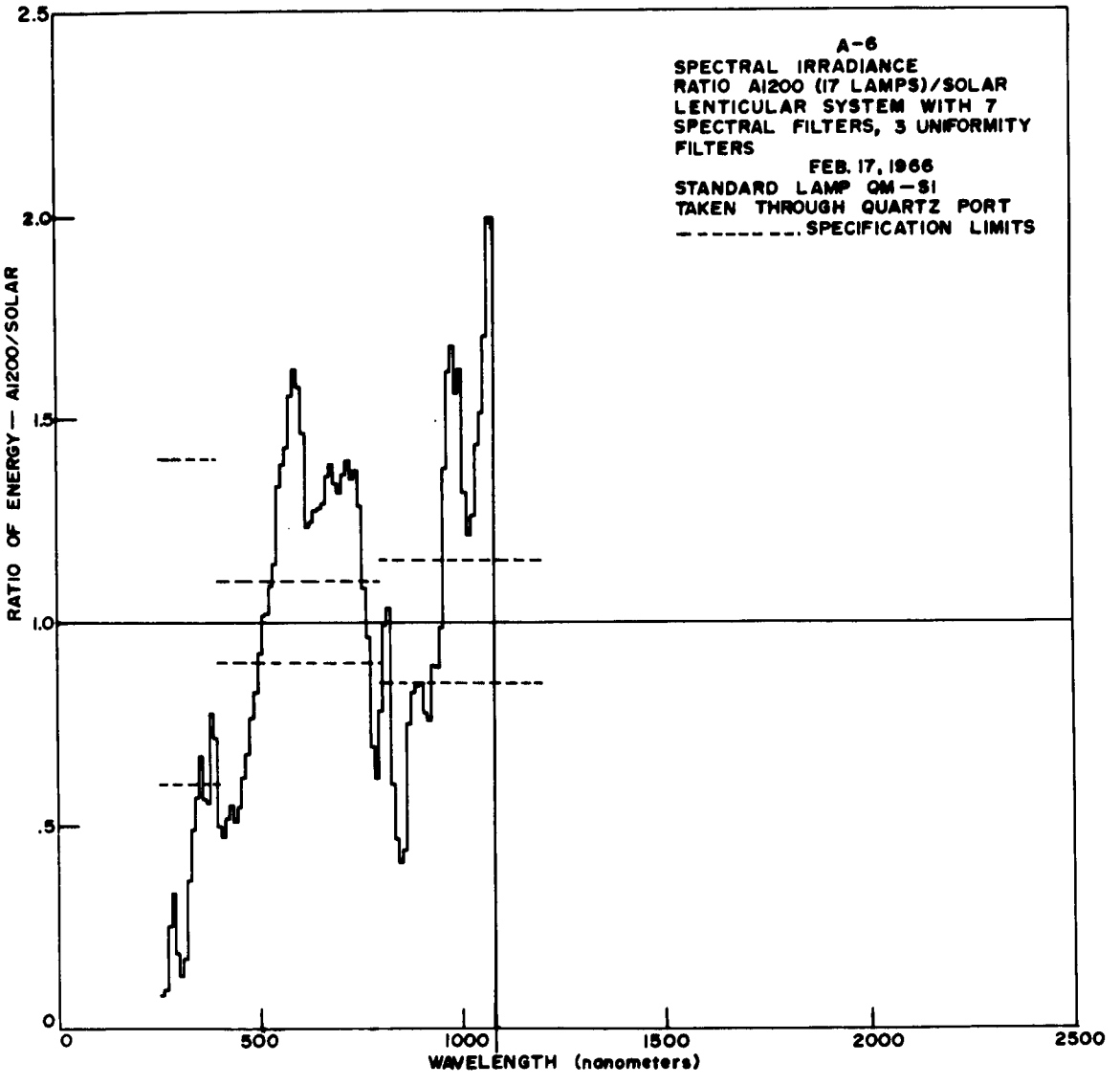

Figure 36. Ratio - A1200/Solar, Xenon, 17 Lamps, 7 Spectral Filters, 3 Uniformity Filters

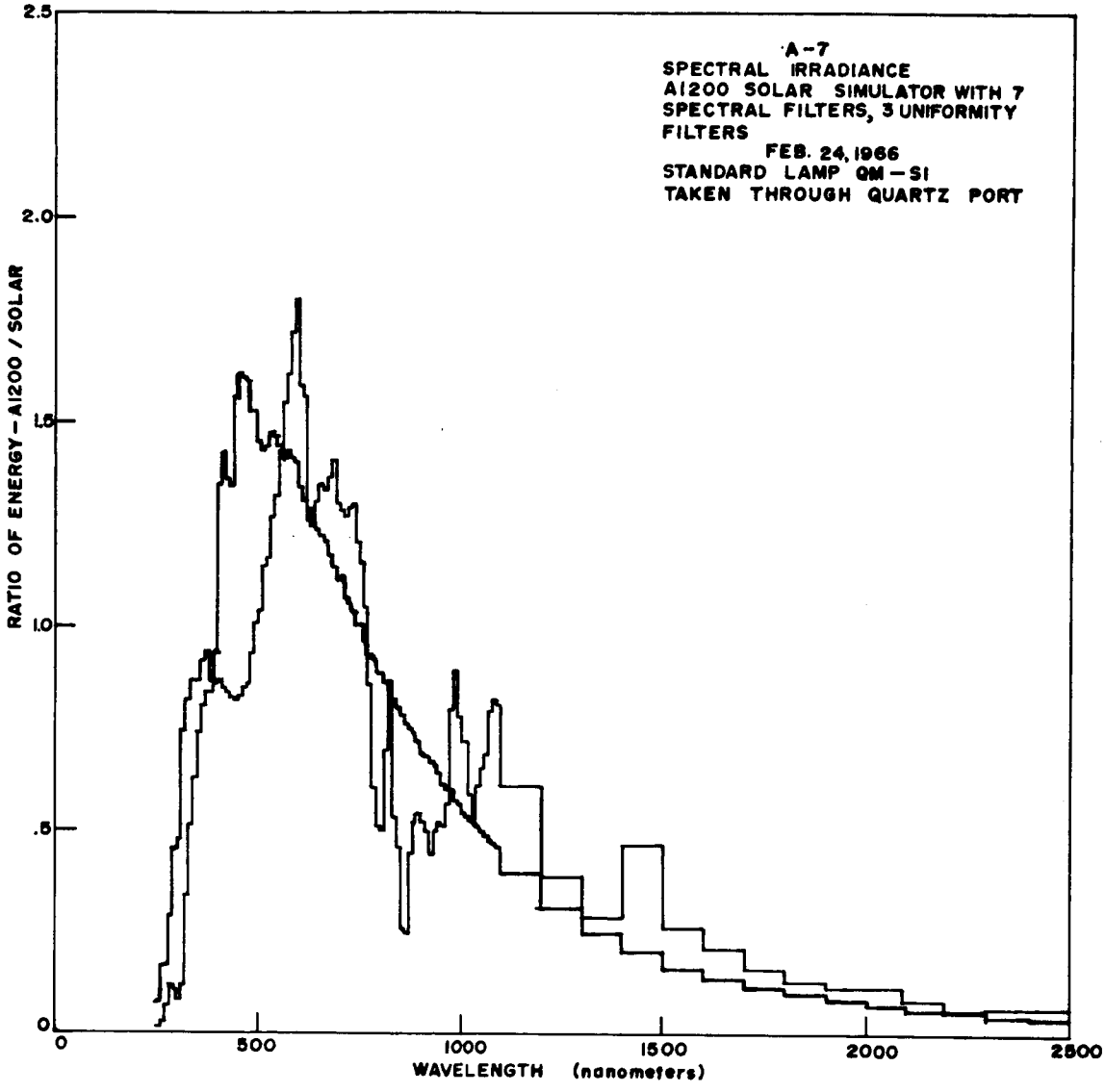

Figure 37. A1200 Spectral Irradiance, Xenon, 17 Lamps, 7 Spectral Filters, 3 Uniformity Filters

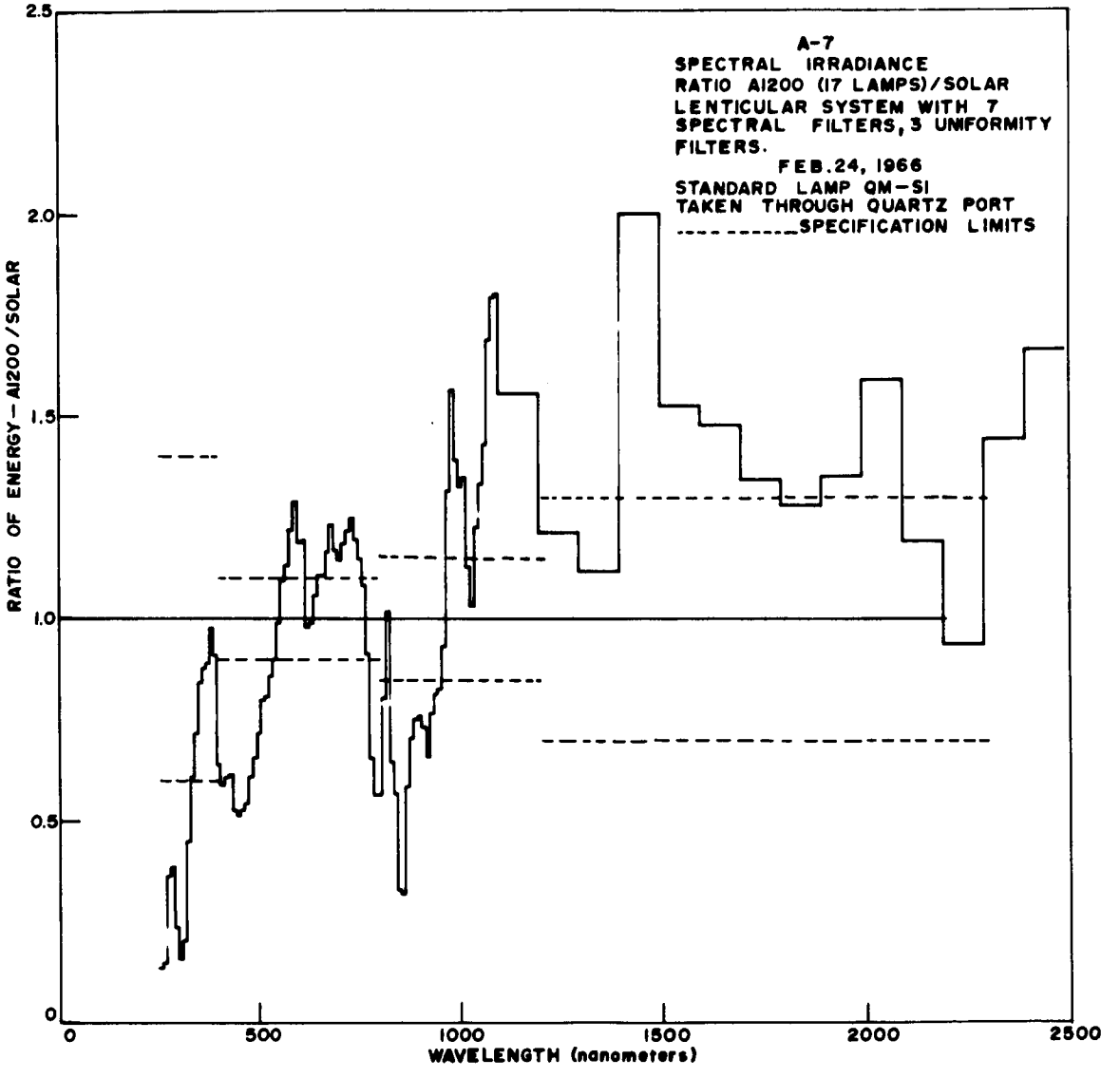

Figure 38. Ratio - A1200/Solar, Xenon, 17 Lamps, 7 Spectral Filters, 3 Uniformity Filters

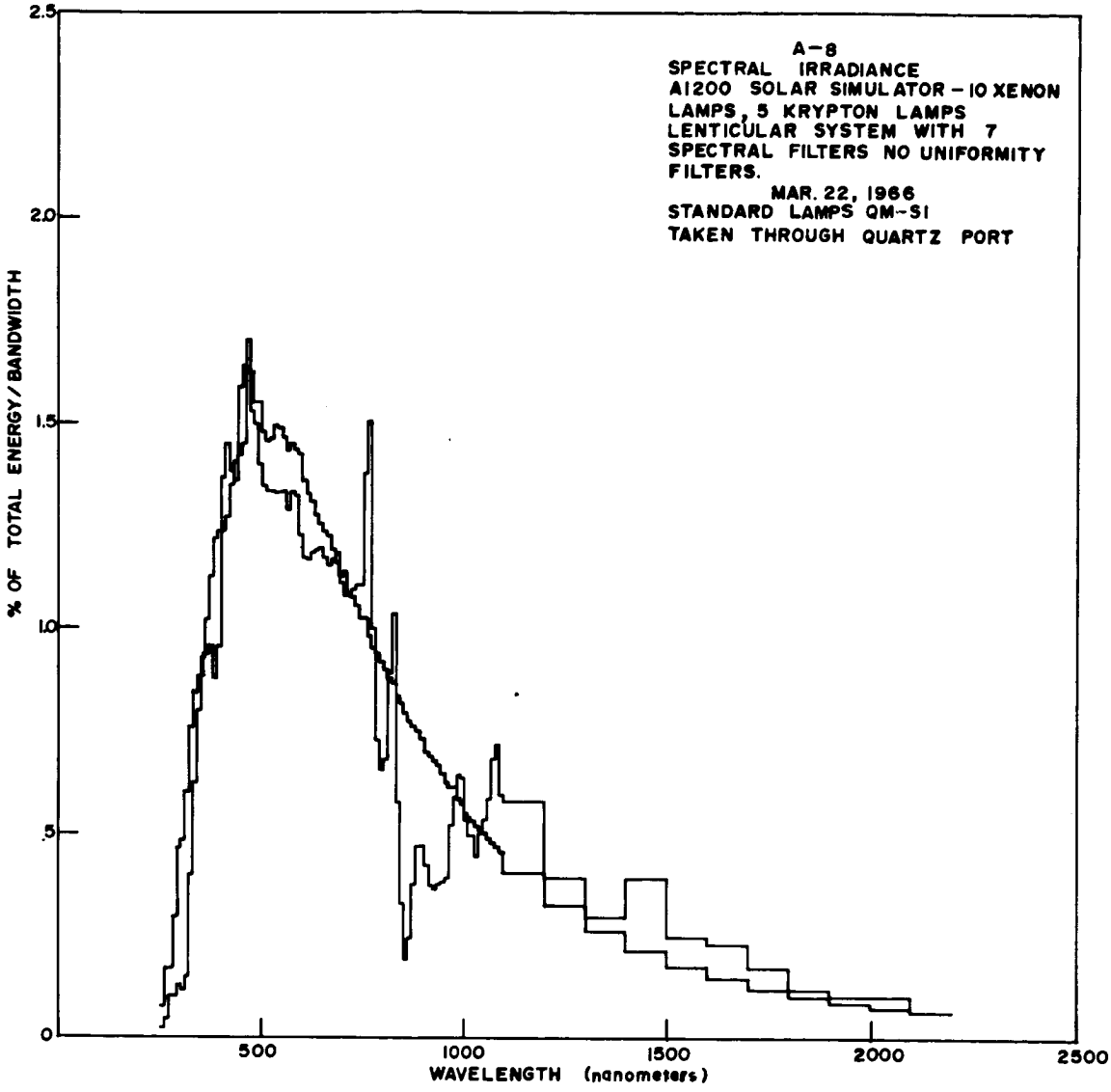

Figure 39. A1200 Spectral Irradiance, 10 Xe, 5 Kr Lamps, 7 Spectral Filters, No Uniformity Filters

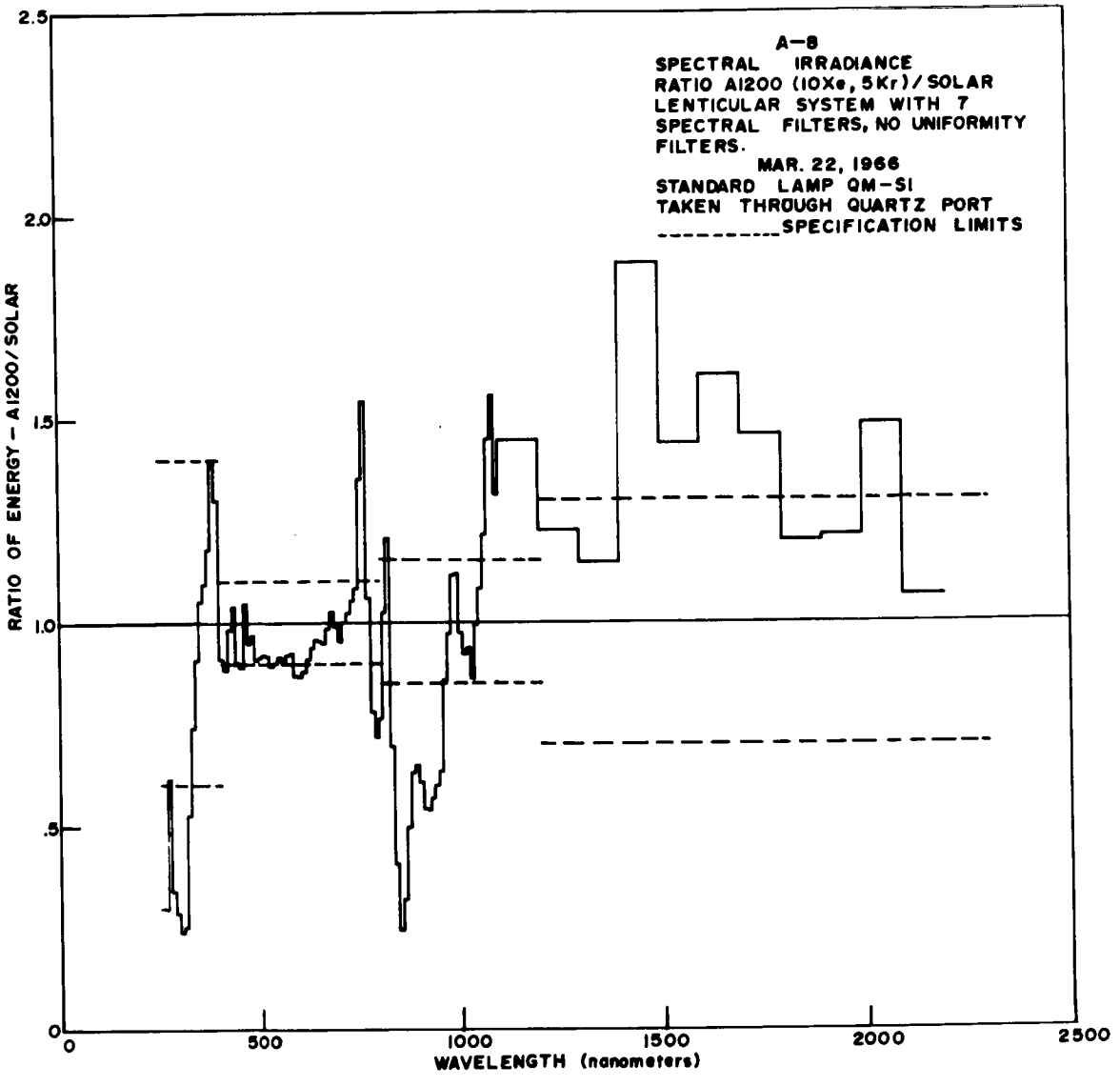

Figure 40. Ratio - A1200/Solar, 10 Xe, 5 Kr Lamps, 7 Spectral Filters, No Uniformity Filters

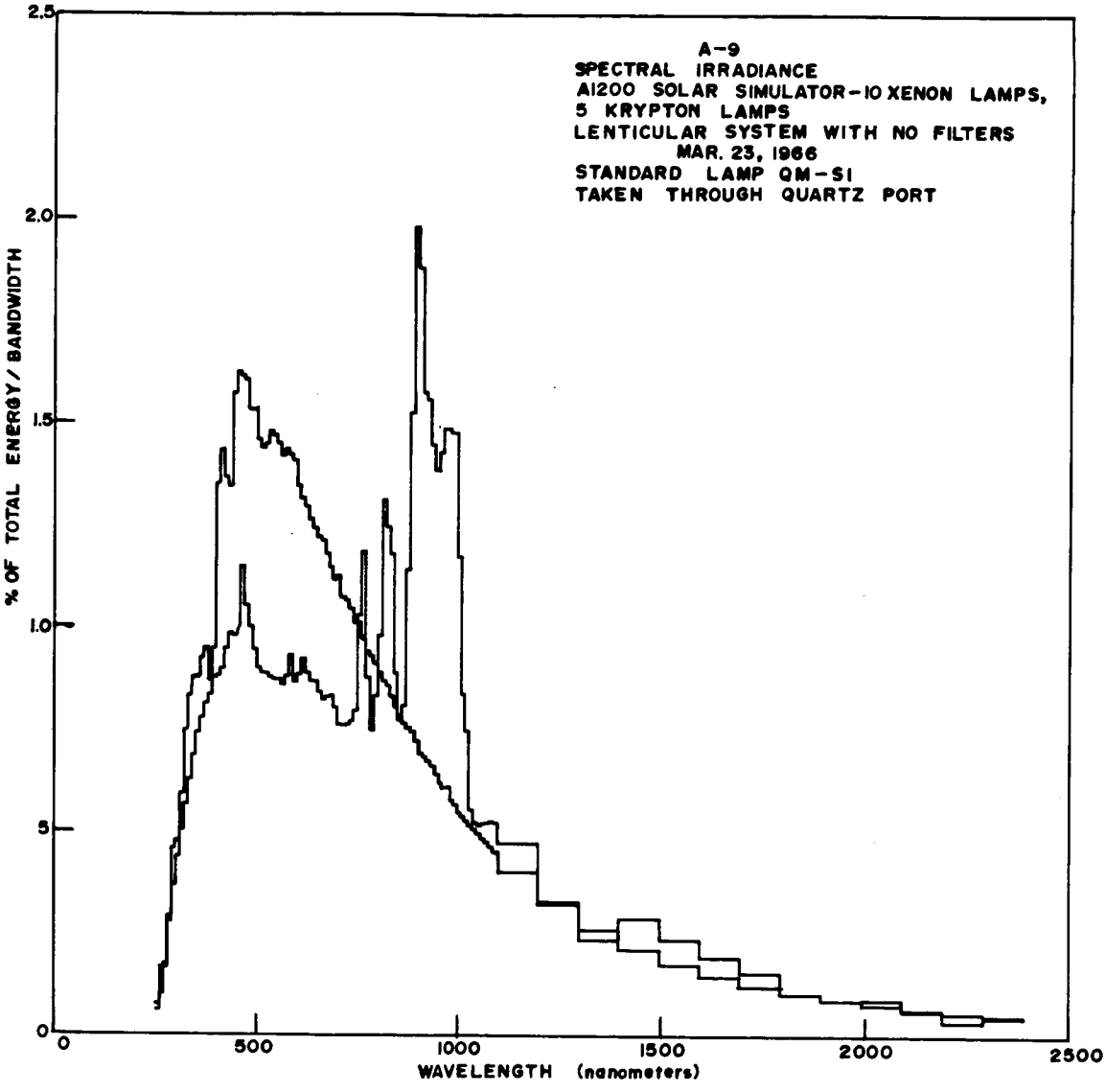

Figure 41. A1200 Spectral Irradiance, 10 Xe, 5 Kr Lamps, No Spectral Filters, No Uniformity Filters

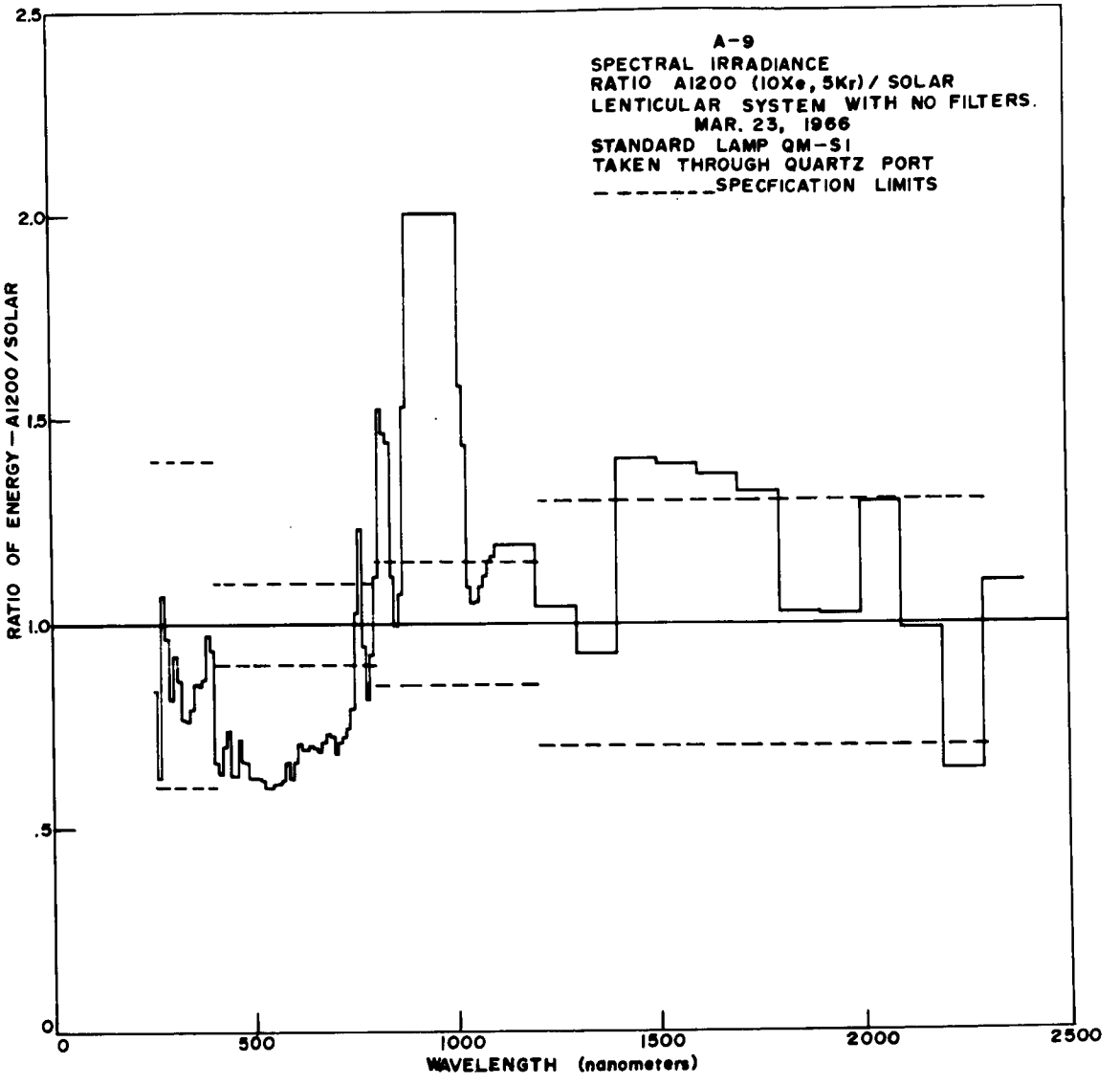

Figure 42. Ratio - A1200/Solar, 10 Xe, 5 Kr Lamps, No Spectral Filters, No Uniformity Filters

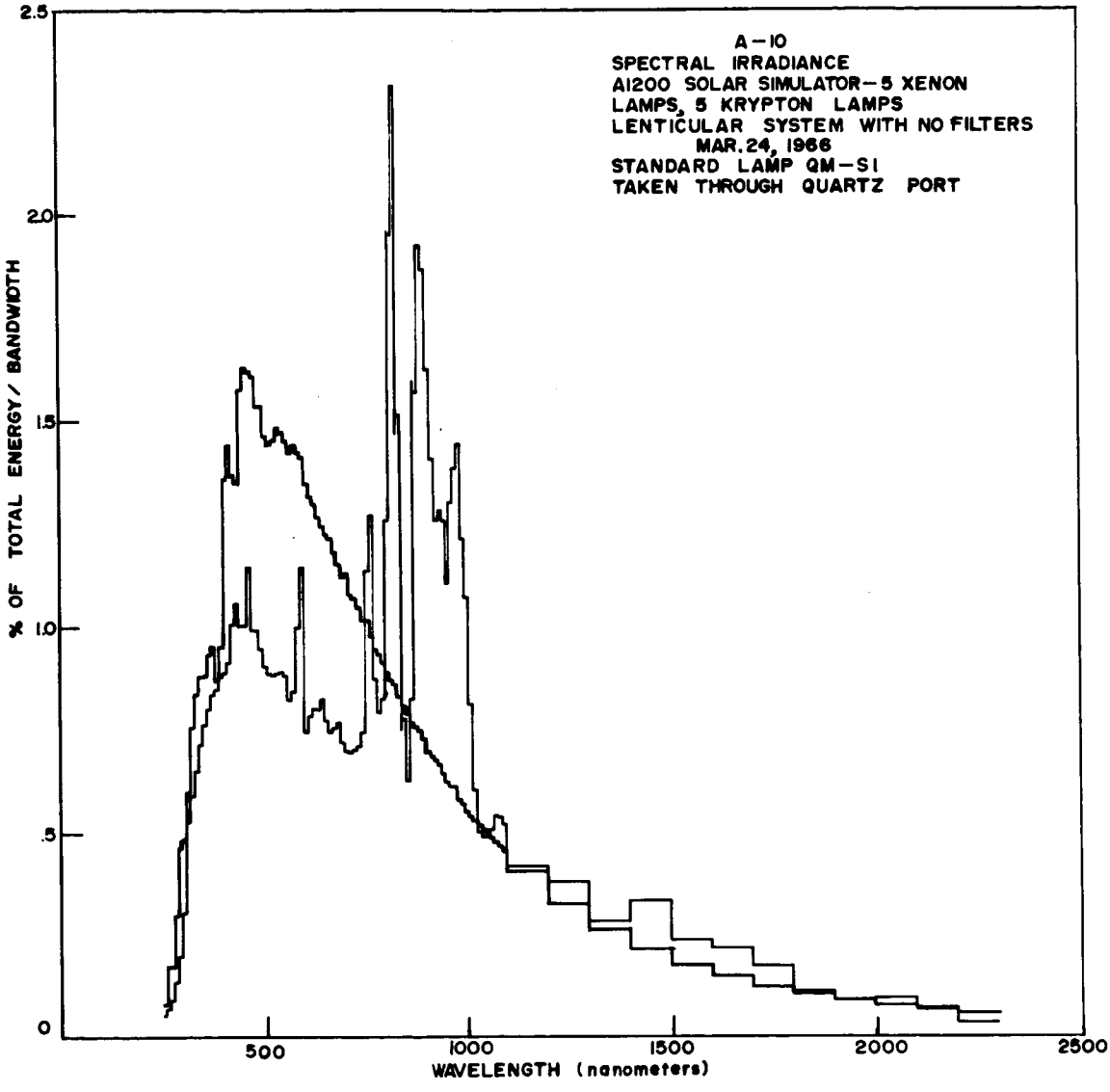

Figure 43. A1200 Spectral Irradiance, 5 Xe, 5 Kr Lamps, No Spectral Filters, No Uniformity Filters

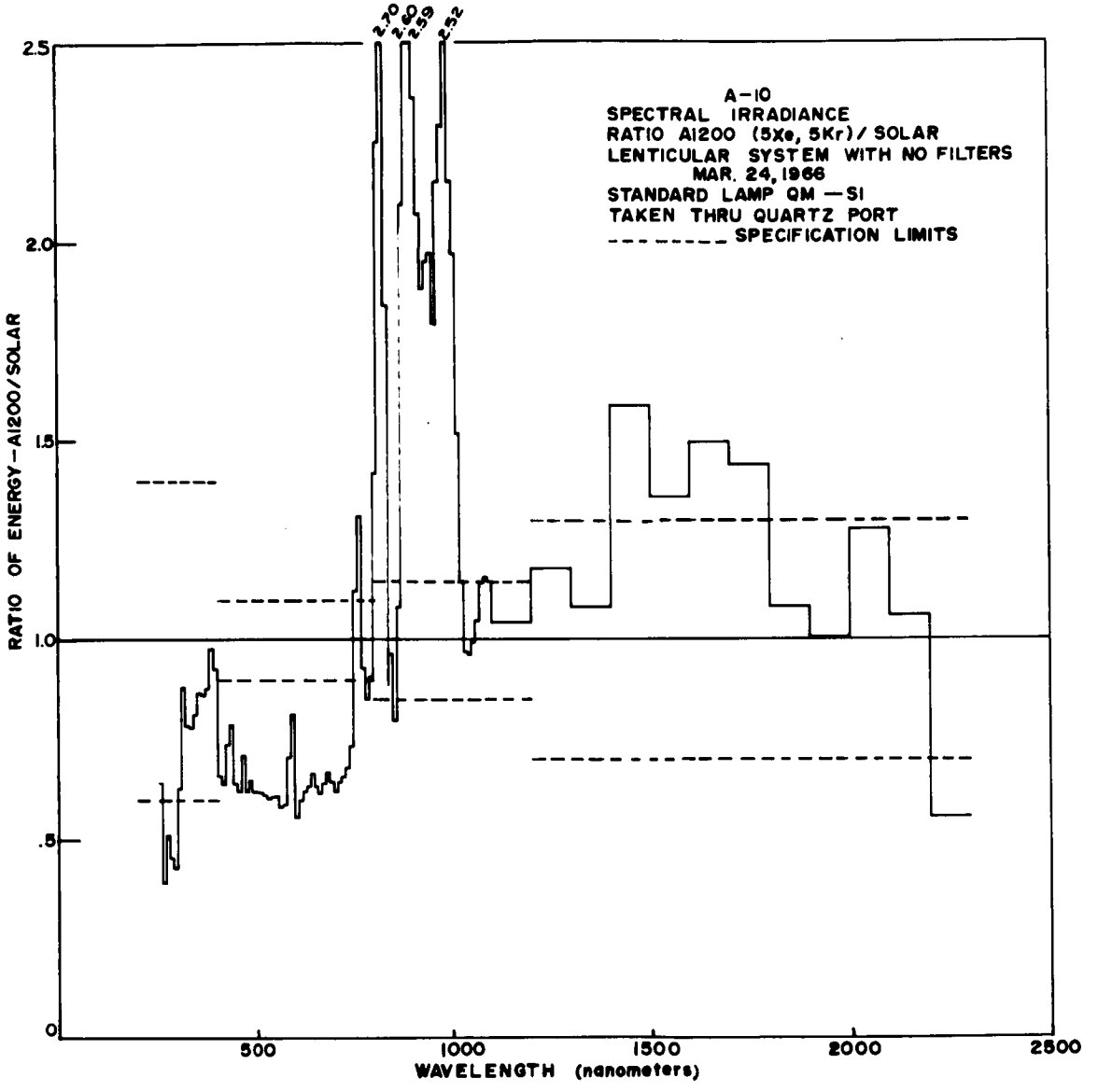

Figure 44. Ratio - A1200/Solar, 5 Xe, 5 Kr Lamps, No Spectral Filters, No Uniformity Filters

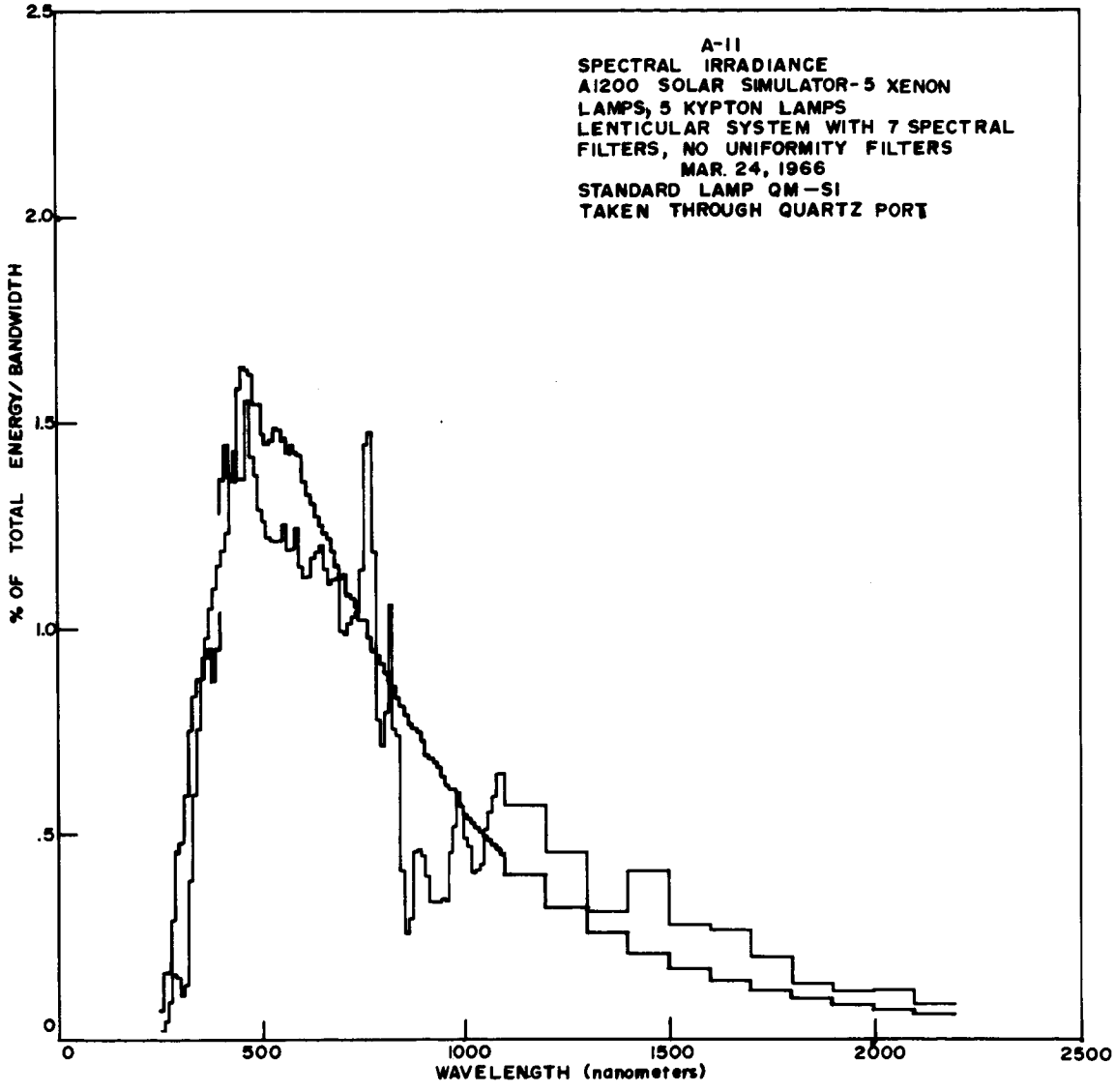

Figure 45. A1200 Spectral Irradiance, 5 Xe, 5 Kr Lamps, 7 Spectral Filters, No Uniformity Filters

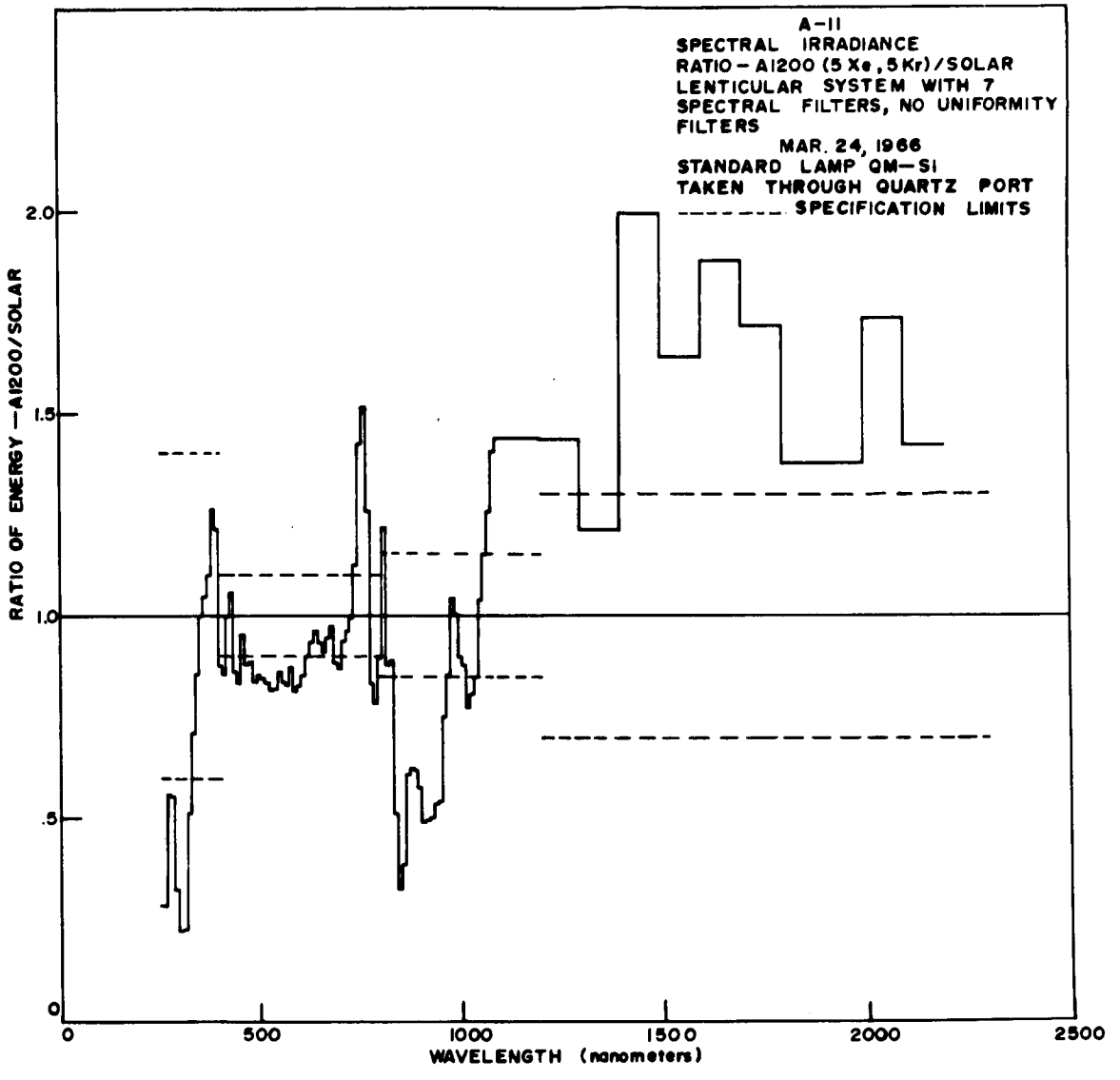

Figure 46. Ratio - A1200/Solar, 5 Xe, 5 Kr Lamps, 7 Spectral Filters, No Uniformity Filters

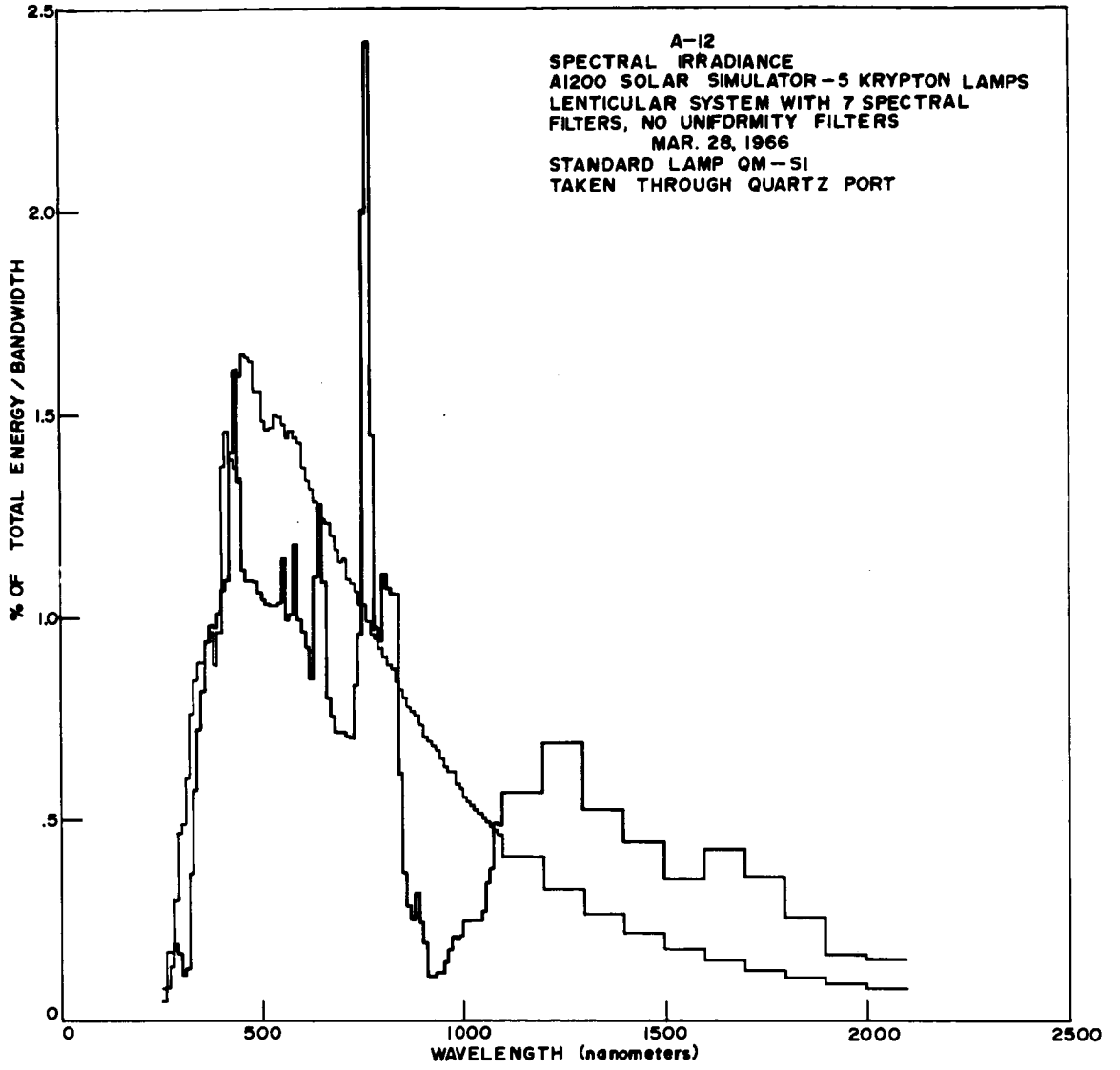

Figure 47. A1200 Spectral Irradiance, 5 Kr Lamps, 7 Spectral Filters, No Uniformity Filters

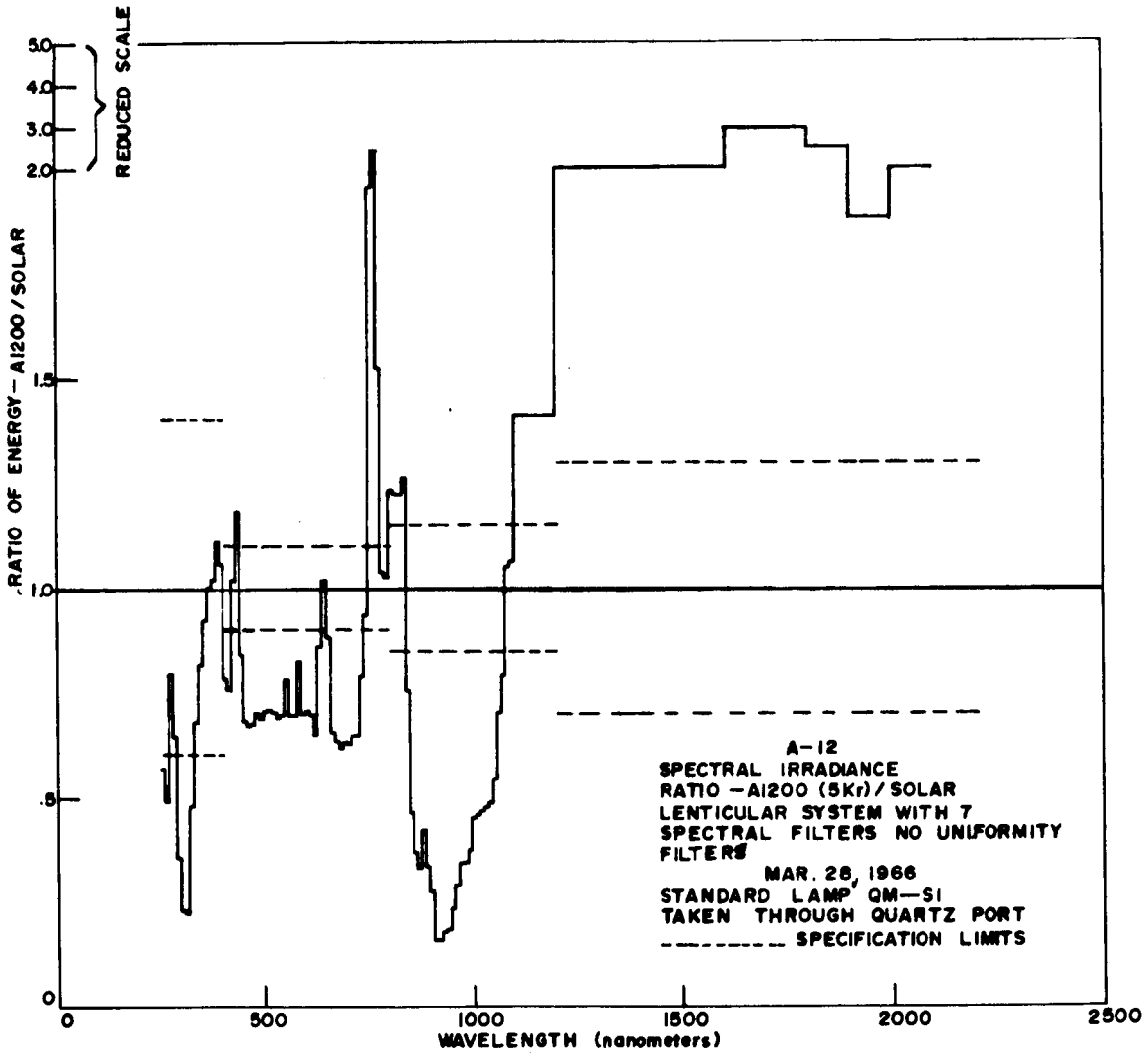

Figure 48. Ratio - A1200/Solar, 5 Kr Lamps, 7 Spectral Filters, No Uniformity Filters

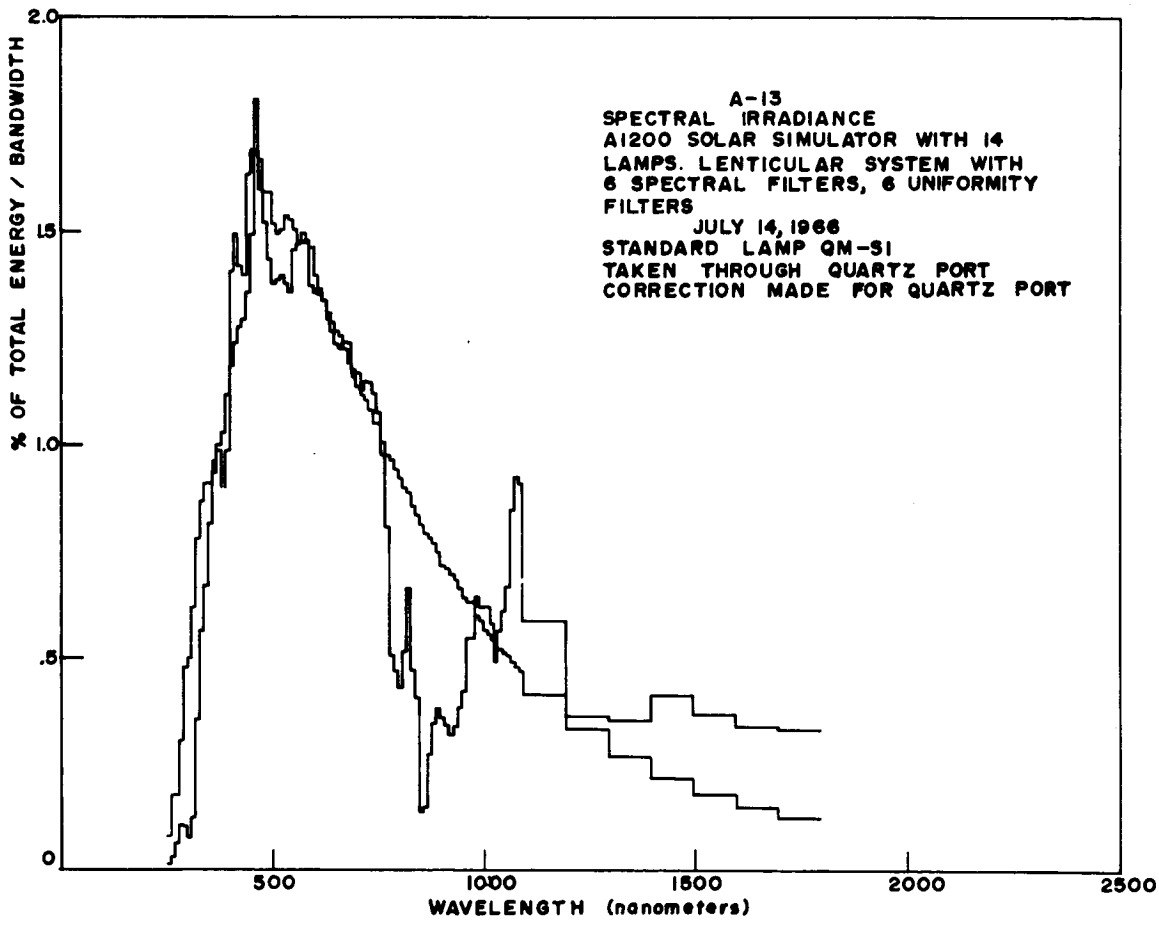

Figure 49. A1200 Spectral Irradiance, Xenon, 14 Lamps, 6 Spectral Filters, 6 Uniformity Filters

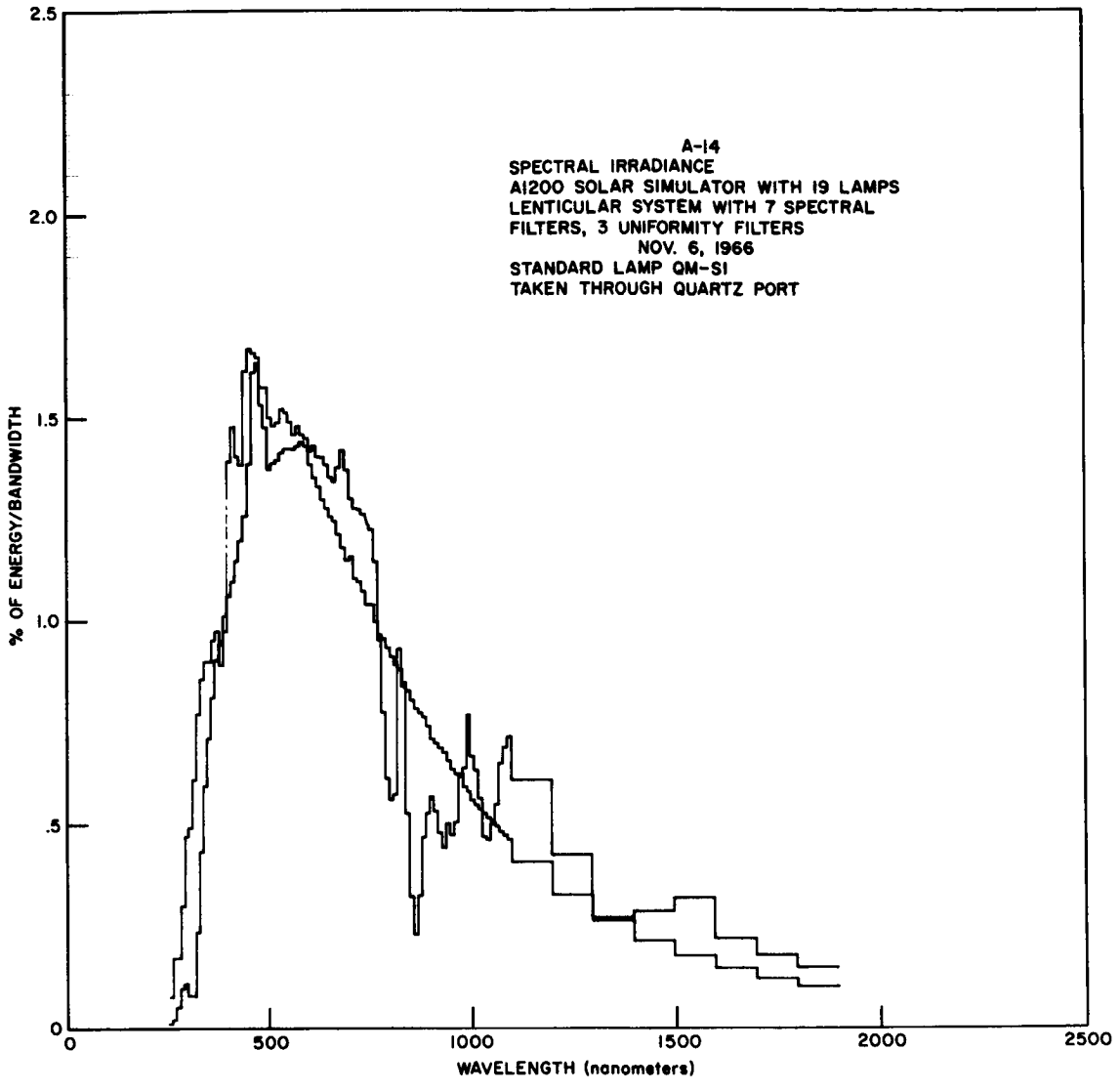

Figure 50. A1200 Spectral Irradiance, Xenon, 19 Lamps, 7 Spectral Filters, 3 Uniformity Filters

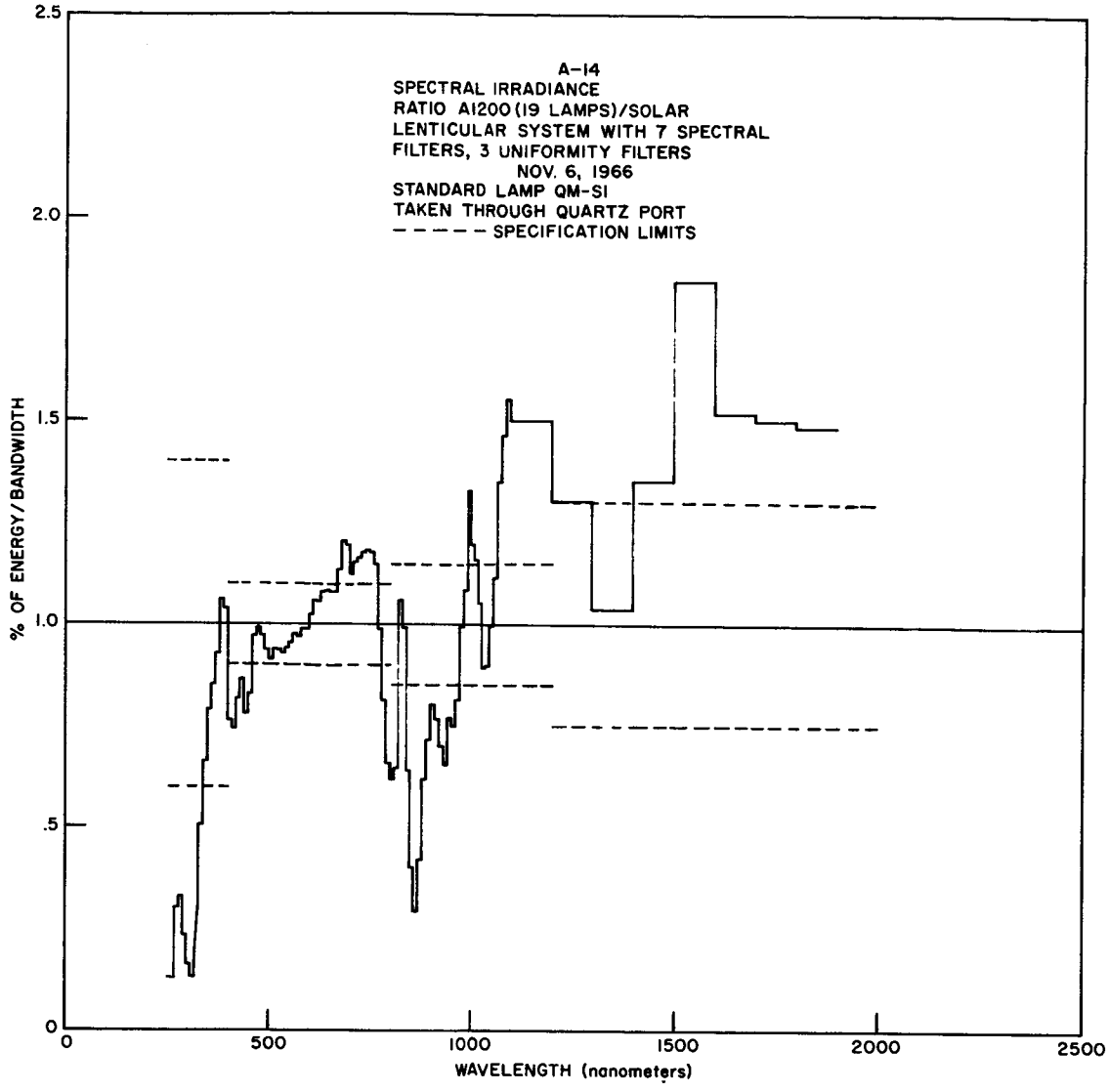

Figure 51. Ratio - A1200/Solar, Xenon, 19 Lamps, 7 Spectral Filters, 3 Uniformity Filters

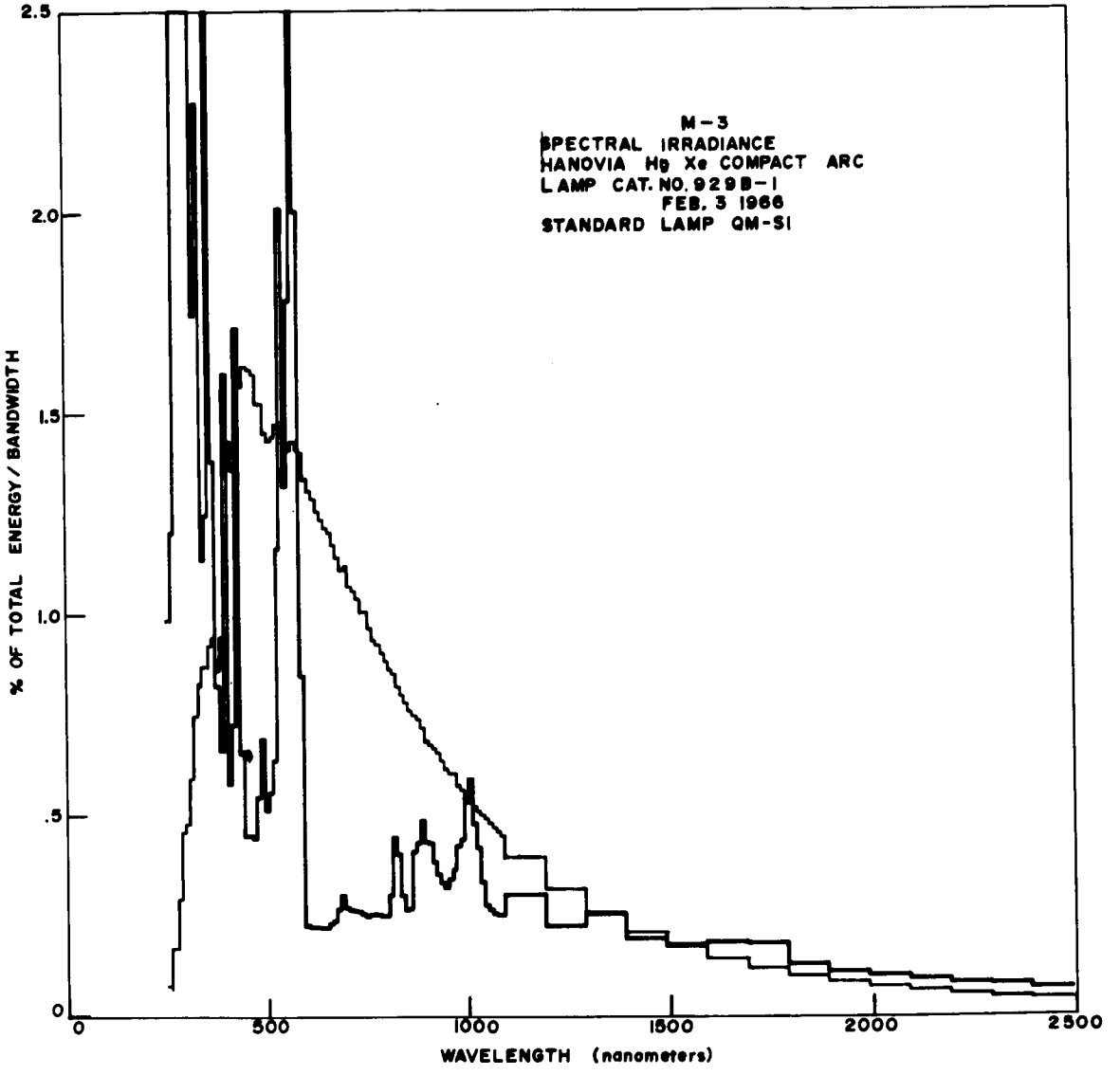

Figure 52. Spectral Irradiance, Hq Xe 2.5kw Lamp

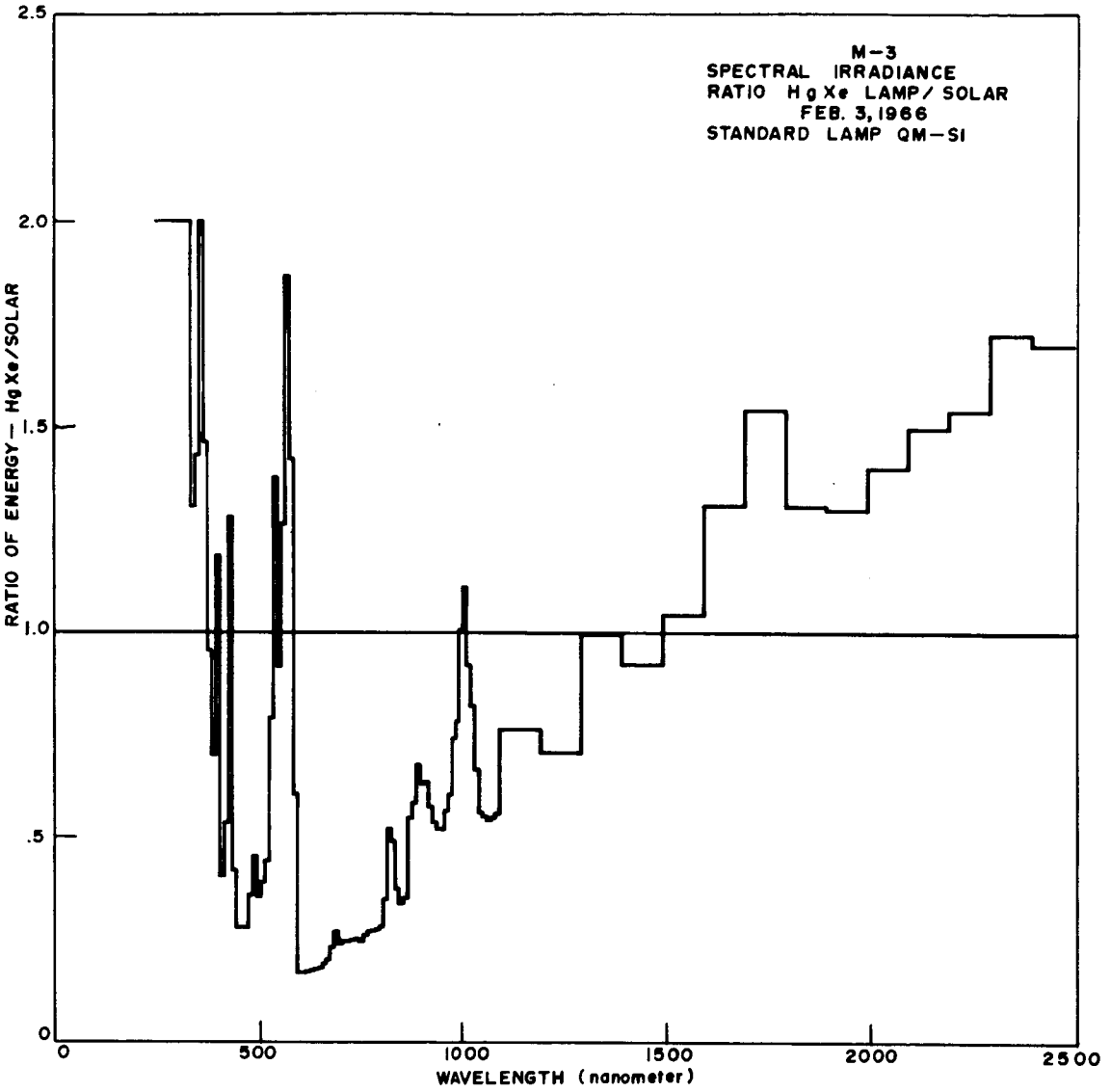

Figure 53. Ratio - Hq Xe 2.5kw Lamp/Solar

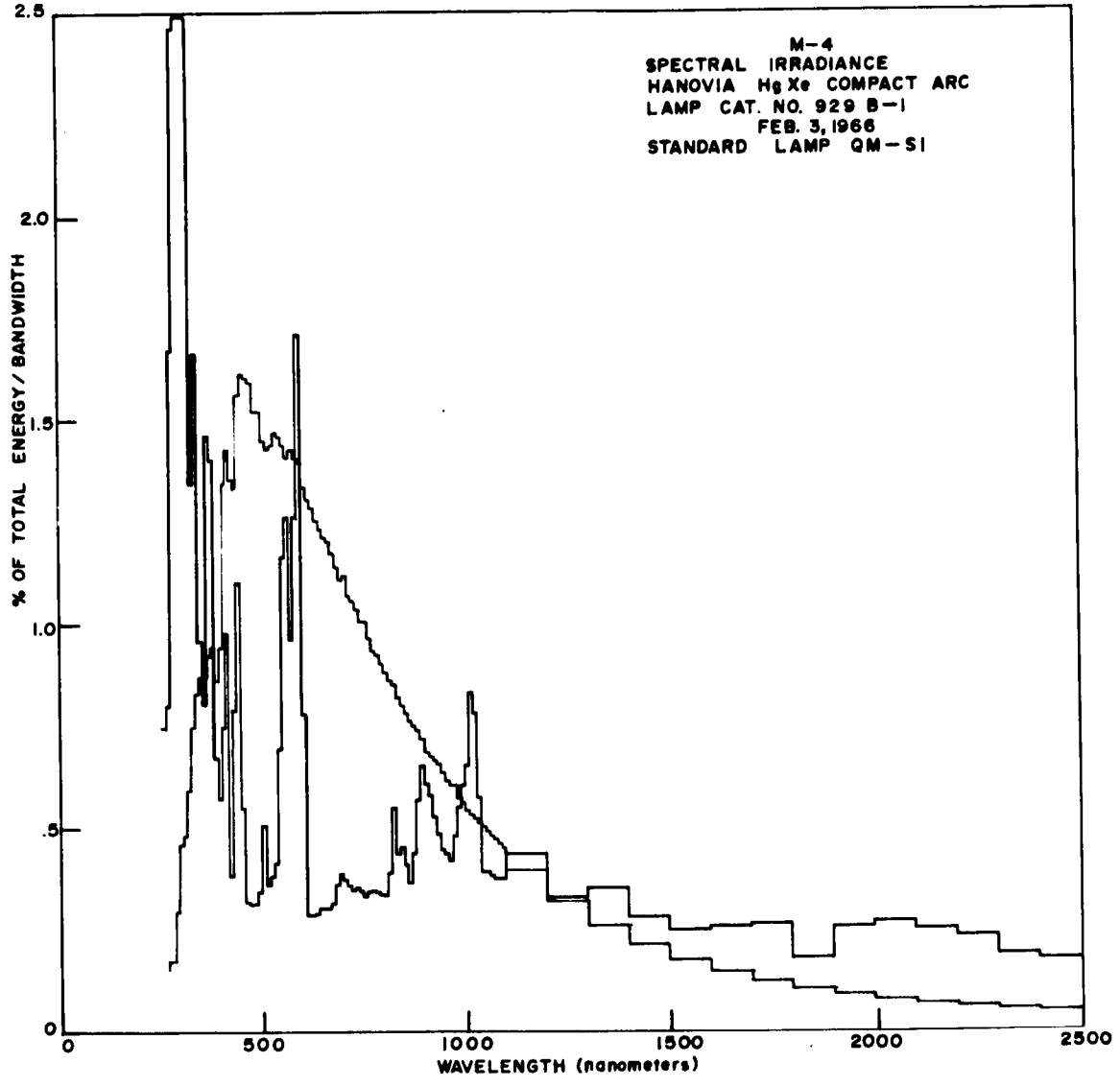

Figure 54. Spectral Irradiance, Hq Xe 2.5kw Lamp

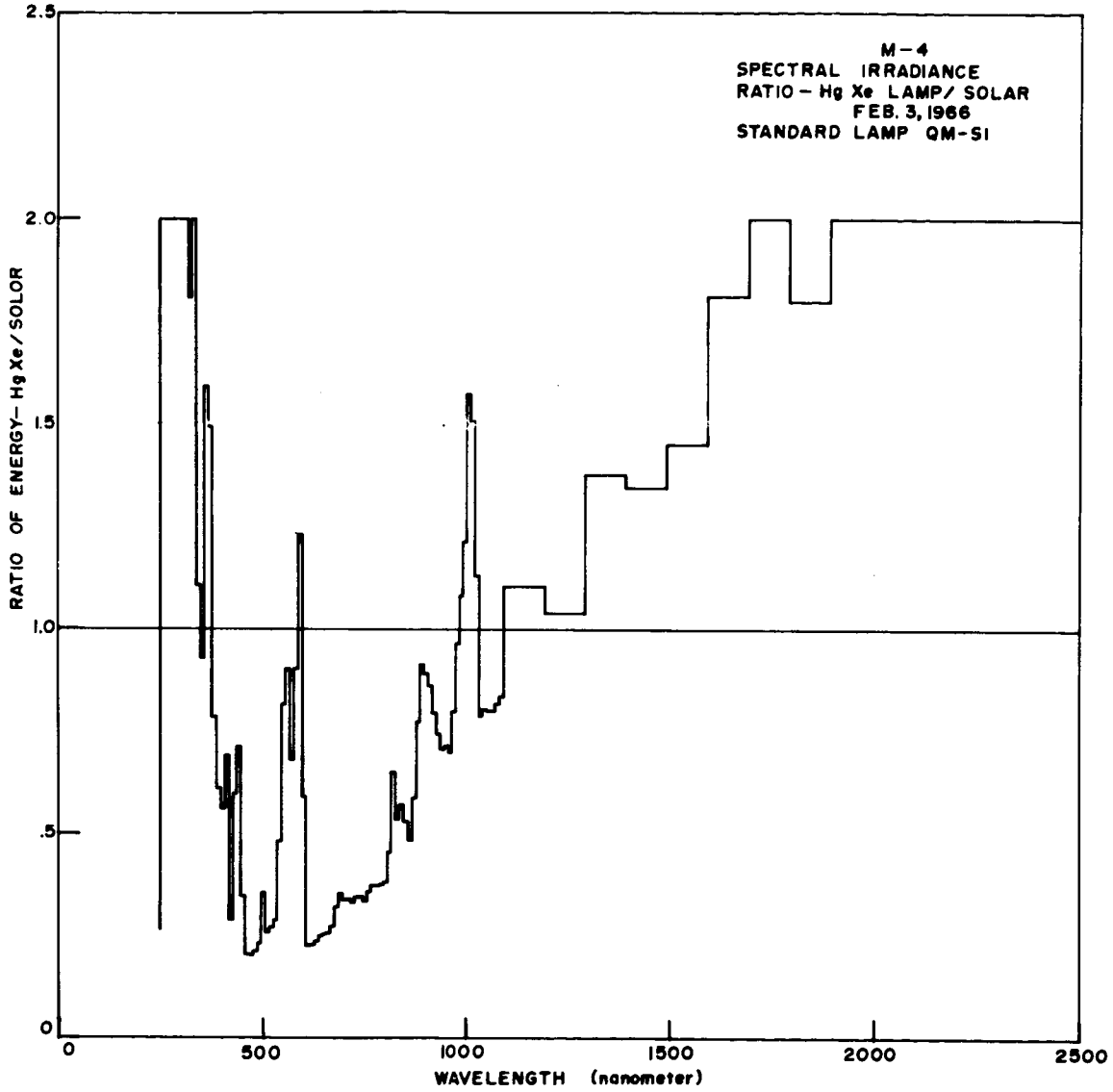

Figure 55. Ratio - Hq Xe 2.5kw Lamp/Solar

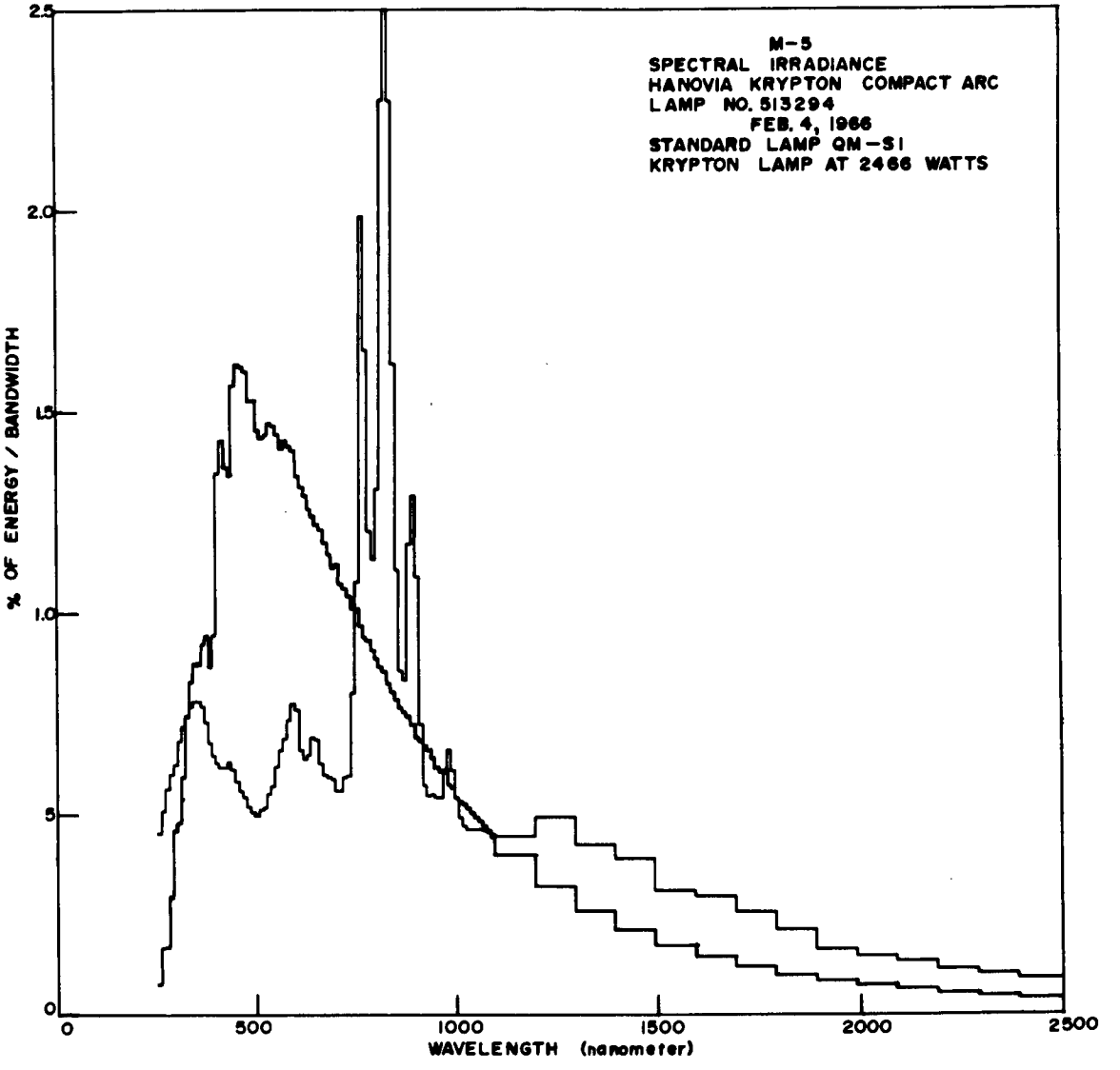

Figure 56. Spectral Irradiance, Krypton 2.4kw Lamp

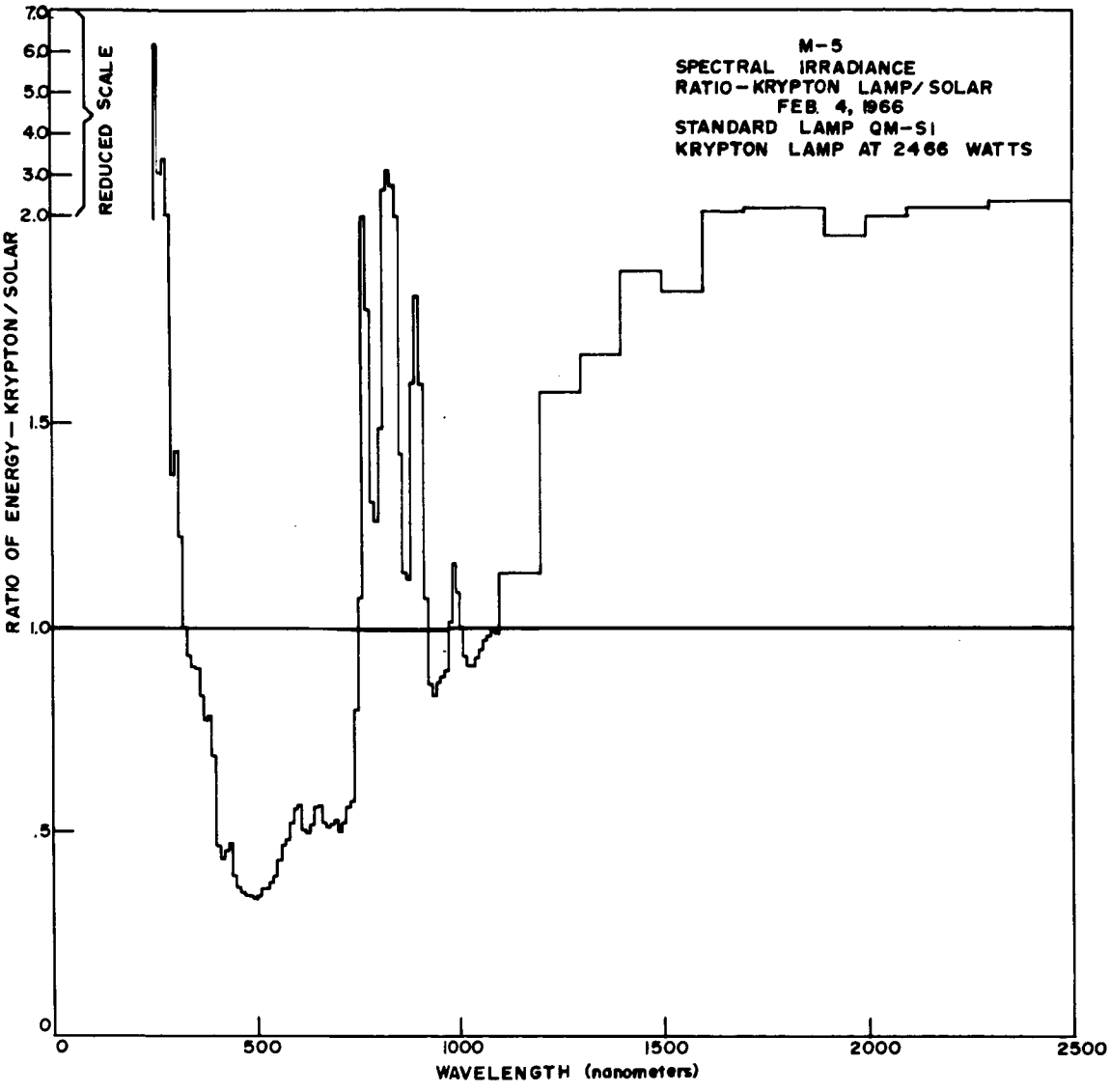

Figure 57. Ratio - Krypton 2.4kw Lamp/Solar

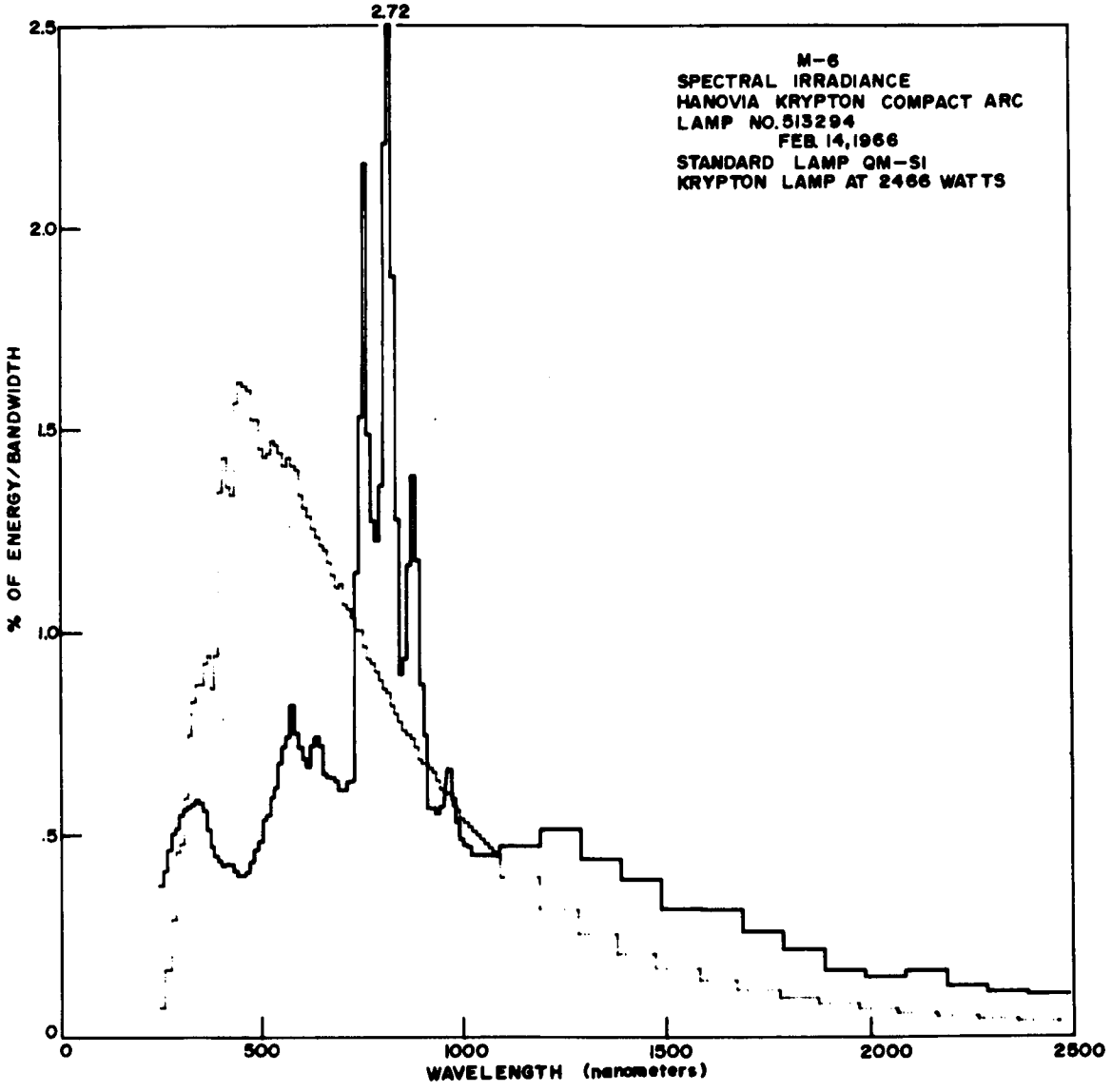

Figure 58. Spectral Irradiance, Krypton 2.4kw Lamp

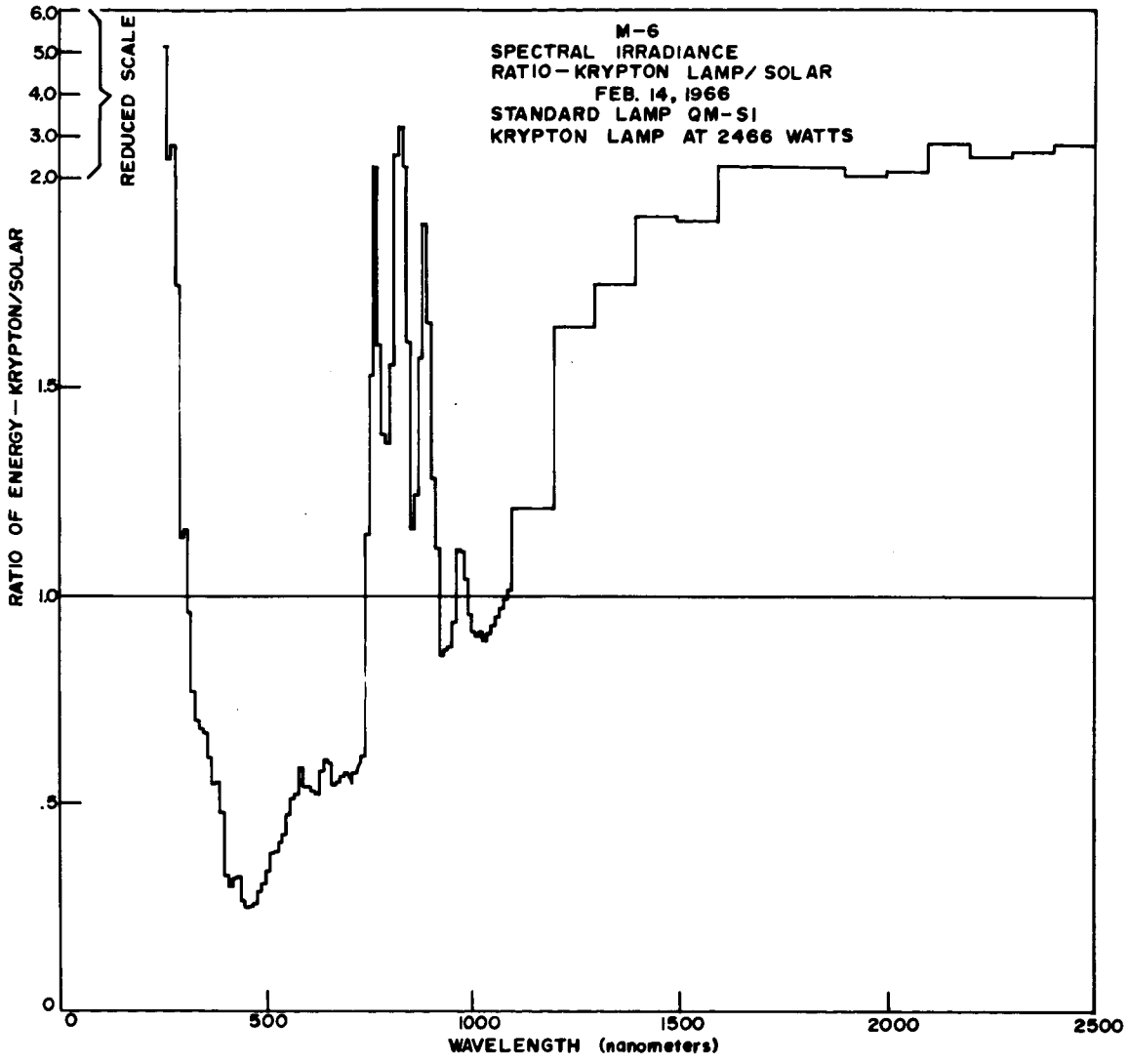

Figure 59. Ratio - Krypton 2.4kw Lamp/Solar

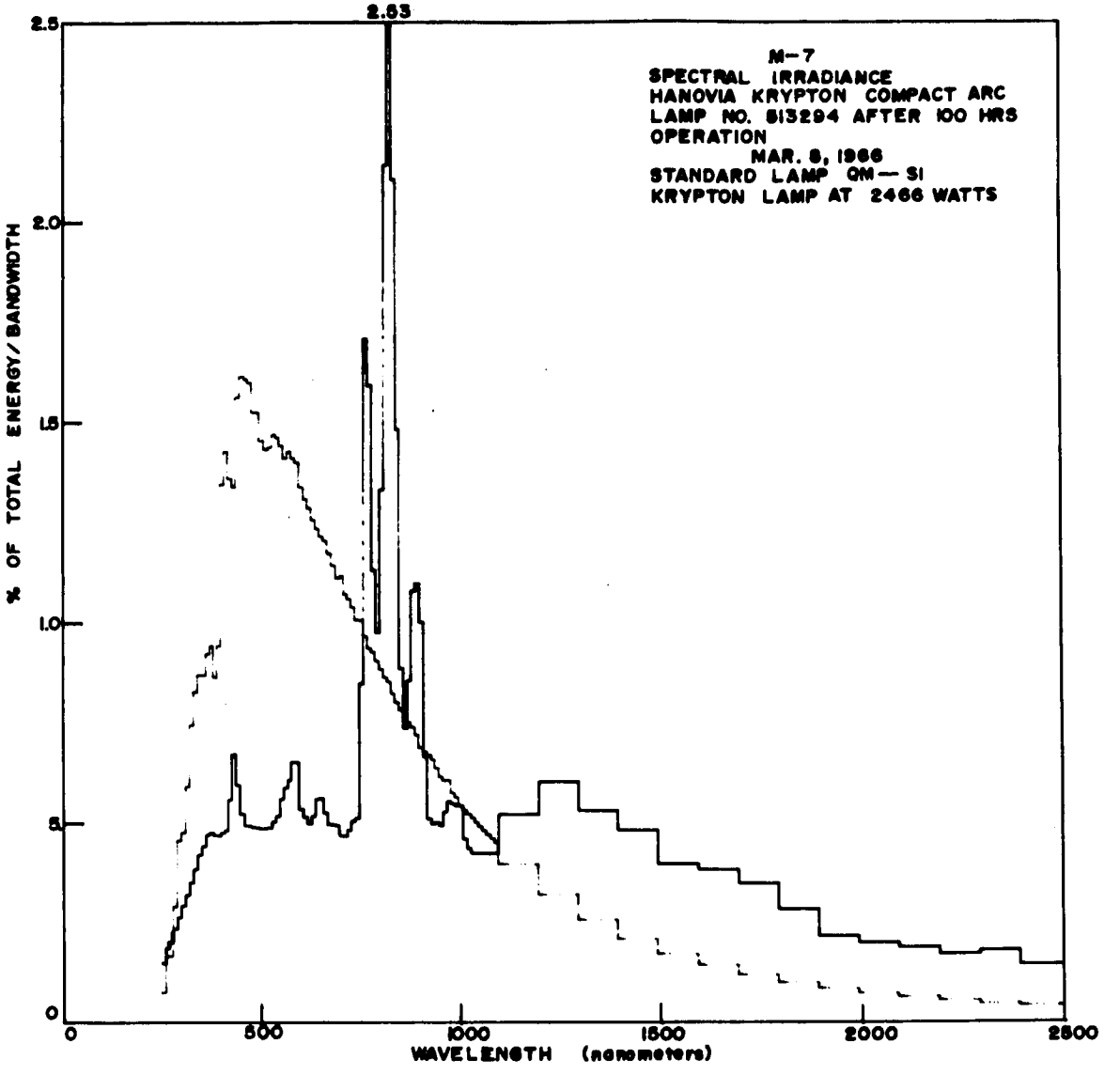

Figure 60. Spectral Irradiance, Krypton 2.4kw Lamp After 100 Hours

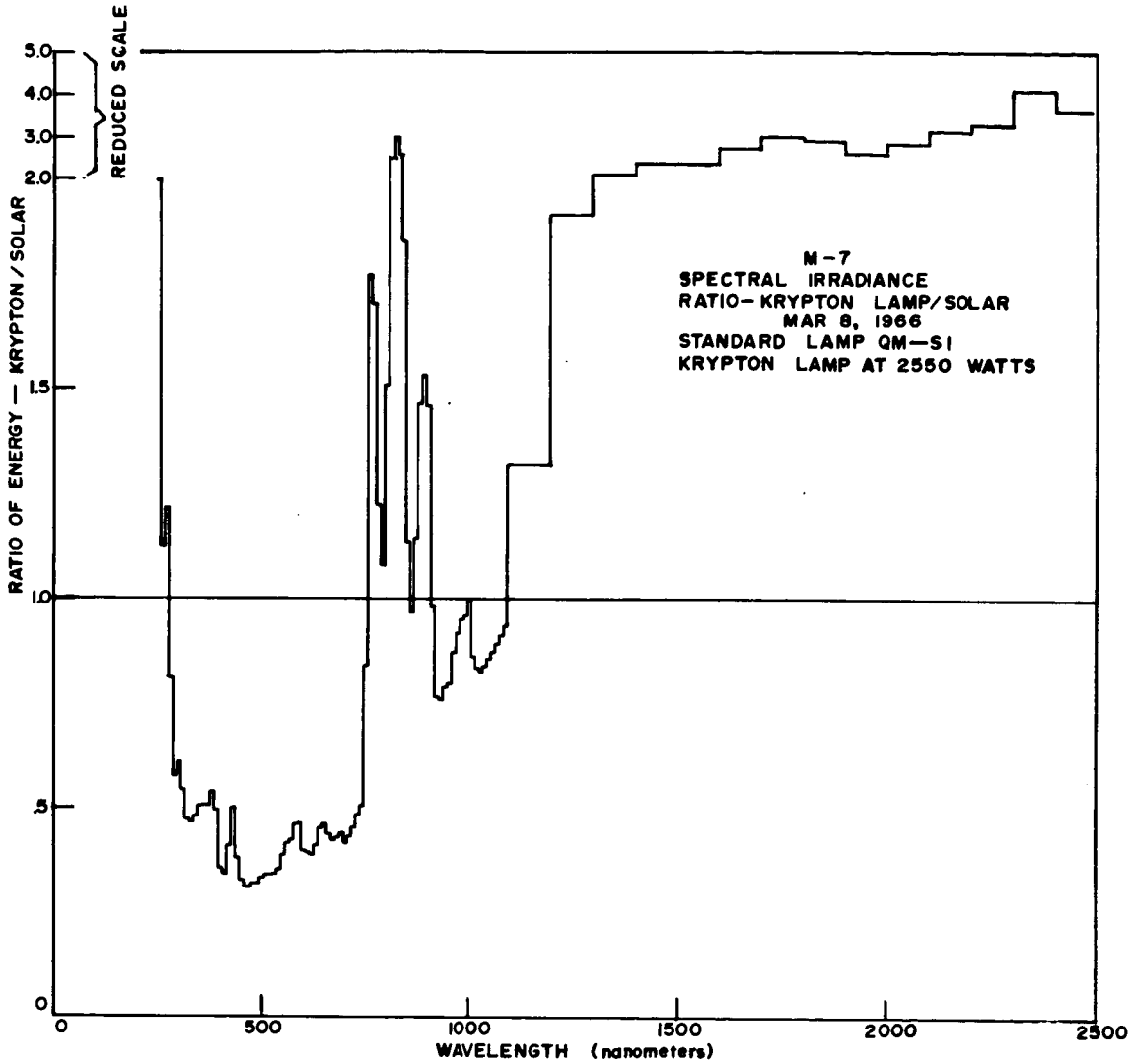

Figure 61. Ratio - Krypton 2.4kw Lamp/Solar (After 100 Hours)

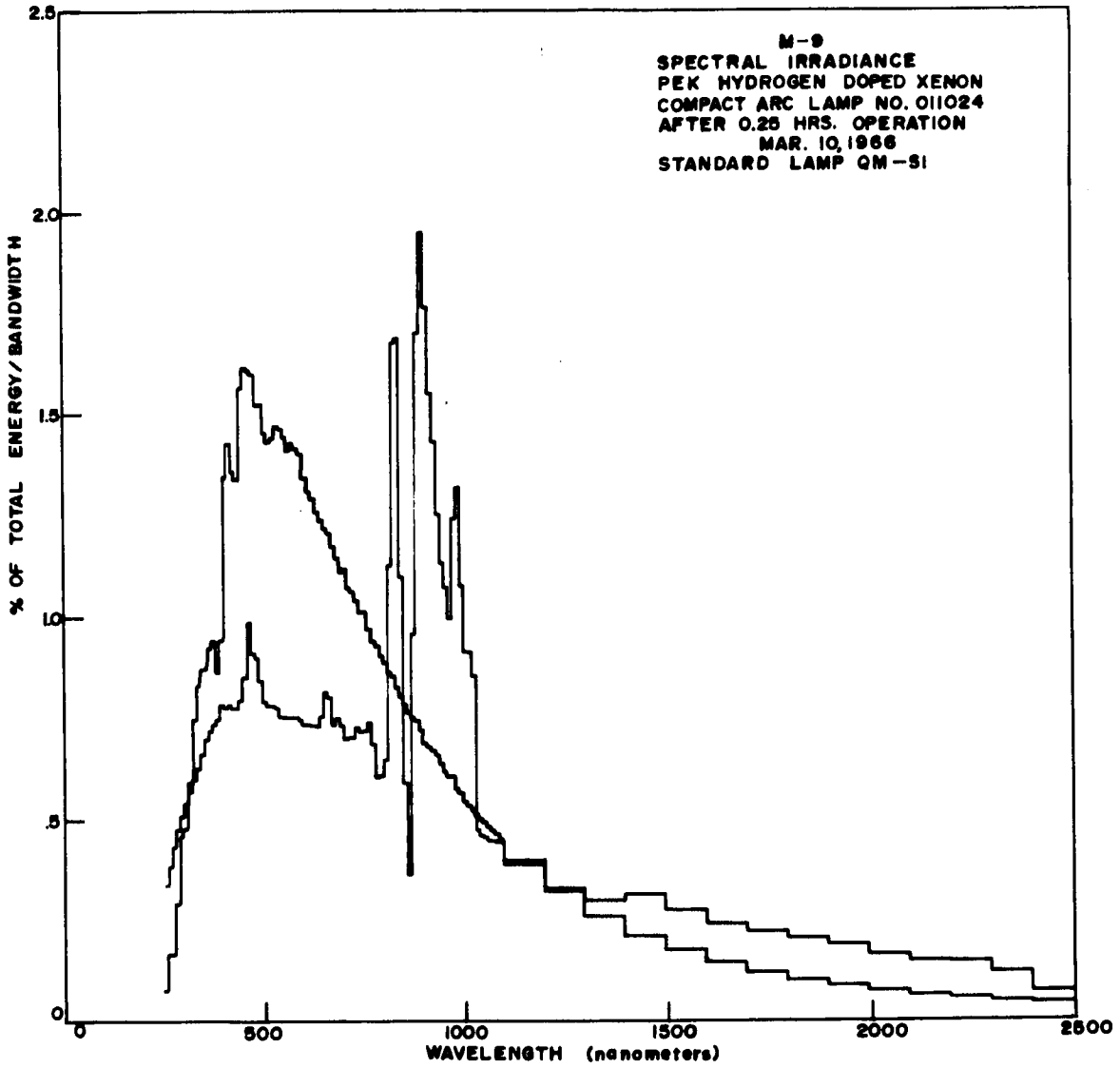

Figure 62. Spectral Irradiance, Hydrogen Doped Xenon 2.0kw Lamp

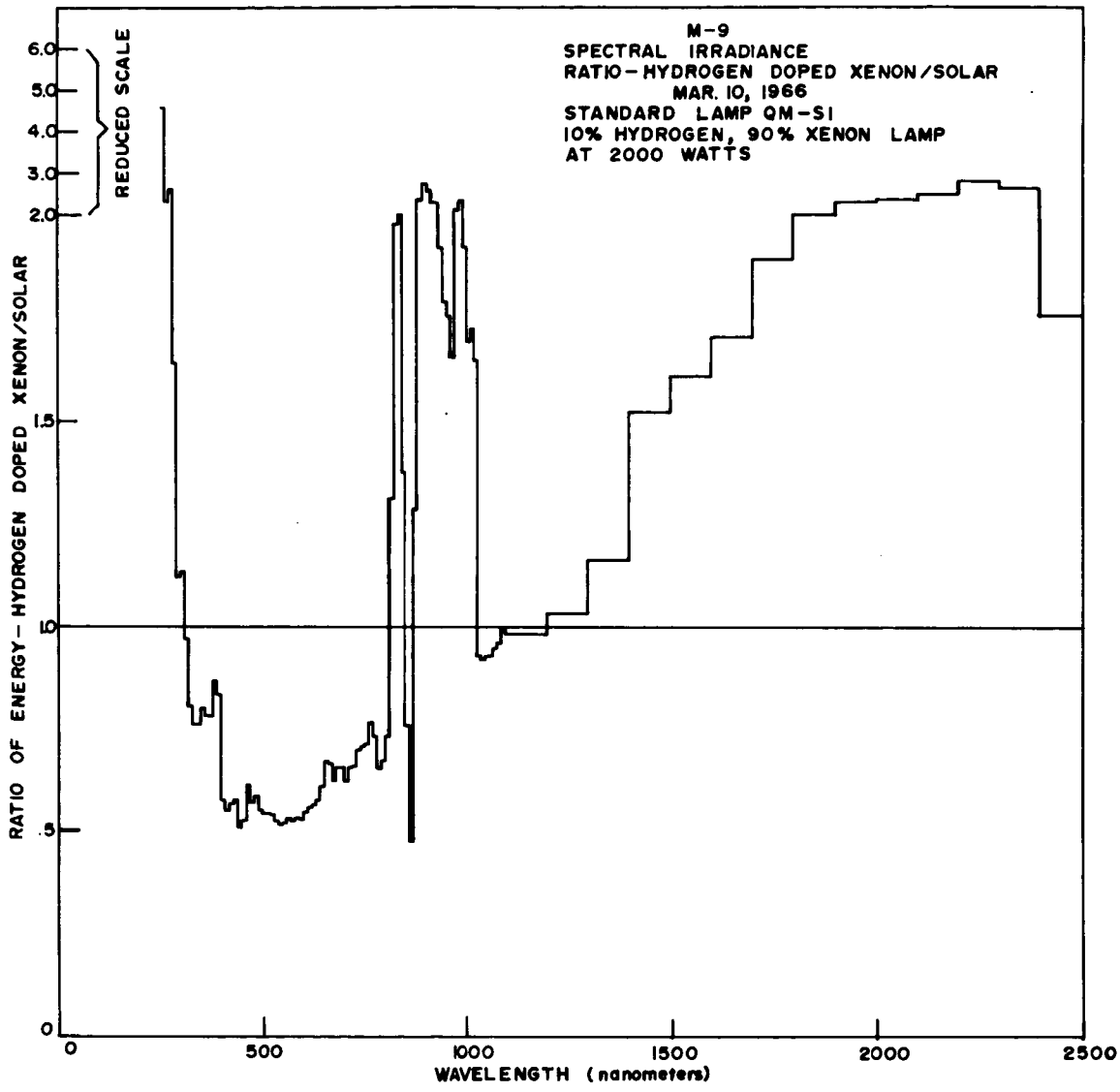

Figure 63. Ratio - Hydrogen Doped Xenon 2.0kw Lamp/Solar

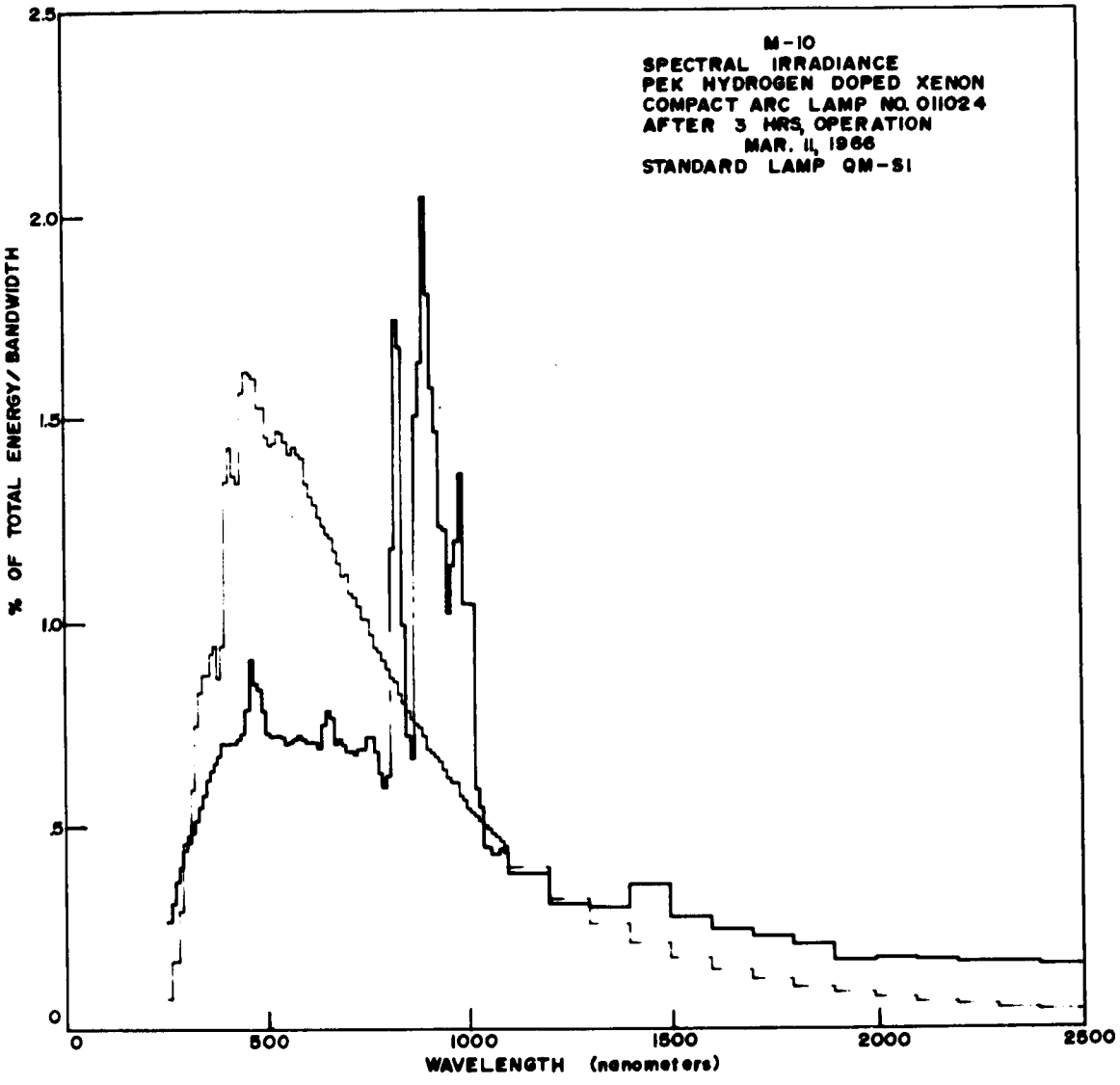

Figure 64. Spectral Irradiance, Hydrogen Doped Xe 2.0kw Lamp

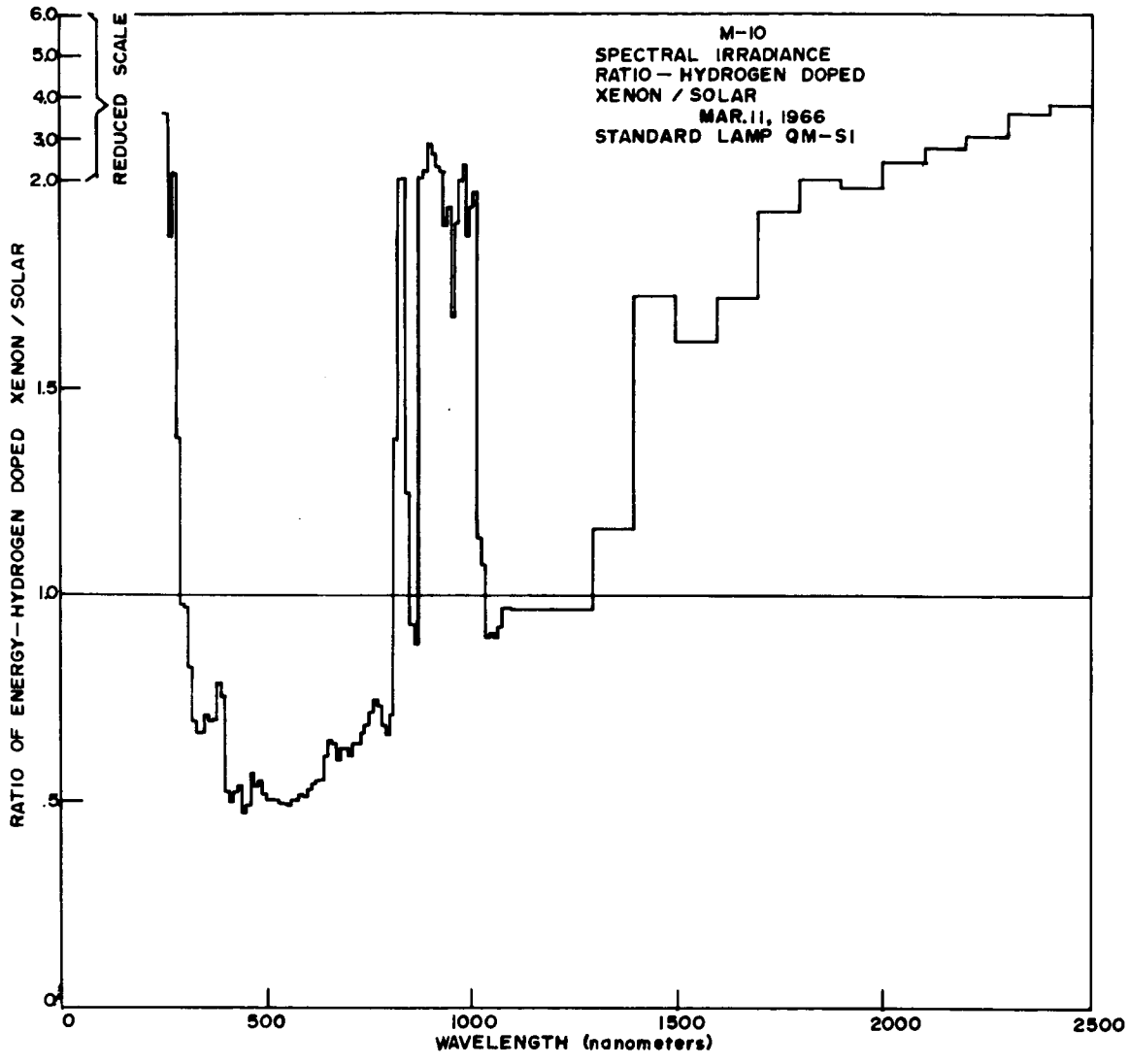

Figure 65. Ratio - Hydrogen Doped Xe 2.0kw Lamp/Solar

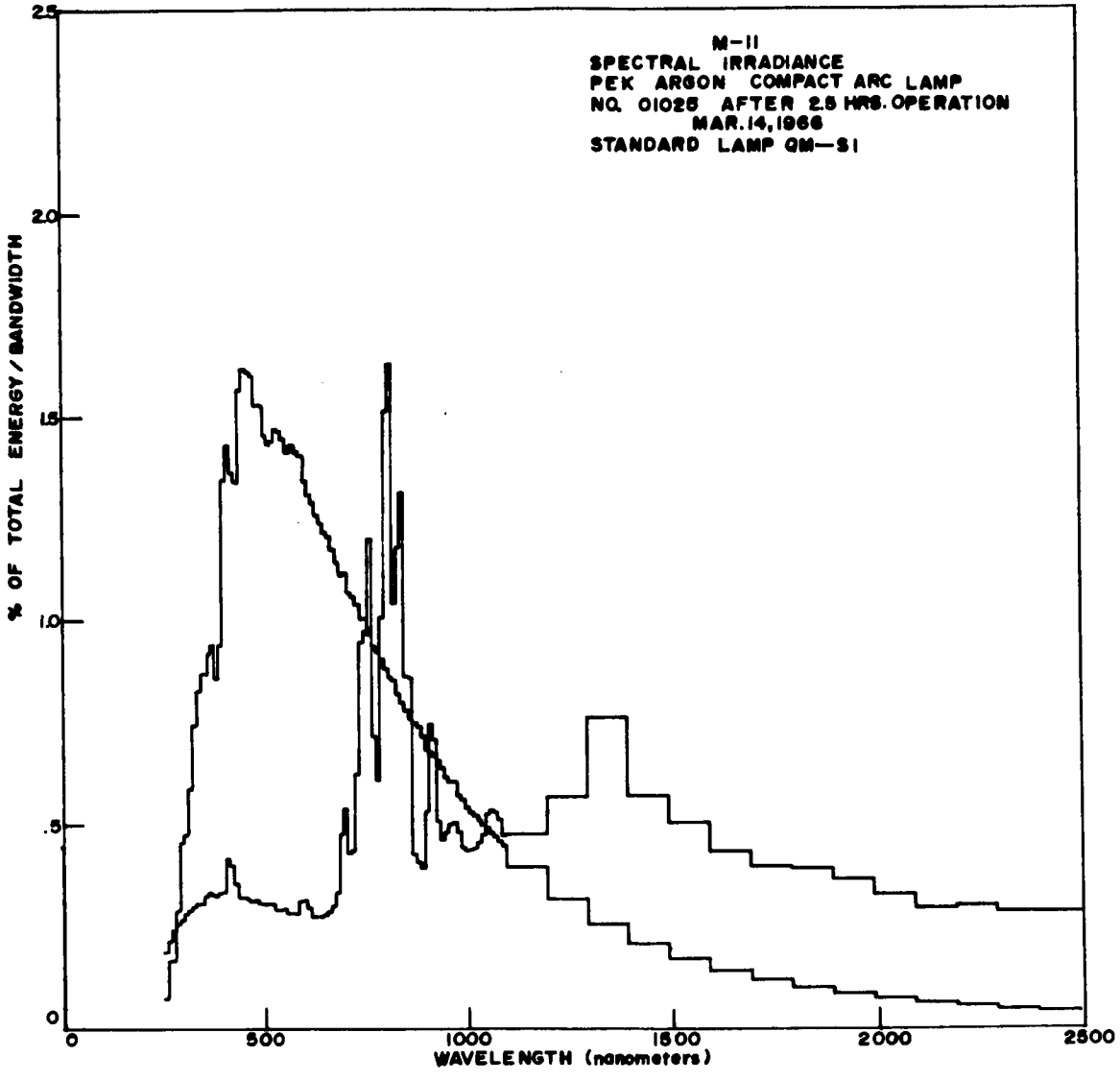

Figure 66. Spectral Irradiance, Argon 2.3kw Lamp

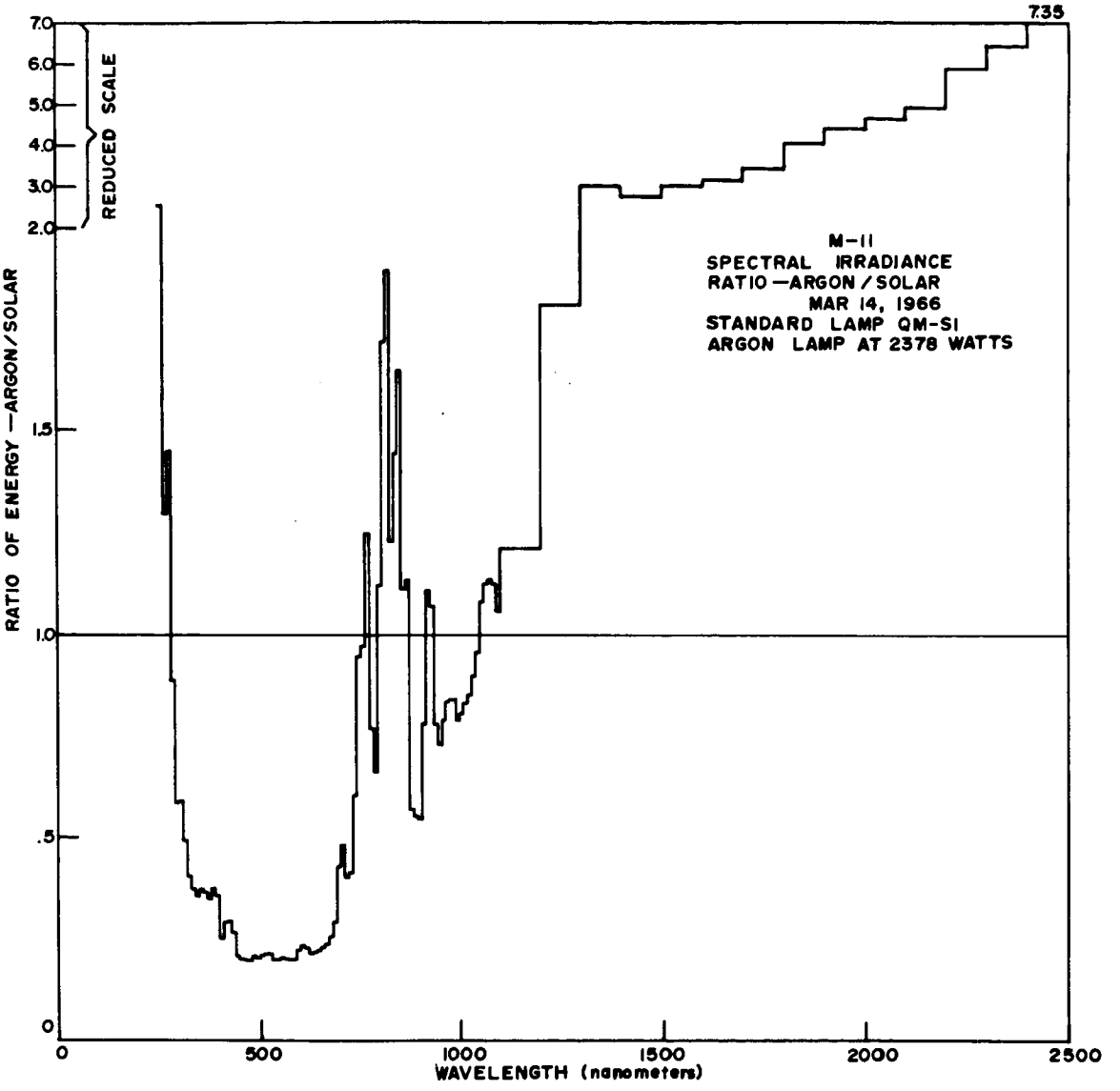

Figure 67. Ratio - Argon 2.3kw Lamp/Solar

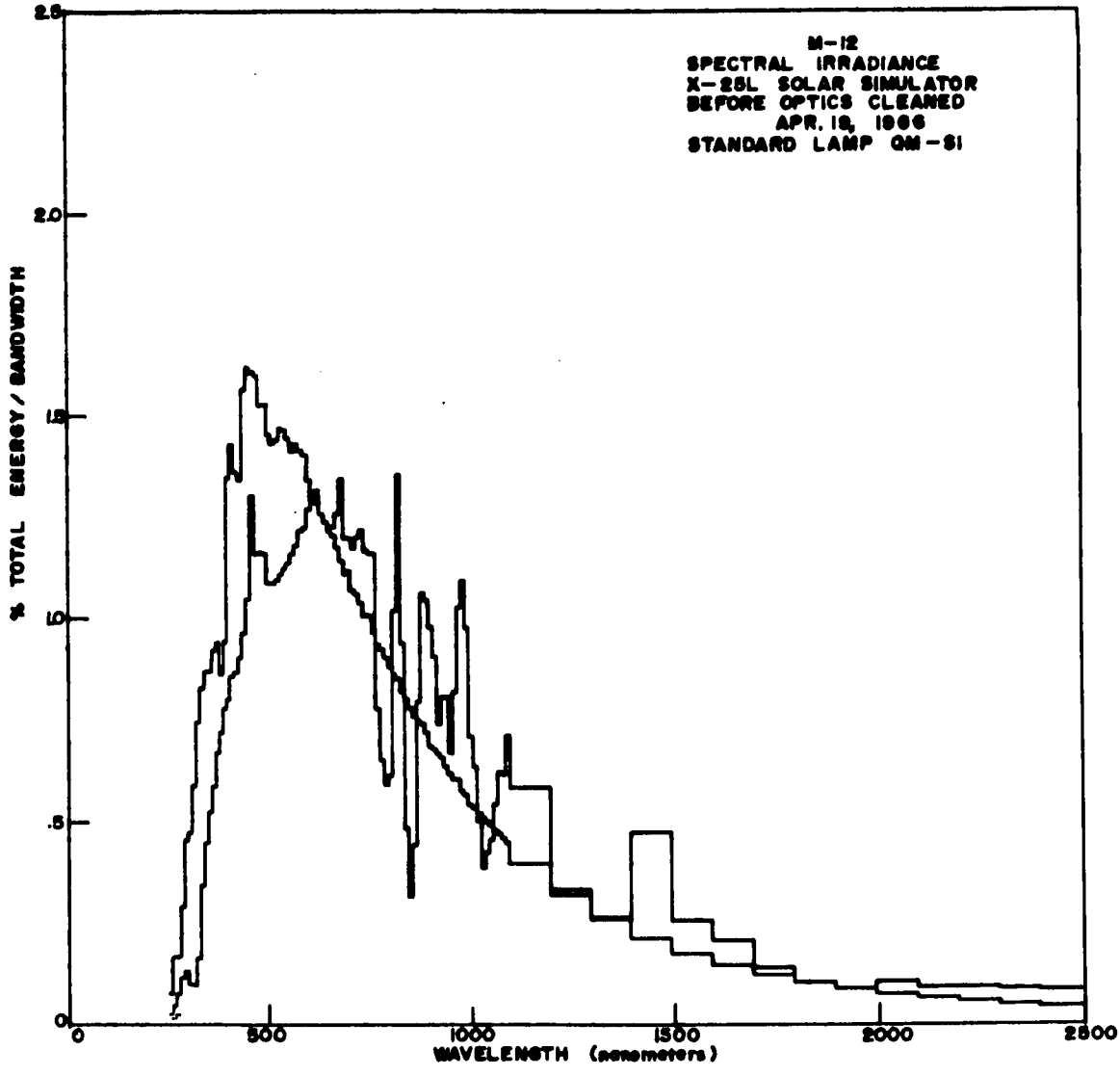

Figure 68. Spectral Irradiance, X-25L Solar Simulator

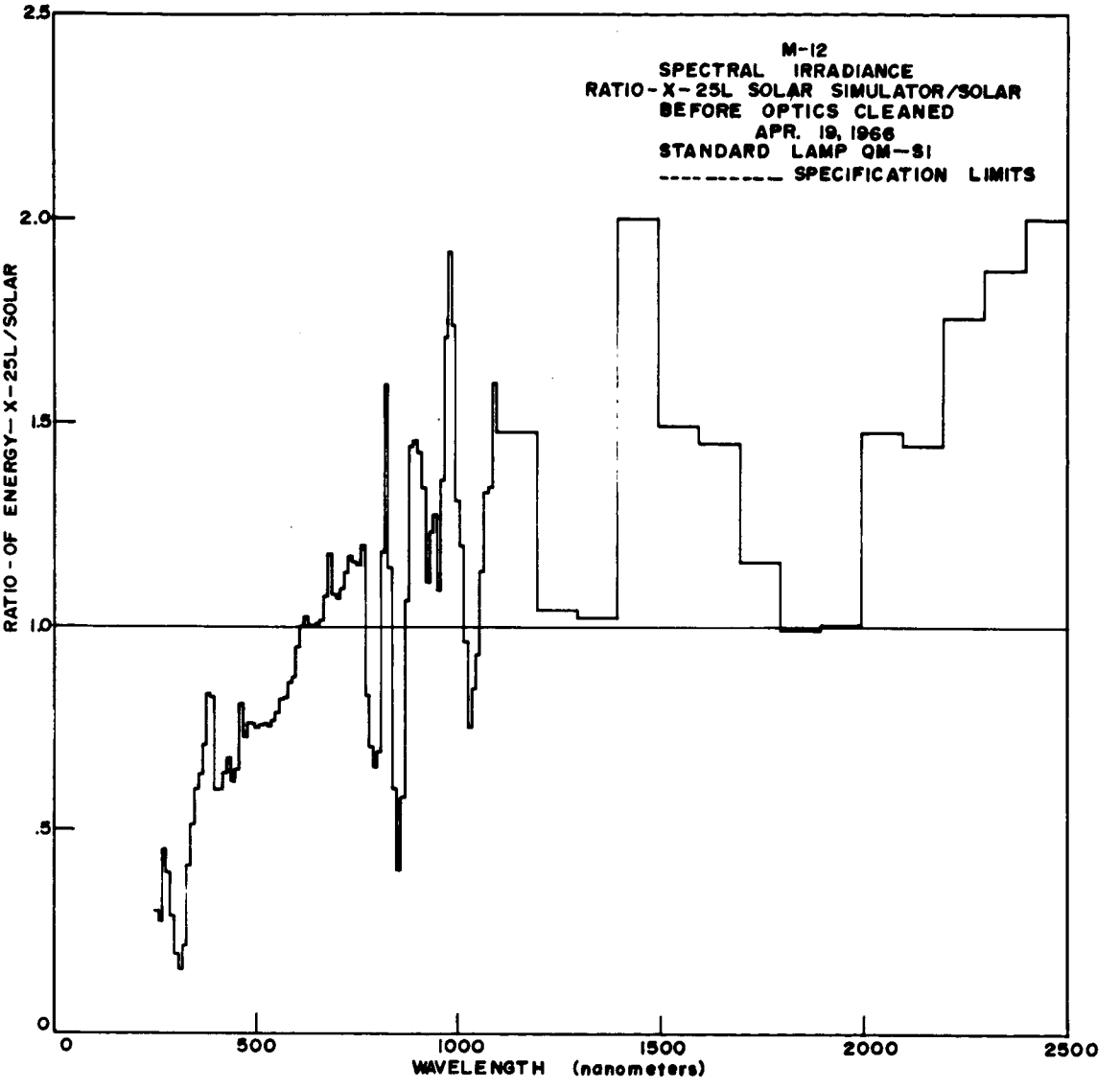

Figure 69. Ratio - X-25L Solar Simulator/Solar

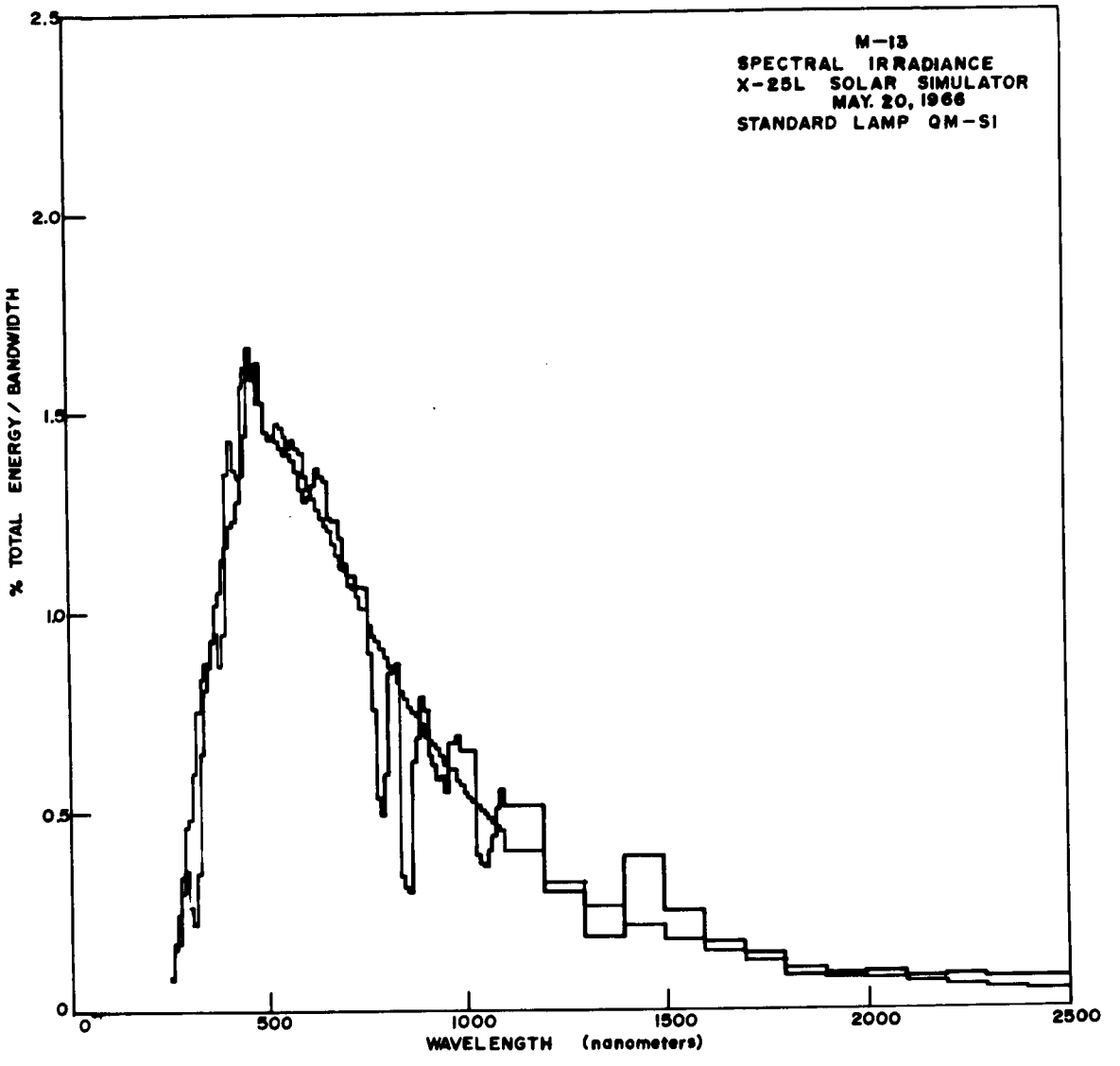

Figure 70. Spectral Irradiance, X-25L Solar Simulator

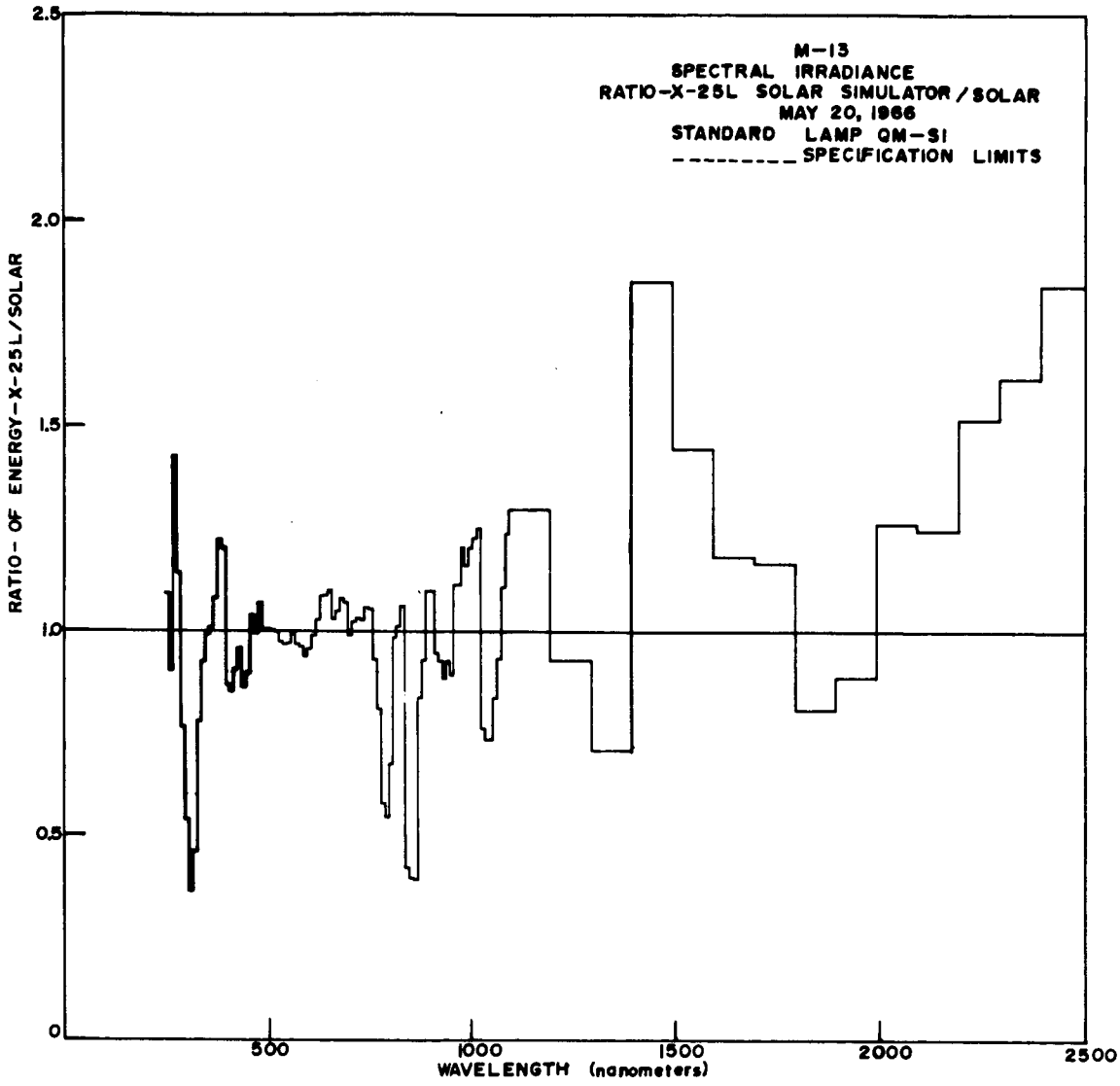

Figure 71. Ratio - X-25L Solar Simulator/Solar

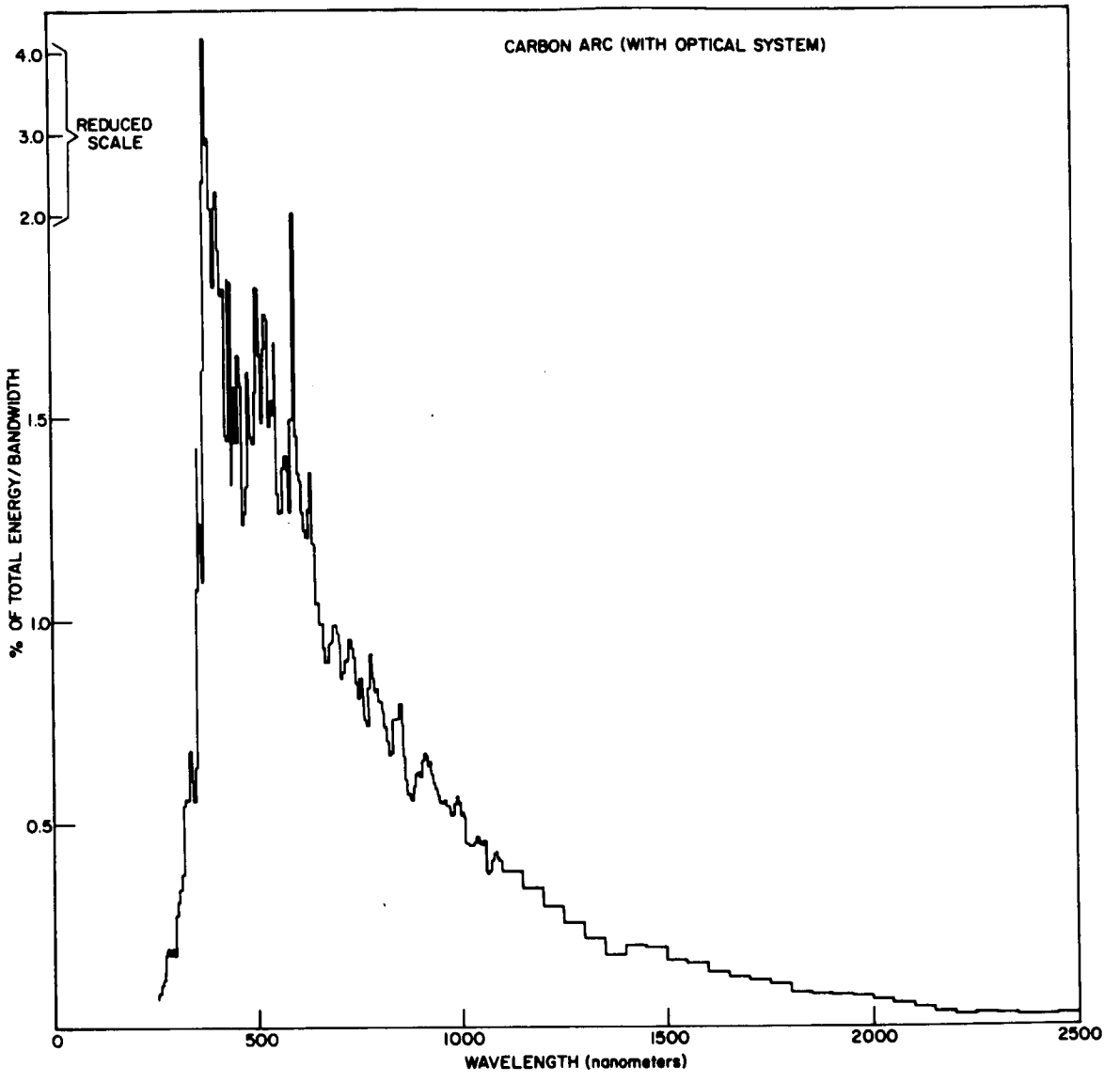

Figure 72. Spectral Irradiance, Carbon Arc

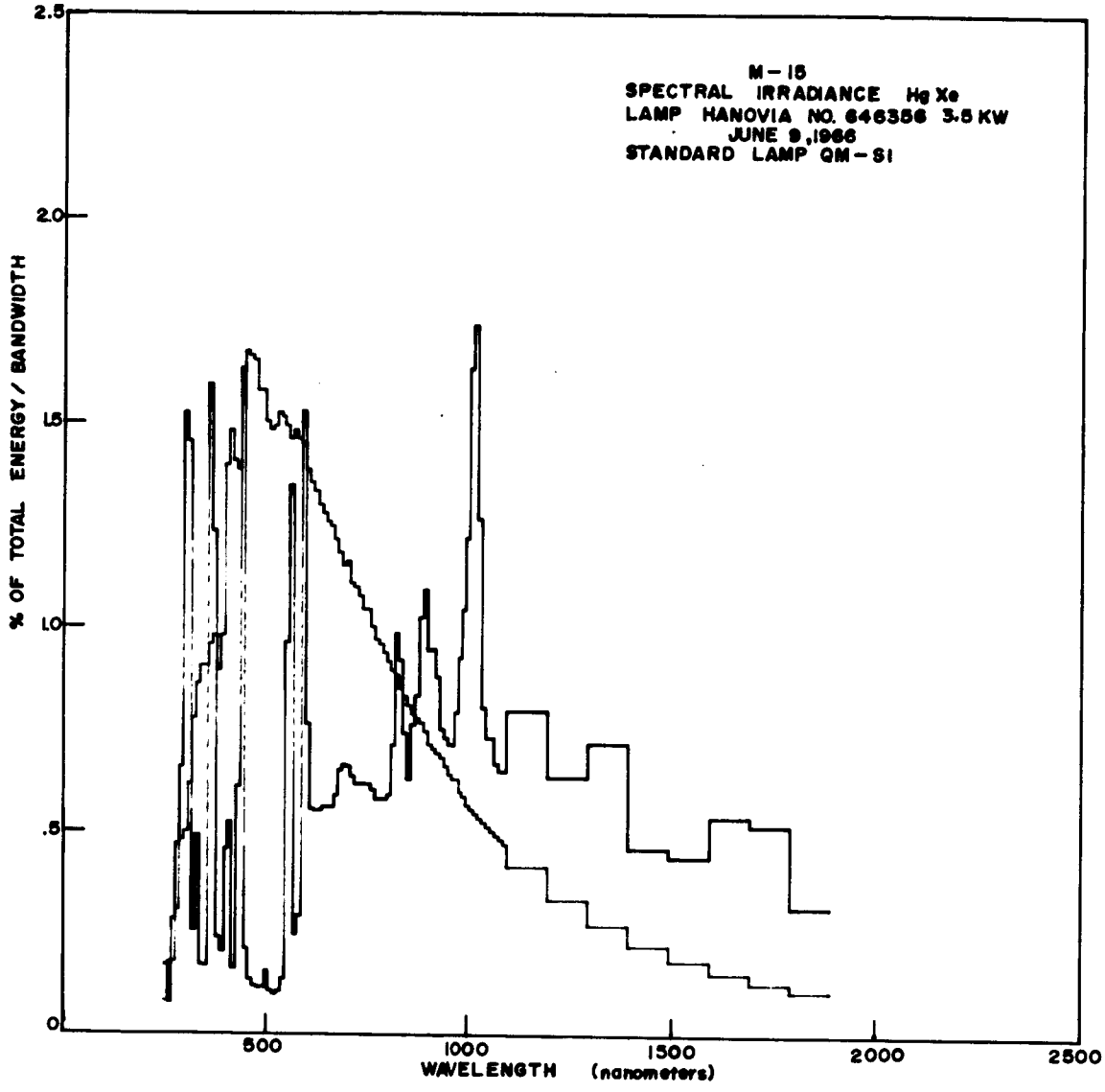

Figure 73. Spectral Irradiance, Hg Xe 3.5kw Lamp

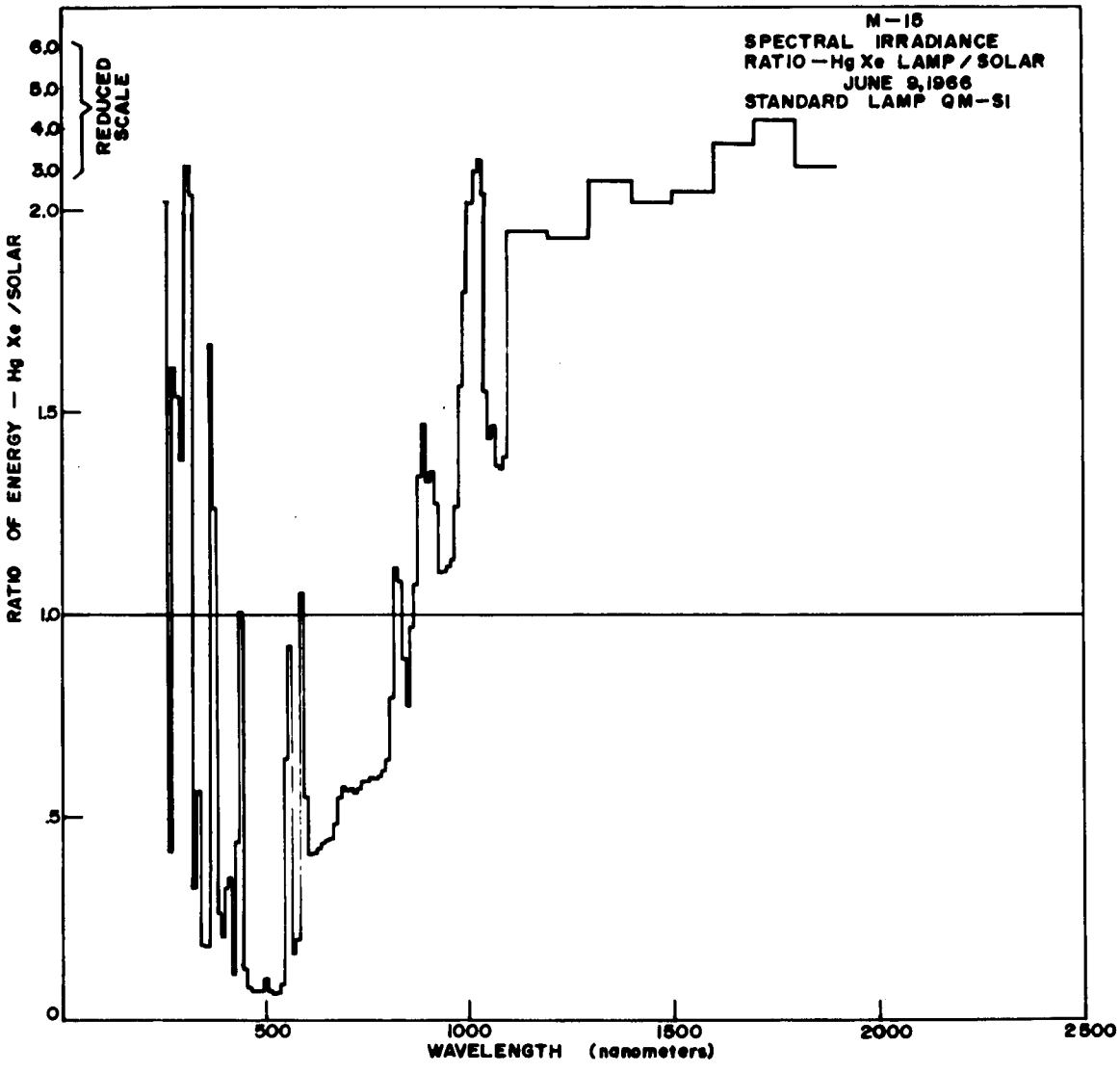

Figure 74. Ratio - Hg Xe 3.5kw Lamp/Solar

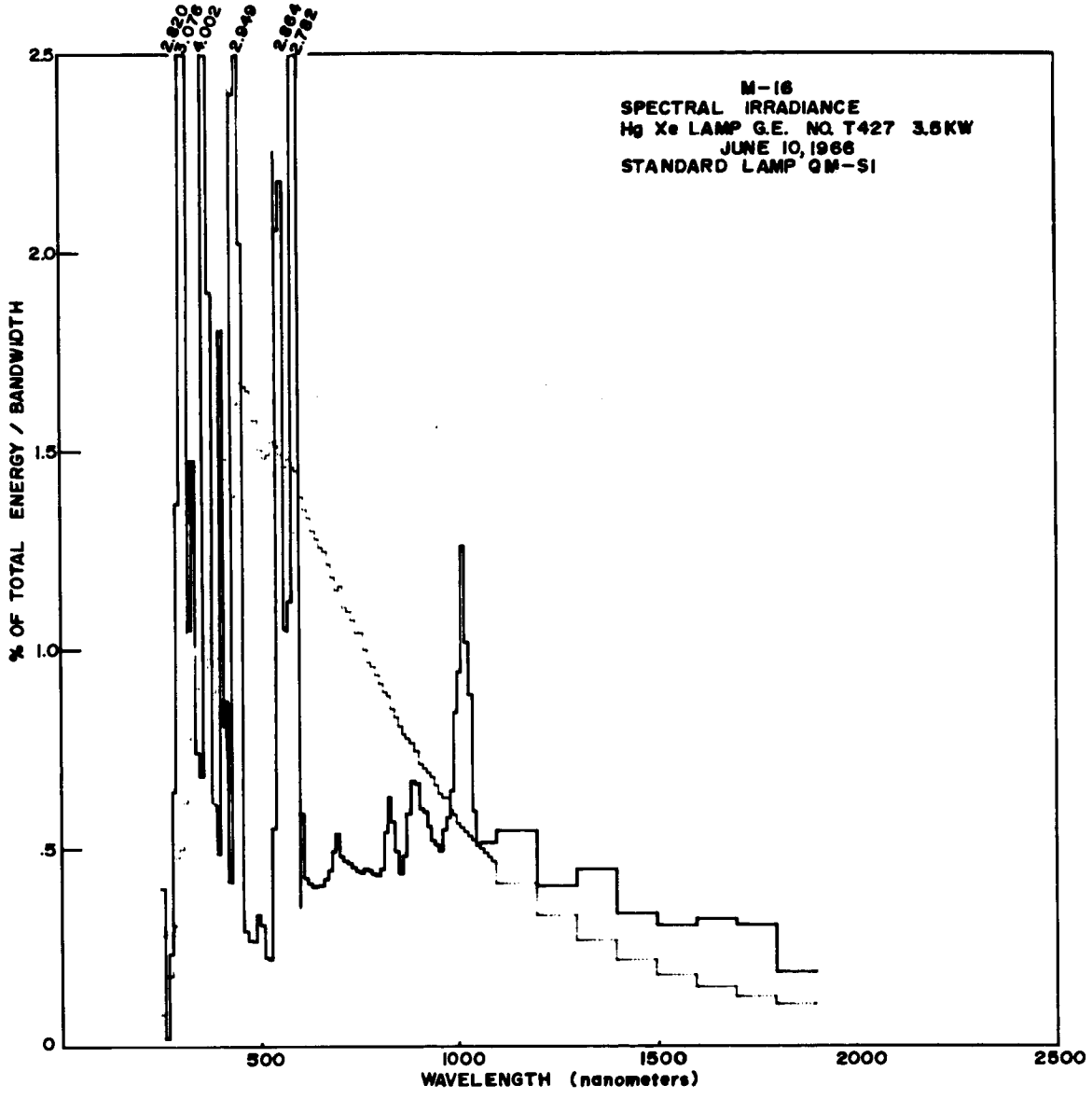

Figure 75. Spectral Irradiance, Hg Xe 3.5kw Lamp

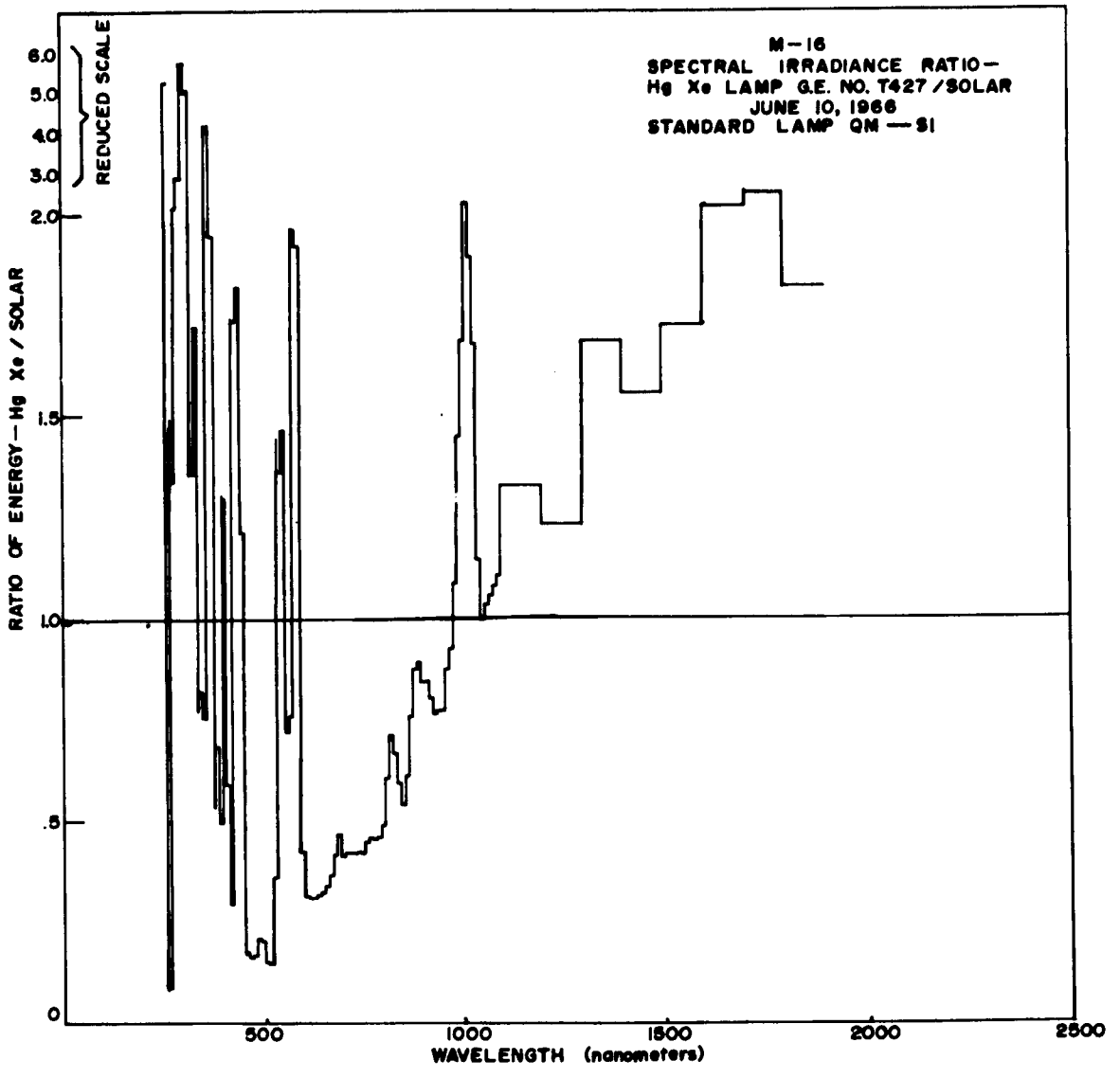

Figure 76. Ratio - Hg Xe 3.5kw Lamp/Solar

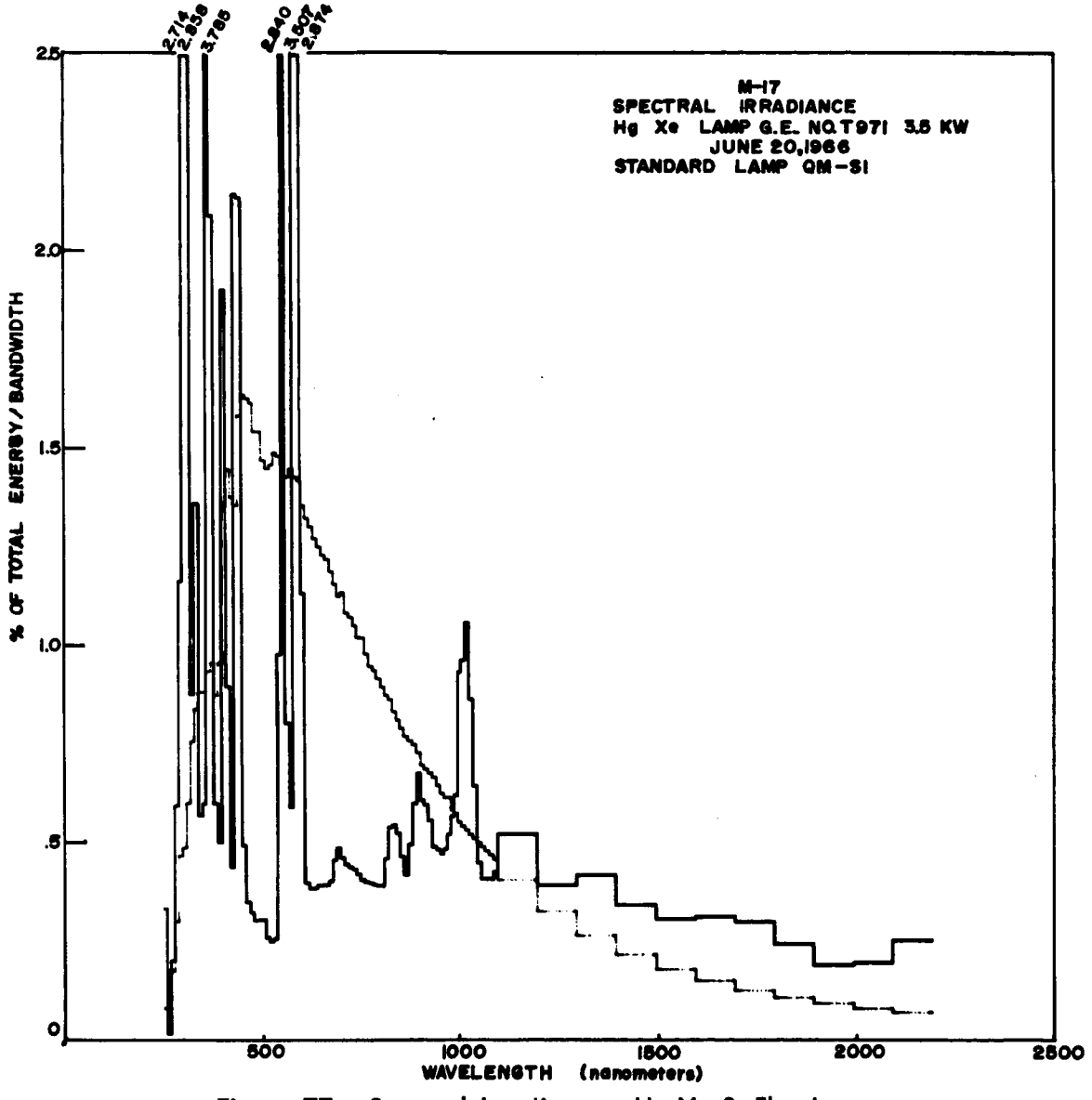

Figure 77. Spectral Irradiance, Hg Xe 3.5kw Lamp

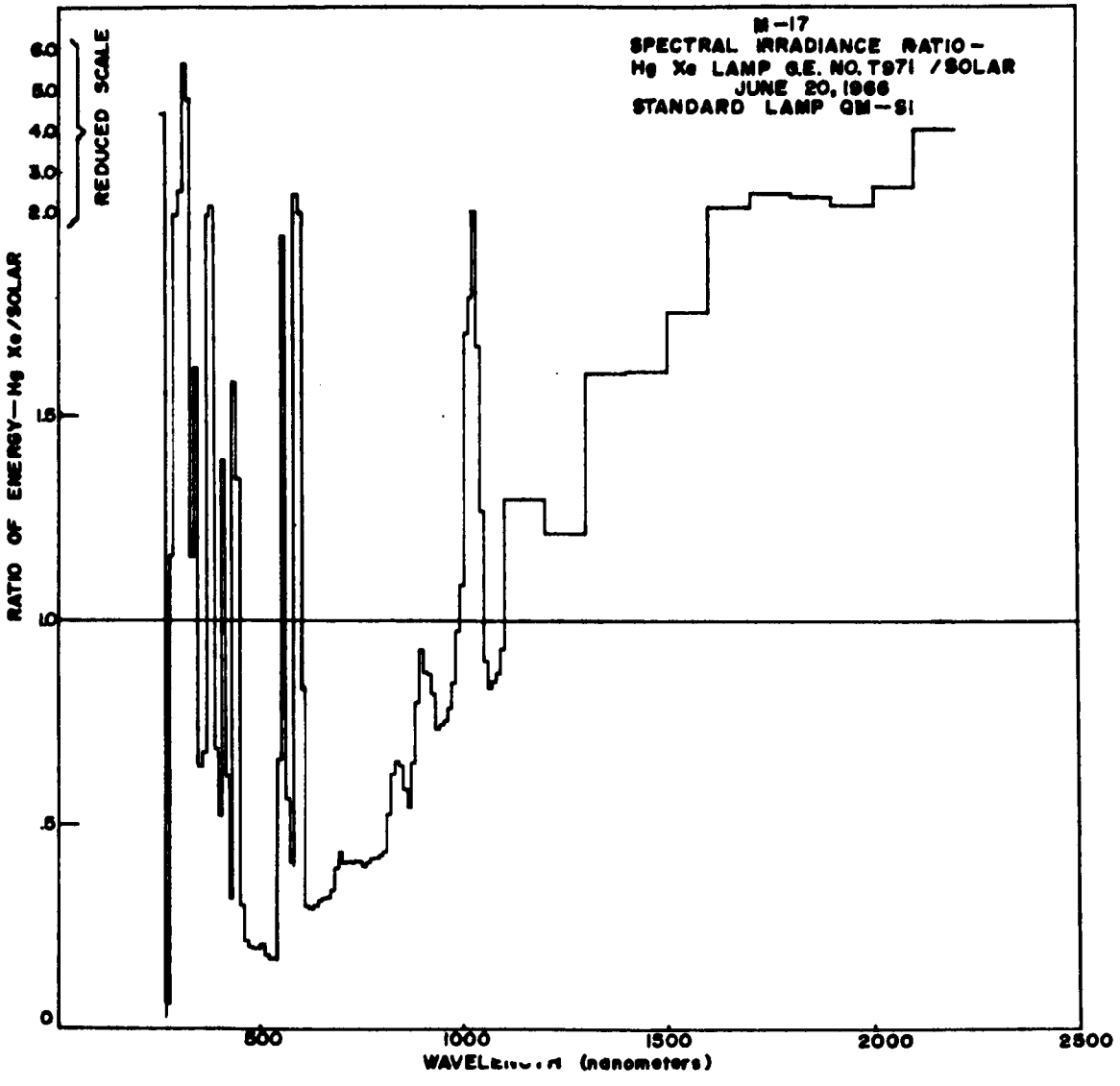

Figure 78. Ratio - Hg Xe 3.5kw Lamp/Solar

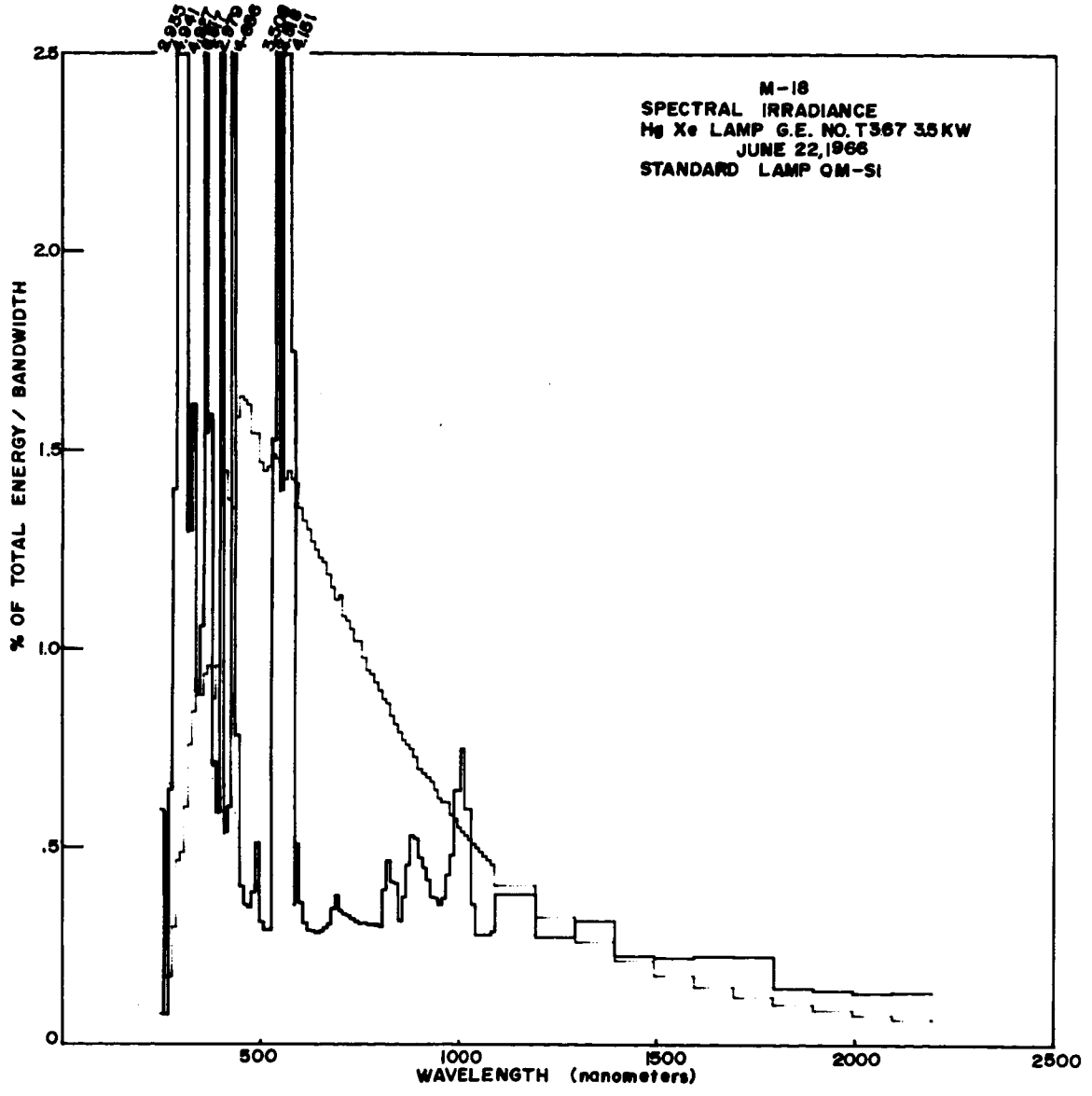

Figure 79. Spectral Irradiance, Hg Xe 3.5kw Lamp

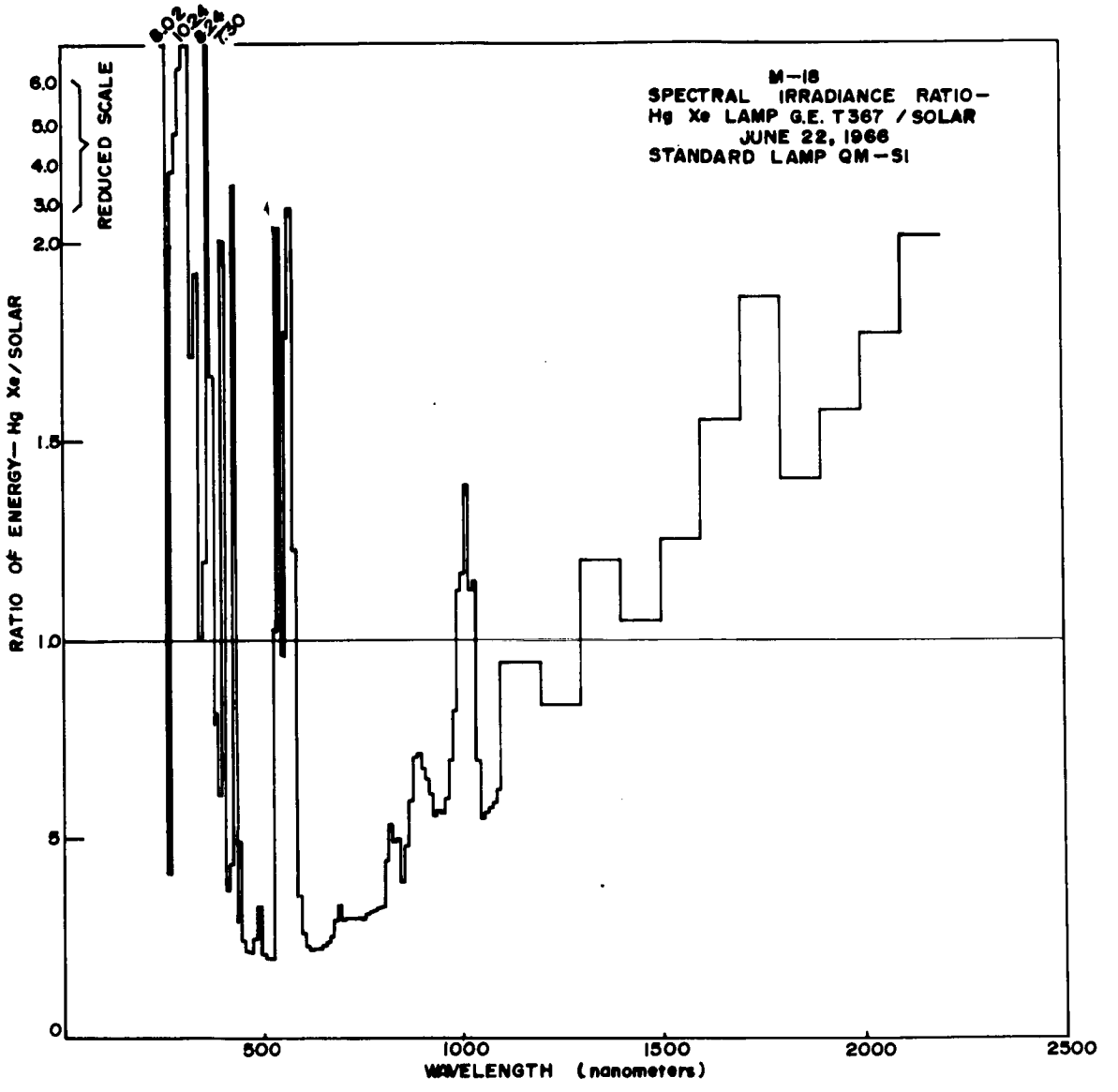

Figure 80. Ratio - Hg Xe 3.5kw Lamp/Solar

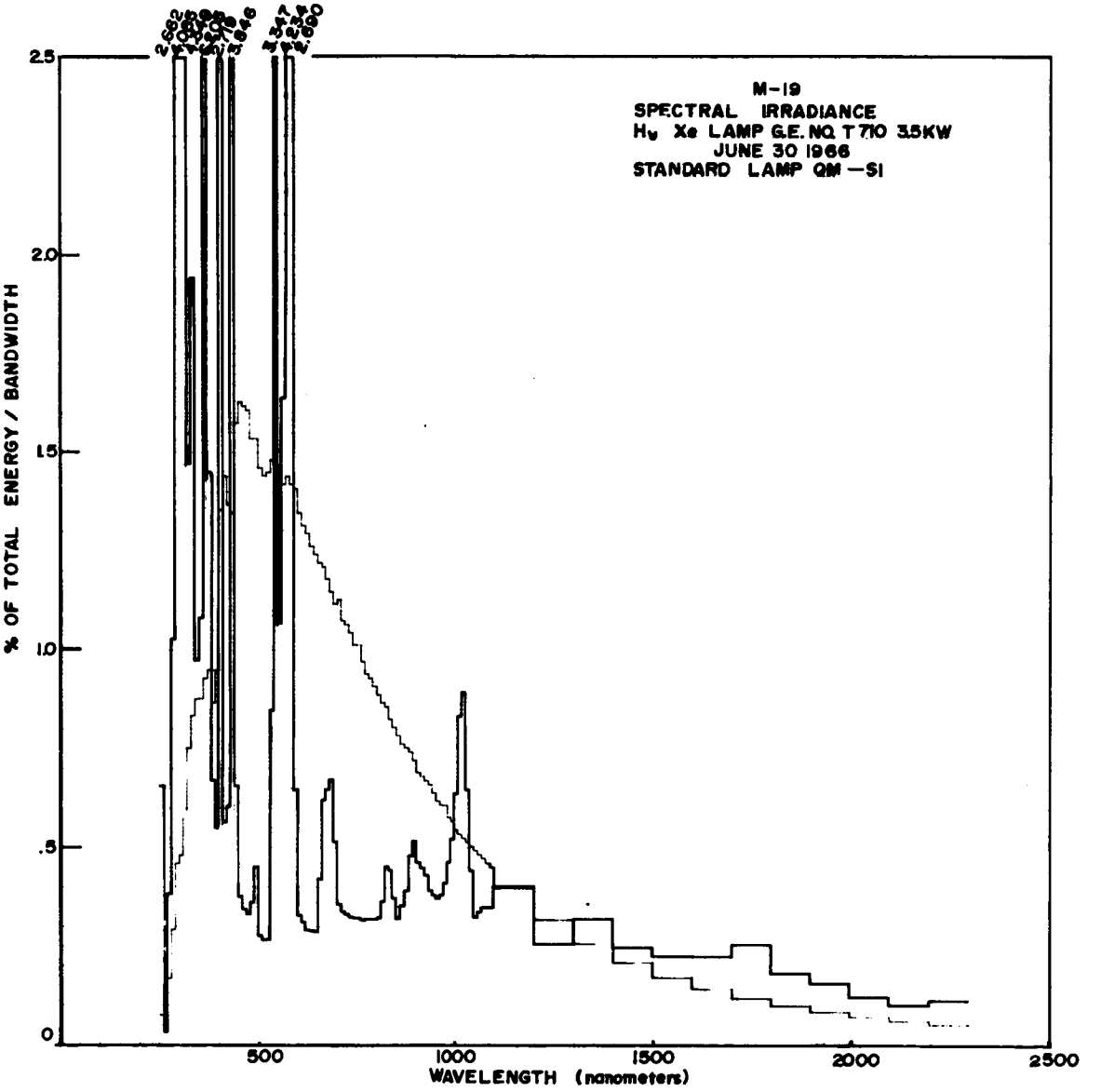

Figure 81. Spectral Irradiance, Hg Xe 3.5kw Lamp

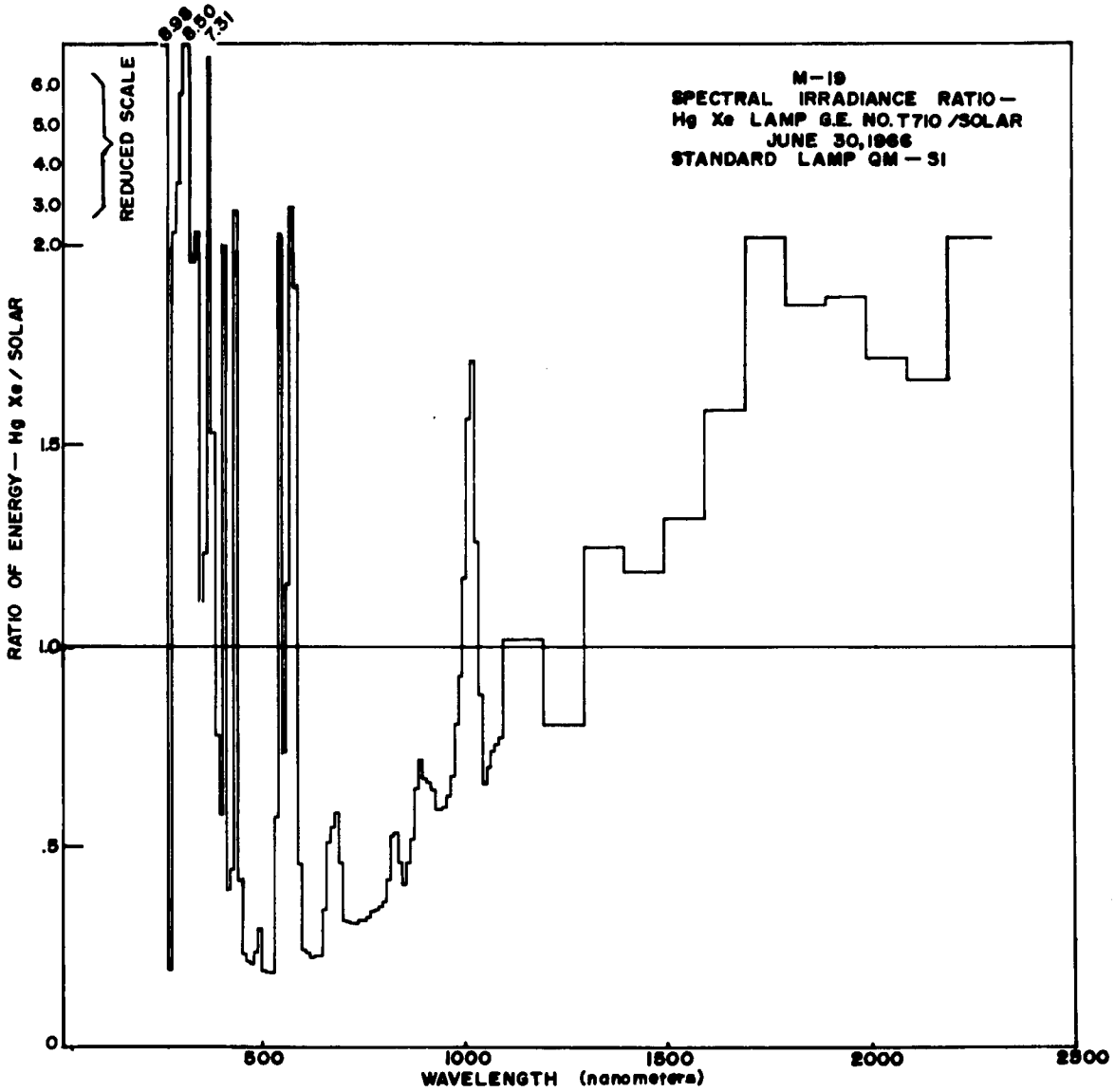

Figure 82. Ratio - Hg Xe 3.5kw Lamp/Solar

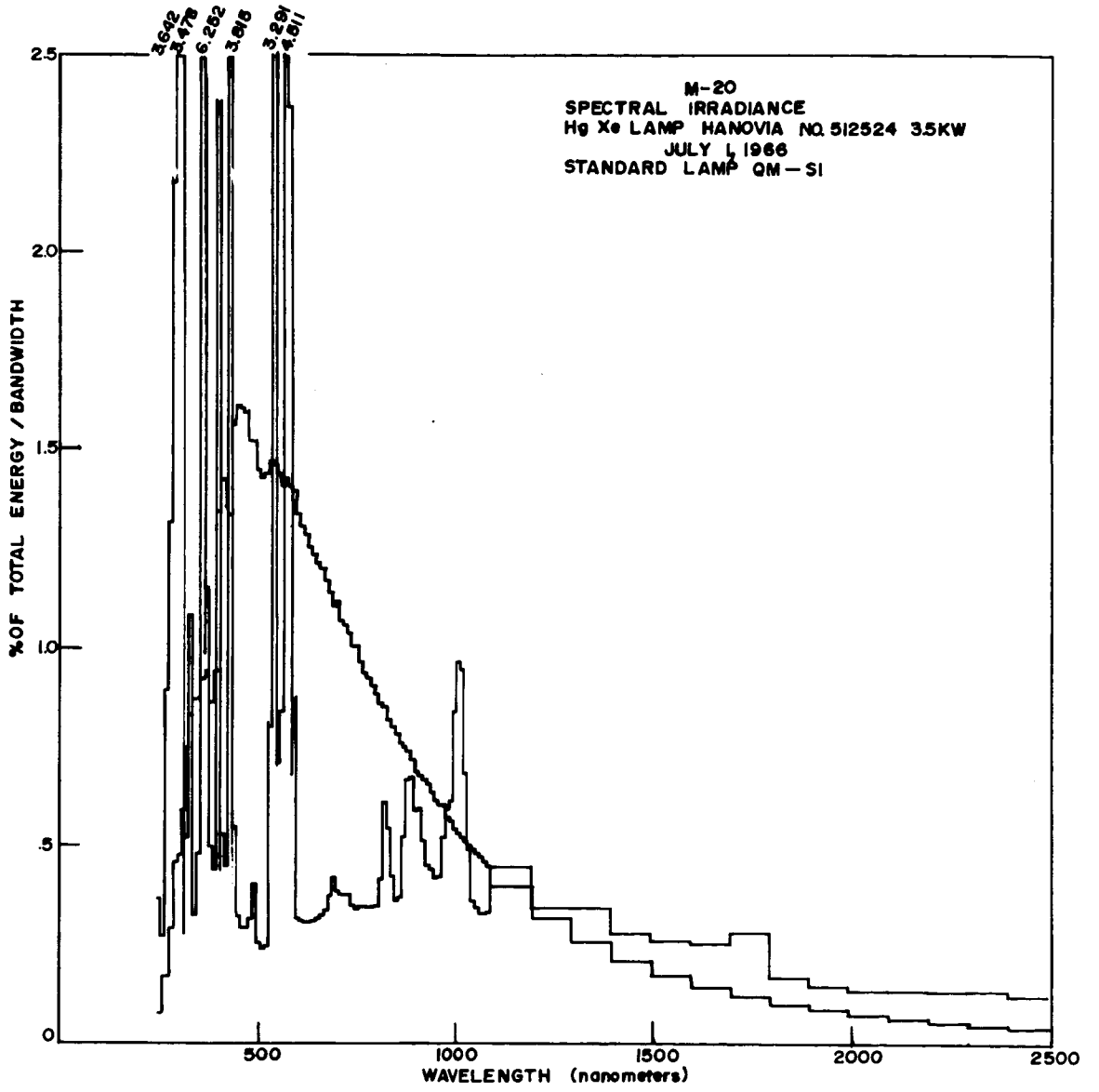

Figure 83. Spectral Irradiance, Hg Xe 3.5kw Lamp

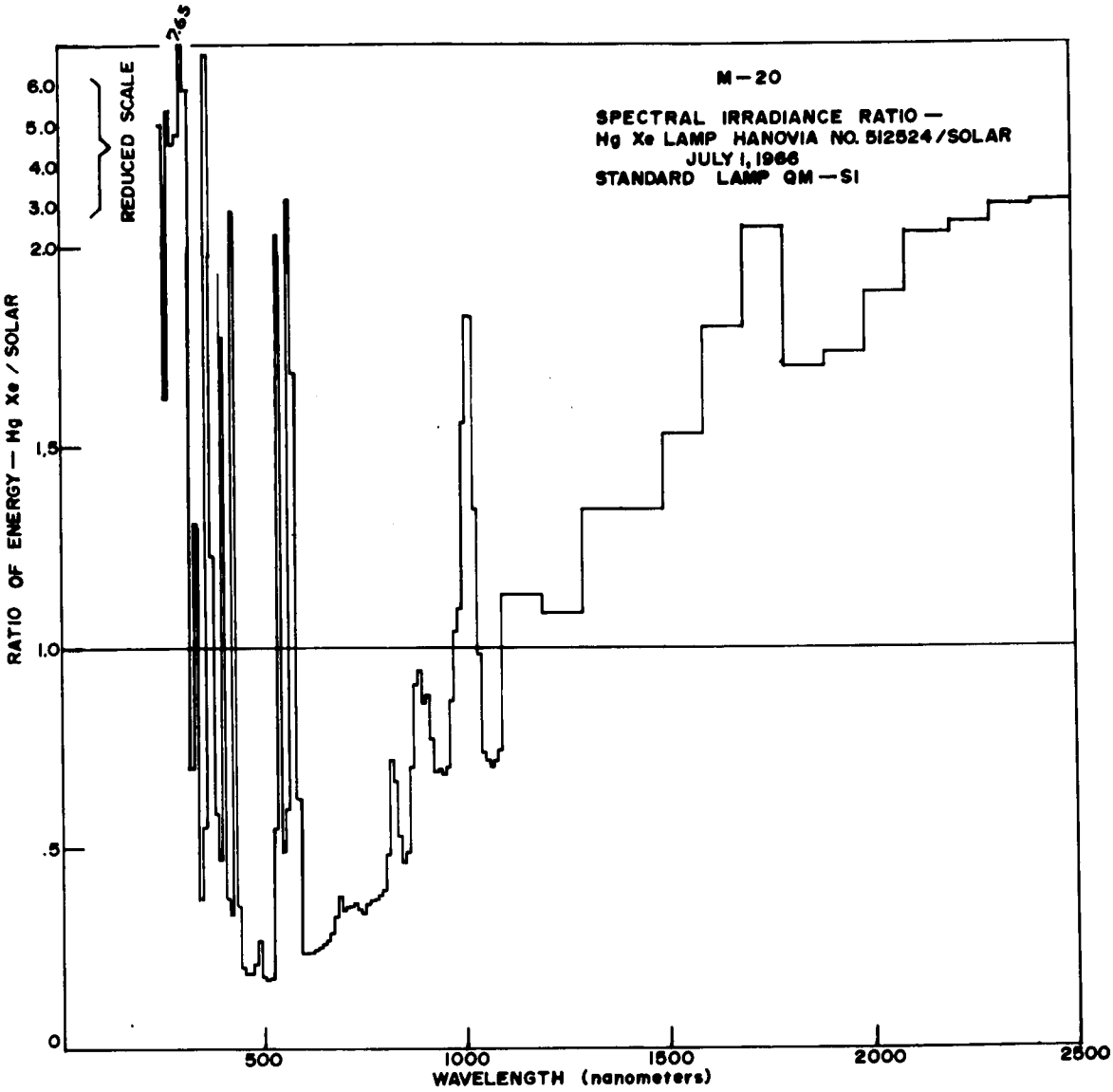

Figure 84. Ratio - Hg Xe 3.5kw Lamp/Solar

APPENDIX I

TEST REPORT ON THE JARRELL ASH 0.5 METER EBERT SCANNING SPECTROMETER

In general the Jarrell Ash Model 82000 Ebert grating scanning spectrometer meets the specifications quoted for it, and the instrument is fairly easy to use once it is set up and checked out. The instrument manual is complete and understandable and contains a considerable amount of maintenance information and sufficient theory for intelligent operation of the equipment.

The wavelength can be read directly in Angstrom units from a digital counter when an 1180 grooves/mm grating is used, wavelengths for other gratings are found by simply multiplying the counter reading by 2 or 4. The digital counter reads to an accuracy of ±1 Å and tenths of Angstroms can be estimated when an 1180 grooves/mm grating is used.

The wavelength accuracy over the spectrum is within ±2 Å in the 1900 Å to 9100 Å range when the instrument is calibrated for a known spectral line. This calibration must be repeated whenever the grating is changed. When gratings for the 3800 Å to 1.8μ range and for the 7600 Å to 3.6μ range are used the accuracy is within 4 Å and 8 Å respectively (the accuracy is within ±2 units of the counter with any grating). There is a 2 Å to 5 Å backlash in the wavelength drive which affects the accuracy when the scanning direction is reversed. Best accuracy is obtained by approaching a desired wavelength from a higher wavelength.

The calibration of the wavelength drive, which must be accomplished after changing gratings, involves finding a known line, removing the counter, setting it for the wavelength of that line and replacing it. The error in this setting may be as much as ±0.5 counter divisions.

The wavelength drive may be manually operated or motor driven. The eight speeds of the motorized drive showed no deviation from the given values. When using gratings with other than 1180 grooves/mm, proper adjustments must be made in scanning speeds because the speeds are given as Å/min when in actuality they are counter units/min.

When the gratings for the longer wavelength ranges are used there may be some problem with higher order lines if the detector used has a fairly high response at lower wavelengths than those under study. Orders as high as the 6th are easily picked up and could be mistaken for lines of longer wavelength.

The resolution obtained in the factory inspection did not reach the optimum quoted in the instruction manual but was better than that obtained in the laboratory here at Goddard, although both the factory test and the one performed here did meet the basic instrument specifications of 0.2 Å in the first order with the 1180 groove/mm grating and 0.4 Å in the first order with the 590 groove/mm grating.

Scattered light is no more than 0.23% of primary radiation at 5800 Å for any of the gratings supplied.

APPENDIX II


```
C      TEST LAMP IRRADIANCE CALCULATIONS
C
C
       DIMENSION A(36),B(36),G(150),H(150),C(100),D(400),STD(650),
      1PE(65 ),RI(650),GE(650),RO(650),RU(650),GI(650),P(650),R(650),
      2WL(65 ),W(450),EN(450),SUNSAV(100),PER(100),ABA(300),ABB(300),
      3ABC(3 0),ABD(300),TITLE(480),DECNAM(12),MXSAV(40),ABASAV(4000),
      4ABBSAV(4000),SUN(100)
    2 FORMAT(12F6.4)
    3 FORMAT (18F4.0)
    4 FORMAT(1H1)
    5 FORMAT(10E12.3)
    6 FORMAT(24F3.2)
    7 FORMAT (2(7F5.1))
    8 FORMAT(14F5.1)
    9 FORMAT(13I5)
   10 FORMAT(F10.0,F16.3,F16.3,F16.2)
   11 FORMAT(72H  WAVELENGTH   TEST LAMP ENERGY    SOLAR ENERGY    RATIO
      1TESTLAMP/SOLAR    )
   12 FORMAT(46H                        PER 10NM WAVELENGTH INTERVAL)
   13 FORMAT(109H   THE  SPECTRAL  ENERGY DISTRIBUTION IN PERCENT OF
      1  THE  TOTAL  ENERGY  PER  GIVEN  WAVELENGTH  INTERVAL)
   14 FORMAT(25H   NORMALIZATION  FACTORS)
   15 FORMAT(94H          THE  WAVELENGTHS  LISTED  ARE  THE  CENTER  WAV
      1ELENGTHS  OF  THEIR  RESPECTIVE  BANDS)
   16 FORMAT(118H   THE  SPECTRAL  ENERGY  DISTRIBUTION  NORMALIZED  AND
      1  EXPRESSED  AS  A  RATIO  RELATIVE  TO  THE  FIRST  WAVELENGTH)
   17 FORMAT(32H           AFTER  500  NANOMETERS)
   18 FORMAT(41H AREA UNDER CURVE AFTER NORMALIZATION WAS  ,F12.3)
   20 FORMAT(5(F12.3,F10.3))
   21 FORMAT(3(F12.3,F10.3,F8.2))
   22 FORMAT(12A6)
   23 FORMAT(24F3.1)
   24 FORMAT(F15.3)
   25 FORMAT(2F10.3)
   27 FORMAT (68H SPECTRAL ENERGY DIST. NORMALIZED,REL. TO FIRST WAVELEN
      1GTH AFTER 500  )
   28 FORMAT(3(F12.3,F10.3))
   29 FORMAT(F12.3,3F10.3)
C      STANDARD AND LEISS CALIBRATION, JOHNSON DATA
       READ(5,9) IGH
C      STANDARD
       READ(5,2)(A(J),J=1,35)
       READ(5,3)(B(J),J=1,35)
C      LEISS
       READ(5,8)(G(K),K=1,IGH)
       READ(5,8)(H(K),K=1,IGH)
       READ(5,6)(SUNSAV(J),J=1,99)
C      ABSORPTIVITY DATA
       KT=1
       JT=1
       READ(5,9)NX
       DO 99 J=1,NX
       JBT=JT+1
       JT=J*2
```

```
      READ( ,22)(TITLE(K),K=JBT,JT)
      READ( ,9)MXSAV(J)
      KS=KT+1
      KT=KT+MXSAV(J)
C     ABSORPTIVITY
      READ( ,23)(ABASAV(JJ),JJ=KS,KT)
C     WAVELENGTH
      READ( ,3)(ABSSAV(JJ),JJ=KS,KT)
   99 CONTINUE
C     TEST LAMP DATA
  112 READ( ,22)DECNAM
      IF(DECNAM)111,112,111
  111 WRITE(6,4)
      WRITE(6,22)DECNAM
      READ( ,9)L1,LL2,LL3
      L2=L1+1
      L3=L1+LL2
      L4=L3+1
      L5=L3+LL3
      M=L5
      IF(LL3.EQ.0) M=L3
      READ( ,7)(P(J),RE(J),RI(J),GE(J),RO(J),RU(J),GI(J),J=1,M)
C     CONVERT DS TO WAVELENGTH
      CALL LAGIN (H,G,P,WL,1,M,IGH)
C     INTERPOLATE STANDARD TO GIVEN WAVELENGTH
      CALL LAGIN(B,A,WL,STD,1,M,35)
      WRITE(6,9)L1,L2,L3,L4,L5
C     R=R*STD/RO
      DO 30 J=1,M
      RE(J)=(RE(J)-RI(J))*GE(J)
      RO(J)=(RO(J)-RU(J))*GI(J)
   30 R(J)=RE(J)*STD(J)/RO(J)
      WRITE(6,25)(R(J),WL(J),J=1,M)
      IF(LL2.EQ.0) GO TO 113
C     NORMALIZATION
C     FIRST OVERLAP, FIRST SECTION
      DO  1 J=1,L1
      NF=J
    51 IF(WL(L2).LE.WL(J))GO TO 52
    52 S1=0.
      DO 53 J=NF,L1
    53 S1=S1+R(J)
      S1=(2.0*S1)-R(NF)-R(L1)
      NL=2*L2-NF-1
C     FIRST OVERLAP, SECOND SECTION
      S2=0.
      DO 54 J=L2,NL
    54 S2=S2+R(J)
      S2=(2.0*S2)-R(L2)-R(NL)
      NOV1=L2-NF
      M1=(NF+L2)/2
      N1=M1-NF+1
      L2=L2+N1
      IF(LL3.EQ.0) GO TO 48
C     SECOND OVERLAP, SECOND SECTION
      DO 55 J=L2,L3
```

```
      NF=J
   55 IF(WL(L4).LE.WL(J))GO TO 56
   56 S3=0.
      DO 57 J=NF,L3
   57 S3=S3+R(J)
      S3=(2.0*S3)-R(NF)-R(L3)
      NL=2*L4-NF-1
C     SECOND OVERLAP, THIRD SECTION
      S4=0.
      DO 58 J=L4,NL
   58 S4=S4+R(J)
      S4=(2.0*S4)-R(L4)-R(NL)
      NOV2=L4-NF
      M2=(NF+L4)/2
      M2=M2-NF+1
      L4=L4+M2
      GO TO 47
   48 S3=0.
      S4=0.
      M2=L3
   47 WRITE(6,5)S1,S2,S3,S4
C     NORMALIZATION FACTORS
      FA1=S1/S1
      FA2=1.0
      FA3=S3/S4
      WRITE(6,14)
      WRITE(6,5)FA1,FA2,FA3
C     NORMALIZE FIRST SECTION
      DO 63 J=1,M1
   63 R(J)=R(J)*FA1
C     NORMALIZE SECOND SECTION
      DO 64 J=L2,M2
      K=J-NOV1
      R(K)=R(J)*FA2
   64 WL(K)=WL(J)
      IF(LL.EQ.0) GO TO 46
C     NORMALIZE THIRD SECTION
      DO 65 J=L4,L5
      K=J-NOV1-NOV2
      R(K)=R(J)*FA3
   65 WL(K)=WL(J)
      KG=L5-NOV1-NOV2
      GO TO 45
   46 KG=L3-NOV1
      GO TO 45
  113 KG=L1
C     TOTAL ENERGY UNDER CURVE
   45 SUM=0.
      DO 301 J=1,KG
      SUM=SUM+(R(J)+R(J+1))*(WL(J+1)-WL(J))/2.0
  301 CONTINUE
      WRITE(6,18) SUM
C     SET R RELATIVE TO FIRST WAVELENGTH AFTER 500 NM
      DO 67 J=1,KG
      RMAX=R(J)
   67 IF(WL(J).GE.500.)GO TO 68
```

```
   68 DO 69 J=1,KG
   69 R(J)=R(J)*100./RMAX
      WRITE(6,16)
      WRITE(6,17)
      WRITE(6,20)(R(J),WL(J),J=1,KG)
C     OUTPUT FOR PLOT
      L2=KG-1
      PUNCH 22,DECNAM
      PUNCH 27
      PUNCH 9,L2
      PUNCH 28,(R(J),WL(J),J=1,KG)
      WRITE(6,4)
      WRITE(6,22)DECNAM
C     GENERATE DESIRED WAVELENGTH TABLE
      CALL WAGEN(250.,1100.,10.,W,1,KJ)
      IF(LL.EQ.0) GO TO 44
      CALL WAGEN(1100.,2800.,100.,W,KJ,KK)
C     SET R TO INTEGRATED VALUE FOR INTERVAL
   44 NN=KG-1
      DO 70 J=1,NN
      RI(J)=WL(J+1)
   70 R(J)=(R(J)+R(J+1))*(WL(J+1)-WL(J))/2.0
      WRITE(6,13)
      SUM=0.0
      DO 15  J=1,NN
C     SET R RELATIVE TO TOTAL ENERGY
  150 SUM=SUM+R(J)
      DO 15. J=1,NN
  151 R(J)=R(J)*100./SUM
      WRITE(6,21)(R(J),WL(J),RI(J),J=1,NN)
      WRITE(6,4)
      WRITE(6,22)DECNAM
C     EN IS R ADJUSTED TO FIT W
      IF(LL.EQ.0) KK=KJ
      DO 71 J=1,KK
      NF=J
   71 IF(W(J).GT.WL(1))GO TO 72
   72 DO 73 J=1,KK
      NL=J
   73 IF(W(J).GE.WL(NN))GO TO 74
   74 IF(W(J+1).GT.WL(KG))GO TO 75
      GO TO 78
   75 IF(W(J)-WL(KG))76,76,77
   76 NL=NL-1
      GO TO 78
   77 NL=NL-2
   78 N=1
      DO 109 J=NF,NL
  100 IF(WL(N).GT.W(J))GO TO 101
      N=N+1
      GO TO 100
  101 IF(WL(N)-W(J+1))103,102,108
  102 EN(J)=(WL(N)-W(J))*R(N-1)/(WL(N)-WL(N-1))
      GO TO 109
  103 EN(J)=(WL(N)-W(J))*R(N-1)/(WL(N)-WL(N-1))
      N=N+1
```

```
  106 IF(WL(N)-W(J+1))105,104,107
  104 EN(J)=EN(J)+R(N-1)
      GO TO 109
  105 EN(J)=EN(J)+R(N-1)
      N=N+1
      GO TO 106
  107 EN(J)=EN(J)+(W(J+1)-WL(N-1))*R(N-1)/(WL(N)-WL(N-1))
      GO TO 109
  108 EN(J)=(W(J+1)-W(J))*R(N-1)/(WL(N)-WL(N-1))
  109 CONTINUE
      SUM=0
      DO 81 J=NF,NL
   81 SUM=SUM+EN(J)
      DO 82 J=NF,NL
   82 EN(J)=EN(J)*1.0/SUM
      DO 83 J=NF,NL
   83 W(J)=(W(J)+W(J+1))/2.0
      WRITE(6,13)
      WRITE(6,15)
      WRITE(6,20)(EN(J),W(J),J=NF,NL)
      WRITE(6,4)
      WRITE(6,22)DECNAM
C     ABSORPTIVITY CALCULATIONS
C     PICK UP TABLES
      JBT=0
      LSAV=
      KSAV=
      DO 326 JB=1,NX
      JT=JBT+1
      JBT=JB*12
      WRITE(6,22)(TITLE(K),K=JT,JBT)
      ABAC=0.0
      MX=MXSAV(JB)
      DO 97 J=1,MX
      KSAV=KSAV+1
   97 ABA(J)=ABASAV(KSAV)
      DO 98 J=1,MX
      LSAV=LSAV+1
   98 ABB(J)=ABBSAV(LSAV)
C     ADJUST TO FIT W
      CALL LAGIN(ABB,ABA,W,ABC,NF,NL,MX)
C     CALCULATE ABSORPTIVITY
      DO 324 J=NF,NL
  324 ABD(J)=ABC(J)*EN(J)
      DO 325 J=NF,NL
  325 ABAC=ABAC+ABD(J)
      ABACT=ABAC/100.
      WRITE(6,24)ABACT
      JX=JB
  326 CONTINUE
      WRITE(6,4)
      WRITE(6,22)DECNAM
C     ADJUST SUN TO FIT NF AND NL
      TOT=0.0
      DO 90 J=NF,NL
   90 TOT=TOT+SUNSAV(J)
```

```
      DO 91 J=NF,NL
   91 SUN(J)=SUNSAV(J)*100./TOT
      DO 92 J=NF,NL
   92 PER(J)=EN(J)/SUN(J)
      WRITE(6,11)
      WRITE(6,12)
      KL=KJ-1
      WRITE(6,10)(W(J),EN(J),SUN(J),PER(J),J=NF,KL)
C     PLOT OUTPUT
      PUNCH 11
      PUNCH 12
      PUNCH 9,KJ
      PUNCH 29,(W(J),EN(J),SUN(J),PER(J),J=NF,KL)
      IF(LL.EQ.0) GO TO 43
      DO 93 J=KJ,NL
      EN(J)=EN(J)/10.
   93 SUN(J)=SUN(J)/10.
      WRITE(6,10)(W(J),EN(J),SUN(J),PER(J),J=KJ,NL)
      KKG=NL-KJ+1
      PUNCH 9, KKG
      PUNCH 29,(W(J),EN(J),SUN(J),PER(J),J=KJ,NL)
   43 WRITE(6,4)
      GO TO 112
  110 STOP
      END
```

SYMBOLS

A	Standard lamp energy table
B	Standard lamp wavelength table, parallel to A
G	Leiss wavelength table
H	Leiss drum setting table, parallel to G
SUNSAV	Table used to save Johnson's data for repeated use
SUN	SUNSAV x 100/TOT
STD	Standard lamp data. This table is parallel to the test lamp data and corresponding wavelength
RE	Test lamp data (voltage). Also used for corrected test lamp data (voltage), (RE-RI) GE
RI	At 300, the error voltage corresponding to RE for the device used to read the voltage. At 70, a table parallel to WL containing the next WL in each position
GE	The range on the measuring device
RO	Standard lamp data (voltage). Also used for corrected data (voltage), (RO-RU) GI
RU	Error voltage for RO
GI	Range for RO
P	The drum setting array parallel to RE, RI, GE, RO, RU, and GI
R	At 300, the relative intensity using (RE x STD)/RO. At 70, the integrated intensity calculated from the intensity relative to the 1st intensity after 500 nm
WL	The wavelengths calculated from P using H and G. This table replaces P and will be called given wavelengths
W	The wavelengths desired for output
EN	The integrated energy calculated from the last R. These tables are parallel to W
PER	The ratio of the test lamp to Johnson's data, EN/SUN
ABA	The absorptivities for various paint samples
ABASAV	Used to save ABA data for repeated use
ABB	The wavelengths corresponding to the absorptivities given in ABA
ABBSAV	Used to save ABB

ABC	ABA interpolated to fit the wavelength table W
ABD	ABC x EN parallel to W
TITLE	An array used to save the names of the absorptance samples
DECNAM	The name of the source that generated the data RE
NX	The number of absorptivity tables
MX	The number of items in each table
MXSAV	An array used to save the MX's
JT	Used as end of each absorptivity title in storing them sequentially
JBT	Used as beginning of each absorptivity title in storing them sequentially
KT	Used as end of each absorptivity ABA & ABB array in storing them sequentially
KS	Used as beginning of each absorptivity ABA & ABB array in storing them sequentially
L1	The number of points in the 1st region
L2	After 111, the beginning of second region, after 54 changes to start of 1st overlap
L3	End of second region
L4	Beginning of third region
L5	End of third region
LL2	Number of points in second region
LL3	Number of points in third region
M	End of data, set to L3 or L5 for 1 or 2 overlap regions
IGH	Number of points in the Leiss calibration tables
NF	At 51, a pointer indicating the start of the 1st overlap region in the 1st section. At 55, the beginning of the 2nd overlap in the 2nd section. At 72, the 1st wavelength in the desired wavelength table (W) after 1st wavelength in WL
S1	The sum of the intensities (R) for the 1st overlap region of the 1st section
NL	After 53, the end of the 1st overlap region in the 2nd section, after 57, the end of the 2nd overlap region in the 3rd section, after 74, the 1st wavelength in the desired wavelength table after the last wavelength in the given table

S2	The sum of the intensities for the 1st overlap in 2nd section
NOV1	The end points, in the 1st overlap region for both sections
M1	The middle points of the 1st overlap for both sections
N1	The beginning of the 1st overlap in the 1st section
S3	Sum of intensities for 2nd overlap in 2nd section
S4	Sum of intensities for 2nd overlap in 3rd section
NOV2	No. of points in 2nd overlap for both sections
M2	Middle of 2nd overlap
N2	Beginning of 2nd overlap in 2nd section
FA1	Normalization for 1st section - S2/S1
FA2	Normalization for 2nd section - 1
FA3	Normalization for 3rd section - S3/S4
KG	The end of the normalized intensity table (R) with the overlap region(s) removed
SUM	At 301, the area under the curve after normalization. At 81, the total energy (EN) summed
RMAX	The first wavelength after 500 nm
KK	The end of the desired wavelengths table (W)
KSAV	Used to pick up ABA's from ABASAV
LSAV	Used to pick up ABB's from ABBSAV
ABAC	$\sum_{J=NF}^{NL} ABD_j$
ABACT	ABAC/100, the energy after the absorptance data is applied to the lamp data
TOT	$\sum_{J=NF}^{NL} SUNSAV_j$

PART III

SOLAR CELL CALIBRATION-EVALUATION

Quarterly Progress Report
Period Covered

September 1 - November 30, 1966

Prepared for:

National Aeronautics and Space Administration
Goddard Space Flight Center
Greenbelt, Maryland

Contract NAS5-9244

Prepared by: _____
William G. Gdula

Approved by: _____
M. J. Brown

Work performed by: William Gdula
Segun Park

Electro-Mechanical Research, Inc.
Aerospace Sciences Division
College Park, Maryland

CONTENTS

CONTENTS (Continued)

ILLUSTRATIONS

ILLUSTRATIONS (Continued)

TABLES

SOLAR CELL CALIBRATION EVALUATION

William G. Gdula

ABSTRACT

During this quarterly report period from September through November 1966, all activities of the solar cell calibration effort conducted for the Thermal Systems Branch GSFC were relocated at EMR's College Park Laboratory. In view of the limited experimental portion of the program, a review of all solar cell measurements developed during this program is presented with a brief description of the theoretical, experimental and application aspects. In addition, a series of 1 MeV electron radiation experiments were performed to define the radiation damage characteristics of silicon solar cells fabricated from 1 ohm-cm and 10 ohm-cm resistivities with thicknesses of 8 mils to 16 mils.

Preliminary results of the angular dependence studies of the electron damage rate in silicon solar cells indicate a higher damage coefficient as the incident angle of the electron flux is increased. Experimental results have not been corrected for a cosine projection factor which would further increase the apparent damage. Proton damage is presently being investigated.

Electron damage characteristics of lithium doped silicon solar cells, fabricated from 20 ohm-cm float-zone material, indicate 300°K annealing only partially effective in short-circuit current recovery. Degradation of the voltage characteristics, remained after 15 days of annealing.

INTRODUCTION

The primary function of the solar cell calibration effort is to provide the Thermo Physics Branch with a comprehensive calibration and evaluation of present day solar cells. Because of the necessary support activities - solar simulation research and development - conducted by the Branch, the efforts of precise evaluation of solar cell characteristics is readily achieved. Included in this report period is a complete calibration and electron radiation evaluation experiment of one ohm-cm and ten ohm-cm silicon cells contained in Section 1. A summary of the measurement procedures developed during this program is presented in Sections 2 and 3.

1.0 SOLAR CELL CALIBRATION AND RADIATION EVALUATION

An evaluation study was performed by request of the Space Power Technology Branch in order to define the radiation damage characteristics of silicon solar cells fabricated from one and ten ohm-cm material with 8 mil and 16 mil thicknesses. Four lots of ten samples each were subsequently exposed to 1 MeV electrons with incremental flux dosages of 10^{13}, 10^{14}, 10^{15} and a final accumulated flux level of 10^{16} e/cm^2. The EMR standard electron radiation procedure was followed as outlined in Report No. 766-7142 with the exception of the 4×10^{15} flux increment which was added to more accurately define the degradation rates near the 10^{16} e/cm^2 level. The complete radiation schedule is included in Table 1.

Current Voltage (I-V) characteristics of the cells were measured immediately after each incremental flux dosage with the X-25$_L$ solar simulator adjusted to one solar constant. Typical I-V characteristics of representative samples are included in Figures 1 and 2. Seventy-four spectral response and quantum yield measurements were also made as time permitted during the radiation procedure. Experimental data including the current, voltage and conversion efficiency parameters is included in Table 2.

1.1 EXPERIMENTAL RESULTS

Typical results of the comparative study are summarized in Figure 3 which is a plot of the energy conversion efficiency vs accumulated 1 MeV electron flux. It was not to be expected that the 8 mil 1 ohm-cm cells would maintain a higher conversion efficiency than the 16 mil 1 ohm-cm cells after an initial flux of about 5×10^{13} e/cm^2. Considering all factors the probable explanation is that the initial properties of the bulk 16 mil material differed from the 8 mil

with a possible higher oxygen concentration. The cross-over of the open-circuit voltage shown in Figure 4 would substantiate this conjectural argument. Among solar cell manufacturers, there is an understanding that higher resistivity material inherently has intrinsically superior radiation resistent characteristics. This is quite true if the sole interest were in the current collection efficiency at short circuit conditions, short circuit degradation is included in Figure 5. Because of longer bulk lifetime and diffusion length due to the lesser number of impurity atoms in the bulk, current-densities of solar cells fabricated from 10-25 ohm-cm material normally are about 10% higher than the lower resistivity cells, considering other fabrication factors and surface reflectance properties equal. Impurity concentration vs resistivity data for both N and P type material shown in Figure 6 indicates the magnitude of change, 1 ohm-cm P type containing 1.5×10^{16} impurity atoms/cm^3 vs. 10 ohm-cm material which contains 1.3×10^{15}. However, the additional decade of impurity atoms results in a greater open circuit voltage which, as a direct result of Fermi level considerations, is a well defined function of temperature and majority donor and acceptor concentrations. A comparison of the diode characteristic in Figure 7 for 1 ohm-cm and 10 ohm-cm cells with equal efficiency shows the dependence of the 10 ohm-cm cells upon the higher current density to maintain conversion efficiency comparable to the 1 ohm-cm cells. The lower resistivity 1 ohm-cm cells, have a V_{oc} of 0.575 volts at 300K compared to 0.545 for the 10 ohm-cm cells, but the increased number of impurity atoms has decreased the bulk minority carrier lifetime and a subsequent decrease in the collected minority carriers.

With all factors considered it has always been apparent for other than academic reasons to evaluate cell radiation characteristics by selecting η_{eff}, the energy conversion efficiency as the comparative parameter. It is this unifying complex parameter which relates the individual characteristics, including the total voltage across the junction, space charge region and current flow through the junction. The data in Figure 3 support the conclusion that the 1 ohm-cm cells, with the initially higher conversion efficiency, maintain superior performance over the 10 ohm-cm cells when exposed to accumulated 1 MeV flux levels of 8×10^{15} electrons-cm^2, results which are subjected to the limitations of any atypical conditions of the one ohm-cm and 10 ohm-cm material utilized.

1.2 EFFECTS OF SOLAR CELL THICKNESS

The intrinsic optical absorption properties of silicon, are such that approximately 200 microns (8 mils) of material is required to absorb over 95% of the solar energy. This makes it feasible to optimize the amount of base material required to collect the generated free carriers.

By combining the optical absorption function with photon density distribution of air mass zero and assuming a unity quantum yield a spatial current density can be derived. This normalized relationship shown in Figure 8 for the current density to a depth of 50 microns indicates that once this function is obtained, detailed considerations can be given to performance requirements not only for conversion properties, but also to radiation damage characteristics.

Using this criteria, there has been a general trend by the cell manufacturers to reduce silicon solar cell thickness from 16 mils to 8 mils or less, in order to achieve both material economy and a higher watts/lb performance figure. (A developmental 12.5KW deployable array over greater than 1200 ft is presently being developed by the Boeing Aero Space Division.)

Quantum yield measurements of cells with varying thickness fabricated from the same boule indicates as shown in Figure 9, very little difference between 4000 Å to 7000 Å (the slight differences are due in part to a variance in the SiO coating). From 7000 Å to 12000 Å the Q.Y. of the 8 mil cells decrease at a higher rate than the 16 mils samples as a direct result of the lesser amount of base material.

Four mil samples were measured but unfortunately, all data was returned to the manufacturer and copies have not been returned to date. The average loss in short-circuit current density in making cells 8 mils rather than 16 mils is approximately 8.3% for cells fabricated from 10 ohm-cm material and 5.8% for cells made from 1 ohm-cm material. The comparative results of V_{oc}, I_{sc}, and η_{eff} are given in Table 2 for all samples measured.

It is of considerable interest to determine if there are any adverse effects upon the cell diode properties as a result of the back surface recombination characteristics. Cells of similar diode properties but different thicknesses, were exposed to 1 MeV electrons with I-V measurements made after each flux increment, the purpose of the electron flux being to remove the current contribution from the bulk of the thick cells. This procedure then allowed I-V measurement at the cells with current output essentially being equal and still maintaining the same incident photon flux. Typical results given in Figure 10 indicate that after about 1×10^{15} 1 MeV electrons, the current densities for the 8 mil and 16 mil cells are approximately equal and importantly, there is no distinguishable difference in the I-V characteristics. There are several interesting conclusions that may be advanced from these conditions. It is obvious that the degradation rates are logarithmic functions of integrated flux. If the 8 mil 1 ohm-cm cells with no shielding were pre-irradiated to a flux level of 10^{15} 1 MeV electrons, the conversion efficiency would still be 8.1% and would only have degraded 8% if exposed to another increment of 1×10^{15} e/cm^2. Initial degradation

of cells which were not pre-irradiated would be approximately 18% in conversion efficiency, a result which complicates the panel design considerations because of the greater variations in power output. Rather than add more shielding to maintain higher conversion efficiencies after specified flux exposures, it might then be possible to maintain a superior watts/lb factor by the addition of pre-irradiated cells with reduced shielding and still maintain similar performance characteristics without the variations in conversion efficiency produced by the radiation damage.

1.3 ANGULAR DEPENDENCE OF DAMAGE RATES

Preliminary results in the determination of angular dependence in the change of solar cell characteristics during electron radiation indicates an increase in damage as the flux angle of incidence is increased from the normal. Data in Figure 11 indicates an increase in damage as the samples are rotated from 0°, 30°, 45°, to 60°. Because of the ionization properties of the electron beam in air and subsequent spatial variation of the incident flux the samples essentially are exposed to varying conditions of flux. It is extremely difficult to assess the possible magnitude of deviation. If the angular dependence is a real function for the 1 MeV electrons, damage rates incurred during proton irradiation would be expected to be highly significant.

2.0 CONSIDERATIONS IN THE MEASUREMENT AND EVALUATION OF SOLAR CELL PROPERTIES

Prerequisite to the accurate measurement and definition of solar cell energy conversion characteristics is the tacit assumption that the pertinent information describing the energy source (solar simulator) namely the energy distribution as a function of wave length and total incident energy is reasonably well described. It is sufficient to state that in the majority of experimental procedures, this is not the circumstance. The radiometric procedure and spectrophotometric instrumentation is indeed formidable and only a few groups have cultivated the proper disciplines required for what could be called measurements is germane to the complete understanding of the validity in applying solar cell data on an absolute basis.

A great deal of confusion arises when the parameters of cells with dissimilar spectral responses are calibrated under varying conditions of solar simulation. A typical measurement of the energy distribution of the solar simulation source used by EMR for solar cell calibration, shown in Figure 12, indicates an excellent match to the known solar energy distribution at the air-mass-zero

environment. To further substantiate the degree of accuracy achieved in laboratory measurements, extensive interchange of solar cells calibrated at altitudes of 47,000 and 78,000 feet have resulted in comparative accuracies which are compiled in Table 3. For cells with similar spectral responses, EMR's calibrations agree within less than 2% of the short-circuit currents of the NASA-Lewis flight calibrated cells; extreme deviations in spectral responses produce a correlation figure of 2.85%. In consideration of the limitation of known absolute standards and the uncertainties of the NRL data, a 2% correlation figure is totally acceptable. EMR's standard radiometric procedure involves use of silicon cells calibrated with the JPL standards and a primary working standard Angstrom Pyrheliometer, which is shown in Figure 13.

3.0 BASIC SOLAR CELL MEASUREMENTS

Most of the present day solar cell measurements are oriented towards the overt features of the energy conversion process, i.e., a photon flux incident on the cell surface is measured and an energy conversion efficiency parameter is derived from the current-voltage characteristic generated by the cell under varying load conditions.

Because the conventionally fabricated silicon cell is a P/N junction device, it has all of the expected attributes including among others a space charge region, electrostatic potential and an effective junction capacitance, each of which is highly dependent upon unique fabrication processes and the intrinsic properties of the parent material.

An awareness of all of the characteristics of the solar cell is needed when measuring any single parameter and because of the interrelated functions a brief, but in no sense complete, summary of each measurement is presented in order to add significance and possibly clarify just what properties are being measured and how this measured physical property relates to the entire energy conversion process.

3.1 CURRENT-VOLTAGE (I-V) MEASUREMENT

Fortunately, the most common and widely used of all solar cell measurements, the I-V characteristic from which the energy conversion efficiency is obtained, can be measured with comparative ease and requires a nominal investment in instrumentation.

Normal procedure in measuring the current-voltage relationship requires use of a precision variable load across the cell with solar energy incident on the cell surface: The short-circuit current, I_{sc}, open circuit voltage V_{oc}, and the conversion efficiency η_{eff}, derived from knowledge of the maximum power point are obtained from the generated diode property. When photon energy is being absorbed within the cell, the intrinsic optical absorption process creates free minority carriers, and as a result of the tendency to maintain dynamic equilibrium the solar cell junction becomes biased in the forward direction in a compensation effort to neutralize the generated carriers. The simple characteristic diode property of large area solar cells in actuality has parameters which have extremely complicated physical inter-relationships. An elementary verbal picture in further defining the current voltage relationship can be described as follows:

When in thermal equilibrium, the net concentrations of electrons and holes in the highly diffused surface region and base portion of the solar cell are kept in balance by means of a potential barrier developed at the solar cell junction region; the magnitude of this barrier electrostatic potential, corresponds to the difference in Fermi levels in the N-type and P-type material, the Fermi level being an explicit function of temperature and density of the electron and hole concentrations.

During the process of ie./and carrier creation by the absorption of photon energy, minority carriers, electrons in the P-region, eventually diffuse to the vicinity of the junction and as a result of the aiding field in this region are returned to a potential of lower state in the N-region; a similar argument applies for the holes in the N-region. The P-type material becomes positively charged and the N-type, negatively charged, a voltage being developed which now biases the P/N junction of the solar cell in the forward direction. This voltage produces a forward current composed of majority carriers which counteracts the flow of charge in the reverse direction due to normal injection of holes from the P-region and electrons from the N-region are related by the ideal diode equation stated in the generalized form by:

$$I = I_o \left(e^{\frac{qv}{KT_{-1}}}\right) \qquad (1)$$

where

KT = Thermal Energy
I_o = Thermally generated reverse saturation current
q = Electronic charge

The current due to the optical injection during normal photon flux density conditions is not affected so that the total current, I, of the solar cell can be reasonably approximated by:

$$I = I_o \left(e^{\frac{qv}{KT}} - 1\right) - q\, G(L_N + L_p) \qquad (2)$$

where

G = minority carrier generation rate
L_n, L_p = diffusion lengths of the carriers

With open circuit conditions I = 0 and the open-circuit voltage is:

$$V_o = \frac{KT}{q} \ln \frac{\left[1+q\, G(L_n + L_p)\right]}{I_o} \qquad (3)$$

V_o is proportional to G at low injection levels. When the photon flux absorbed is high then the voltage generated will increase until it removes the barrier and no further increase will ensue. The maximum photo-voltage which can be generated is equal to that obtained from the difference in Fermi levels of the N-type and P-type sections of the cell and for silicon cells this is approximately equal to the voltage corresponding to the energy gap, (Eg) of 1.11 volts.

With an appropriate curve shaping factor added in the exponential term qv/Akt to compensate for deviations from the idealized conditions, the I-V function can be readily synthesized for most silicon solar cells.

3.1.1 Experimental Data

Typical current-voltage characteristics illustrated in Figure 14 for one ohm-cm and ten ohm-cm silicon solar cells demonstrate the more obvious features of differences in material properties even though the conversion efficiencies are equal.

Because of the effect of the additional impurities in reducing the parent material minority carrier lifetime, the one ohm-cm cells have current densities of 3 to 4 ma/cm^2 less than the ten ohm-cm cells. However, the increased number of boron atoms in the bulk enhance the voltage factor for the lower resistivity material so that the maximum power derived is about the same.

From the power supply design viewpoint, ten ohm-cm cells have lower voltage at maximum power, a slightly smaller temperature dependence and generally exhibit a higher electron radiation resistance than lower resistivity cells.

3.1.2 EMR Instrumentation Procedure

For measurements in which only the general form of the I-V function is required and the simulation source can be adjusted to achieve the proper current density, exact match to air-mass-zero is of less significance. EMR, however, has realized the difficulty in correlating measurements taken of solar cells such as GaAs and CdS under less precise solar simulation conditions, (e.g., 2800° K tungsten energy filtered with water) and has adopted the procedure of only using a solar simulator which has a known energy distribution matched to the air-mass-zero solar radiance. The variable electronic load used in generating the I-V function is uniquely designed for this specific measurement and has internal standards with measurement error of less than 0.05%. An external digital voltmeter monitors the open-circuit voltage and short-circuit current and an X-Y plotter records the complete diode function along with the product of the current and voltage. The solar cell temperature is controlled by cooling the sample holder with a re-circulating heat exchanger and measurements are normally taken at 27°C.

3.2 SOLAR CELL QUANTUM YIELD MEASUREMENTS

Fundamental to the characterization of the current-voltage properties of solar cells is the determination of the physical parameters and inter-related functions which control the collected current density. This essential information is derived from the solar cell quantum yield measurement which in the practical definition relates the ability of the P/N junction and the parent bulk material to collect the minority carriers created by the material absorption of photon energy, each photon being loosely described as possessing a discrete quantum of energy. The wavelength dependent ratio of the collected current density to the photon density incident on the cell surface is the quantum yield $QY_{(\lambda)}$.

where

$$QY(\lambda) = \frac{I_{sc}(\lambda)}{(q)\, N_o(\lambda)} \qquad (4)$$

and

$I_{sc}(\lambda)$ = collected current density
q = electronic charge
$N_o(\lambda)$ = photon density

In material investigations of a fundamental nature it is often pertinent to deal with the absolute quantum yield. In this measurement energy reflected from the surface is considered and the current density qualified as originating

from the incident photon density being absorbed in the material. The absolute quantum yield QY_{ab} is

$$QY_{ab} = \frac{I_{sc}(\lambda)}{q(1-R\lambda)\ N_o(\lambda)} \tag{5}$$

and

$R(\lambda)$ = surface reflectance

3.2.1 Instrumentation

The wave-length dependence of solar cell characteristics requires use of an optical dispersion instrument equipped with the necessary detectors and light source.

A grating monochrometer with comparatively high efficiency and constant bandwidth was selected in order to have the maximum amount of monochromatic energy on the sample surface and to eliminate any variations of response near the band edge as a result of large variations in bandwidth, typical of prism monochrometers. The complete instrumentation set-up (illustrated in Figure 15) is primarily composed of the 1 meter Zerny Turner grating monochrometer, high intensity light source, beam-splitting transfer optics and rationing electronics with the output recorded on an X-Y-Y^1 plotter. A function generator has been designed which allows the concurrent plotting of the cell output in both equal energy and equal photon density modes which are the spectral response and quantum yield measurements. Typical experimental data of production type silicon solar cells is included in Figure 16. With prior knowledge of the optical absorption characteristics of the material various physical parameters can be derived from the QY measurement, including the bulk diffusion length, surface recombination characteristics, and an approximation of the function depth. A computer program has been prepared which enables the experimental data to be compared with generated functions of varying solar cell parameters.

3.3 SOLAR CELL SURFACE REFLECTANCE AND ANTI-REFLECTION COATINGS

Although the EMR Aerospace Sciences Division presently does not have the in-house facilities for optical coatings and other thin-film deposition activities, its awareness of the importance of anti-reflection SiO coatings and the more complex multi-layer dielectric films in establishing ultimate current densities and thermal properties of solar cells has fostered the cultivation of mutual

cooperative programs between members of the EMR staff and the Thermal System Branch GSFC Coatings Laboratory which has the necessary fabrication capabilities.

The surface reflectance properties of thirteen varieties of solar cell coatings received from ten manufacturers were measured. Subsequent calculation of the surface effects in changing the current densities, showed extreme variations among manufacturers. It was, therefore, decided to objectively determine what parameters need be more precisely defined in order to establish what constituted a "good" anti-reflection coating for silicon solar cells and to clarify some of the proprietary mystery of the overall coatings process. Initial efforts have been conducted with the excellent cooperation of the GSFC Thermal Systems Branch Coatings Laboratory to define the necessary parameters to achieve maximum performance with a single layer SiO coating.

3.3.1 Performance Requirements and Physical Considerations

A typical cross section of a finished solar cell structure shown in Figure 17 demonstrates that there are, in reality, two optical coatings applied in the final cell structure:

1. A unique multi-layer dielectric film, whose typical reflectance, properties are shown in Figure 18 where in this instance, no SiO coating has been applied to the solar cell; the primary purpose of this multi-layer coating is to protect the adhesive which bonds the radiation cover slip to the cell proper. It is hoped that this expensive addition may be eliminated by future improvements in applying integral quartz cover slips by sputtering techniques. In addition to the protection offered to the adhesive, the unique "window cutoff offered by the multi-layer properties effectively eliminates the absorption of infrared energy which normally is dissipated in the cell base.

2. The conventional SiO coating which decreases the cell surface reflectance in its region of response, which is 3750 Å to 12000 Å for silicon solar cells.

In dealing only with the SiO coating which is applied directly to the solar cell, it has been found that in order to reduce the reflected energy from the heavily doped N-type surface layer to a minimum, an intermediate layer is required to form an interference type optical coating with such an index of refraction n_1, that:

$$n_1 = \sqrt{n_c n_r} \qquad (6)$$

where

n_c = refractive index of silicon = 3.5 to 4.0
n_r = refractive index of the bonding resin = 1 to 1.5

For practical considerations solar cells are invariably used with radiation quartz cover slips and this requires using the refractive properties of the bonding resin which covers the cell. Simple calculations indicate that the intermediate material should have a refractive index of approximately 2.0, a requirement reasonably satisfied by SiO which has the values, dependent upon deposition parameters, between 1.7 and 1.9.

In addition to the proper index of refraction the optical thickness, which is defined as the physical thickness multiplied by n, should be a 1/4 wavelength in the solar cell response region near 6000 Å where minimum reflectivity is desired. Although the maximum energy in the solar spectrum is at 4800 Å, the nature of the conversion process, i.e., electron-hole pair creation as a function of photon density distribution which peaks at 6000 Å more significant than the total energy values. Increasing the thickness to achieve minimum reflectivity at the 6000 Å wavelength region must be optimized, however, since the reflective properties begin to increase at the shorter wavelengths.

3.3.2 Establishment of Deposition Parameters

With the general physical requirement for maximum cell performance taken into consideration SiO_x in layer thicknesses of 3/16 λ to 1/2 λ were deposited on 2 x 2 cm N/P chem-etched uncoated silicon cells selected from the production variety used in the Nimbus Program. Short-circuit current measurements taken before and after the evaporation process to document the changes in solar cell performance as a result of the applied coatings are compiled in Table 4. Applications of the SiO_x coating were performed in a 72" evaporator at rates of approximately 200 Å/min with the samples being positioned 30" from the SiO source; vacuum conditions were maintained at 10^{-4} Torr with small amounts of oxygen bled into the system.

3.3.3 Experimental Results

Typical results of the achieved reflectance values shown in Figure 19 indicate very obvious trends in the requirements for establishing an optimum single layer SiO coating. It is readily apparent that an optimum layer slightly greater than 1/4λ, (1100 Å, results in a respectable reflectance value of approximately 6% from 4750 Å to 6000 Å;) the 3/16 λ layer indicates a decrease at all wavelengths measured but still has a high reflectance value of approximately 25%.

As the thickness of the SiO layer increases to a $1/2\lambda$ the minimum reflectivity is shifted to longer wavelengths which results in a considerable loss in the solar cell quantum yield from 4000 Å to 6000 Å.

It is apparent that an overall optimization process must be considered, which includes the photon density function, quantum yield characteristics of the solar cell, and the surface reflectance in order to achieve maximum solar cell current density.

The difficulties in achieving low reflectance values at the shorter wavelengths are presently being overcome by the addition of magnesium flouride coatings; this addition plus the optimized SiO layer tends to give the cells superior current outputs and also radiation resistance characteristics.

3.4 BASIC SOLAR CELL MEASUREMENTS APPLIED TO THERMAL ANALYSIS

The fact that solar cells perform as energy converters and a portion of the absorbed photon energy is directly removed from the cell proper in the form of electrical energy to be utilized by the spacecraft leads to the logical conclusion that knowledge of the power conversion process can certainly be extended to aid in determining the net energy absorbed.

With the additional knowledge of the thermal radiative properties principally defined by the total hemispherical emittance characteristics of the cell structure a more precise analytical determination can be made in the calculation of operational temperatures of solar cell arrays.

Measurements of the required physical parameters are presently being made in the EMR Thermal Systems Group but here-to-fore have not been applied to this precise analysis.

It would be difficult to over emphasize the importance in the precise measurement of these basic solar cell properties and their immediate application in achieving maximum power performance by optimizing, wherever possible, relationships between the variables which determine the power-temperature function.

3.4.1 Solar Cell Absorptance Characteristics

A pertinent function which should be considered when measuring the optical absorptance, $\alpha(\lambda)$, of solar cells where

$$\alpha(\lambda) = 1-R(\lambda) \tag{7}$$

and $R(\lambda)$ = surface reflectance

is the process of energy conversion within the cells; the fact that a part of the absorbed energy is removed from the cell needs to be considered when total absorptance properties are to be defined.

Because of the nature of the energy transformation - a photon absorption process which creates free electron - hole pairs - only a discrete portion of the absorbed energy is capable of being transferred to the created free carriers. Intrinsic properties of the band structure of silicon material results in a 1.11eV indirect transition; this means that the excess energy of photons possessing energies above this level is normally dissipated within the silicon lattice structure. It is this excess energy plus a portion of the transformed electrical energy which is not delivered to the load which help determine the thermal characteristics of the cells.

By considering the photon density in the solar spectrum as a function of eV energy where:

$$eV = \frac{hc}{\lambda} \tag{8}$$

h = Planck's Constant
c = Velocity of Light
λ = Wavelength

and weighting this function which is given in Figure 20 by the energy which is absorbed within the material and importantly, the fraction of converted energy which is transferred to an external load, a more precise value of energy absorptance can be obtained. Presented in a very general form the total energy absorbed, Q_t, is

$$Q_t = \int_{\lambda=0}^{\lambda=2.5} \left[1-R(\lambda)\right] \frac{hc}{\lambda} N_{o(\lambda)} d\lambda \tag{9}$$

where

$N_o(\lambda)$ = photon density incident on surface

For silicon solar cells the net amount of energy absorbed within the cell can be more clearly expressed by dividing the photon density of the solar spectrum into three wavelength regions.

1. The extremely shallow absorption coefficient of α below 3750 Å results in no current collectipn; letting the function $K(\lambda) = 1-R(\lambda)\ hc/\lambda$, the UV energy absorbed is

$$Q_1 = \int_{\lambda = 0}^{\lambda = 0.3750\mu} K(\lambda)\, d \tag{10}$$

2. From 0.3750 to 1.12 microns the thermal energy created is determined by the current collection efficiency and excess energy function above 1.11 eV.

   The current collection efficiency is the parameter indicative of the ability to collect the free carriers generated by the photon absorption and is experimentally determined by the quantum yield measurement. The photon energy above the band gap value of 1.11 which is absorbed and converted to heat in this region of cell response is given by:

$$Q_2 = \int_{\lambda = 0.375\,\mu}^{\lambda = 1.12\,\mu} QY(\lambda)\ \left[1-R(\lambda)\right]\ N_o(\lambda)\ \left[\frac{hc}{\lambda} - 1.15\ \ d\lambda\right] \tag{11}$$

   there is also a finite amount of energy Q_3, retained in this region of cell response as indicated by QY values, less than unity which can be expressed by:

$$Q_3 = \int_{\lambda = 0.375\,\mu}^{\lambda = 1.12\mu} K(\lambda)\ \left[1-QY(\lambda)\right]\ d\lambda \tag{12}$$

3. Finally the photon energy Q_4, beyond the band gap of 1.11 eV can be considered completely absorbed and dissipated by thermal means where:

$$Q_4 = \int_{\lambda = 1.12\,\mu}^{\lambda = 2.5\,\mu} K(\lambda)\, d\lambda \tag{13}$$

The summation of the simply energy integrals of Equation 10 to Equation 13 is a straight forward process and since an existing program contains the necessary weighting functions, calculations of effective $\bar{a}$ values can be readily accomplished. Typical measurements of the quantum yield and surface reflectance for a Texas Instrument N/P solar cell is illustrated in Figure 21.

In a recent survey absorptance values for a variety of cells received from 10 manufacturers indicated a wide range of absorptance $\bar{a}$ values from 0.72 to 0.87.

Because of EMR's early awareness of the advantages gained in measuring absolute quantum yield characteristics of solar cells this information can now be readily applied in the complete analysis of the thermal characteristics of individual cells and solar cell arrays.

3.5 DIFFUSION LENGTH MEASUREMENTS

The fundamental parameter of the bulk silicon material which determines the current collection efficiency of a P/N junction-type solar cell is the minority carrier diffusion length, L, which, in a general sense, can be construed at the dimunition of the minority carrier density by a factor of e^{-1} in each interval of L. For the simplified case in which minority carriers are uniformily generated in the base material at a rate g_0, carriers per cm^3 per second, the collected current density, I_{sc}, assuming that each created excess minority carrier is collected, it is given by:

$$I_{sc} = qg_0L \tag{14}$$

where

q = the electronic charge
g = generation rate

The diffusion length is related to the steady state minority carrier lifetime by:

$$(D\tau)^{\frac{1}{2}} \tag{15}$$

where

$D\tau$ = diffusion coefficient
τ = minority carrier lifetime

The diffusion length, as stated in section 3.2 can be derived from the quantum yield measurement but the difficulty in measuring the surface reflectance, the accuracy of available optical absorption data, and the fact that the absorption function is rapidly changing in the near infra-red region creates a complicated condition conductive to large experimental errors.

3.5.1 Experimental Procedure

Techniques using penetrating electron radiation have been adopted by EMR which effectively eliminates the reliance on optical absorption data and the required reflectance measurements. The original details of the experimental procedure developed by Rosenzweig of BTL involves the concurrent measurement of the electron intensity and solar cell ionization current in a double aperture vacuum Faraday cup. With the proper selection of an absorber thickness covering the cell it is possible to achieve a uniform generation function and with prior knowledge of a spatial ionization function, i.e., the number of electron-hole pairs created per micron per electron particle at a discrete energy level, the effective averaged diffusion length can readily be calculated. It has been argued and always with a considerable degree of justification that L is a unique function of spatial position created by the minority carrier recombination characteristics of the bulk material.

However, the typically high quality of the bulk material used in making silicon solar cells which reduces the recombination effects results in minority carrier lifetimes in the range of 10-25 microseconds; a vast amount of experimental data which supports the bulk diffusion length concept have given sufficient credulence in utilizing the average bulk diffusion length as a comparative parameter for both collection efficiency evaluation and radiation damage studies.

3.5.2 EMR Experimental Results and Applications

Typical experimental data shown in Figure 22 indicates that linearity of cell response can be established over three decades of injection levels while establishing the diffusion length at the same time. Use of the dynamic range capabilities of a Van deGraaff accelerator can resolve any doubts about linearity considerations when extrapolating for example, cell properties measured under low level monochromatic energies to AMO conditions. Figure 23 presents another application of the diffusion length measurement where it is used to derive the K parameter from the relationship

$$\frac{1}{L^2} = \frac{1}{L_o{}^2} + K\phi \qquad (16)$$

where

L_o = initial diffusion length
L = final diffusion length
ϕ = particle flux

Here the rate of degradation under 0.5 MeV electrons is shown for silicon solar cells fabricated from wafers cut in the <111>, <110>, and <100> planes. The linear rate of degradation gives added credulence to the evaluative K parameter in this situation.

All experimental hardware has been fabricated, experimental procedure established and the measurements are ready to be performed by EMR upon proper scheduling of accelerator facilities.

3.6 SOLAR CELL P/N JUNCTION CHARACTERISTICS

One of the less defined areas in the field of basic solar cell measurements and in which EMR is now actively involved is the definition of the electrical properties of the P/N junction. This investigation has been relegated to one of no apparent significance for reasons engendered, partly because the information at first appearance is not directly applicable to the solar cell performance. And yet, it must be stated that this measurement can yield more detailed information than any made concerning the characteristic cell structure and further, it is quite possible to derive valid performance characteristics without the use of any solar simulation source providing knowledge of the surface reflection properties is known.

3.6.1 Theoretical and Experimental Considerations

EMR's conventional analysis of the P/N junction properties of solar cells involves use of the Schottky relationship for an abrupt impurity transition region and because of the inter-relationship of the physical parameters a capacitance function evolves where C is given by:

$$C^{-2} = \frac{8\pi V}{\epsilon q N_x} \qquad (17)$$

and

C = junction capacitance $-cm^{-2}$
N_x = impurity concentration of base region
ϵ = dielectric constant
q = electronic charge
V = total voltage across the junction

The voltage total is the sum of the internal electrostatic potential and any externally applied dc bias voltage. Effects of a reverse bias voltage changes the equilibrium conditions in the junction region and for an increasing reverse bias condition, the space charge region (depletion width) broadens into regions of higher resistivity which is the base region for solar cells. The change in the volume of the space charge region is determined by the dielectric constant of the material, impurity concentrations and profiles on either side of the junction region and magnitude of the total potential across the junction. The relationship of the space charge region, W, to the capacitance is readily derived and becomes:

$$W = \frac{\epsilon\epsilon_o A}{C} \tag{18}$$

where

A = total junction area
$\epsilon = 11.8$
$\epsilon_o = 8.85 \times 10^{-14}$ farad/cm^2

For convenience in quickly establishing the magnitude of W in certain types of silicon solar cells this function is plotted in Figure 24.

From Equation 17 it is apparent that the slope of the curve is determined primarily by the impurity concentration in the bulk region, the magnitude of which can readily be calculated. Large area solar cells with shallow junction formations of one micron or less ordinarily have impurity profiles of the complementary error function form shown in Figure 25, the exact nature of the impurity profile being governed by the diffusion coefficient, the time of diffusion, initial concentrations and the boundary conditions. Since the diffusion coefficient generally has an exponential temperature dependence, precise control of the impurity profile requires accurate control of the diffusion temperature. It is found that the experimental data for the silicon solar cells up to junction breakdown voltage is in reasonably good agreement with the Schottky abrupt-transition model. Typical experimental data and the comparison of the calculated impurity concentrations with figures given by the manufacturer are shown in Figure 26 for silicon solar cells.

It has been found that measurements of the junction properties of GaAs single crystal solar cells using similar experimental methods does not follow the abrupt transition scheme but more appropriately is applicable to a graded junction model. Experimental data of the V vs C^{-3} relationship derived from the graded junction theory is plotted in Figure 27 and indicates agreement with

this concept. Also of obvious interest is the value of the extrapolated diffusion voltage of 1.38 volts which is exactly the band gap of GaAs.

3.6.2 Experimental Details

Present EMR methods of analysis involve measuring the complex impedance of the solar cells by standard bridge techniques in the experimental setup shown in Figure 28 and outlined diagrammatically in Figure 29. The samples are in dark conditions on a temperature-control holder assembly with applied external bias conditions. The capacitance relationship as a function of applied voltage is then calculated from knowledge of the complex impedance at 1536 cps and is then related to the physical characteristics of the junction by the Schottky theory for both abrupt and graded junctions.

Physical constants of the solar cell P/N junction including the depletion width, impurity concentration in the base, and the extrapolated diffusion potential, can then be used in defining the parameters which lead to better cell performance. It is the lack of such precise data which has hindered the efforts in improving present performance of solar cells and it is unlikely that any major gain from present day silicon solar cell conversion efficiency values of 10 to 11% can be envisioned without an increased understanding of the fabrication parameters which influence the junction properties

Measurements of the junction properties of solar cells are currently being performed at EMR to correlate the junction properties of cells which demonstrate higher efficiency values.

4.0 NEW TECHNOLOGY

This section is not applicable in the main efforts of the existing program.

5.0 PROGRAM FOR NEXT REPORT PERIOD

In accordance with the conclusion of the present form of effort and the conductance of this effort on initiated job orders as outlined by the Technical Monitor the following efforts will be completed as specifically outlined in Job Order 713-861-51-75-01.

I Prepare type III Report in accordance with Specification NASA TIB-5-100 on the McPherson spectral measurement system. Include data on absolute accuracy of instrument; comparisons between flight calibrated

cells and other instrumentation measurements with McPherson measurements; and, advantages of system over other measurement systems and techniques.

II Design System to obtain "in situ" spectral reflectances of 15/16 inch samples using the ULTEK vacuum system and the Perkin-Elmer spectrophotometer. Consider particle and ultraviolet irradiation of samples.

III Obtain V-14 curves for 25 solar cells.

IV Obtain quantum yields for 25 solar cells.

6.0 CONCLUSIONS AND RECOMMENDATIONS

The total progress in consideration of the nominal amount of engineering hours allocated has been very encouraging. Detailed considerations have been given to the fundamental properties of the solar cell structure. Most measurements can be conducted on a routine basis. In addition to the calibration radiation damage evaluation capabilities have been firmly established and experiments are now conducted on a routine basis.

Table 1

1 MeV Electron Radiation Schedule
(Solar cell bulk resistivity and thickness)

Date	Run	Radiation Time	Flux Density e/cm^2-sec.	Flux Increment e/cm^2	$\Sigma\Phi$ Integrated Flux e/cm^2
11/1/66	1	:7:20	2.3×10^{10}	1×10^{13}	1×10^{13}
11/2/66	2	0:36:40	6.17×10^{11}	9×10^{13}	1×10^{14}
11/2/66	3	1:43:49	1.8×10^{12}	9×10^{14}	1×10^{15}
11/3/66	4	5:51:54	1.8×10^{12}	3×10^{15}	4×10^{15}
11/4/66	5	12:57:45	2.1×10^{12}	6×10^{15}	1×10^{16}

Cup-Cell factor 850

Table 2

1 MeV Electron Radiation Experiment

	0			1			2			3			4			5		
	0			10^{13} e/m^2			10^{14} e/m^2			1×10^{15} e/m^2			4×10^{15} e/m^2			1×10^{16} e/m^2		
Cell #	I_{sc}(ma)	Voc(mv)	n(%)	I_{sc}	Voc	n	I_{sc}	Voc	n	I_{sc}	Voc	n	I_{sc}	Voc	n	I_{sc}	Voc	n
8-1-1	131	563	10															
8-1-2	132	567	10.1															
8-1-3	131	564	10	129.4	563	9.8												
8-1-4	131	567	10	129.3	566	9.8												
8-1-5	134.3	567	10	132.5	567	9.8	131	560	9.6									
8-1-6	130	567	10	128.3	566	9.8	126	560	9.6									
8-1-7	131	575	10.1	129.3	573	10.0	126.5	567	9.7	111.0	535	8.0						
8-1-8	131	572	10.3	129.5	566	10.0	128	563	9.8	113.0	530	8.2						
8-1-9	130.5	570	10.2	129	567	10.0	126	560	9.6	112	529	8.0	100	508	6.8	90	487	5.9
8-1-10	131	567	10	130	567	10	127	558	9.6	113	530	8.1	97	508	6.8	90	487	5.8
																		5.6
16-1-1	140	577	10.8															
16-1-2	140	580	10.8															
16-1-3	140	580	10.75	138	575	10.5												
16-1-4	138	576	10.75	135.4	573	10.3												
16-1-5	140	575	10.6	138	573	10.3	130	560	9.4									
16-1-6	138	577	10.6	136.3	574	10.4	128.5	558	9.6									
16-1-7	139	575	10.8	137	574	10.6	130	560	9.75	114	525	8.0						
16-1-8	137	578	10.7	135.5	574	10.5	128	560	9.5	112	527	7.8						
16-1-9	139	575	10.74	136	570	10.4	130	557	9.6	114	525	7.8	101	505	6.7	91.7	485	5.75
16-1-10	140	575	10.75	138.5	570	10.5	130	578	9.5	114	525	7.8	101	505	6.7	91.6	487	5.8

Table 2 (Continued)

	0			1			2			3			4			5		
	0			10^{13} e/m^2			10^{14} e/m^2			10^{15} e/m^2			4×10^{15} e/m^2			10^{16} e/m^2		
Cell #	I_{sc}(ma)	Voc(mv)	n(%)	I_{sc}	Voc	n	I_{sc}	Voc	n	I_{sc}	Voc	n	I_{sc}	Voc	n	I_{sc}	Voc	n
8-10-1	64.3	525	8.6															
8-10-2	64.7	525	8.75															
8-10-3	65.5	520	8.75	65.2	520	8.75												
8-10-4	64.5	525	8.75	64	525	8.75												
8-10-5	67.5	535	9.3	67	533	9.25	65	525	8.9									
8-10-6	66.5	528	9.1	66.2	528	9.0	64	522	8.75									
8-10-7	67	530	9.25	66.2	528	9.0	64	525	8.8	57.5	494	7.3						
8-10-8	66.5	528	9.0	66.0	527	8.9	65	526	8.8	59	495	7.4						
8-10-9	67	533	9.0	66.8	530	9.0	65	530	8.8	58.5	496	7.4	52.5	480	6.35	48.7	460	5.60
8-10-10	67.7	532	9.25	67.5	528	9.2	66.3	525	8.9	59	493	7.4	53.5	475	6.4	50	458	5.75
15-10-1	72.3	543	10.25															
15-10-2	72.3	547	10.3															
15-10-3	72.6	550	10.3	72.5	546	10.25												
15-10-4	72.7	543	10.1	72.1	542	10.0												
15-10-5	71.5	547	10.2	70.5	546	10.0	66.7	527	9.1									
15-10-6	71.8	547	10.2	71.0	544	10.0	67.5	528	9.2									
15-10-7	71.8	550	10.4	71.2	547	10.25	67.5	532	9.3	58.5	495	7.5						
15-10-8	71.8	555	10.4	71.5	550	10.3	67.0	532	9.3	58.6	495	7.5						
15-10-9	71.6	547	10.3	71.4	543	10.1	68.5	530	9.3	60	495	7.6	54.3	476	6.6	50.8	460	5.93
15-10-10	72.6	555	10.6	72.3	550	10.3	68.5	535	9.0	60	496	7.6	54.0	475	6.5	50.4	461	5.87

Table 3
Solar Cell Short-Circuit Current Correlations

	A-2	A-13	C-1	C-2	C-3	D-1	D-2	D-3	E-1	E-2	E-3	F-1	F-3
Lewis Air Flight[1]	126[1]	121.4	119.3	124.0	127.3	115.4	115.5	111.9	97.6	99.8	99.8	77.3	75.3
NRL[2]	126	120.2	117.3	123.2	129.6	114.8	115.8	111.6	98.0	100.8	100.2	77.9	75.7
APL[3]	126	- - -	117.0	123.0	130.0	114.7	115.9	112.8	99.0	101.0	101.0	- - -	76.5
EMR[4]	125.9	119.7	118.0	122.1	129.2	114.2	115.8	111.7	99.5	101.8	101.8	79.5	76.6
EMR % Dev.[5]	0	1.4	1.09	1.5	1.5	1.04	.26	.12	1.9	2.0	2.0	2.85	2.6

1. Aircraft calibrated at 47,000 feet by NASA-Lewis
2. Aircraft calibrated spectral intergrating method at Naval Research Lab (NRL)
3. Measured with OCLI Simulator at APL
4. Measured with Spectrolab X-25 Solar Simulator
5. % Deviation from flight values

Table 4

Effects of SiO Thickness in Altering Solar Cell Parameters

CELL NO.	I_{sc} - ma UNCOATED	I_{sc} - ma 3/16 λ_o	I_{sc} - ma 1/4 λ_o	I_{sc} - ma 1/2 λ_o
N-44	101			
N-47	103			
N-58	101			
N-60	104.4			
N-4	101			
N-37	103.5	107		
N-40	100	104		
N-41	100	105		
N-42	99	103		
N-43	101	105		
N-17	102		11.5	
N-39	104		118.5	
N-49	102		117	
N-53	102		115	
N-61	106		121	
N-20	100			119
N-23	103			118
N-24	101.6			120
N-27	102.4			122
N-28	98.3			117

SILICON SOLAR CELLS I_{sc} vs SiO COATING THICKNESS λ_o = 4000 Å

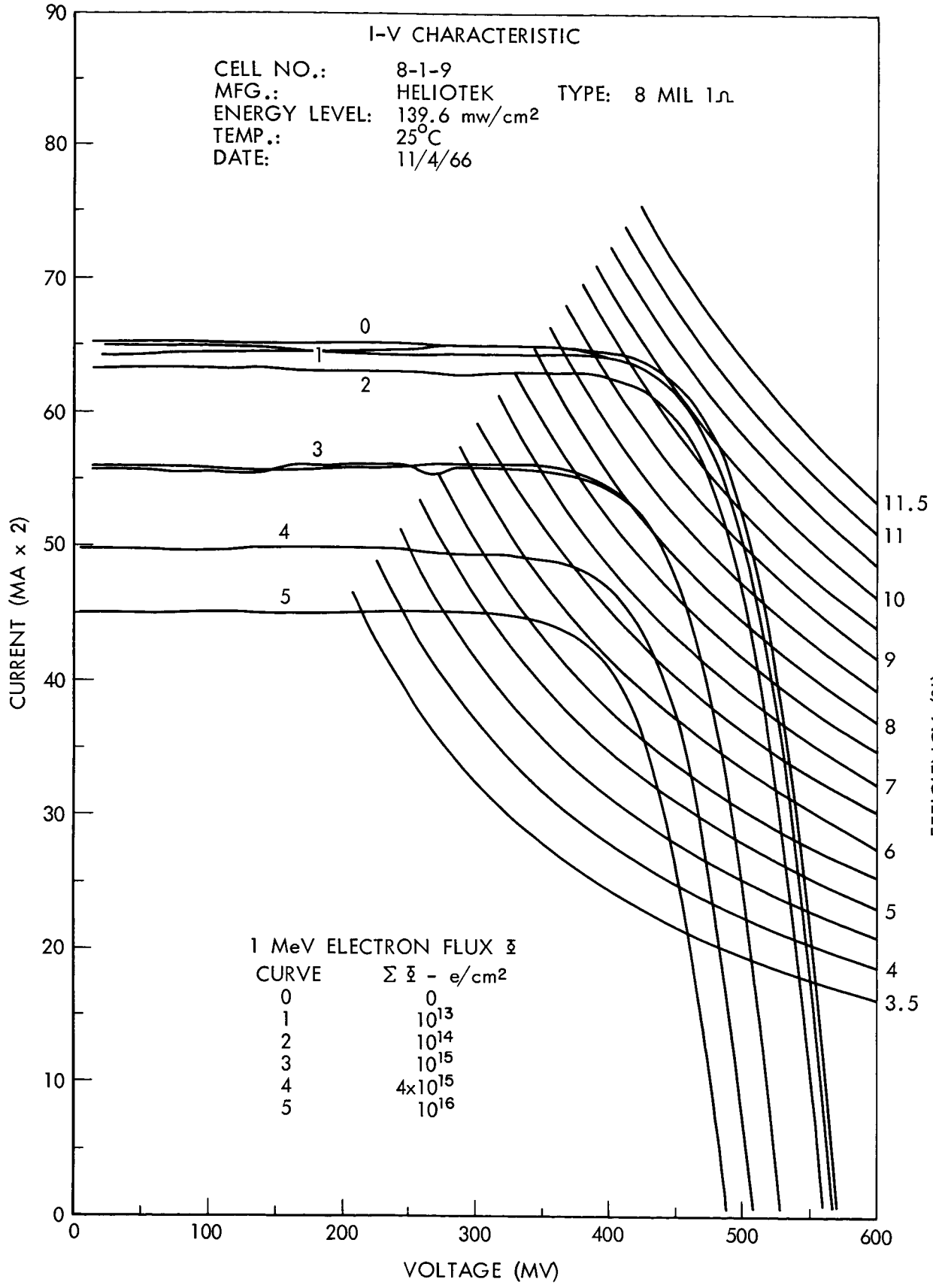

Figure 1. 8 mil, 1 ohm-cm I-V Characteristic

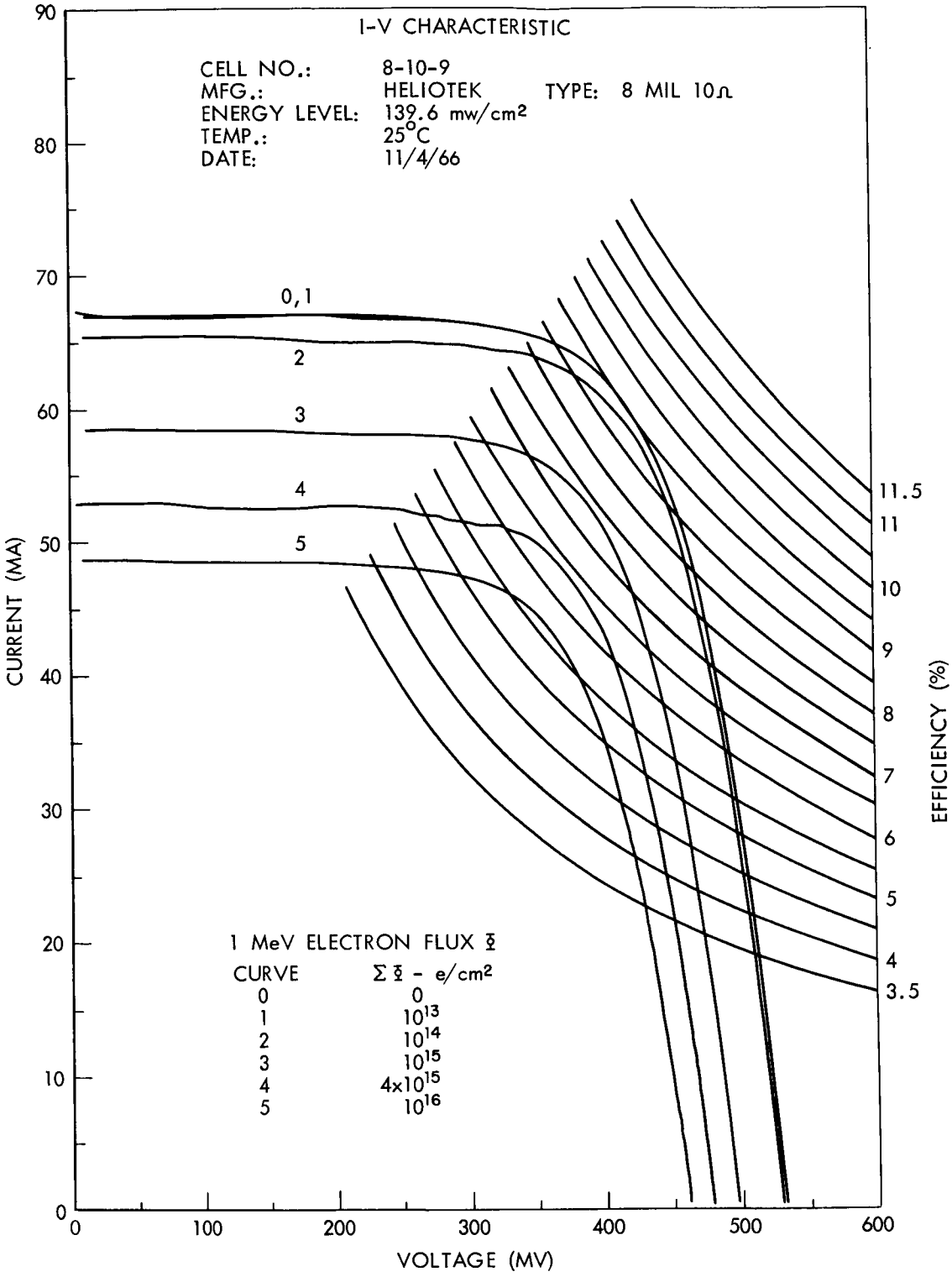

Figure 2. 8 mil, 10 ohm-cm I-V Characteristic

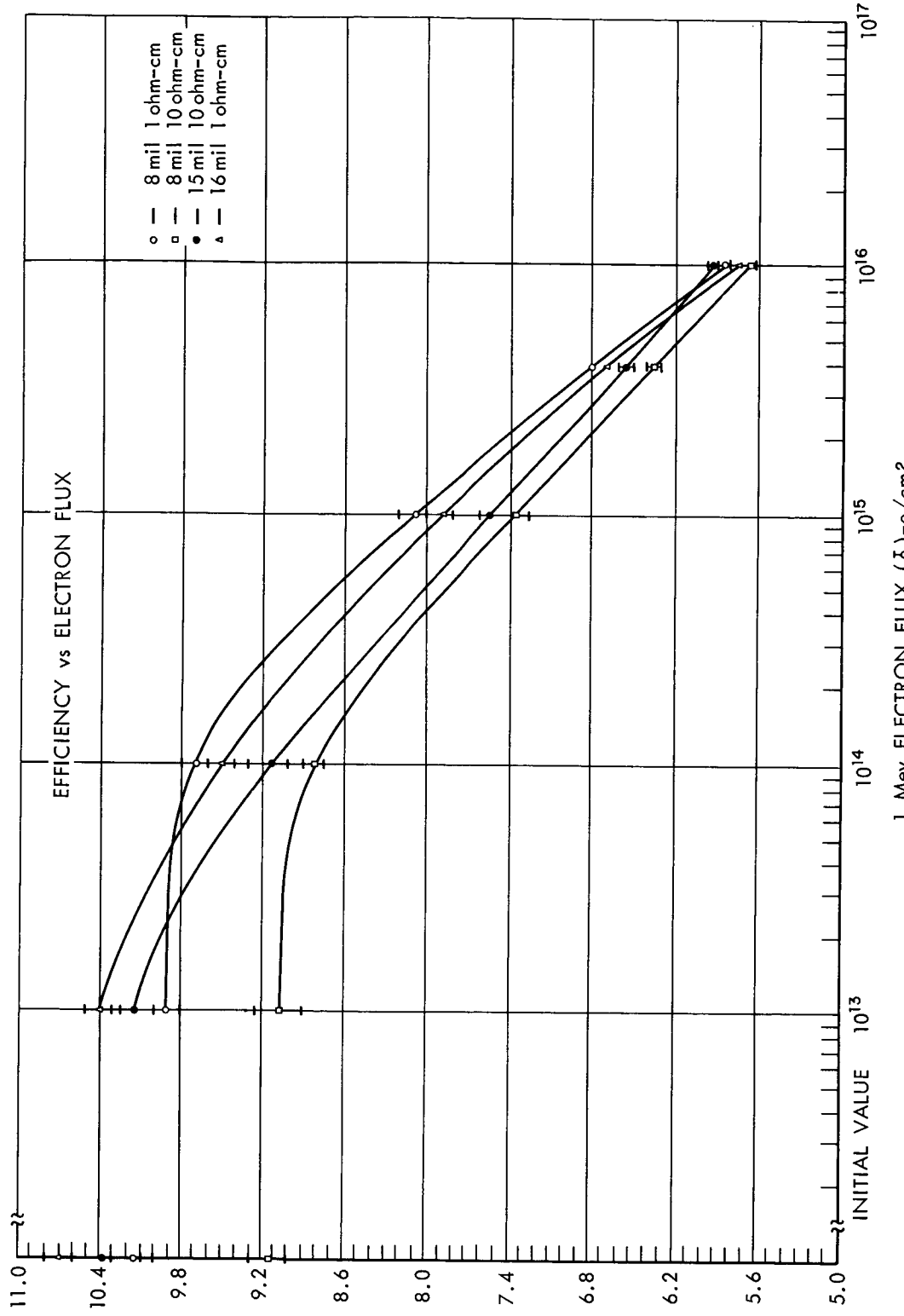

Figure 3. Efficiency vs 1 MeV Electron Flux

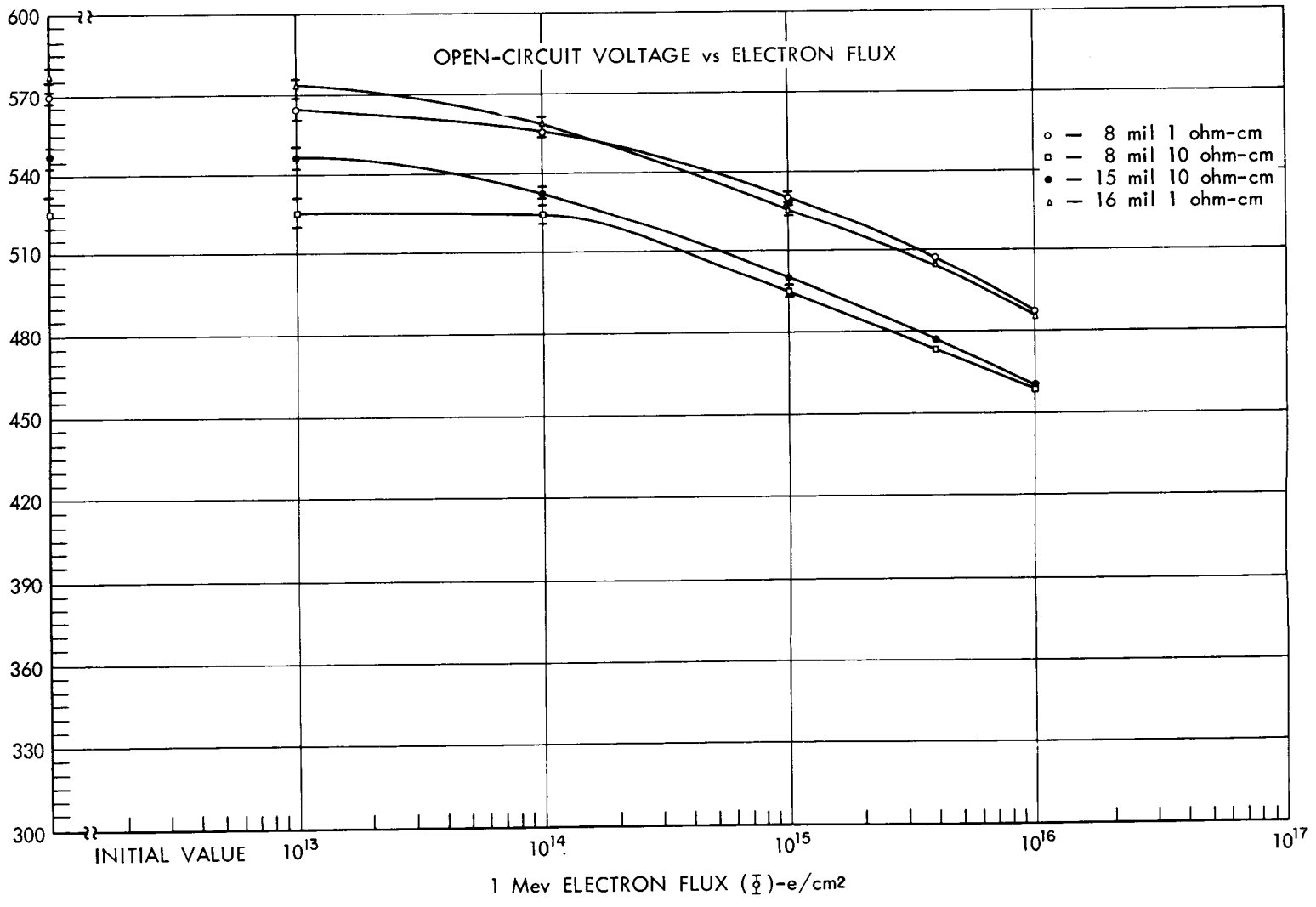

Figure 4. Open Circuit Voltage, Voc vs 1 MeV Flux

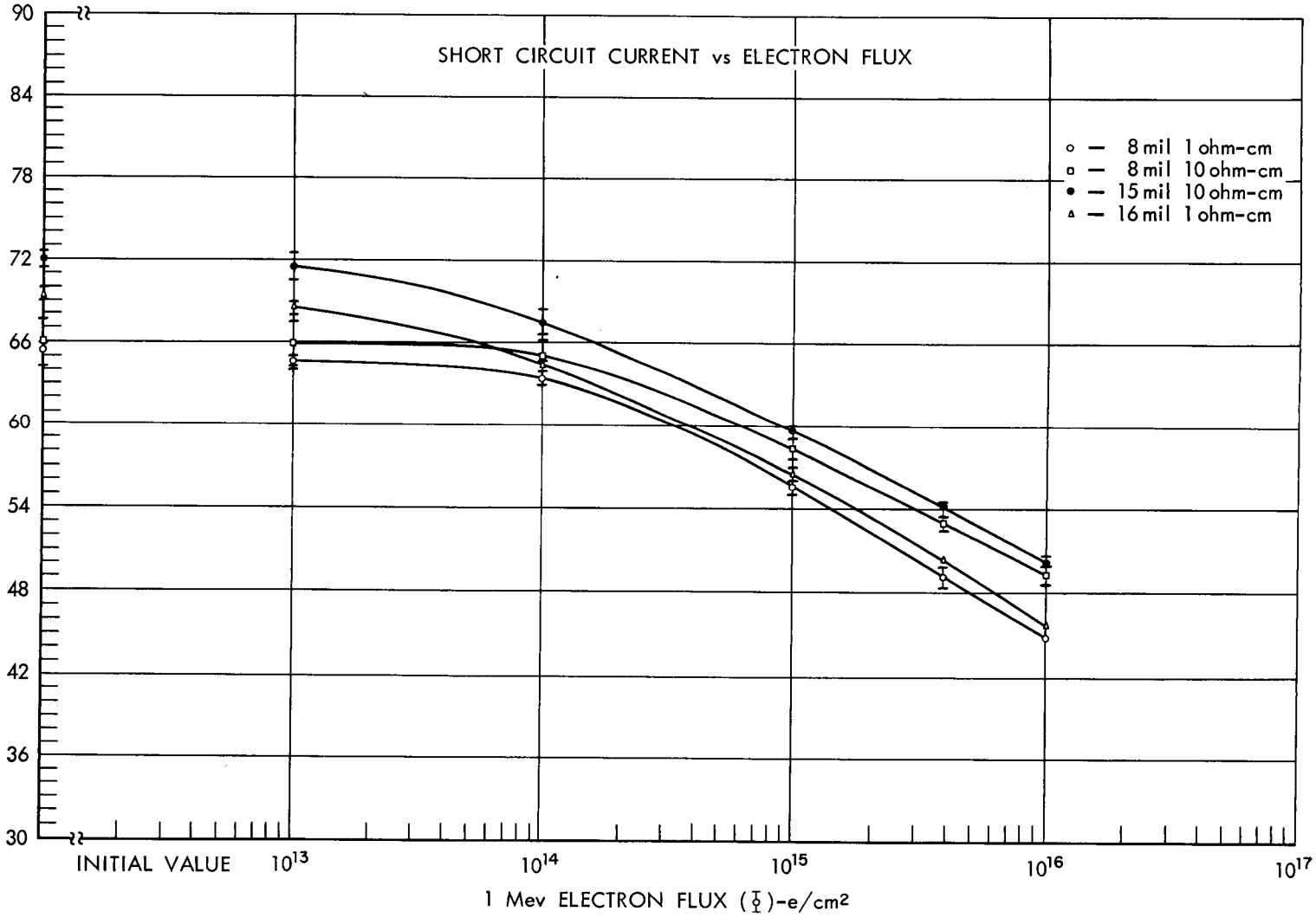

Figure 5. Short Circuit Current vs 1 Mev Flux

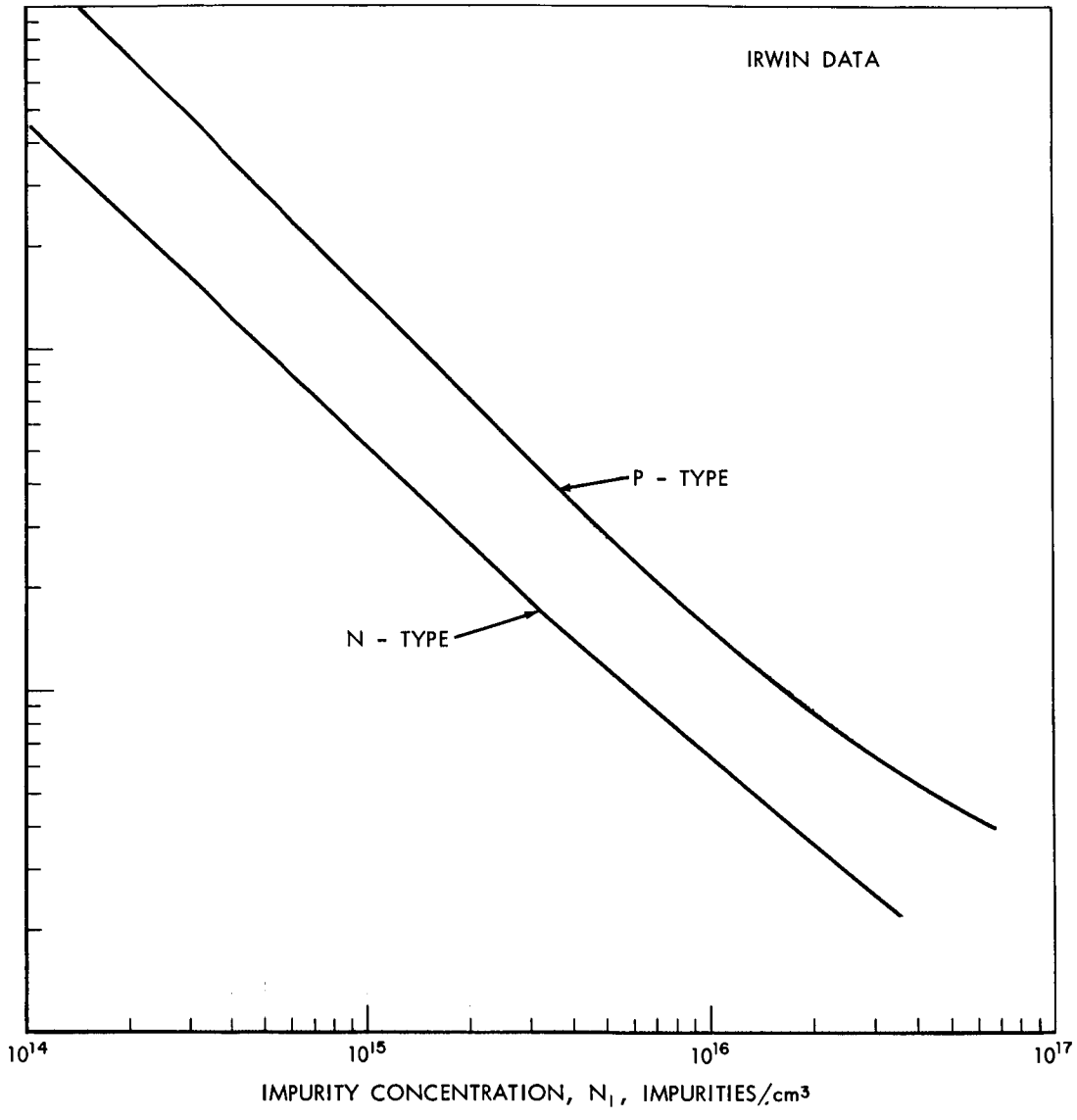

Figure 6. Electrical Resistivity vs Impurity Concentration Data by Irwin

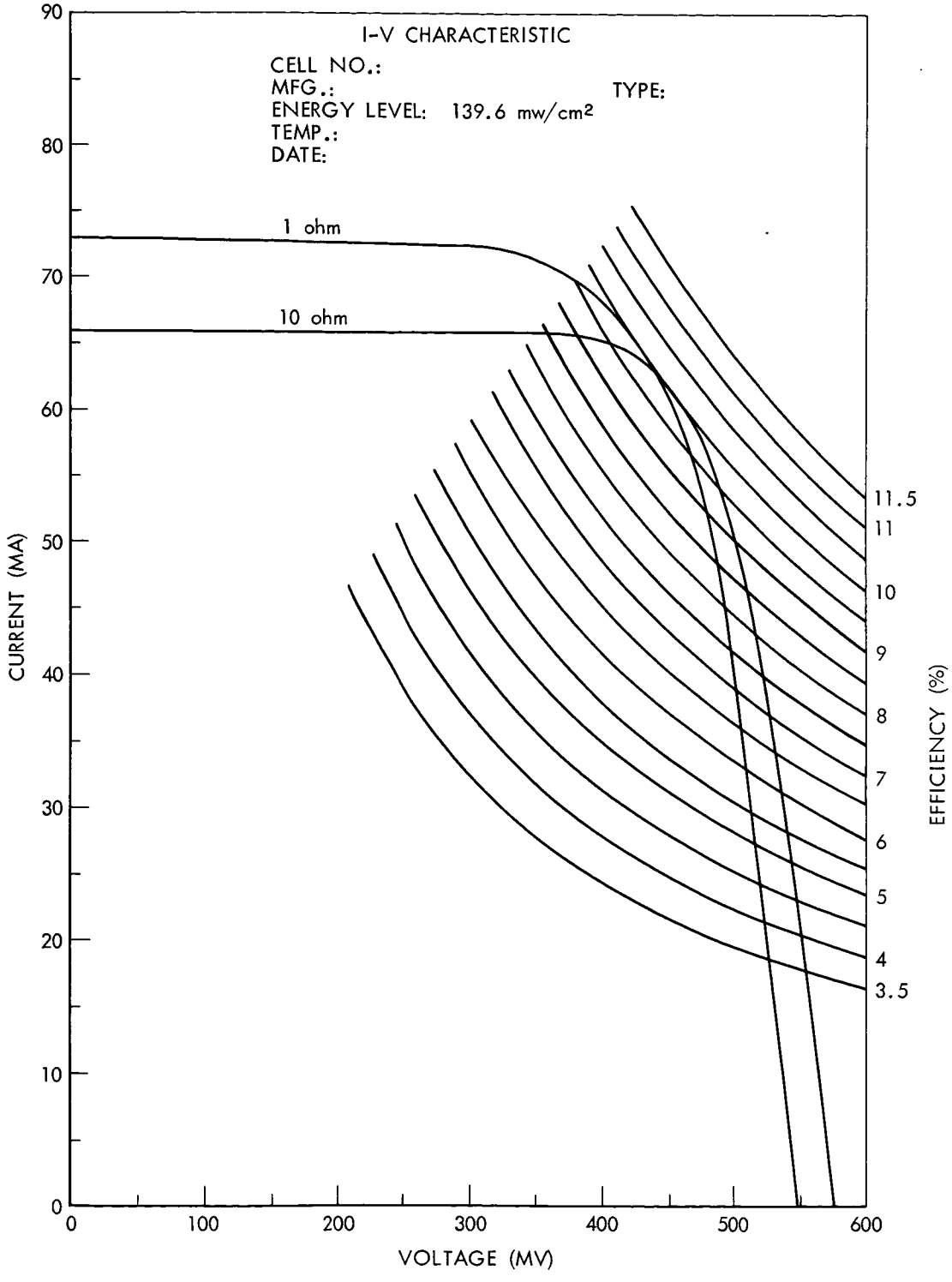

Figure 7. I-V Characteristics, 1 ohm-cm and 10 ohm-cm Solar Cells

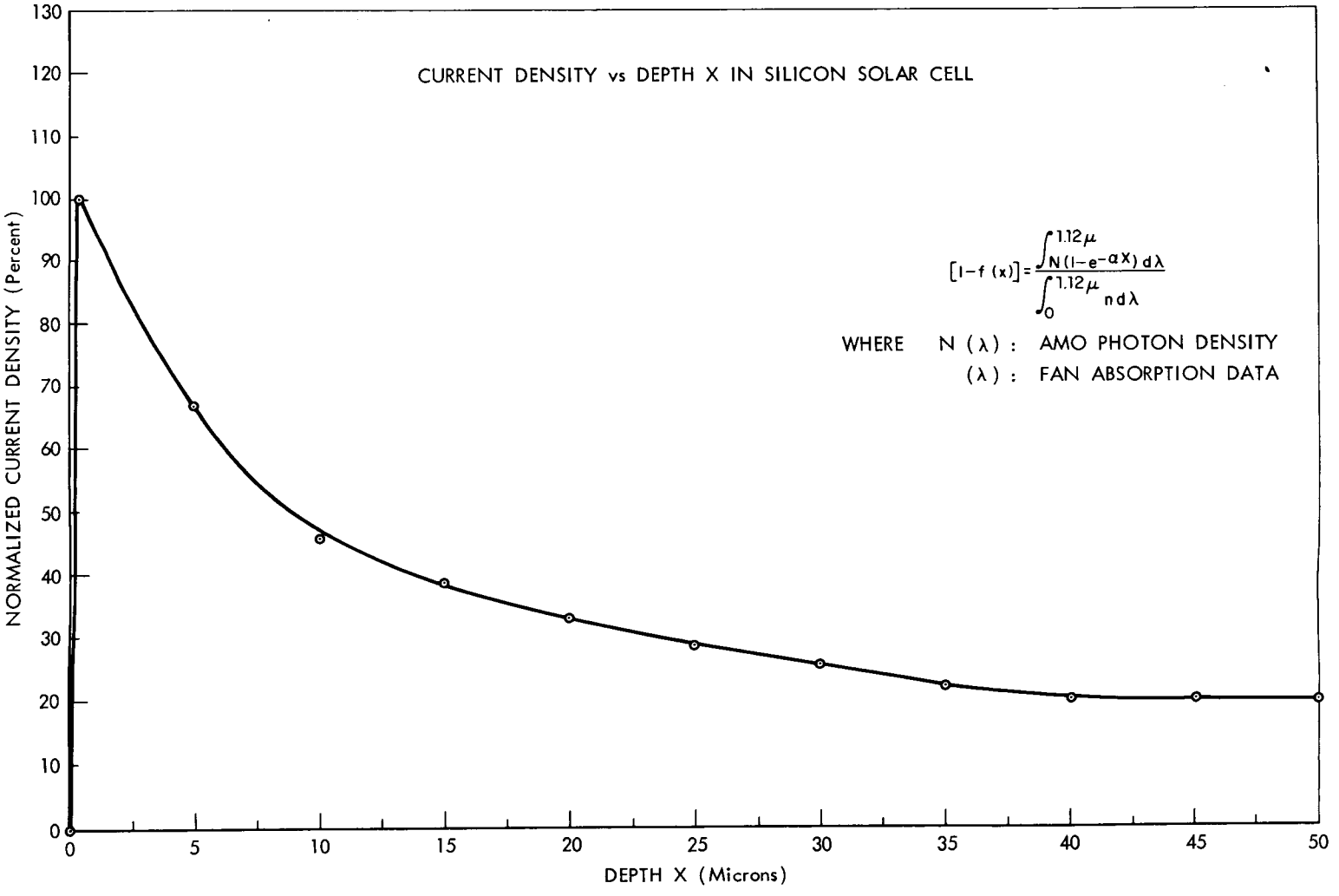

Figure 8. Spatial Current Density Function

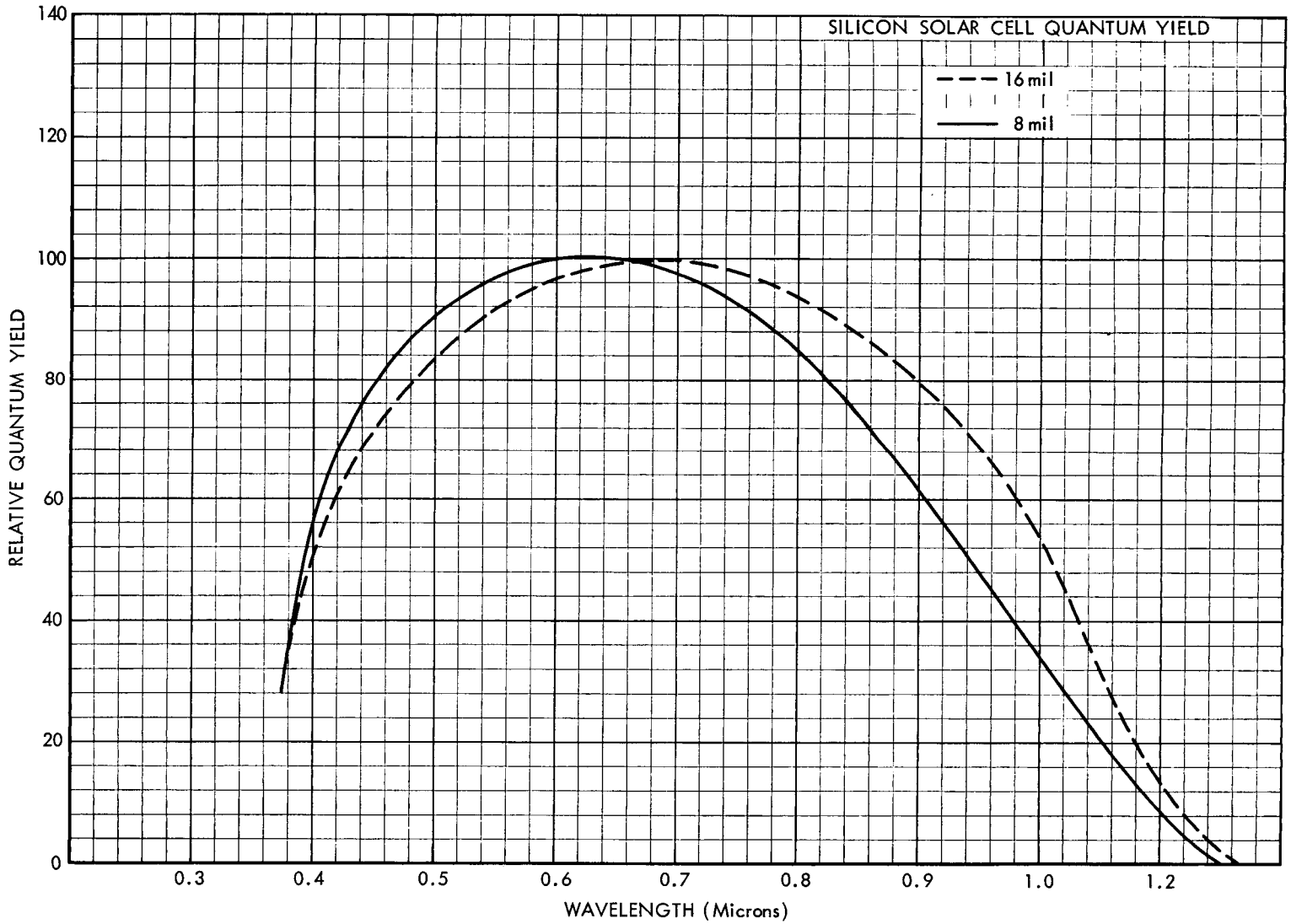

Figure 9. Quantum Yields. One ohm-cm 8 mil and 16 mil Thicknesses

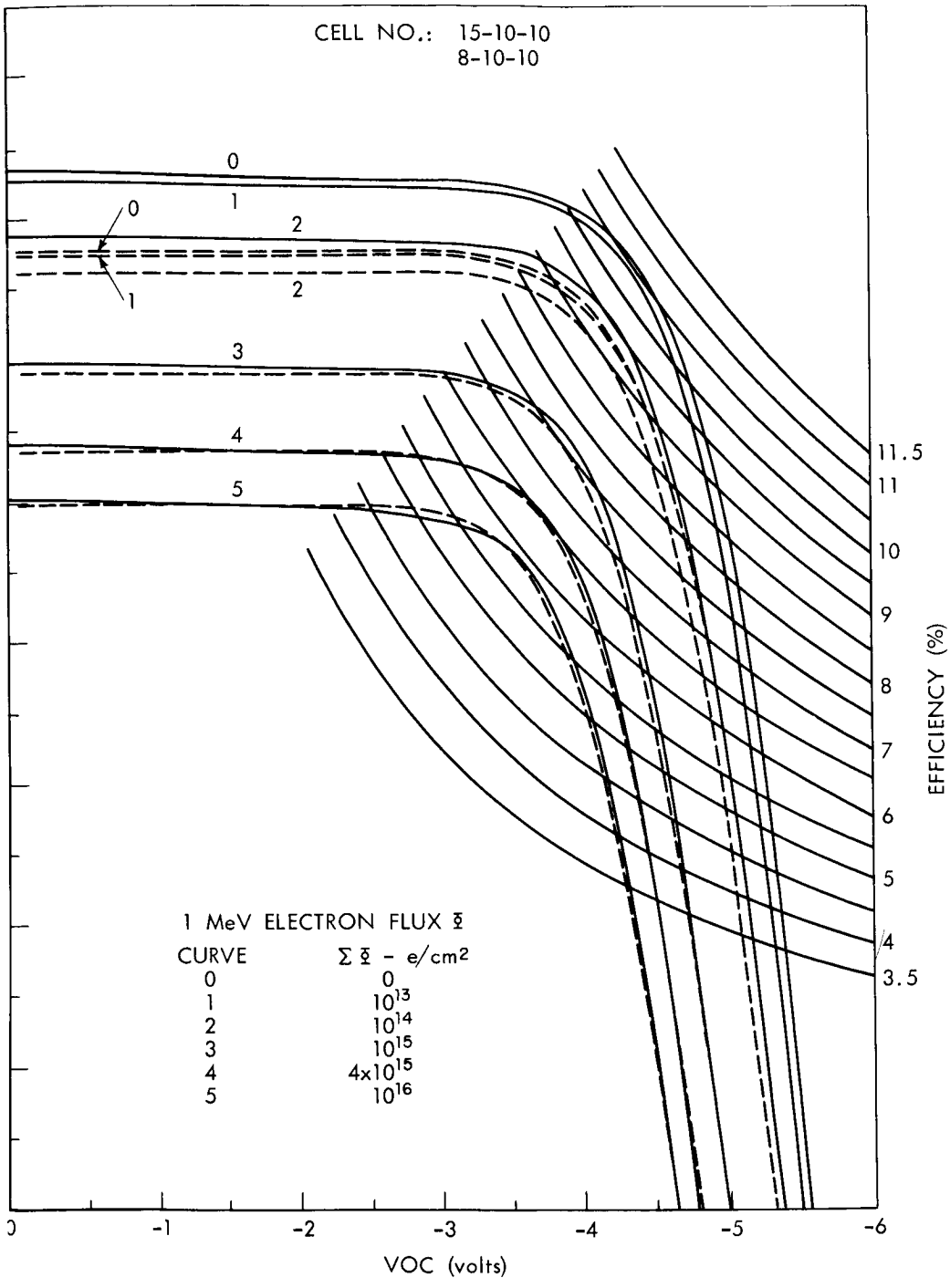

Figure 10. I-V Characteristics of 8 mil, 15 mil 10 ohm-cm Solar Cells vs 1 MeV electrons

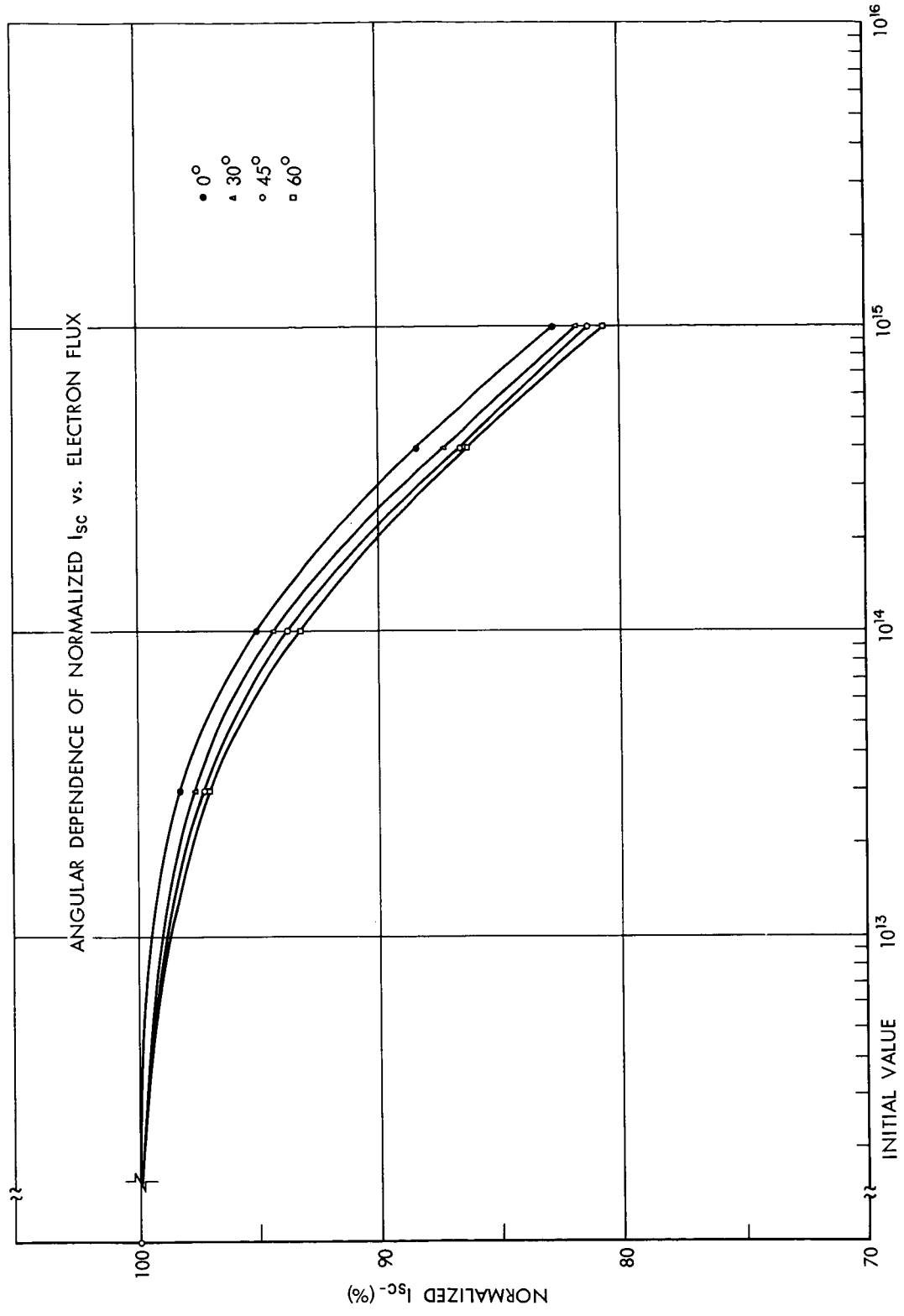

Figure 11. Angular Dependence of I_{SC} vs 1 MeV Electrons

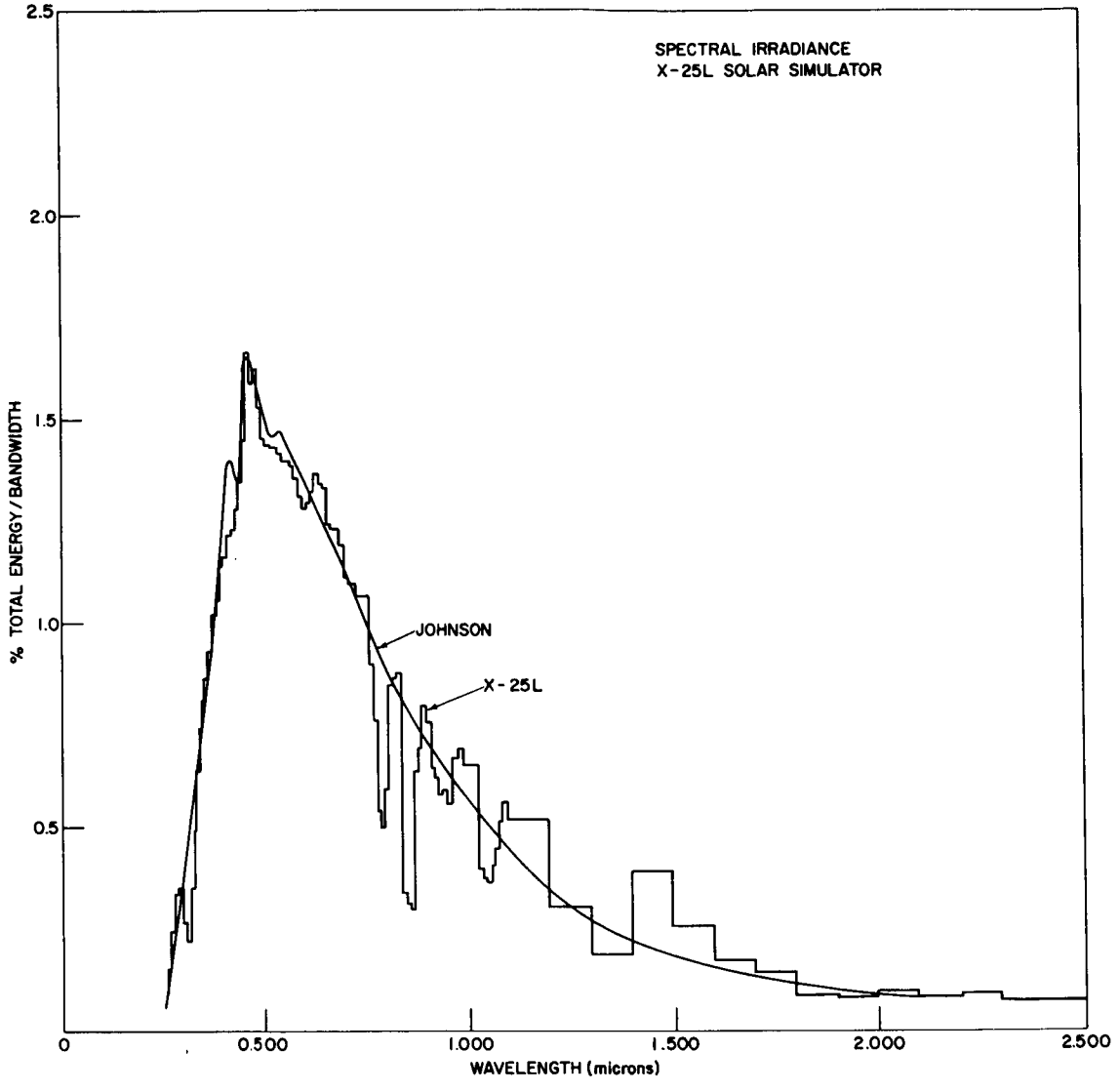

Figure 12. Spectral Energy Distribution of Solar Simulation

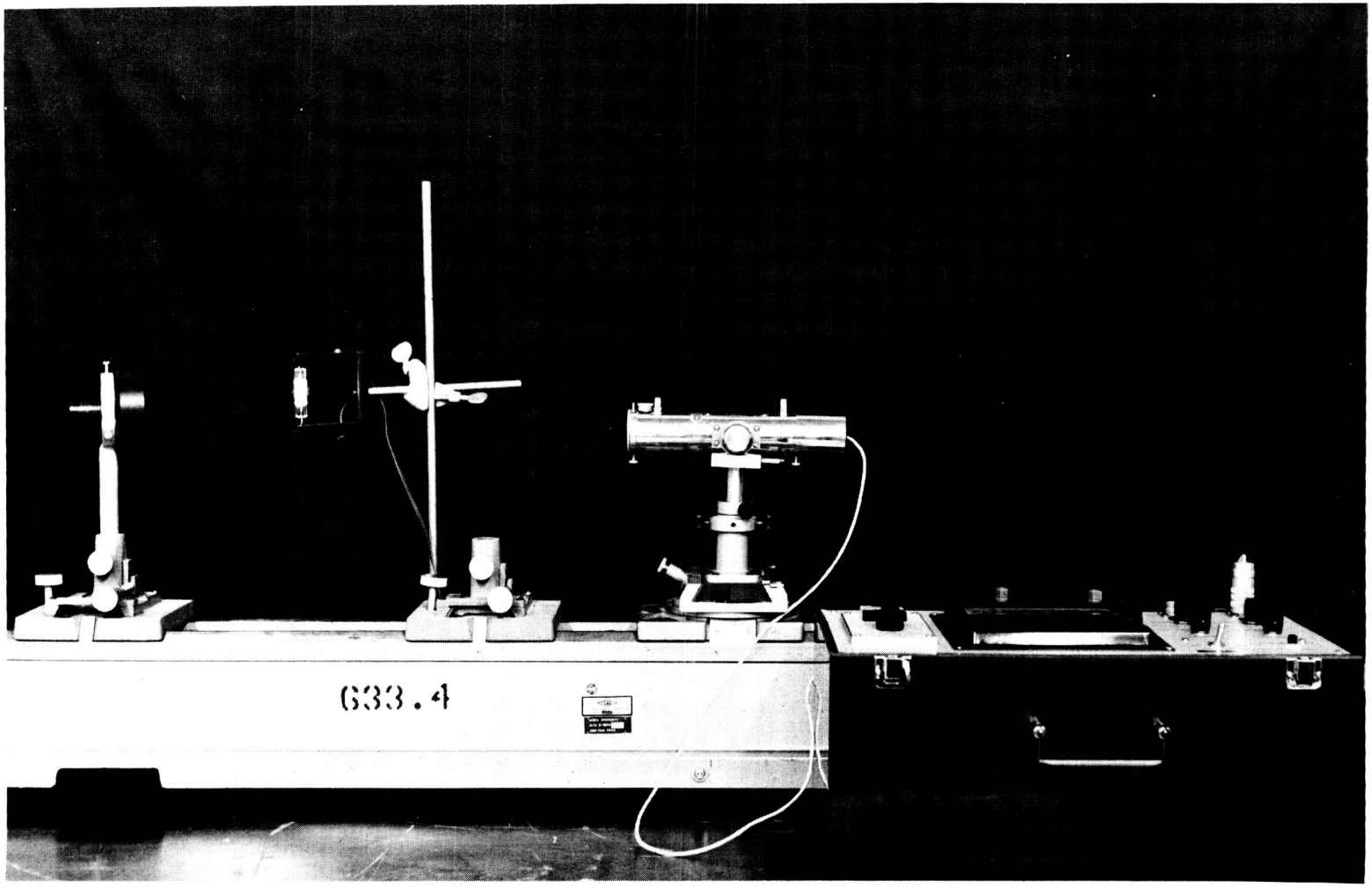

Figure 13. The Primary Working Standard Angstrom Pyrheliometer

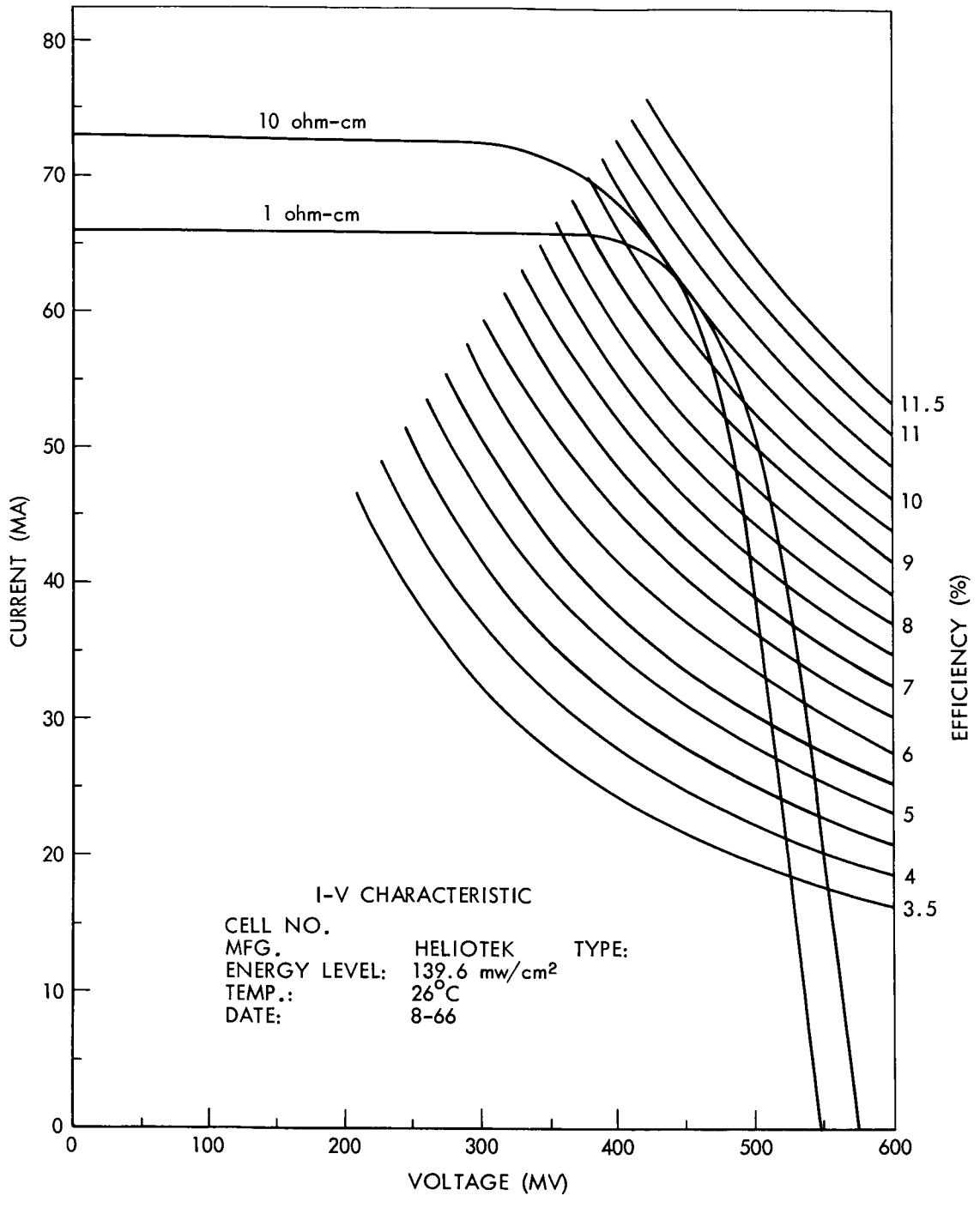

Figure 14. Current-Voltage Functions of One Ohm-cm and Ten Ohm-cm Silicon Solar Cells

Figure 15. Quantum Yield Instrumentation Set-up

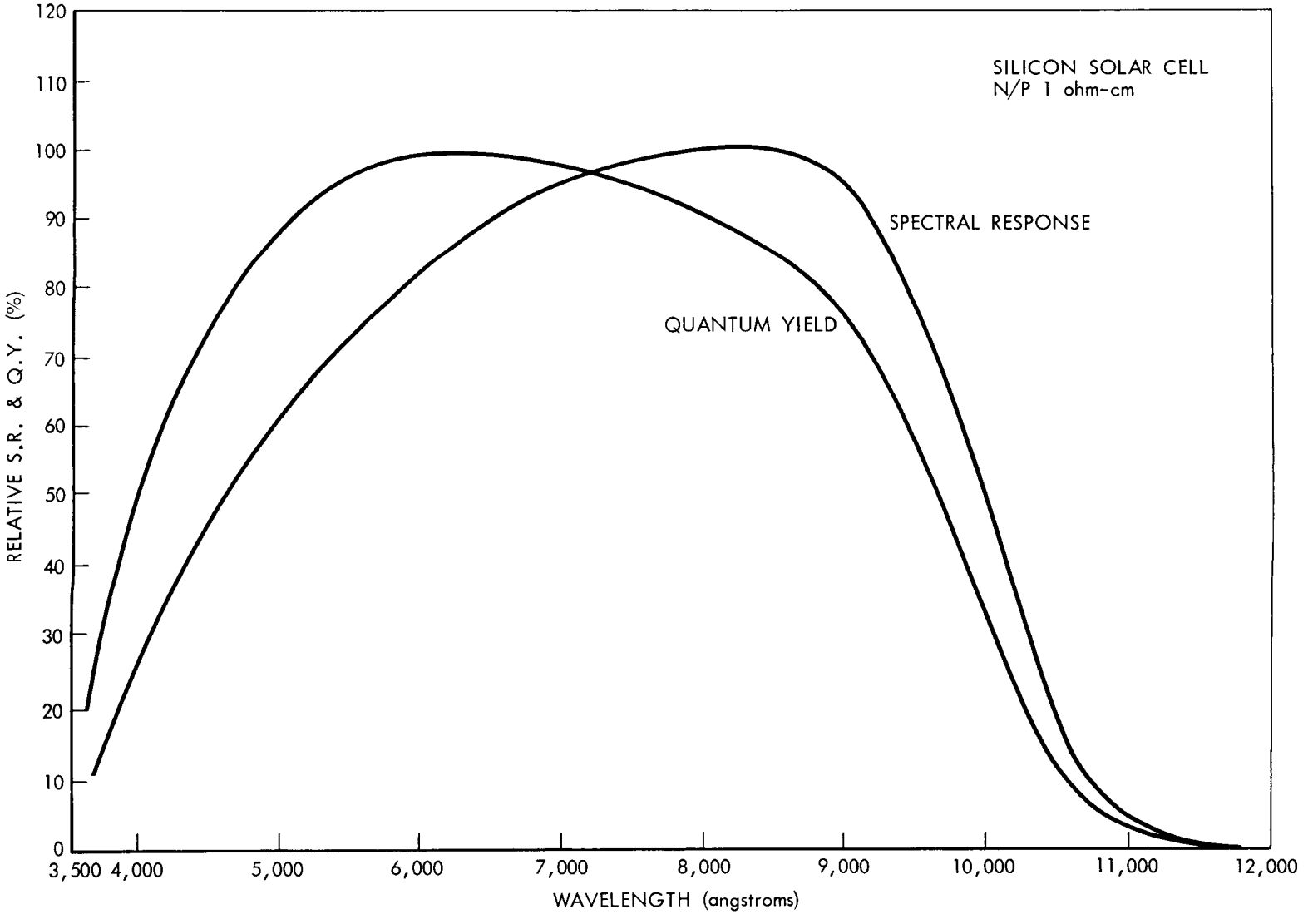

Figure 16. Typical Quantum Yield and Spectral Response

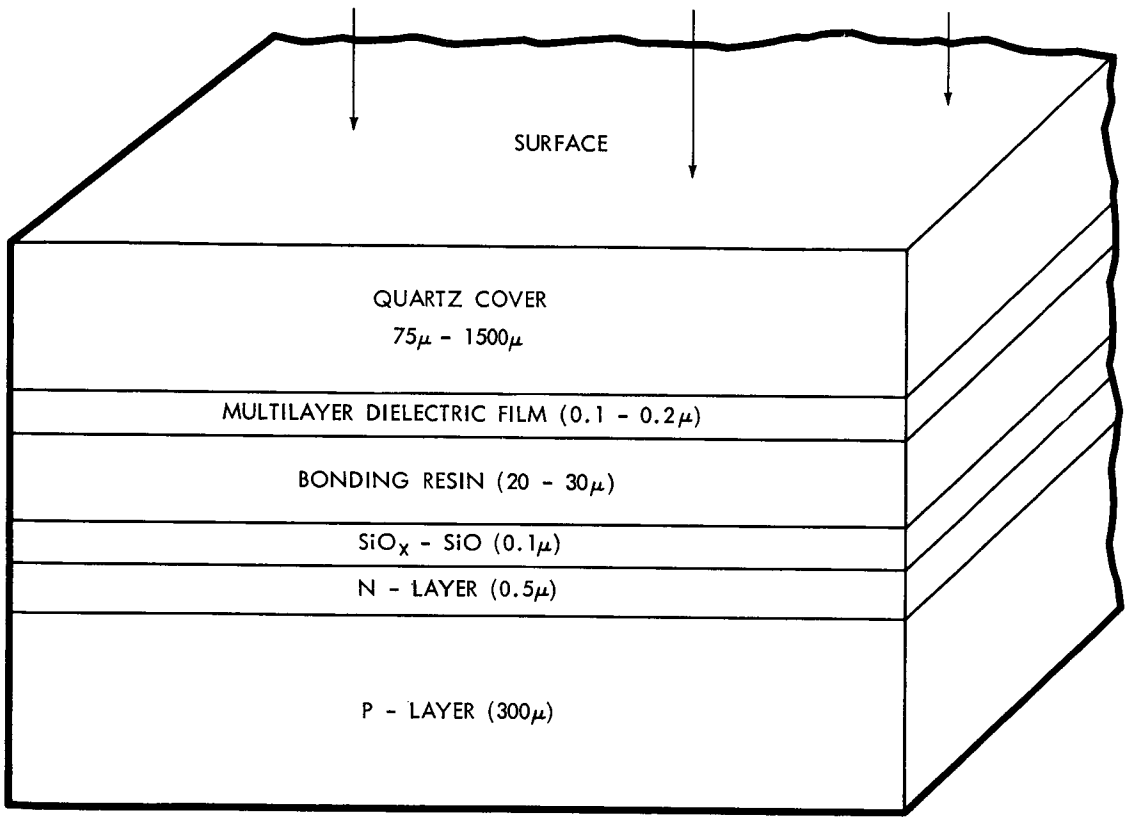

TYPICAL FINISHED SOLAR CELL CROSS SECTION (not drawn to scale)

Figure 17. Cross Section of Solar Cell Structure

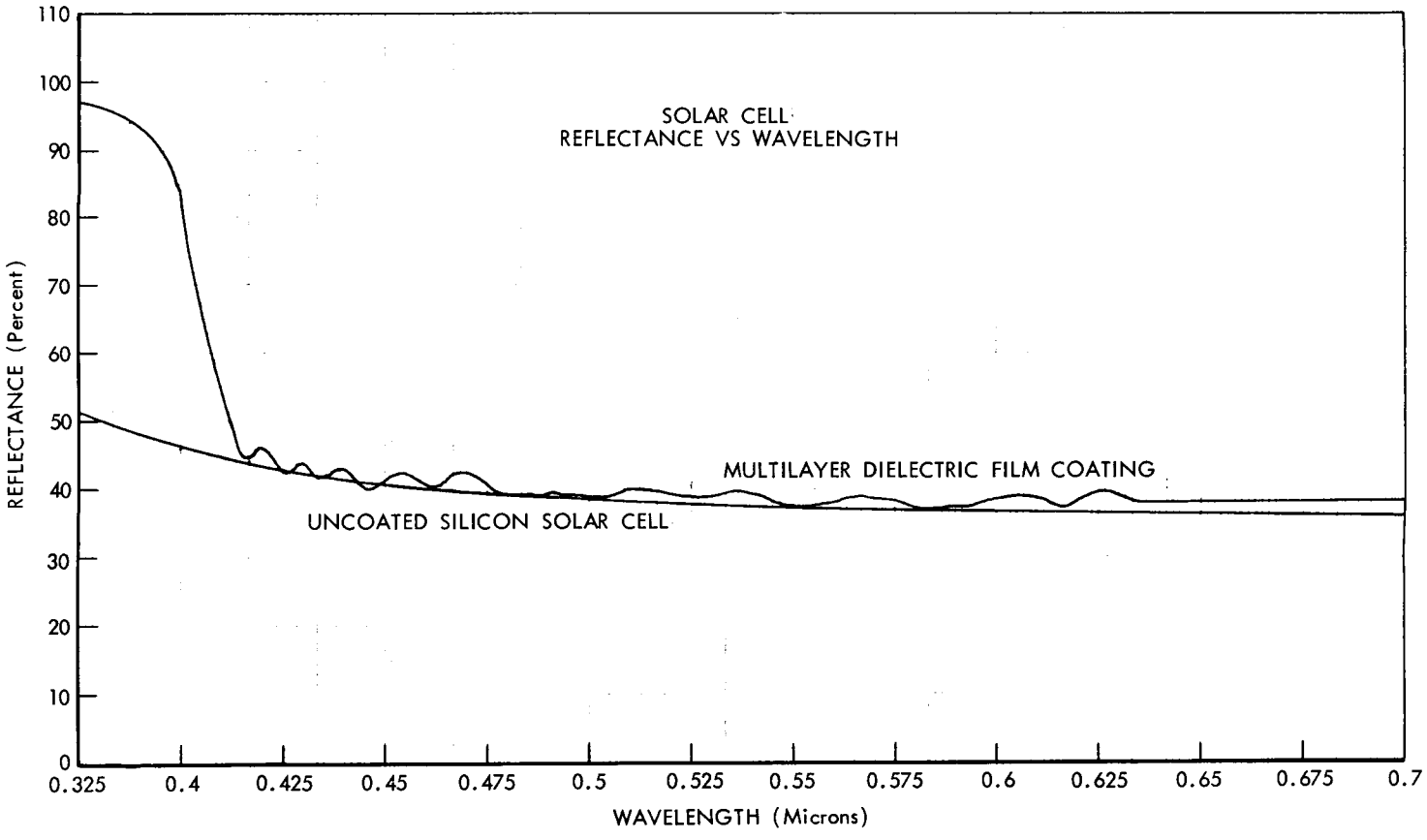

Figure 18. Surface Reflectance Properties of Coated and Uncoated Silicon Solar Cells

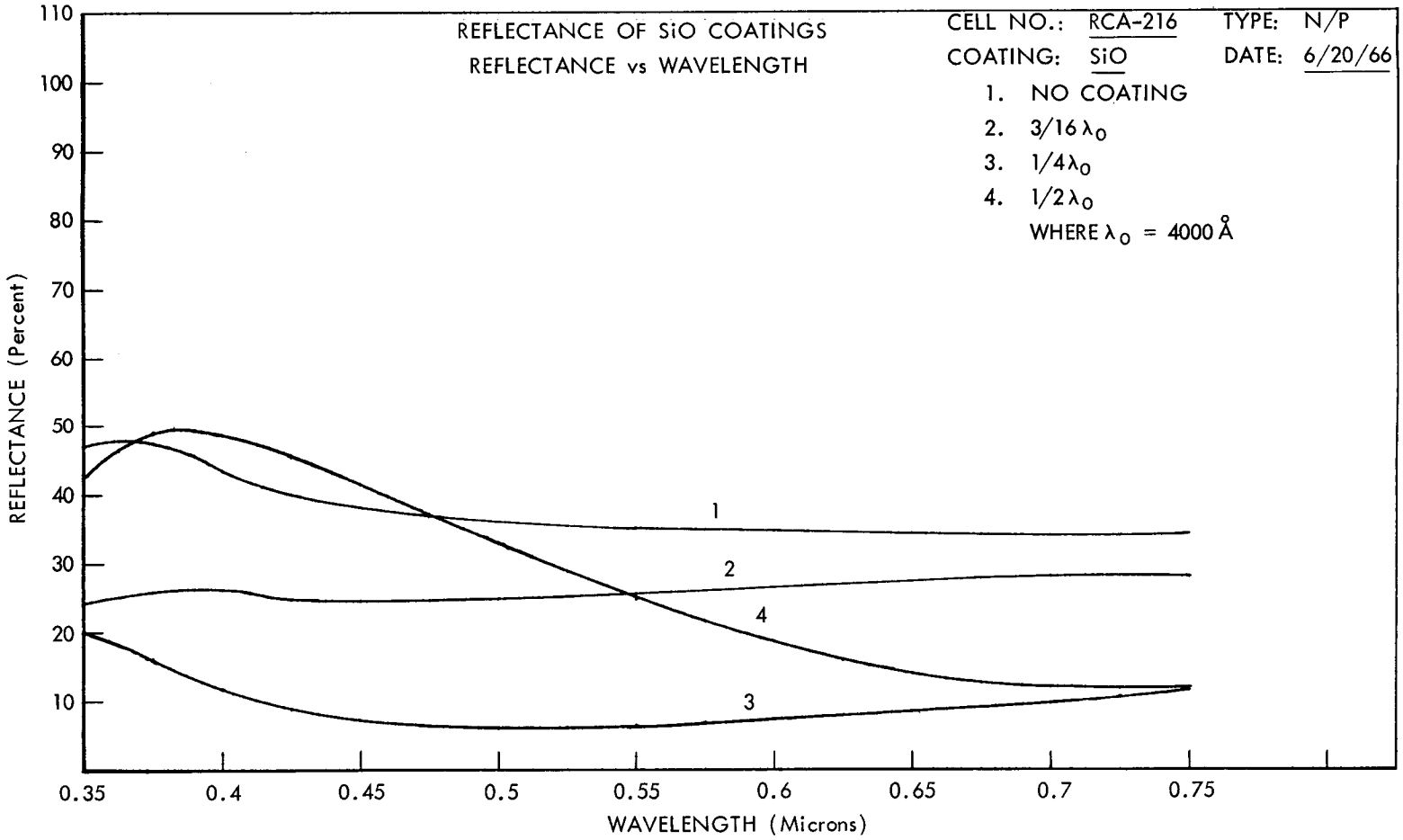

Figure 19. Surface Reflectance of N/P Silicon Solar Cell as a Function of SiO Thickness

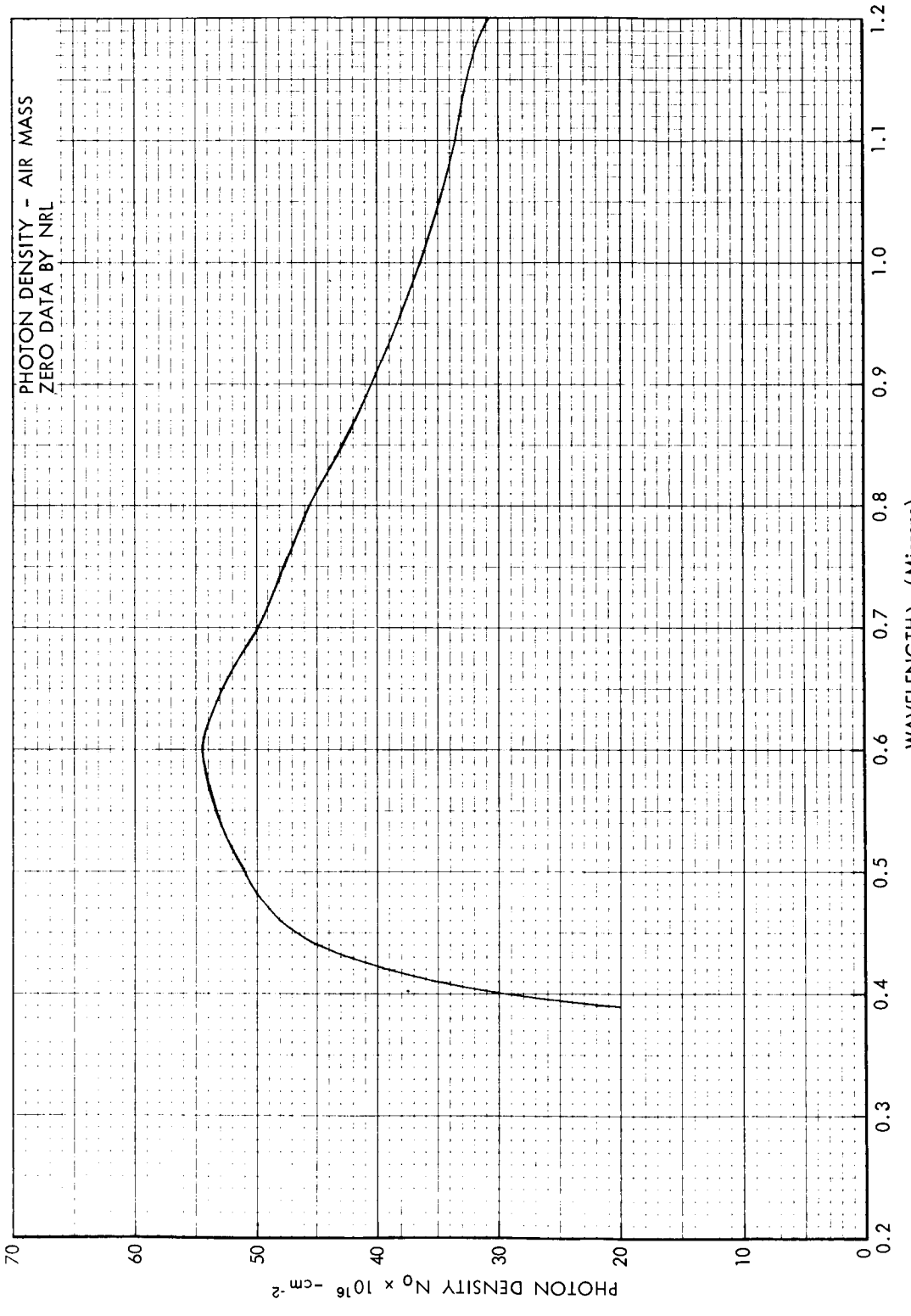

Figure 20. AMO Photon Density Function

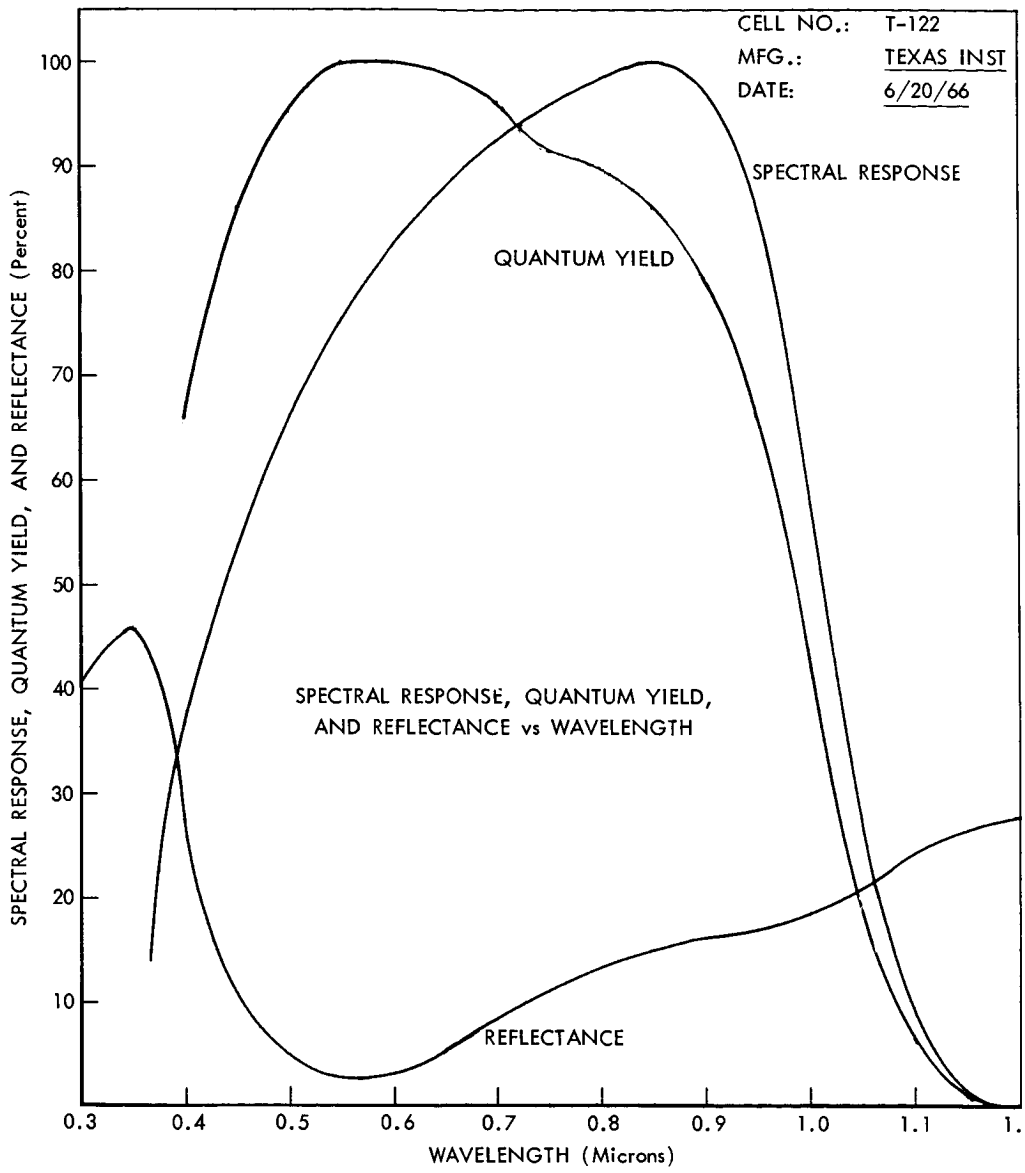

Figure 21. Surface Reflection, Quantum Yield and Spectral Response of Silicon Solar Cells

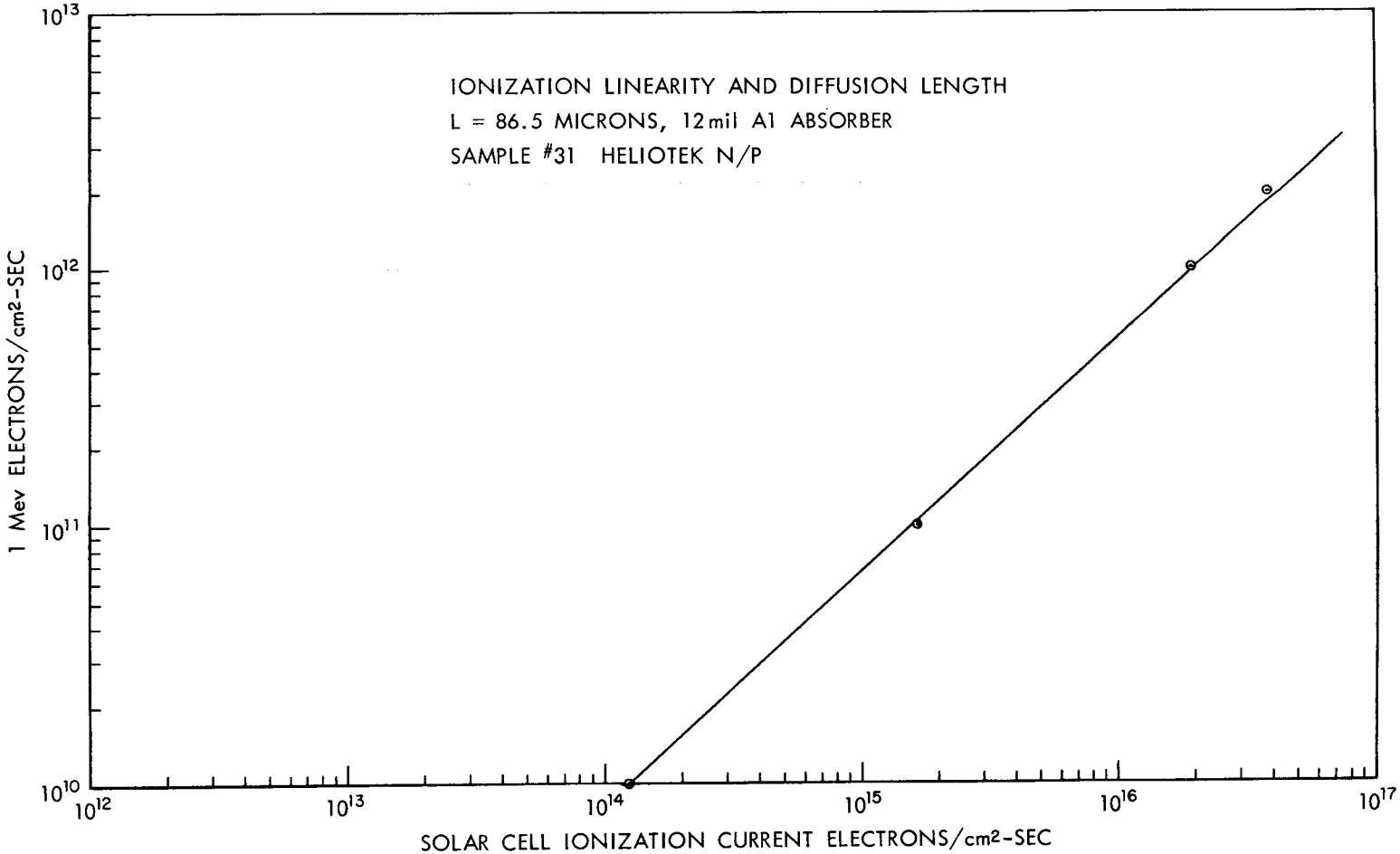

Figure 22. Solar Cell Ionization Current vs 1 MeV Electron Flux

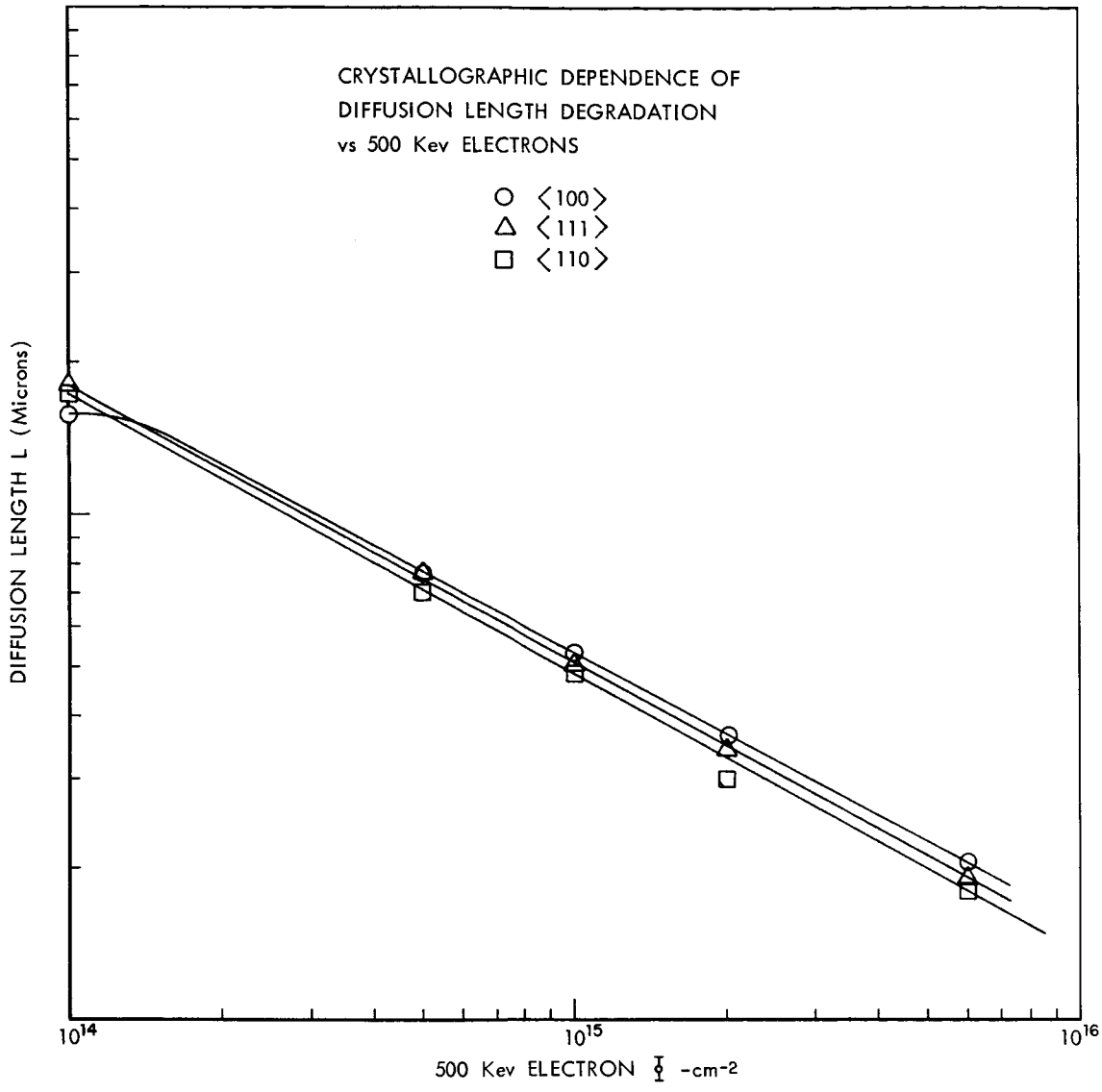

Figure 23. Crystallographic Dependence of Diffusion Length Degradation vs 0.5 MeV Electron Flux

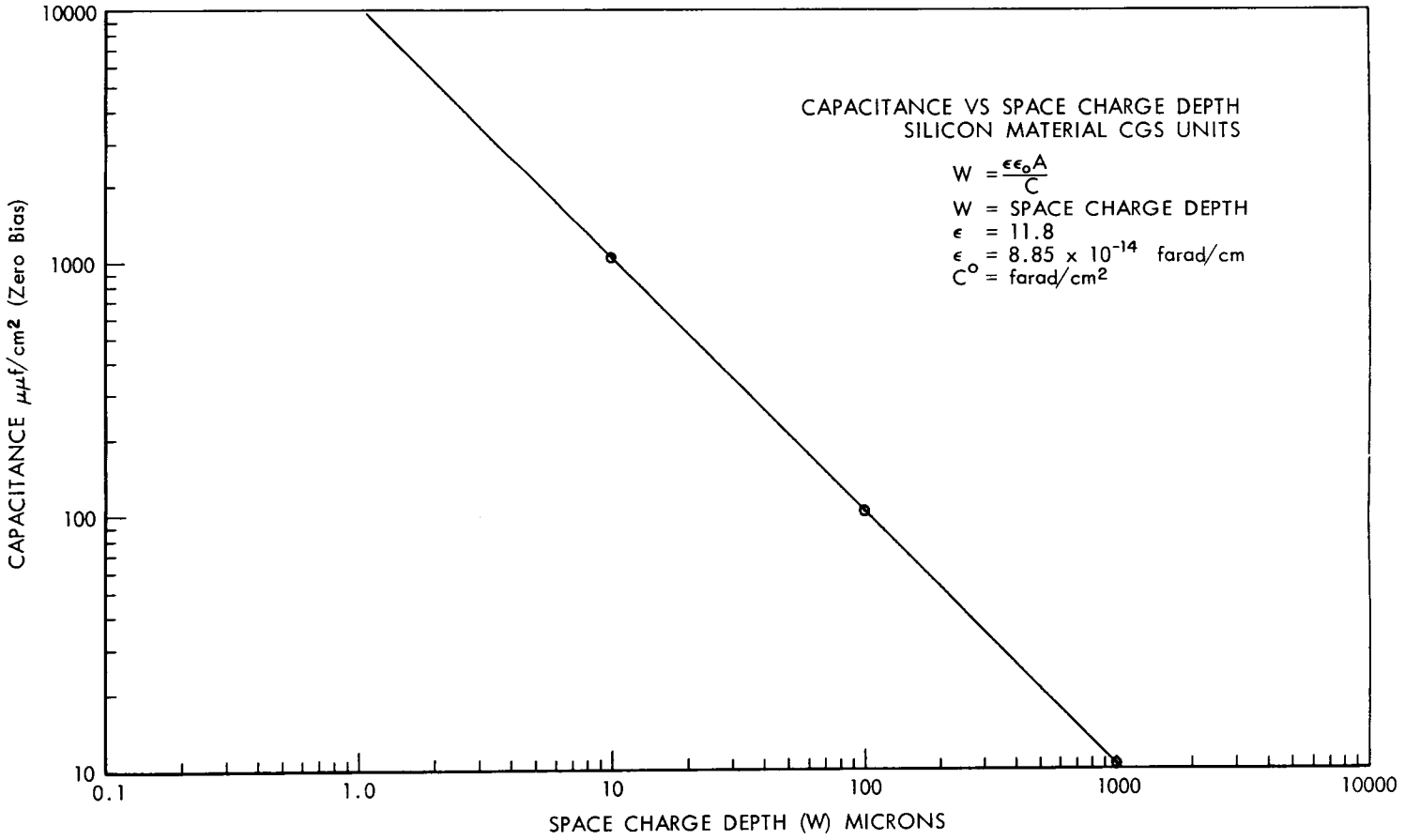

Figure 24. Capacitance vs Space Charge Depth of Silicon Solar Cells

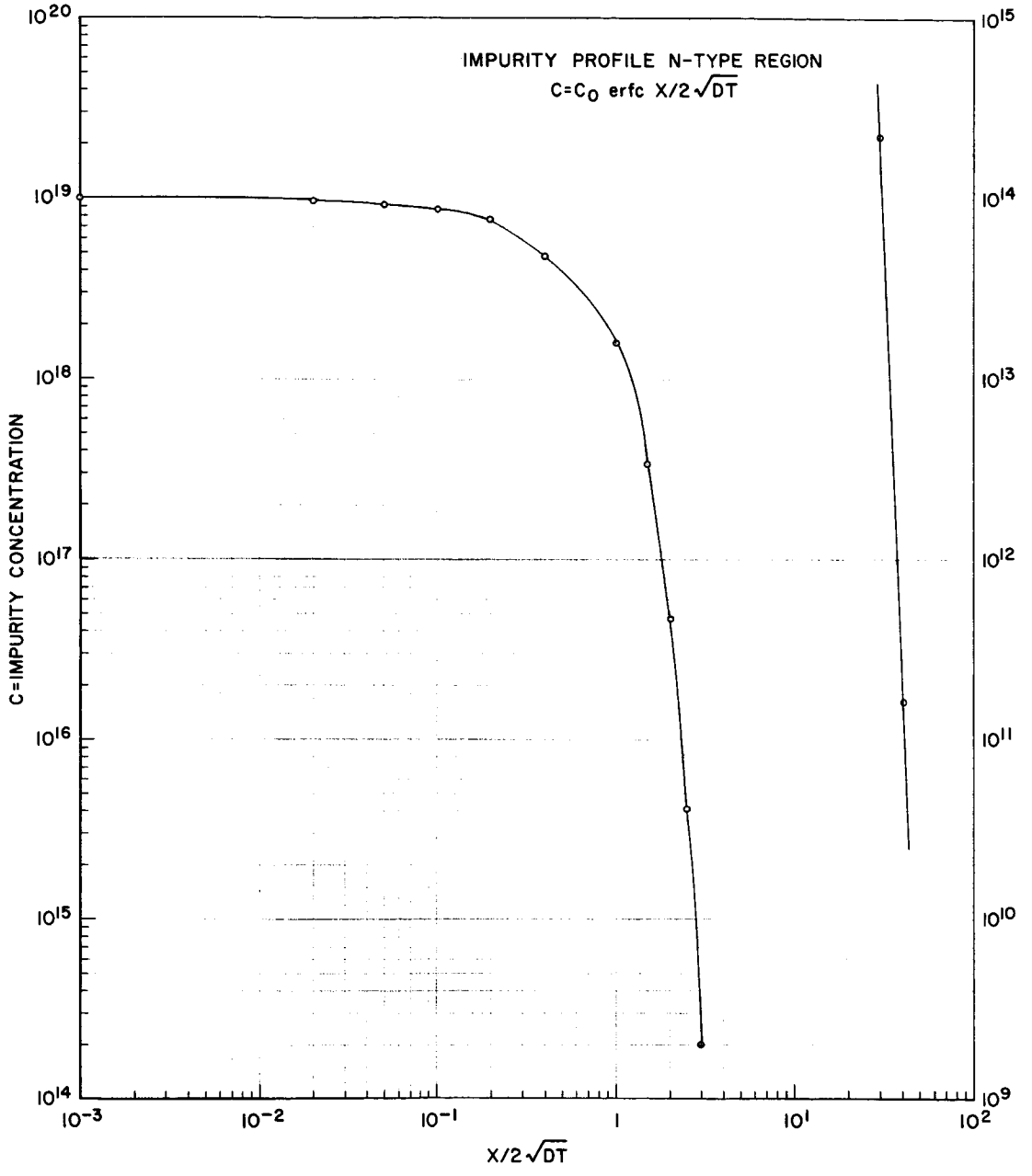

Figure 25. Impurity Profile of Solar Cell Calculated by Means of the Complementary Error Function

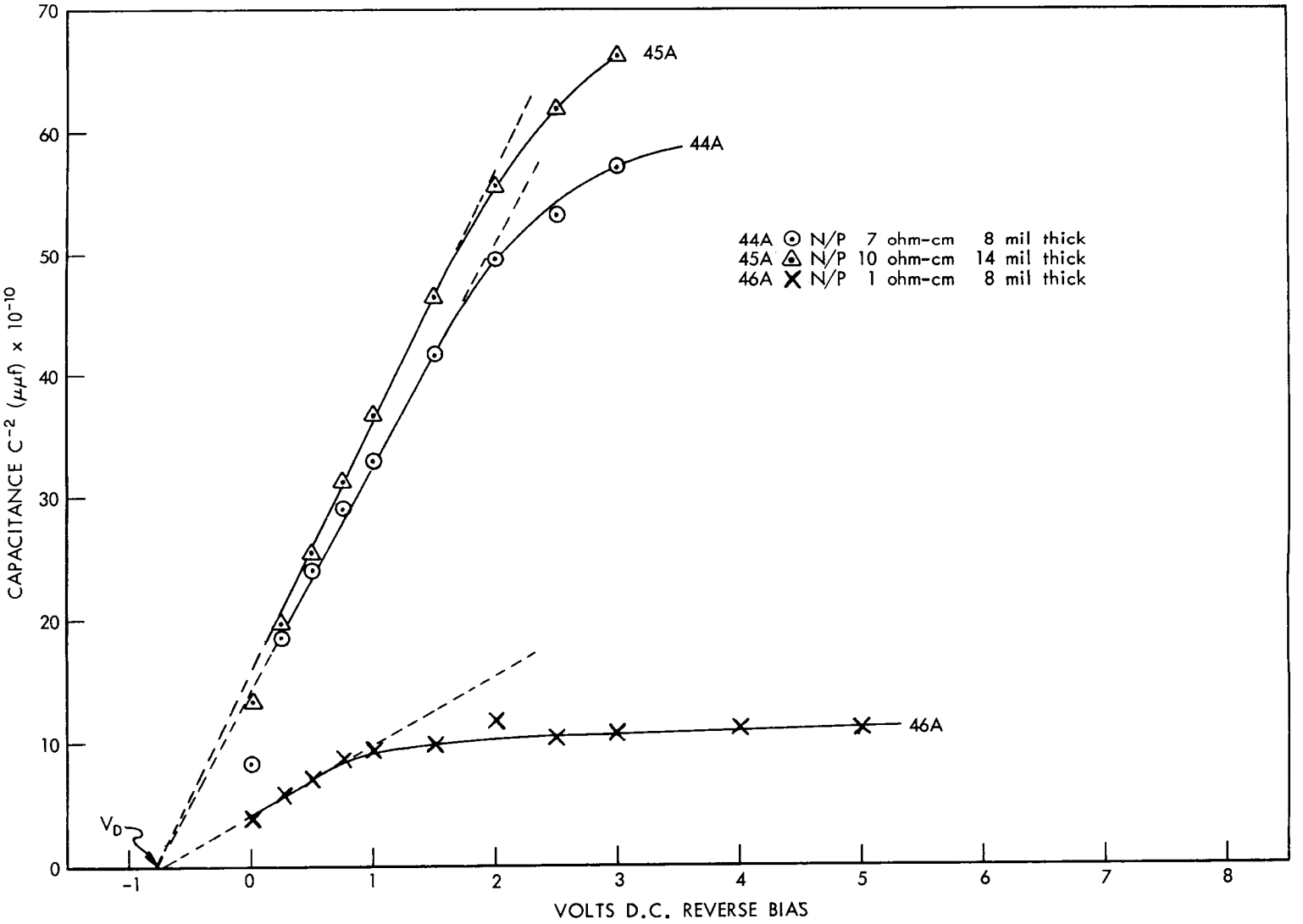

Figure 26. Silicon Solar Cell Capacitance vs Reverse Bias Voltage, C^{-2} vs V

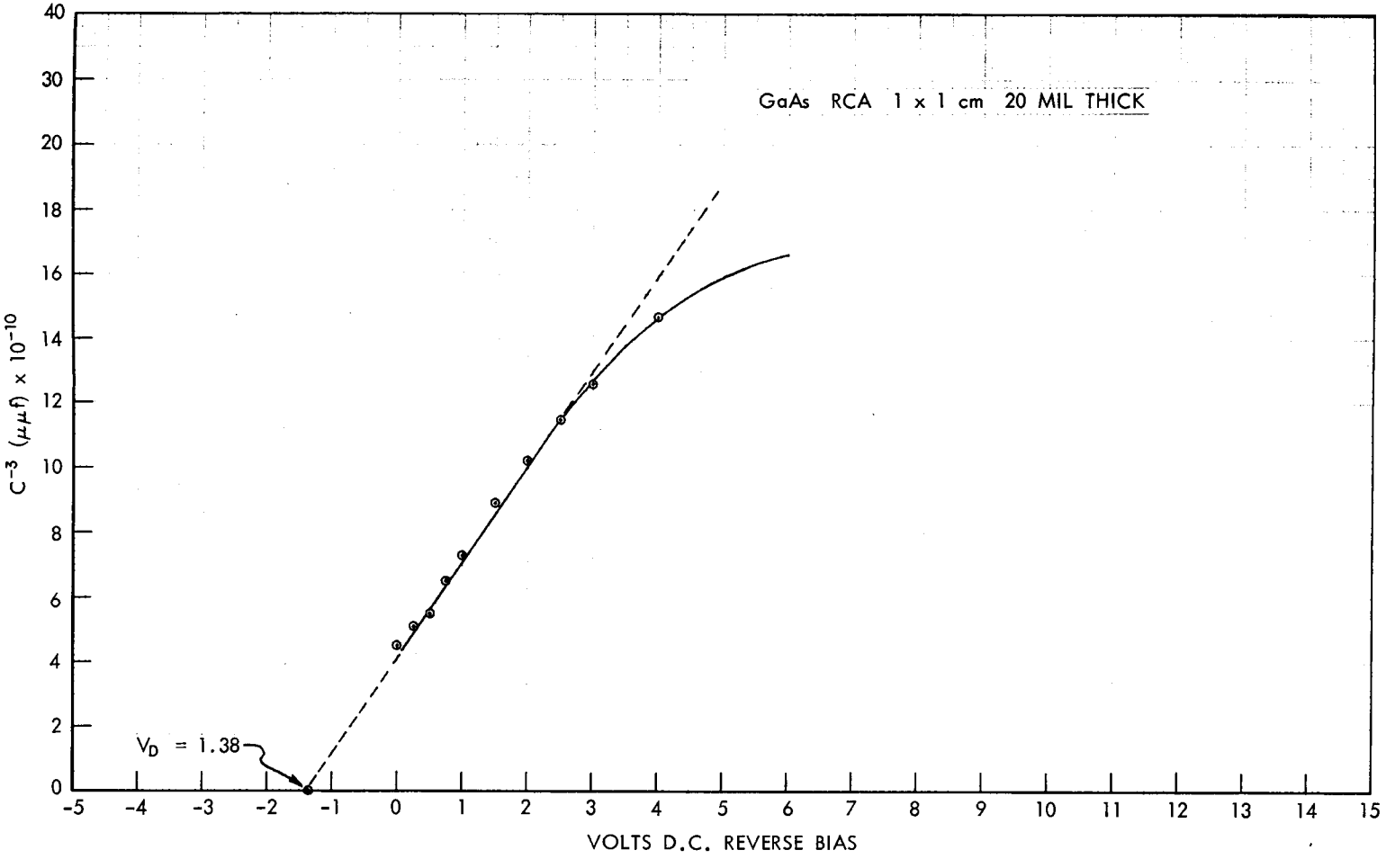

Figure 27. GaAs Solar Cell Capacitance vs Reverse Bias Voltage, C^{-3} vs V

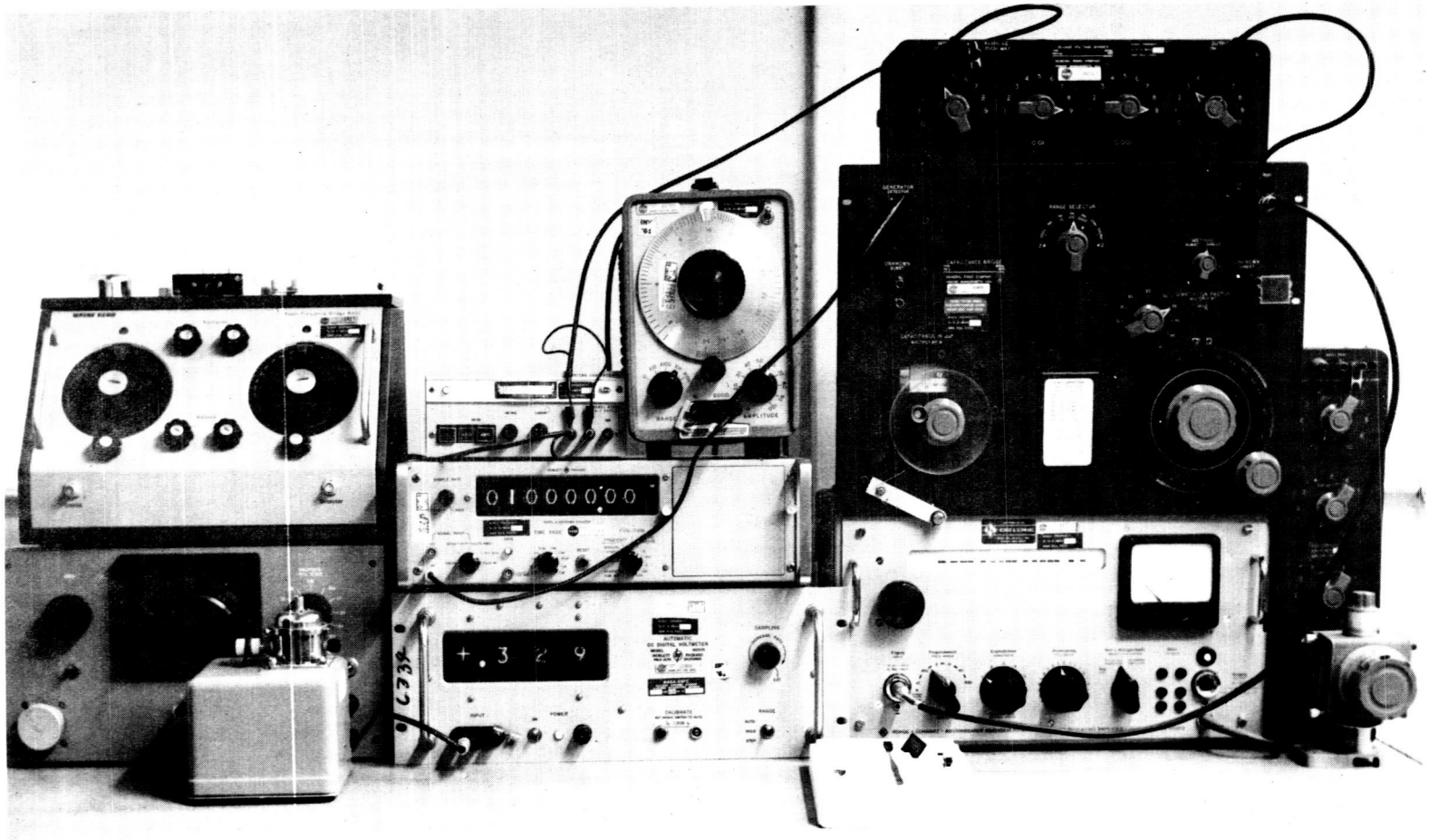

Figure 28. Instrumentation for the Measurement of Solar Cell Junction Properties

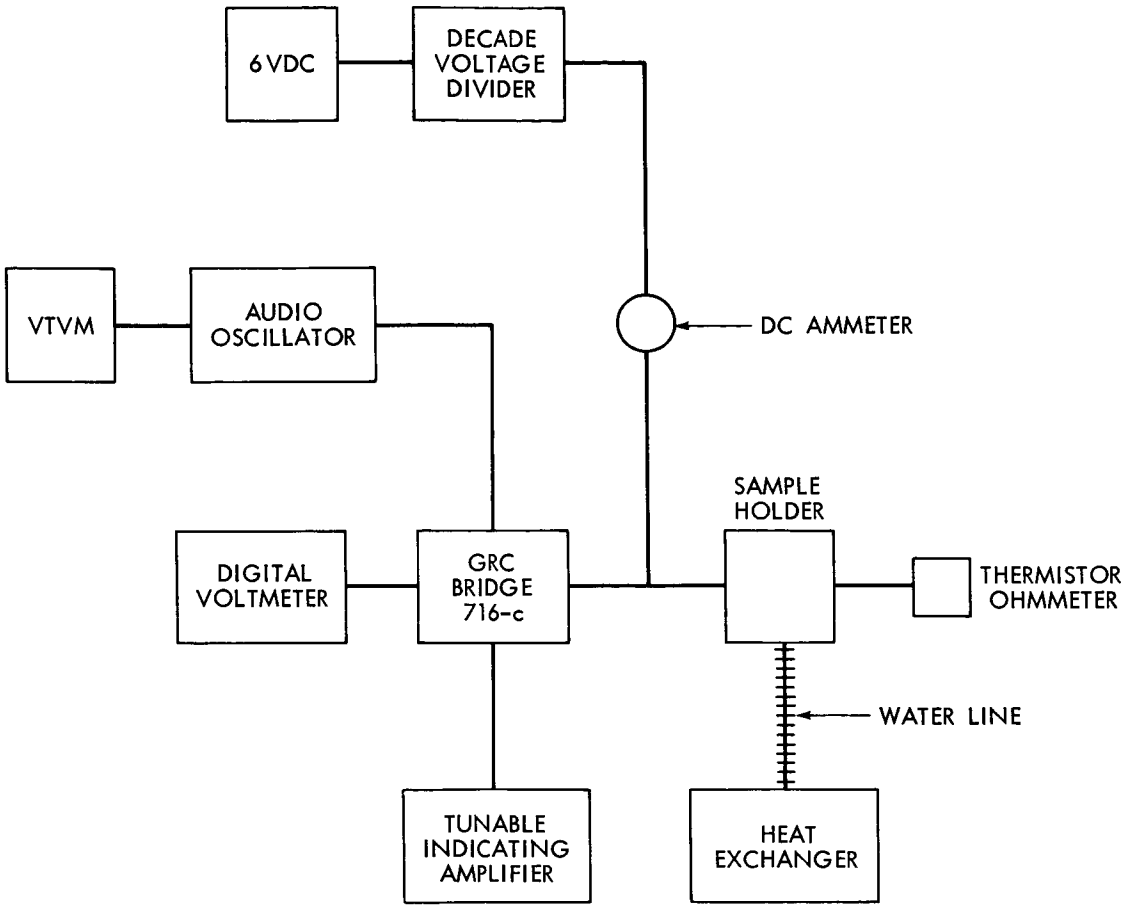

Figure 29. Pictorial Layout of Impedance Measurements